

**Broadband electromagnetic analysis of dispersive, periodic
structures for radiometer calibration**

by

S. Sandeep

M.S., University of Colorado, Boulder 2011

A thesis submitted to the
Faculty of the Graduate School of the
University of Colorado in partial fulfillment
of the requirements for the degree of
Doctor of Philosophy
Department of Electrical, Energy and Computer engineering
2012

This thesis entitled:
Broadband electromagnetic analysis of dispersive, periodic structures for radiometer calibration
written by S. Sandeep
has been approved for the Department of Electrical, Energy and Computer engineering

Prof. Albin Gasiewski

Prof. Dejan Filipovic

Prof. Edward Kuester

Prof. Bob McLeod

Dr. David Walker

Date _____

The final copy of this thesis has been examined by the signatories, and we find that both the content and the form meet acceptable presentation standards of scholarly work in the above mentioned discipline.

Sandeep, S. (Ph.D., Electrical and Computer engineering)

Broadband electromagnetic analysis of dispersive, periodic structures for radiometer calibration

Thesis directed by Prof. Albin Gasiewski

This thesis primarily focusses on the full wave electromagnetic analysis of radiometer calibration targets using doubly dispersive 3D Finite Difference Time Domain (FDTD) formulation. The boundary conditions are set up to solve for doubly periodic structures. The thesis contains very detailed derivation and equations regarding this formulation. One of the novelty in this formulation is the handling of magnetically and electrically dispersive media (usually it is just the electrical dispersion which is incorporated). Using a custom developed code which can be run on a distributed computing system, the reflectivity spectrum of calibration targets of different geometries, coating thicknesses and aspect ratios are analyzed. The results are well validated using commercial simulation softwares and custom Geometric Optics (GO) code. The geometries analyzed include square pyramids, conical pyramids, truncated square pyramids and truncated conical pyramids with spherical top. The coating thicknesses used are 1 mm, 2 mm and 3 mm. The aspect ratios (ratio of base to height) used include 1 : 1, 1 : 2 and 1 : 4. The nominal target structure has 1 : 4 aspect ratio and 2mm coating thickness. The material used for simulation is ECCOSORB MF112. The material properties of other materials such as MF110 and MF114 are listed. It should be remarked that measured material properties are available only in the frequency range [8, 26] GHz and a Debye series extrapolation was used for simulation at frequencies outside this range. Throughout this work 0.5" base was used. Some significant conclusions include the following: 1) 1:4 aspect ratio or better is required to achieve a -50 dB reflectivity or lower 2) Low frequency reflectivity is independent of the target geometry. 3) At high frequencies, the conical target results in better performance when compared to square pyramids (by about 10 dB). 4) The reflectivity spectrum exhibits a general trend of high reflectivity at low frequencies followed by decreasing reflectivity as frequency is increased. There is a reflectivity jump at frequencies where non-specular Floquet modes start

propagating. This is followed by nearly sinusoidal oscillations at high frequencies. 5) Asymptotic techniques can be used at high frequencies instead of full wave analysis. The plane wave reflectivity estimated using full wave analysis is an approximate method to calculate brightness temperature as measured by antenna during radiometer calibration. It assumes two conditions: 1) The calibration targets have a uniform temperature profile. 2) Antenna is in the far field. These two conditions are never met in practice. In order to estimate the near field thermal emission, Fluctuation Dissipation Theorem (FDT) must be used. Dyadic Green Function (DGF) along with FDT can be used to calculate the thermal emission from simple geometries. Analytical formulations to this end is given in this thesis.

The rest of the thesis ($\sim 50\%$) contains work related to numerical methods applied to radiative transfer and computational electromagnetics. In the first part, a novel method to calculate the absorption coefficient, scattering coefficient, backscattering coefficient and phase asymmetry parameter of a polydispersed distribution of liquid water and ice hydrometeors is presented. The conventional method of calculating these coefficients can be time consuming, because of the Mie series summation to calculate Mie coefficients and the numerical quadrature over a distribution of spheres to calculate the required coefficients. By using spline interpolation on a precomputed look up table, the calculation procedure can be accelerated. The second part deals with time domain analysis of dispersive, periodic structures for oblique plane wave incidence. This is a difficult problem with only one work available in literature till now. The proposed method uses Laguerre Marching-In-On-Degree (MoD) where time dependant quantities are expressed as an expansion of Laguerre basis functions. Using several properties of Laguerre basis functions, the time dependant problem is converted to a time independent problem in Laguerre basis coefficients. This in turn is solved using the familiar finite difference format. The novel method was validated with analytical results for incident angles as large as 75° .

Dedication

To my parents

Acknowledgements

I would like to thank Prof. Albin Gasiewski for providing me an opportunity to do PhD with funding and for his patience. His broad knowledge in several fields (both practical and theoretical) inspired me tremendously. The last four years of grad school made me realize that my knowledge from undergrad textbooks was nothing! (I would have been in the same state of mind, if I continued working in industry). I would also like to thank Dr. David Walker of NIST for the NIST PREP fellowship. I hope the invaluable experience and knowledge which I obtained in last four years will help me in solving more difficult and important problems in electromagnetics and applied mathematics.

Contents

Chapter

1	Introduction	1
2	FDTD formulation	5
2.1	Piecewise Linear Recursive Convolution	6
2.2	Uniaxial Perfectly Matched Layer	12
2.3	Boundary conditions	14
2.4	Parallel computation	15
2.5	Microwave characterization of radar absorbing material	17
2.6	Numerical validation	19
3	Results and Discussion	25
3.1	Total reflectivity formulation	25
3.2	Reflectivity spectrum of square pyramid array	27
3.3	Geometrical optics validation	29
3.4	Floquet mode reflectivity analysis	30
3.5	Reflectivity spectrum of conical pyramid array	31
3.6	Reflectivity spectrum of truncated square pyramid array	33
3.7	Target base width scaling	34
3.8	Unscented transformation sensitivity analysis	34
3.9	Uncertainty in material properties	35

3.10	Stability and convergence	37
3.11	Conclusions	38
4	Transient analysis of dispersive, periodic structures for obliquely incident plane wave using Laguerre Marching-On-In Degree (MoD)	48
4.1	Introduction	48
4.2	Laguerre MoD formulation for periodic, dispersive structure	49
4.3	UPML formulation in Laguerre MoD	53
4.4	Numerical validation	56
4.5	Conclusions	57
5	Near Field Thermal Emission	60
5.1	Fluctuation Dissipation Theorem	61
5.2	Dyadic Green's Function	61
5.3	Formulation of stochastic electromagnetic power density	63
5.4	Cylindrical Vector Wave Functions	65
5.4.1	Orthogonality of VWFs	66
5.5	DGF for dielectric cylinder	67
6	Fast Jacobian Mie Library for Terrestrial Hydrometeors	71
6.1	Introduction	72
6.2	Mie theory	74
6.3	Look-up table calculation	76
6.4	B-spline interpolation	79
6.5	Results and discussion	82
6.5.1	Memory and Computational Overhead Reduction	82
6.5.2	Radiation Jacobian	83
6.5.3	Computational Savings	84

6.5.4	Reconstruction Error Analysis	84
6.5.5	Radiative Transfer Simulations	87
6.6	Conclusions	88
7	Conclusions and Future work	99
7.1	Conclusions	99
7.2	Future work	102
7.2.1	Heat Diffusion Equation	104
	Bibliography	106
	Appendix	
A	3D dispersive FDTD code	113
B	Genetic algorithm Debye series fitting code	171
C	Periodic surface reflectivity using Geometric Optics (GO)	173
D	Truncated pyramid geometry	178
E	Laguerre MoD code	181
F	ADE (Auxiliary Differential Equation) formulation for TM_z case (Debye media)	192

Tables

Table

2.1	5 pole Debye parameters for MF-112	20
2.2	5 pole Debye parameters for MF-114	21
2.3	5 pole Debye parameters for MF-110	21

Figures

Figure

1.1	Radiometer calibration target	3
2.1	FDTD computational engine	6
2.2	FDTD unit cell	15
2.3	Symmetry/Antisymmetry boundary conditions on x,z boundaries	16
2.4	1D Domain Decomposition for parallel computation	17
2.5	1D Domain Decomposition in the case of 1D FDTD	17
2.6	MF112 permittivity : Measured data and 5 pole Debye fit	21
2.7	MF112 permeability : Measured data and 5 pole Debye fit	22
2.8	MF110 permittivity : Measured data and 5 pole Debye fit	22
2.9	MF110 permeability: Measured data and 5 pole Debye fit	23
2.10	Reflectivity spectrum of 0.5" base,1:1 pyramid with 1 mm MF112 coating	23
2.11	Numerical validation of the code	24
3.1	2D cross section of calibration target	26
3.2	Reflectivity of pyramidal targets with MF112 coating for various aspect ratios and coating thicknesses in the frequency range [6,26] GHz.	28
3.3	HFSS model for square pyramid specular mode reflectivity calculation	39
3.4	Reflectivity of pyramidal targets with MF112 coating for various aspect ratios and coating thicknesses 1 mm,2 mm in the frequency range [6,200] GHz	39

3.5	Reflectivity of pyramidal targets with MF112 coating for various aspect ratios and coating thickness 3 mm in the frequency range [6,200] GHz. GO validation is also shown for each case.	40
3.6	Front view of pyramid showing facets for GO modelling	40
3.7	Floquet mode reflectivity spectrum for 1:2, 0.5'' base pyramid with 2 mm MF112 coating	41
3.8	Reflectivity spectrum of conical pyramid array with 1 mm of MF112 coating	41
3.9	Reflectivity spectrum of conical pyramid array with 2 mm of MF112 coating	42
3.10	Reflectivity spectrum of conical pyramid array with 3 mm of MF112 coating	42
3.11	Reflectivity spectrum comparison of circular and square pyramids with 2 mm MF112 coating. Periodicity is $\frac{0.5''}{\sqrt{2}}$	43
3.12	Reflectivity spectrum of truncated radiometer calibration targets	43
3.13	Reflectivity spectrum of truncated, conical pyramid array. Aspect ratio of 1:4 and 2 mm MF112 coating.	44
3.14	Reflectivity spectrum of square pyramid array. Base = 0.2833'', 1:4 aspect ratio and 2 mm MF112 coating.	44
3.15	Uncertainty bounds in the reflectivity spectrum of 1:4, 2 mm square pyramid target with MF112 coating	45
3.16	Late time instability	45
3.17	Prony extrapolation of scattered field time series	46
3.18	Effect of late time instability on reflectivity spectrum	46
3.19	Convergence study: 0.5'' base, 1:4 circular pyramid with 1 mm MF112 coating	47
3.20	Observation plane location : 0.5'' base, 1:4 circular pyramid with 1 mm MF112 coating	47
4.1	Transmission spectrum of dispersive slab at 0° angle of incidence	58
4.2	Transmission spectrum of dispersive slab at 45° angle of incidence	58
4.3	Transmission spectrum of dispersive slab at 60° angle of incidence	59

4.4	Transmission spectrum of dispersive slab at 75° angle of incidence	59
6.1	Logarithmic ratio of the calculation time for B-spline interpolation to that for exact Mie series calculation of polydispersed liquid hydrometeor absorption coefficients. An exponential drop-size distribution, temperature $T = 0^\circ\text{C}$ and fractional volume $f = 10^{-6}$ are assumed	90
6.2	Fractional error in reconstructed values of liquid and ice hydrometeor absorption coefficient vs. liquid and ice hydrometeor absorption values. The maximum allowable error bounds for $T_{DB} = 0.01\text{K}$ and 0.1K are shown.	90
6.3	Liquid hydrometeor $\kappa_a(\text{dB/km})$ vs. $(f, \langle D \rangle)$ at $T = 0^\circ\text{C}$	91
6.4	Ice hydrometeor $\kappa_a(\text{dB/km})$ vs. $(f, \langle D \rangle)$ at $T = 0^\circ\text{C}$	91
6.5	Liquid hydrometeor $\kappa_s(\text{dB/km})$ vs. $(f, \langle D \rangle)$ at $T = 0^\circ\text{C}$	92
6.6	Ice hydrometeor $\kappa_s(\text{dB/km})$ vs. $(f, \langle D \rangle)$ at $T = 0^\circ\text{C}$	92
6.7	Liquid hydrometeor $\kappa_b(\text{dB/km})$ vs. $(f, \langle D \rangle)$ at $T = 0^\circ\text{C}$	93
6.8	Ice hydrometeor $\kappa_b(\text{dB/km})$ vs. $(f, \langle D \rangle)$ at $T = 0^\circ\text{C}$	93
6.9	Liquid hydrometeor g vs. $(f, \langle D \rangle)$ at $T = 0^\circ\text{C}$	94
6.10	Ice hydrometeor g vs. $(f, \langle D \rangle)$ at $T = 0^\circ\text{C}$	94
6.11	Liquid hydrometeor $\frac{d\kappa_a}{d\langle D \rangle}$ vs. $(f, \langle D \rangle)$ at $T = 0^\circ\text{C}$	95
6.12	Ice hydrometeor $\frac{d\kappa_a}{d\langle D \rangle}$ vs. $(f, \langle D \rangle)$ at $T = 0^\circ\text{C}$	95
6.13	Liquid hydrometeor $\frac{d\kappa_s}{d\langle D \rangle}$ vs. $(f, \langle D \rangle)$ at $T = 0^\circ\text{C}$	96
6.14	Ice hydrometeor $\frac{d\kappa_s}{d\langle D \rangle}$ vs. $(f, \langle D \rangle)$ at $T = 0^\circ\text{C}$	96
6.15	Liquid hydrometeor $\frac{d\kappa_b}{d\langle D \rangle}$ vs. $(f, \langle D \rangle)$ at $T = 0^\circ\text{C}$	97
6.16	Ice hydrometeor $\frac{d\kappa_b}{d\langle D \rangle}$ vs. $(f, \langle D \rangle)$ at $T = 0^\circ\text{C}$	97
6.17	Liquid hydrometeor $\frac{dg}{d\langle D \rangle}$ vs. $(f, \langle D \rangle)$ at $T = 0^\circ\text{C}$	98
6.18	Ice hydrometeor $\frac{dg}{d\langle D \rangle}$ vs. $(f, \langle D \rangle)$ at $T = 0^\circ\text{C}$	98
7.1	Reflectivity spectrum as shown in [1]	100

D.1 Truncated pyramid geometry	178
D.2 Spherical cap	179

Chapter 1

Introduction

Microwave and millimeter wave remote sensing offer several advantages over infrared and visible observations. This is primarily due to the fact that microwave radiation is transparent to clouds and aerosols, thereby aiding in the accurate determination of temperature and water-vapor profiles. Passive microwave remote sensing of planetary atmospheres and surfaces provides a valuable means of mapping a variety of atmospheric and surface variables with minimal adverse influence from clouds and aerosols. Variables regularly measured and imaged include temperature and water vapor profiles, cloud liquid and ice content, soil moisture, sea surface salinity and wind vector, snow water equivalent, and sea ice extent. Increasingly, these variables are the object of climate studies which seek to link anthropogenic forcings to regional or global changes in one or several of them. Unambiguous determination of changes in any of these variables generally requires absolute radiometric accuracy of a small fraction of a Kelvin over decadal time scales. For example, instrumental biases as small as 0.05K or better out of a total system temperature of 500-1500K or more are required over the typical lifetime of a sounding instrument (several years) in order to unambiguously identify climatological temperature trends of order 0.1C per decade. Such accuracy is difficult to achieve across generations of instruments without traceable and accurate calibration methods. Radiometer calibration is the process by which a relationship is obtained between the output indicator of the radiometer usually voltage or current and the noise temperature at the radiometer input (usually the antenna temperature, when an antenna is connected to the radiometer receiver input) [2].

Radiometer calibration is most practically accomplished by periodic observations of highly emissive thermal references whose physical temperature is used to determine the measured antenna temperature [2]. Precise absolute calibration of radiometers for many Earth remote sensing applications requires knowledge of the antenna temperature to ± 100 mK [3], or even a factor of ten better in the case of atmospheric temperature trend estimation. To achieve such precision - on the order of -40 dB or better - highly stable and emissive thermal microwave references are used for external calibration of spaceborne radiometers. Sensors relying on such external references for calibration include the JAXA AMSR-E [4], AMSR-2 [5], DMSP SSM/I and SSMIS [6], NRL WindSat [7], Suomi ATMS, and NASA GMI [8]. Reference targets are typically periodic 1-dimensional arrays of wedges or two-dimensional arrays of pyramids constructed of a highly thermally-conductive substrate (e.g., Al or Mg) coated with a thin layer of microwave absorbing material as shown in Fig. 1.1. Microwave absorbing materials are often mixtures of iron particles in an epoxy matrix, and are electrically dispersive in nature. The ideal radiometer calibration reference should be a blackbody radiator with an emissivity of unity at all radiometric bands of interest. However, this is not achieved in practice, in which case the emitted brightness temperature of the reference $T_B(\theta, \phi)$ becomes

$$T_B(\theta, \phi) = e(\theta, \phi)T_P + \int_0^{\frac{\pi}{2}} \int_0^{2\pi} (1 - e(\theta', \phi'))T_R(\theta', \phi') d\Omega' \quad (1.1)$$

where the emissivity $e(\theta, \phi)$ is related to reflectivity $r(\theta, \phi)$ by Kirchoff's law, $e(\theta, \phi) = 1 - r(\theta, \phi)$ and $d\Omega' \equiv \sin\theta' d\theta' d\phi'$. T_P is the physical temperature of the reference and $T_R(\theta', \phi')$ is the background temperature. Accordingly, we seek thermally conductive structures with low and well known reflectivities at key microwave sounding and imaging bands often spanning a decade or more in frequency. Since the background radiation field is often difficult to control and predict, accurate estimation of target reflectivity is therefore essential for precise calibration.

In order to efficiently design wideband calibration targets, an accurate electromagnetic and thermal analysis of these structures is essential. Electromagnetic and thermal analysis of one-dimensional periodic wedge shaped structures was studied by Jackson and Gasiewski [9, 10]. This

work used the coupled-wave approach for the electromagnetic field analysis [11]. However the work was not able to be extended to 2-D periodic pyramidal structures due to computational and numerical accuracy limitations. The Extended Boundary Condition (EBC) was used for predicting surface scattering from doubly periodic pyramidal structures in [12]. This method has the disadvantage of being ill-conditioned when the surface corrugation is deep or when the corrugation depth divided by the period is large. The method also is not easily able to handle inhomogeneous calibration references which might involve a number of layers or even gradations in material parameters. Geometrical optic techniques have been used to study wedge shaped structures [13]. However, these optical techniques provide accurate results only at sufficiently high frequencies.

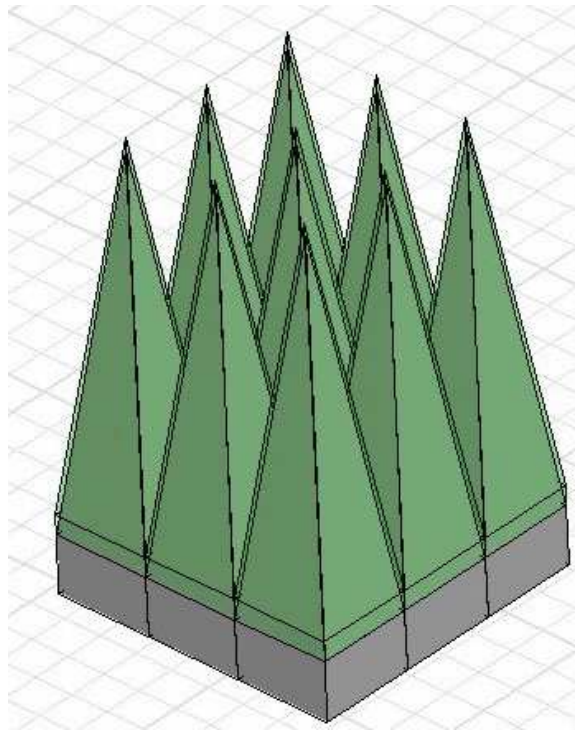


Figure 1.1: Radiometer calibration target

In chapter 2, the formulation of Finite Difference Time Domain (FDTD) method for estimating the reflectivity of periodic, dispersive (electric and magnetic dispersion) structures is outlined. The results obtained by the developed code is detailed in chapter 3. In chapter 4, a novel method for transient analysis of electrically dispersive periodic structures for oblique plane wave incidence is

presented. This method is based on Laguerre Marching-On-In-Degree (MoD), which can eliminate the constraint on the temporal discretization interval of the FDTD. Near field thermal emission from a surface with non uniform temperature profile is the subject of chapter 5. The formulations based on Fluctuation Dissipation Theorem (FDT) and Dyadic Green's Function (DGF) is explained. Chapter 6 deals with a faster way of calculating absorption, scattering and phase asymmetry coefficients of a polydispersed distribution of liquid water or ice hydrometeors. The method uses 3D spline interpolation rather than the conventional Mie series expansions and time consuming numerical quadratures. The technique was found to have significant advantages particularly for large hydrometeors (or alternatively at high frequency atmospheric radiative transfer simulations).

Chapter 2

FDTD formulation

Finite Difference Time Domain (FDTD) is a time domain numerical electromagnetic method introduced by K.S.Yee [14]. Several decades of research had resulted in the method being one of the most powerful and commonly used Computational Electromagnetic (CEM) method. The introduction to this method and its application to wide range of electromagnetic problems can be found in [15, 16, 17]. In this section, the FDTD notation which is required to understand the rest of the chapter is outlined. In FDTD, the spatial domain is discretized into rectangular cubical cells called Yee cells of dimension $\Delta x \times \Delta y \times \Delta z$. Electric field components are located at the edge centers and magnetic field components at the face centers of the Yee cell. Similarly, the time axis is discretized into intervals of Δt . The electric field components are evaluated at $n\Delta t$ and magnetic field components are evaluated at $(n + 0.5)\Delta t$. The notation used for FDTD difference equations in this work is given by,

$$\begin{aligned} E_x|_{i,j,k}^n &\rightarrow E_x((i + 0.5)\Delta x, j\Delta y, k\Delta z; n\Delta t) \\ E_y|_{i,j,k}^n &\rightarrow E_y(i\Delta x, (j + 0.5)\Delta y, k\Delta z; n\Delta t) \\ E_z|_{i,j,k}^n &\rightarrow E_z(i\Delta x, j\Delta y, (k + 0.5)\Delta z; n\Delta t) \\ H_x|_{i,j,k}^{n+0.5} &\rightarrow H_x(i\Delta x, (j + 0.5)\Delta y, (k + 0.5)\Delta z; (n + 0.5)\Delta t) \\ H_y|_{i,j,k}^{n+0.5} &\rightarrow H_y((i + 0.5)\Delta x, j\Delta y, (k + 0.5)\Delta z; (n + 0.5)\Delta t) \\ H_z|_{i,j,k}^{n+0.5} &\rightarrow H_z((i + 0.5)\Delta x, (j + 0.5)\Delta y, k\Delta z; (n + 0.5)\Delta t) \end{aligned}$$

(2.1)

where i, j, k are the spatial discretization indices and n is the temporal discretization index. This notation is more helpful in software implementation than using integer and half indices for spatial discretization, such as $E_x^n|_{i+0.5, j, k}$, since software array indexing is interger based. The components of the FDTD formulation for this problem is given in Fig. 2.1. Piecewise Linear Recursive Convolution (PLRC) is used to handle dispersive coating material. The problem space is bounded by Uniaxial Perfectly Matched Layers (UPML) on the y - axis boundaries and Periodic Boundary Condition (PBC) is used to simulate an infinite 2D array of pyramids. In order to simulate electrically large structures, parallel computation is used in the form of 1D domain decomposition.

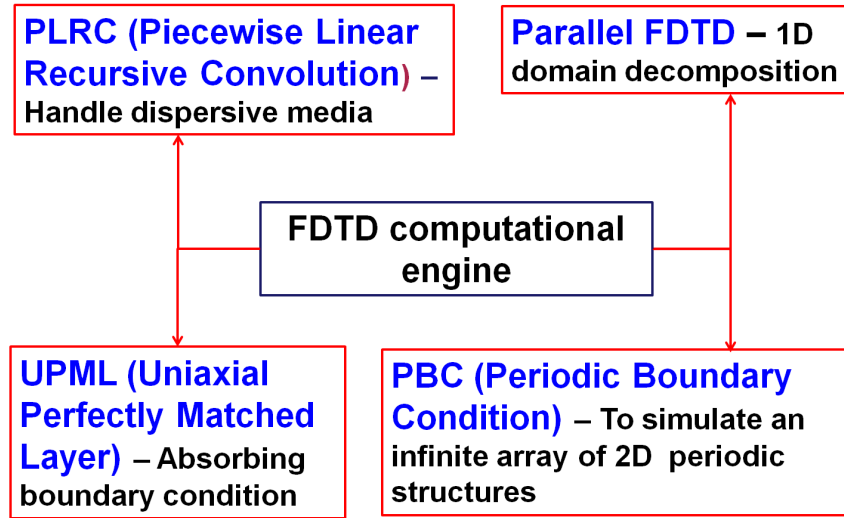


Figure 2.1: FDTD computational engine

2.1 Piecewise Linear Recursive Convolution

Temporal dispersion is characterized by frequency dependent electric and magnetic susceptibility as given by,

$$\varepsilon_r(\omega) = \varepsilon_\infty + \chi_e(\omega) \quad (2.2)$$

$$\mu_r(\omega) = \mu_\infty + \chi_m(\omega) \quad (2.3)$$

where $\chi_e(\omega), \chi_m(\omega)$ are the frequency domain electric and magnetic susceptibility functions, respectively. Depending on the functional form of these susceptibility functions, the material is classified as Debye, Lorentz, Drude media etc. The time domain form of (2.2),(2.3) is obtained by inverse Fourier transform as,

$$\varepsilon_r(t) = \varepsilon_\infty \delta(t) + \chi_e(t) \quad (2.4)$$

$$\mu_r(t) = \mu_\infty \delta(t) + \chi_m(t) \quad (2.5)$$

where $\chi_e(t), \chi_m(t)$ are associated time domain electric and magnetic susceptibility functions. In order to derive the FDTD update equation for the field component H_x , we start with the following continuous domain PDE and its discretized version as shown below,

$$\frac{\partial E_z(x, y, z; t)}{\partial y} - \frac{\partial E_y(x, y, z; t)}{\partial z} = -\frac{\partial B_x(x, y, z; t)}{\partial t} \quad (2.6)$$

$$\begin{aligned} & \left[\frac{E_z|_{i,j+1,k}^n - E_z|_{i,j,k}^n}{\Delta y} - \frac{E_y|_{i,j,k+1}^n - E_y|_{i,j,k}^n}{\Delta z} \right] \\ & = - \left[\frac{B_x|_{i,j,k}^{n+0.5} - B_x|_{i,j,k}^{n-0.5}}{\Delta t} \right] \end{aligned} \quad (2.7)$$

In time domain, $B_x(t)$ is related to $H_x(t)$ through the convolution integral,

$$B_x(t) = \mu_o [\mu_r(t) \otimes H_x(t)] = \mu_o \mu_\infty H_x(t) + \mu_o \int_0^t \chi_m(\tau) H_x(t - \tau) d\tau \quad (2.8)$$

In the discrete space, the equation (2.8) can be written as,

$$B_x|_{i,j,k}^{n+0.5} = \mu_o \mu_\infty |_{i,j,k} H_x|_{i,j,k}^{n+0.5} + \mu_o \int_0^{n\Delta t} \chi_m|_{i,j,k}(\tau) H_x|_{i,j,k}[(n+0.5)\Delta t - \tau] d\tau \quad (2.9)$$

It should be noted that in (2.9), $n\Delta t$ rather than $(n+0.5)\Delta t$ is used as the upper limit of the integral. This is due to the fact that when τ ranges from $n\Delta t$ to $(n+0.5)\Delta t$, the argument of the H_x ranges between 0 and $0.5\Delta t$. In this interval, all the magnetic fields are assumed to be zero. In (2.9), it can be seen that the values of H_x between temporal discretization points is required for integration. This problem is overcome by using linear interpolation in the interval between

two time discretization points. This is the main idea behind PLRC. In order to facilitate linear interpolation, (2.9) can be rewritten in the following summation form.

$$B_x|_{i,j,k}^{n+0.5} = \mu_o \mu_\infty |_{i,j,k} H_x|_{i,j,k}^{n+0.5} + \mu_o \sum_{d=0}^{n-1} \int_{d\Delta t}^{(d+1)\Delta t} \chi_m|_{i,j,k}(\tau) H_x|_{i,j,k}[(n+0.5)\Delta t - \tau] d\tau \quad (2.10)$$

In the interval $\tau \in [d\Delta t, (d+1)\Delta t]$, $H_x|_{i,j,k}[(n+0.5)\Delta t - \tau]$ can be approximated using a piecewise linear form as follows,

$$H_x|_{i,j,k}[(n+0.5)\Delta t - \tau] = H_x|_{i,j,k}^{n-d+0.5} + \left(\frac{\tau - d\Delta t}{\Delta t} \right) \left[H_x|_{i,j,k}^{n-d-0.5} - H_x|_{i,j,k}^{n-d+0.5} \right] \quad (2.11)$$

By applying (2.11) in (2.10), an expression for $B_x|_{i,j,k}^{n+0.5}$ can be obtained as,

$$B_x|_{i,j,k}^{n+0.5} = \mu_o \mu_\infty H_x|_{i,j,k}^{n+0.5} + \mu_o \sum_{d=0}^{n-1} X_m|_{i,j,k}^d H_x|_{i,j,k}^{n-d+0.5} + \xi_m|_{i,j,k}^d \left(H_x|_{i,j,k}^{n-d-0.5} - H_x|_{i,j,k}^{n-d+0.5} \right) \quad (2.12)$$

where we have used the following coefficients,

$$\begin{aligned} X_m|_{i,j,k}^d &= \int_{d\Delta t}^{(d+1)\Delta t} \chi_m|_{i,j,k}(\tau) d\tau \\ \xi_m|_{i,j,k}^d &= \frac{1}{\Delta t} \int_{d\Delta t}^{(d+1)\Delta t} (\tau - d\Delta t) \chi_m|_{i,j,k}(\tau) d\tau \end{aligned} \quad (2.13)$$

By applying (2.12) and time shifted version of (2.12) to (2.7), the update equation for $H_x|_{i,j,k}^{n+0.5}$ is derived as,

$$\begin{aligned} H_x|_{i,j,k}^{n+0.5} &= \left(\frac{\Delta t}{\mu_o K1|_{i,j,k}} \right) \left[\frac{E_y|_{i,j,k+1}^n - E_y|_{i,j,k}^n}{\Delta z} \frac{E_z|_{i,j+1,k}^n - E_z|_{i,j,k}^n}{\Delta y} \right] \\ &\quad + \left(\frac{K2|_{i,j,k}}{K1|_{i,j,k}} \right) H_x|_{i,j,k}^{n-0.5} + \frac{\Psi^{Hx}|_{i,j,k}^{n-0.5}}{K1|_{i,j,k}} \\ K1|_{i,j,k} &= \mu_\infty|_{i,j,k} + X_m|_{i,j,k}^0 - \xi_m|_{i,j,k}^0 \\ K2|_{i,j,k} &= \mu_\infty|_{i,j,k} - \xi_m|_{i,j,k}^0 \end{aligned} \quad (2.14)$$

$\Psi^{Hx}|_{i,j,k}^{n-0.5}$ is called the recursive accumulator and is given by

$$\Psi^{Hx}|_{i,j,k}^{n-0.5} = \sum_{d=0}^{n-2} \Delta X_m|_{i,j,k}^d H_x|_{i,j,k}^{n-d-0.5} + \Delta \xi_m|_{i,j,k}^d \left(H_x|_{i,j,k}^{n-d-1.5} - H_x|_{i,j,k}^{n-d-0.5} \right) \quad (2.15)$$

$$\Delta X_m|_{i,j,k}^d = X_m|_{i,j,k}^d - X_m|_{i,j,k}^{d+1} \quad (2.16)$$

$$\Delta \xi_m|_{i,j,k}^d = \xi_m|_{i,j,k}^d - \xi_m|_{i,j,k}^{d+1} \quad (2.17)$$

From (2.15), it can be seen that for calculating $H_x|_{i,j,k}^{n-0.5}$, all the previous $H_x|_{i,j,k}$ field components are required. However in FDTD simulations only the latest previous field components are stored due to enormous memory requirements. This difficulty is overcome by recursively calculating $\Psi^{H_x}|_{i,j,k}^{n-0.5}$.

$$\begin{aligned} \Psi^{H_x}|_{i,j,k}^{n+0.5} &= \Psi^{H_x}|_{i,j,k}^{n-0.5} + \Delta X_m|_{i,j,k}^0 H_x|_{i,j,k}^{n+0.5} + \Delta \xi_m|_{i,j,k}^0 \left(H_x|_{i,j,k}^{n-0.5} - H_x|_{i,j,k}^{n+0.5} \right) \\ &+ \sum_{d=0}^{n-2} \left(\Delta X_m|_{i,j,k}^{d+1} - \Delta X_m|_{i,j,k}^d \right) H_x|_{i,j,k}^{n-d-0.5} \\ &+ \left(\Delta \xi_m|_{i,j,k}^{d+1} - \Delta \xi_m|_{i,j,k}^d \right) \left(H_x|_{i,j,k}^{n-d-1.5} - H_x|_{i,j,k}^{n-d-0.5} \right) \\ &= \Delta X_m|_{i,j,k}^0 H_x|_{i,j,k}^{n+0.5} + \Delta \xi_m|_{i,j,k}^0 \left(H_x|_{i,j,k}^{n-0.5} - H_x|_{i,j,k}^{n+0.5} \right) \\ &+ \sum_{d=0}^{n-2} \Delta X_m|_{i,j,k}^{d+1} H_x|_{i,j,k}^{n-d-0.5} + \Delta \xi_m|_{i,j,k}^{d+1} \left(H_x|_{i,j,k}^{n-d-1.5} - H_x|_{i,j,k}^{n-d-0.5} \right) \end{aligned} \quad (2.18)$$

For a multipole Debye model with P poles, $\chi_m(\omega)$ and $\chi_m(t)$ are given by

$$\chi_m(\omega) = \sum_{p=1}^P \frac{\Delta \mu_p}{1 + j\omega\tau_p}; \quad \chi_m(t) = \sum_{p=1}^P \frac{\Delta \mu_p e^{-\frac{t}{\tau_p}}}{\tau_p} \quad (2.19)$$

By substituting (2.19) in (2.13), expressions for $X_m|_{i,j,k}^d$ and $\xi_m|_{i,j,k}^d$ are obtained.

$$\begin{aligned} X_m|_{i,j,k}^d &= \sum_{p=1}^P X_m^p|_{i,j,k}^d \\ X_m^p|_{i,j,k}^d &= \Delta \mu_p e^{-\frac{d\Delta t}{\tau_p}} \left[1 - e^{-\frac{\Delta t}{\tau_p}} \right] \end{aligned} \quad (2.20)$$

$$\begin{aligned} \xi_m|_{i,j,k}^d &= \sum_{p=1}^P \xi_m^p|_{i,j,k}^d \\ \xi_m^p|_{i,j,k}^d &= \Delta \mu_p e^{-\frac{d\Delta t}{\tau_p}} \left[\frac{\tau_p}{\Delta t} - \left(\frac{\tau_p}{\Delta t} + 1 \right) e^{-\frac{\Delta t}{\tau_p}} \right] \end{aligned} \quad (2.21)$$

Using (2.20) and (2.21), it can be shown that

$$\begin{aligned} X_m^p|_{i,j,k}^{d+1} &= e^{-\frac{\Delta t}{\tau_p}} X_m^p|_{i,j,k}^{d+1} \\ \xi_m^p|_{i,j,k}^{d+1} &= e^{-\frac{\Delta t}{\tau_p}} \xi_m^p|_{i,j,k}^{d+1} \end{aligned} \quad (2.22)$$

$$\begin{aligned}
\Delta X_m^p |_{i,j,k}^{d+1} &= e^{-\frac{\Delta t}{\tau_p}} \Delta X_m^p |_{i,j,k}^d \\
\Delta \xi_m^p |_{i,j,k}^{d+1} &= e^{-\frac{\Delta t}{\tau_p}} \Delta \xi_m^p |_{i,j,k}^d
\end{aligned} \tag{2.23}$$

For a multipole Debye media, $\Psi^{Hx} |_{i,j,k}^{n+0.5}$ should be written as a summation of terms corresponding to each pole.

$$\begin{aligned}
\Psi^{Hx} |_{i,j,k}^{n+0.5} &= \sum_{p=1}^P \Psi^{Hx,p} |_{i,j,k}^{n+0.5} \\
\Psi^{Hx,p} |_{i,j,k}^{n+0.5} &= \Delta X_m^p |_{i,j,k}^0 H_x |_{i,j,k}^{n+0.5} + \Delta \xi_m^p |_{i,j,k}^0 \left(H_x |_{i,j,k}^{n-0.5} - H_x |_{i,j,k}^{n+0.5} \right) \\
&\quad + \sum_{d=0}^{n-2} \Delta X_m^p |_{i,j,k}^{d+1} H_x |_{i,j,k}^{n-d-0.5} + \Delta \xi_m^p |_{i,j,k}^{d+1} \left(H_x |_{i,j,k}^{n-d-1.5} - H_x |_{i,j,k}^{n-d-0.5} \right)
\end{aligned} \tag{2.24}$$

By substituting (2.23) in (2.24), a recursive expression for $\Psi^{Hx,p} |_{i,j,k}^{n+0.5}$ is obtained.

$$\begin{aligned}
\Psi^{Hx,p} |_{i,j,k}^{n+0.5} &= \Delta X_m^p |_{i,j,k}^0 H_x |_{i,j,k}^{n+0.5} + \Delta \xi_m^p |_{i,j,k}^0 \left(H_x |_{i,j,k}^{n-0.5} - H_x |_{i,j,k}^{n+0.5} \right) \\
&\quad + e^{-\frac{\Delta t}{\tau_p}} \Psi^{Hx,p} |_{i,j,k}^{n-0.5}
\end{aligned} \tag{2.25}$$

The same procedure can be repeated for the remaining 5 field components. The FDTD-PLRC update equations for electrically and magnetically dispersive multipole Debye media in 3D domain is given by (2.26)-(2.31).

$$\begin{aligned}
E_x |_{i,j,k}^{n+1} &= \left(\frac{\Delta t}{\varepsilon_o K3 |_{i,j,k}} \right) \left[\frac{H_z |_{i,j,k}^{n+0.5} - H_z |_{i,j-1,k}^{n+0.5}}{\Delta y} - \frac{H_y |_{i,j,k}^{n+0.5} - H_y |_{i,j,k-1}^{n+0.5}}{\Delta z} \right] \\
&\quad + \left(\frac{K4 |_{i,j,k}}{K3 |_{i,j,k}} \right) E_x |_{i,j,k}^n + \frac{\Psi^{Ex} |_{i,j,k}^n}{K3 |_{i,j,k}} \\
K3 |_{i,j,k} &= \varepsilon_\infty |_{i,j,k} + X_e |_{i,j,k}^0 - \xi_e |_{i,j,k}^0 + \frac{\sigma_{i,j,k} \Delta t}{2\varepsilon_o} \\
K4 |_{i,j,k} &= \varepsilon_\infty |_{i,j,k} - \xi_e |_{i,j,k}^0 - \frac{\sigma_{i,j,k} \Delta t}{2\varepsilon_o} \\
\Psi^{Ex} |_{i,j,k}^n &= \sum_{p=1}^P \Psi^{Ex,p} |_{i,j,k}^n \\
\Psi^{Ex,p} |_{i,j,k}^n &= \sum_{d=0}^{n-1} \Delta X_e^p |_{i,j,k}^d E_x |_{i,j,k}^{n-d} + \Delta \xi_e^p |_{i,j,k}^d \left(E_x |_{i,j,k}^{n-d-1} - E_x |_{i,j,k}^{n-d} \right) \\
\Psi^{Ex,p} |_{i,j,k}^{n+1} &= \Delta X_e^p |_{i,j,k}^0 E_x |_{i,j,k}^{n+1} + \Delta \xi_e^p |_{i,j,k}^0 \left(E_x |_{i,j,k}^n - E_x |_{i,j,k}^{n+1} \right) \\
&\quad + e^{-\frac{\Delta t}{\tau_p}} \Psi^{Ex,p} |_{i,j,k}^n
\end{aligned} \tag{2.26}$$

$$\begin{aligned}
E_y|_{i,j,k}^{n+1} &= \left(\frac{\Delta t}{\varepsilon_o K3|_{i,j,k}} \right) \left[\frac{H_x|_{i,j,k}^{n+0.5} - H_x|_{i,j,k-1}^{n+0.5}}{\Delta z} - \frac{H_z|_{i,j,k}^{n+0.5} - H_z|_{i-1,j,k}^{n+0.5}}{\Delta x} \right] \\
&+ \left(\frac{K4|_{i,j,k}}{K3|_{i,j,k}} \right) E_y|_{i,j,k}^n + \frac{\Psi^{E_y}|_{i,j,k}^n}{K3|_{i,j,k}} \\
\Psi^{E_y}|_{i,j,k}^n &= \sum_{p=1}^P \Psi^{E_y,p}|_{i,j,k}^n \\
\Psi^{E_y,p}|_{i,j,k}^n &= \sum_{d=0}^{n-1} \Delta X_e^p|_{i,j,k}^d E_y|_{i,j,k}^{n-d} + \Delta \xi_e^p|_{i,j,k}^d \left(E_y|_{i,j,k}^{n-d-1} - E_y|_{i,j,k}^{n-d} \right) \\
\Psi^{E_y,p}|_{i,j,k}^{n+1} &= \Delta X_e^p|_{i,j,k}^0 E_y|_{i,j,k}^{n+1} + \Delta \xi_e^p|_{i,j,k}^0 \left(E_y|_{i,j,k}^n - E_y|_{i,j,k}^{n+1} \right) \\
&+ e^{-\frac{\Delta t}{\tau_p}} \Psi^{E_y,p}|_{i,j,k}^n
\end{aligned} \tag{2.27}$$

$$\begin{aligned}
E_z|_{i,j,k}^{n+1} &= \left(\frac{\Delta t}{\varepsilon_o K3|_{i,j,k}} \right) \left[\frac{H_y|_{i,j,k}^{n+0.5} - H_y|_{i-1,j,k}^{n+0.5}}{\Delta x} - \frac{H_x|_{i,j,k}^{n+0.5} - H_x|_{i,j-1,k}^{n+0.5}}{\Delta y} \right] \\
&+ \left(\frac{K4|_{i,j,k}}{K3|_{i,j,k}} \right) E_z|_{i,j,k}^n + \frac{\Psi^{E_z}|_{i,j,k}^n}{K3|_{i,j,k}} \\
\Psi^{E_z}|_{i,j,k}^n &= \sum_{p=1}^P \Psi^{E_z,p}|_{i,j,k}^n \\
\Psi^{E_z,p}|_{i,j,k}^n &= \sum_{d=0}^{n-1} \Delta X_e^p|_{i,j,k}^d E_z|_{i,j,k}^{n-d} + \Delta \xi_e^p|_{i,j,k}^d \left(E_z|_{i,j,k}^{n-d-1} - E_z|_{i,j,k}^{n-d} \right) \\
\Psi^{E_z,p}|_{i,j,k}^{n+1} &= \Delta X_e^p|_{i,j,k}^0 E_z|_{i,j,k}^{n+1} + \Delta \xi_e^p|_{i,j,k}^0 \left(E_z|_{i,j,k}^n - E_z|_{i,j,k}^{n+1} \right) \\
&+ e^{-\frac{\Delta t}{\tau_p}} \Psi^{E_z,p}|_{i,j,k}^n
\end{aligned} \tag{2.28}$$

$$\begin{aligned}
H_x|_{i,j,k}^{n+0.5} &= \left(\frac{\Delta t}{\mu_o K1|_{i,j,k}} \right) \left[\frac{E_y|_{i,j,k+1}^n - E_y|_{i,j,k}^n}{\Delta z} - \frac{E_z|_{i,j+1,k}^n - E_z|_{i,j,k}^n}{\Delta y} \right] \\
&+ \left(\frac{K2|_{i,j,k}}{K1|_{i,j,k}} \right) H_x|_{i,j,k}^{n-0.5} + \frac{\Psi^{H_x}|_{i,j,k}^{n-0.5}}{K1|_{i,j,k}} \\
K1|_{i,j,k} &= \mu_\infty|_{i,j,k} + X_m|_{i,j,k}^0 - \xi_m|_{i,j,k}^0 \\
K2|_{i,j,k} &= \mu_\infty|_{i,j,k} - \xi_m|_{i,j,k}^0 \\
\Psi^{H_x}|_{i,j,k}^{n-0.5} &= \sum_{p=1}^P \Psi^{H_x,p}|_{i,j,k}^{n-0.5} \\
\Psi^{H_x,p}|_{i,j,k}^{n-0.5} &= \sum_{d=0}^{n-2} \Delta X_m^p|_{i,j,k}^d H_x|_{i,j,k}^{n-d-0.5} + \Delta \xi_m^p|_{i,j,k}^d \left(H_x|_{i,j,k}^{n-d-1.5} - H_x|_{i,j,k}^{n-d-0.5} \right) \\
\Psi^{H_x,p}|_{i,j,k}^{n+0.5} &= \Delta X_m^p|_{i,j,k}^0 H_x|_{i,j,k}^{n+0.5} + \Delta \xi_m^p|_{i,j,k}^0 \left(H_x|_{i,j,k}^{n-0.5} - H_x|_{i,j,k}^{n+0.5} \right) \\
&+ e^{-\frac{\Delta t}{\tau_p}} \Psi^{H_x,p}|_{i,j,k}^{n-0.5}
\end{aligned} \tag{2.29}$$

$$\begin{aligned}
H_y|_{i,j,k}^{n+0.5} &= \left(\frac{\Delta t}{\mu_o K1|_{i,j,k}} \right) \left[\frac{E_z|_{i+1,j,k}^n - E_z|_{i,j,k}^n}{\Delta x} - \frac{E_x|_{i,j,k+1}^n - E_x|_{i,j,k}^n}{\Delta z} \right] \\
&+ \left(\frac{K2|_{i,j,k}}{K1|_{i,j,k}} \right) H_y|_{i,j,k}^{n-0.5} + \frac{\Psi^{Hy}|_{i,j,k}^{n-0.5}}{K1|_{i,j,k}} \\
\Psi^{Hy}|_{i,j,k}^{n-0.5} &= \sum_{p=1}^P \Psi^{Hy,p}|_{i,j,k}^{n-0.5} \\
\Psi^{Hy,p}|_{i,j,k}^{n-0.5} &= \sum_{d=0}^{n-2} \Delta X_m^p|_{i,j,k}^d H_y|_{i,j,k}^{n-d-0.5} + \Delta \xi_m^p|_{i,j,k}^d (H_y|_{i,j,k}^{n-d-1.5} - H_y|_{i,j,k}^{n-d-0.5}) \\
\Psi^{Hy,p}|_{i,j,k}^{n+0.5} &= \Delta X_m^p|_{i,j,k}^0 H_y|_{i,j,k}^{n+0.5} + \Delta \xi_m^p|_{i,j,k}^0 (H_y|_{i,j,k}^{n-0.5} - H_y|_{i,j,k}^{n+0.5}) \\
&+ e^{-\frac{\Delta t}{\tau_p}} \Psi^{Hy,p}|_{i,j,k}^{n-0.5}
\end{aligned} \tag{2.30}$$

$$\begin{aligned}
H_z|_{i,j,k}^{n+0.5} &= \left(\frac{\Delta t}{\mu_o K1|_{i,j,k}} \right) \left[\frac{E_x|_{i,j+1,k}^n - E_x|_{i,j,k}^n}{\Delta y} - \frac{E_y|_{i+1,j,k}^n - E_y|_{i,j,k}^n}{\Delta x} \right] \\
&+ \left(\frac{K2|_{i,j,k}}{K1|_{i,j,k}} \right) H_z|_{i,j,k}^{n-0.5} + \frac{\Psi^{Hz}|_{i,j,k}^{n-0.5}}{K1|_{i,j,k}} \\
\Psi^{Hz}|_{i,j,k}^{n-0.5} &= \sum_{p=1}^P \Psi^{Hz,p}|_{i,j,k}^{n-0.5} \\
\Psi^{Hz,p}|_{i,j,k}^{n-0.5} &= \sum_{d=0}^{n-2} \Delta X_m^p|_{i,j,k}^d H_z|_{i,j,k}^{n-d-0.5} + \Delta \xi_m^p|_{i,j,k}^d (H_z|_{i,j,k}^{n-d-1.5} - H_z|_{i,j,k}^{n-d-0.5}) \\
\Psi^{Hz,p}|_{i,j,k}^{n+0.5} &= \Delta X_m^p|_{i,j,k}^0 H_z|_{i,j,k}^{n+0.5} + \Delta \xi_m^p|_{i,j,k}^0 (H_z|_{i,j,k}^{n-0.5} - H_z|_{i,j,k}^{n+0.5}) \\
&+ e^{-\frac{\Delta t}{\tau_p}} \Psi^{Hz,p}|_{i,j,k}^{n-0.5}
\end{aligned} \tag{2.31}$$

2.2 Uniaxial Perfectly Matched Layer

The Uniaxial Perfectly Matched Layer (UPML) is an uniaxial anisotropic media that is capable of absorbing electromagnetic waves incident on it with minimal reflections. The incident wave can be of arbitrary frequency, incident angle and polarization. The derivation of UPML-FDTD update equations and its software implementation can be found in [18, 15]. The difference in this work is that the UPML absorbing slabs are placed only on the y - axis boundaries. The

UPML update equations for the y -axis slabs are given by (2.32)-(2.43).

$$\begin{aligned}
D_x|_{i+0.5,j,k}^{n+1} &= C1D_x.D_x|_{i+0.5,j,k}^n + C2D_x \left(\frac{H_z|_{i+0.5,j+0.5,k}^{n+0.5} - H_z|_{i+0.5,j-0.5,k}^{n+0.5}}{\Delta y} \right. \\
&\quad \left. - \frac{H_y|_{i+0.5,j,k+0.5}^{n+0.5} - H_y|_{i+0.5,j,k-0.5}^{n+0.5}}{\Delta z} \right) \\
C1D_x &= \frac{2\varepsilon_o - \sigma_y \Delta t}{2\varepsilon_o + \sigma_y \Delta t}; \quad C2D_x = \frac{2\varepsilon_o \Delta t}{2\varepsilon_o + \sigma_y \Delta t}
\end{aligned} \tag{2.32}$$

$$\begin{aligned}
D_y|_{i,j+0.5,k}^{n+1} &= D_y|_{i,j+0.5,k}^n + \Delta t \left(\frac{H_x|_{i,j+0.5,k+0.5}^{n+0.5} - H_x|_{i,j+0.5,k-0.5}^{n+0.5}}{\Delta z} \right. \\
&\quad \left. - \frac{H_z|_{i+0.5,j+0.5,k}^{n+0.5} - H_z|_{i-0.5,j+0.5,k}^{n+0.5}}{\Delta x} \right)
\end{aligned} \tag{2.33}$$

$$\begin{aligned}
D_z|_{i,j,k+0.5}^{n+1} &= D_z|_{i,j,k+0.5}^n + \Delta t \left(\frac{H_y|_{i+0.5,j,k+0.5}^{n+0.5} - H_y|_{i-0.5,j,k+0.5}^{n+0.5}}{\Delta x} \right. \\
&\quad \left. - \frac{H_x|_{i,j+0.5,k+0.5}^{n+0.5} - H_x|_{i,j-0.5,k+0.5}^{n+0.5}}{\Delta y} \right)
\end{aligned} \tag{2.34}$$

$$E_x|_{i+0.5,j,k}^{n+1} = E_x|_{i+0.5,j,k}^n + \frac{D_x|_{i+0.5,j,k}^{n+1} - D_x|_{i+0.5,j,k}^n}{\varepsilon_o} \tag{2.35}$$

$$\begin{aligned}
E_y|_{i,j+0.5,k}^{n+1} &= E_y|_{i,j+0.5,k}^n + C2E_y.D_y|_{i,j+0.5,k}^{n+1} - C3E_y.D_y|_{i,j+0.5,k}^n \\
C2E_y &= \frac{2\varepsilon_o + \sigma_y \Delta t}{2\varepsilon_o^2}; \quad C3E_y = \frac{2\varepsilon_o - \sigma_y \Delta t}{2\varepsilon_o^2}
\end{aligned} \tag{2.36}$$

$$\begin{aligned}
E_z|_{i,j,k+0.5}^{n+1} &= C1E_z.E_z|_{i,j,k+0.5}^n + C2E_z.(D_z|_{i,j,k+0.5}^{n+1} - D_z|_{i,j,k+0.5}^n) \\
C1E_z &= \frac{2\varepsilon_o - \sigma_y \Delta t}{2\varepsilon_o + \sigma_y \Delta t}; \quad C2E_z = \frac{2\varepsilon_o}{\varepsilon_o(2\varepsilon_o + \sigma_y \Delta t)}
\end{aligned} \tag{2.37}$$

$$\begin{aligned}
B_x|_{i,j+0.5,k+0.5}^{n+1.5} &= C1B_x.B_x|_{i,j+0.5,k+0.5}^{n+0.5} - C2B_x. \left(\frac{E_z|_{i,j+1,k+0.5}^{n+1} - E_z|_{i,j,k+0.5}^{n+1}}{\Delta y} \right. \\
&\quad \left. - \frac{E_y|_{i,j+0.5,k+1}^{n+1} - E_y|_{i,j+0.5,k}^{n+1}}{\Delta z} \right) \\
C1B_x &= \frac{2\varepsilon_o - \sigma_y \Delta t}{2\varepsilon_o + \sigma_y \Delta t}; \quad C2B_x = \frac{2\varepsilon_o \Delta t}{2\varepsilon_o + \sigma_y \Delta t}
\end{aligned} \tag{2.38}$$

$$B_y|_{i+0.5,j,k+0.5}^{n+1.5} = B_y|_{i+0.5,j,k+0.5}^{n+0.5} - \Delta t \left(\frac{E_x|_{i+0.5,j,k+1}^{n+1} - E_x|_{i+0.5,j,k}^{n+1}}{\Delta z} - \frac{E_z|_{i+1,j,k+0.5}^{n+1} - E_z|_{i,j,k+0.5}^{n+1}}{\Delta x} \right) \quad (2.39)$$

$$B_z|_{i+0.5,j+0.5,k}^{n+1.5} = B_z|_{i+0.5,j+0.5,k}^{n+0.5} - \Delta t \cdot \left(\frac{E_y|_{i+1,j+0.5,k}^{n+1} - E_y|_{i,j+0.5,k}^{n+1}}{\Delta x} - \frac{E_x|_{i+0.5,j+1,k}^{n+1} - E_x|_{i+0.5,j,k}^{n+1}}{\Delta y} \right) \quad (2.40)$$

$$H_x|_{i,j+0.5,k+0.5}^{n+1.5} = H_x|_{i,j+0.5,k+0.5}^{n+0.5} + \frac{1}{\mu_o} \left(B_x|_{i,j+0.5,k+0.5}^{n+1.5} - B_x|_{i,j+0.5,k+0.5}^{n+0.5} \right) \quad (2.41)$$

$$H_y|_{i+0.5,j,k+0.5}^{n+1.5} = H_y|_{i+0.5,j,k+0.5}^{n+0.5} + C2Hy \cdot B_y|_{i+0.5,j,k+0.5}^{n+1.5} - C3Hy \cdot B_y|_{i+0.5,j,k+0.5}^{n+0.5} \\ C2Hy = \frac{2\varepsilon_o + \sigma_y \Delta t}{2\mu_o \varepsilon_o} ; C3Hy = \frac{2\varepsilon_o - \sigma_y \Delta t}{2\mu_o \varepsilon_o} \quad (2.42)$$

$$H_z|_{i+0.5,j+0.5,k}^{n+1.5} = C1Hz \cdot H_z|_{i+0.5,j+0.5,k}^{n+0.5} + C2Hz \cdot \left(B_z|_{i+0.5,j+0.5,k}^{n+1.5} - B_z|_{i+0.5,j+0.5,k}^{n+0.5} \right) \\ C1Hz = \frac{2\varepsilon_o - \sigma_y \Delta t}{2\varepsilon_o + \sigma_y \Delta t} ; C2Hz = \frac{2\varepsilon_o}{\mu_o(2\varepsilon_o + \sigma_y \Delta t)} \quad (2.43)$$

Polynomial grading is used to define σ_y in the above equations and is given by

$$\sigma_y = \sigma_o(y/d)^m \quad (2.44)$$

where $m = 3.5$, $\sigma_o = \frac{16(m+1)}{2\eta d}$ and d is the length of the PML. y is the distance of the field component from the problem space UPML boundary. For instance, when using (2.44) in calculating $C2Ey$, y should be the distance of E_y component from problem space UPML boundary. In this work, the number of Yee cells in each UPML slab is 12 (i.e. $d = 12\Delta y$). The UPML-main grid interface has to be carefully programmed. These two regions have two different formulations. The main grid PLRC field components are \vec{E}, \vec{H} , while the field components in the UPML regions are $\vec{E}, \vec{H}, \vec{B}, \vec{D}$.

2.3 Boundary conditions

Periodic boundary conditions (PBC) are imposed on the x and z boundaries to simulate a 2D periodic array of pyramidal structures. In this work, incident plane wave is assumed to be normal

to the structure (i.e. wave vector is parallel to y -axis). This simplifies the implementation of the PBC tremendously. PBC for obliquely incident plane wave requires a more complex formulation known as the Split Field Method (SFM) [19]. SFM combined with dispersive FDTD can be even more complex. It is presumed that the immediate results obtained from a normal incidence case outweighs oblique incidence case. Therefore normal incidence PBC is preferred in this work. The FDTD unit cell bounded by PBC's and UPML is shown in Fig. 2.2. In that figure, the red object is the scatterer, which is the coated pyramid in our case. PLRC update equations are used in the problem space. Symmetry and antisymmetry boundary conditions can further be used in our

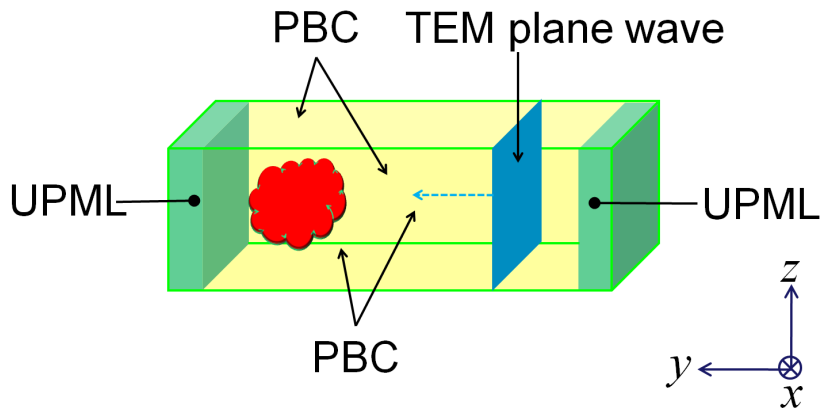


Figure 2.2: FDTD unit cell

problem to reduce the computational burden by a factor of 4 [20]. These conditions are shown in Fig. 2.3. Fig. 2.3 is the front view of the pyramidal structure, where the dashed line represent the pyramidal edges. In the case of normal incidence on a doubly periodic structure each quadrant is indistinguishable. For an incident wave linearly polarized along z direction, PEC and PMC boundaries as shown in Fig. 2.3 is used to simulate the pyramidal quadrant. We note that this boundary condition can only be applied for the case of a normally incident plane wave.

2.4 Parallel computation

FDTD simulation of this particular problem is computationally expensive for two reasons: 1) the structure is electrically large, thus requiring a large number of Yee cells for accurate simulation.

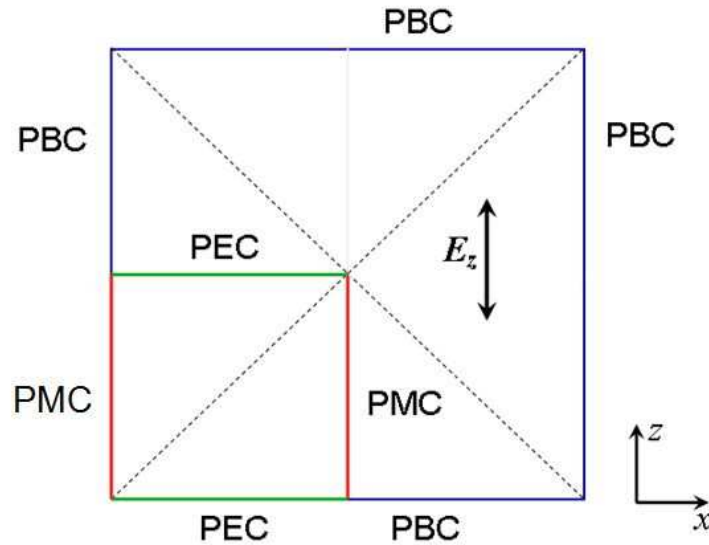


Figure 2.3: Symmetry/Antisymmetry boundary conditions on x, z boundaries

For instance, the nominal calibration target is a pyramid with base equal to $0.5''$ and height $2''$. In addition to this, there is a 2 mm coating and the reflectivity spectrum is required at frequency as high as 200 GHz. 2) memory usage is considerably increased due to the dispersive formulation which results in a large number of precomputed coefficients. This is more pronounced in this problem where material is both magnetically and electrically dispersive. In order to overcome these problems the code was parallelized using a one dimensional Domain Decomposition (DDM) technique [21]. The FDTD computational domain is divided into slabs along the y -axis direction as shown in Fig. 2.4. Each slab was handled on a separate processor. The surface fields at the interface between two slabs are passed through adjacent processors using Message Passing Interface (MPI) commands [22, 23]. The code was developed and executed on 200 cores of NOAA HPCS (High Performance Computing System) distributed computing system. A simple 1D DDM applied to 1D FDTD is depicted in Fig. 2.5. At time instant n , the E_x field components need to be calculated. E_x at y_3 belongs to core j and E_x at y_4 belongs to core $j + 1$. For core j to calculate the E_z at position y_3 , core $j - 1$ passes the H_z at position y_1 and time $n - 0.5$ to core j . Similarly, core j passes H_z value at position y_2 and time $n - 0.5$ to core $j + 1$. At time instant $n + 0.5$, the H_z field components

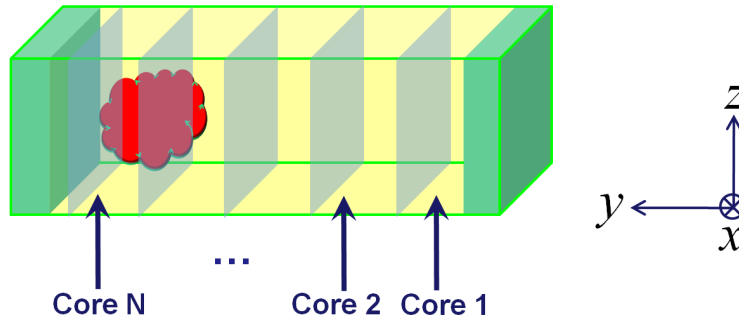


Figure 2.4: 1D Domain Decomposition for parallel computation

need to be updated. In order to calculate H_z at y_1 , core j passes the value of E_z at position y_3 and time n to core $j - 1$. Similarly, core $j + 1$ passes the value of E_z at position y_4 and time n to core j . A C++ code of roughly 5000 lines was developed with the above mentioned formulations and

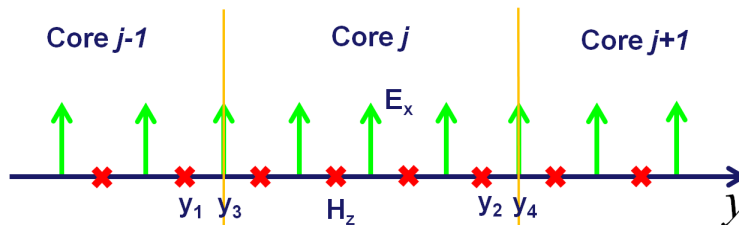


Figure 2.5: 1D Domain Decomposition in the case of 1D FDTD

boundary conditions. The main code (excluding postprocessing codes, library files etc.) is listed in appendix A.

2.5 Microwave characterization of radar absorbing material

The microwave absorbent material used in radiometer calibration references is usually a ferrous-doped epoxy resin composite. These materials consist of ferrous inclusions such as carbonyl iron powder in a dielectric epoxy resin matrix. Commonly used material designations are MF-110, MF-112, MF-114, MF-116 and MF-117 [24]. Since FDTD is a time domain method, the complex permittivity and permeability (along with DC conductivity) of these materials needs to be known as a function of frequency along the entire frequency axis. Inverse Fourier transformation can

then be applied to the frequency domain data to obtain the time domain electric and magnetic susceptibility functions, which are needed in FDTD modeling. The complex permittivity and permeability of microwave absorbent materials in the range 8 GHz to 26 GHz is reported in [24]. Waveguide based Transmission/Reflection (T/R) method is used to measure these quantities. In this work, we have used these measurements for material characterization.

The time domain electric and magnetic susceptibility functions are the impulse responses for the linear time-invariant system with electric/magnetic field intensities as input and polarization as the output. Hence the time domain susceptibility functions have to be causal. In order to ensure causality in the time domain, the transform in the frequency domain, i.e. complex susceptibilities, has to satisfy the Kramers - Kronig relation [25]. In short, the real and imaginary parts of the complex susceptibilities are required to be Hilbert-transform pairs. Moreover the complex susceptibilities should be Hermitian functions in order to assure a real time domain signal. Debye functions satisfy the above mentioned conditions and can be used for approximating frequency characteristics of composites for time domain electromagnetic modeling. The measured data is curve fitted to a series of Debye functions. The curve fitting procedure can be carried out using global optimization techniques such as Genetic Algorithm (GA) or simulated annealing [26].

GA is a robust, stochastic optimization method developed using the concepts of natural selection and evolution. GA is particularly suited for solving complex optimization problems, where traditional optimization methods fail [27]. In GA, a set of trial solutions termed as population is evaluated using a suitable fitness function. Each potential solution in the population is called a chromosome, which essentially consists of a string of variables (or genes). The fitness function will be a function of these variables. This function will evaluate the fitness of each solution in the current generation of population. The chromosomes for the next generation population are selected from the fittest current generation chromosomes. The algorithm is continued until the fitness function of a solution is below some prescribed value. The complex permittivity can be expressed as a series

of Debye terms as

$$\varepsilon_r(\omega) = \varepsilon_\infty + \sum_{i=1}^N \frac{\Delta\varepsilon_i}{1 + j\omega\tau_i} \quad (2.45)$$

where N denotes the number of Debye poles and $\Delta\varepsilon_i$, τ_i represent the parameter for the i^{th} pole.

The fitness function $J(\varepsilon_\infty, \{\Delta\varepsilon_i\}_{i=1}^N, \{\tau_i\}_{i=1}^N)$ can be written as

$$J(\varepsilon_\infty, \{\Delta\varepsilon_i\}_{i=1}^N, \{\tau_i\}_{i=1}^N) = \sum_{m=1}^M \left\| \varepsilon_r^{meas}(\omega_m) - \varepsilon_\infty - \sum_{i=1}^N \frac{\Delta\varepsilon_i}{1 + j\omega_m\tau_i} \right\|^2 \quad (2.46)$$

where M is the total number of measurement points, $\varepsilon_r^{meas}(\omega_m)$ is the measured value of complex relative permittivity at the frequency ω_m . The value of M can be increased by using spline interpolation between measured frequency points. MATLAB[®] GA toolbox can be used to perform GA optimization with the fitness function given by (2.46). The GA code for complex permittivity fitting is listed in appendix B. The initial values for the Debye parameters should be selected reasonably for faster convergence. For instance, the relaxation time τ_i can be bounded in the interval $[10^{-12}, 10^{-4}]$. A 5 pole Debye fit of the complex permittivity and permeability of MF112 and MF110 is shown in Figs. 2.6, 2.7 and Figs. 2.8, 2.9 respectively. The Debye parameters for MF112, MF114 and MF110 are listed in tables 2.1, 2.2 and 2.3 respectively. It should be remarked that the values of Debye coefficients listed in these tables are just mathematical quantities and do not have any physical significance. Moreover a comparison of FDTD results using a 4-pole and 5-pole Debye fit can be seen in Fig. 2.10. This was done a for 0.5'' base, 1:1 pyramid with 1 mm of MF112 coating. From the figure, it can be seen that there is not much difference between the two results, even though the 4 pole and 5 pole Debye fit parameters vary significantly.

2.6 Numerical validation

The numerical accuracy of the developed code was validated by estimating the transmission coefficient of an infinite slab of MF112 material. The slab is infinite along the x, z - directions and has a finite width d (m) along the y -direction. If a plane TEM wave is incident normally on one

side of the slab, the ratio of the magnitude of the transmitted wave (wave on the other side of the slab) to incident wave as a function of frequency is the transmission coefficient, $|S_{21}(f)|$. The analytical expression for $|S_{21}(f)|$ can be shown to be

$$\begin{aligned}
 |S_{21}(f)| &= \left| \frac{4\eta_o\eta_s(f)}{e^{+jk_s d}[\eta_s(f) + \eta_o]^2 - e^{-jk_s d}[\eta_s(f) - \eta_o]^2} \right| \\
 \eta_s(f) &= \eta_o \sqrt{\frac{\mu_{rs}(f)}{\epsilon_{rs}(f)}} \\
 k_s(f) &= \frac{2\pi f}{c} \sqrt{\epsilon_{rs}(f)\mu_{rs}(f)}
 \end{aligned} \tag{2.47}$$

where η_o is the intrinsic impedance of free space and $\epsilon_{rs}(f), \mu_{rs}(f)$ are the relative complex permittivity and permeability of the slab medium. The 5 pole Debye series fit was used for MF112 material in these simulations. The simulation was carried out by exciting a plane TEM wave with a Gaussian time signature. In the first step of the simulation, the incident field (i.e. electric field) is sampled at a suitable observation plane without the presence of an infinite slab. The transmitted field is sampled at this same observation point. A Fast Fourier Transform (FFT) is applied to these time series to obtain the frequency domain electric field intensity. The ratio of the transmitted electric field intensity to the incident field in the frequency domain gives $S_{21}(f)$. Transmission spectrum of a 3.1 mm MF112 slab obtained by the code is compared with analytical results in Fig. 2.11.

Table 2.1: 5 pole Debye parameters for MF-112

$\epsilon_\infty=5.36759\text{e}+000$		$\mu_\infty=6.09930\text{e}-001$	
$\Delta\epsilon_i$	τ_i	$\Delta\mu_i$	τ_i
2.49845e-010	9.76769e-004	1.72594e-009	9.79427e-004
7.50170e-009	9.93680e-004	7.90230e-001	8.30554e-012
2.87363e-009	9.95832e-004	1.57528e-009	8.38797e-004
3.19969e-001	1.88552e-011	1.01232e-009	5.37175e-004
1.94940e-008	8.74442e-004	1.53336e-009	9.29023e-004

Table 2.2: 5 pole Debye parameters for MF-114

$\varepsilon_\infty=1.00102e+001$		$\mu_\infty=6.66467e-001$	
$\Delta\varepsilon_i$	τ_i	$\Delta\mu_i$	τ_i
2.77091e+001	2.71277e-009	2.98554e+001	1.57767e-008
2.99984e+001	8.59746e-008	1.44034e+000	1.38109e-011
2.99384e+001	2.81365e-008	2.98575e+001	1.78864e-008
2.99613e+001	5.71671e-008	2.99943e+001	8.69623e-009
2.99977e+001	1.44155e-007	2.99350e+001	8.78818e-009

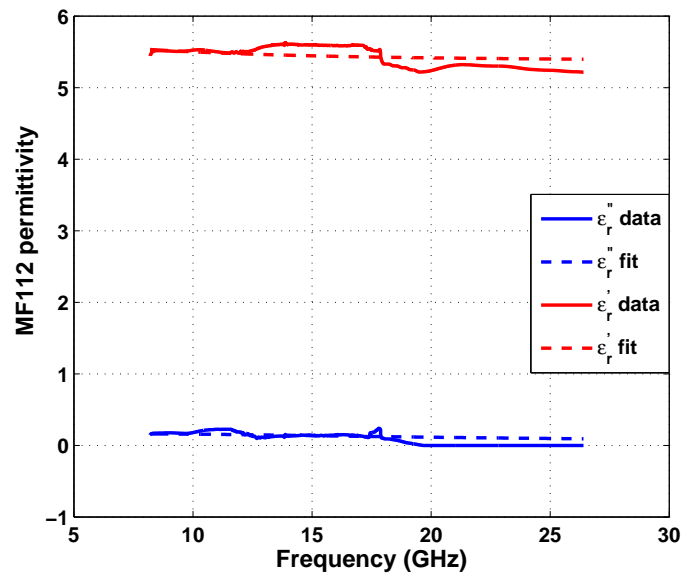


Figure 2.6: MF112 permittivity : Measured data and 5 pole Debye fit

Table 2.3: 5 pole Debye parameters for MF-110

$\varepsilon_\infty=3.91208e+000$		$\mu_\infty=8.70924e-001$	
$\Delta\varepsilon_i$	τ_i	$\Delta\mu_i$	τ_i
3.37157e-010	9.77380e-004	1.99949e+001	1.55559e-008
2.88869e-010	9.73578e-004	7.16149e-004	9.99900e-004
1.21663e-010	6.78805e-004	2.46327e-001	9.86915e-004
4.05910e-010	9.31808e-004	6.65351e-002	9.99272e-004
1.63012e-001	1.99686e-011	3.27121e-001	7.96570e-012

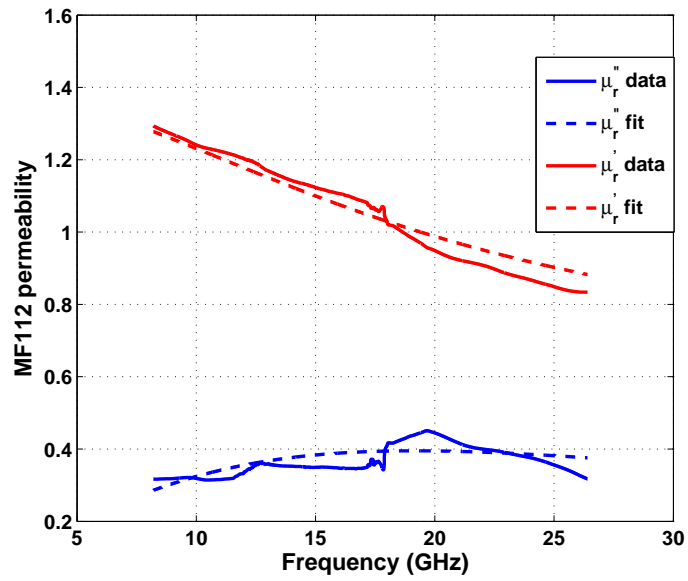


Figure 2.7: MF112 permeability : Measured data and 5 pole Debye fit

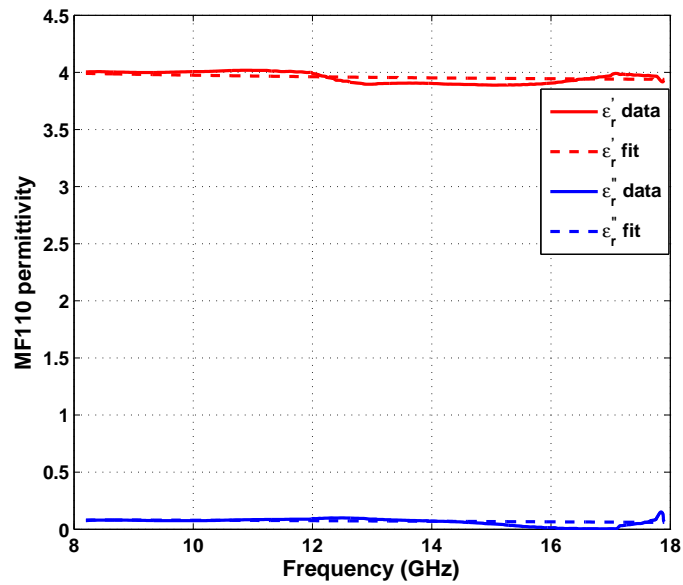


Figure 2.8: MF110 permittivity : Measured data and 5 pole Debye fit

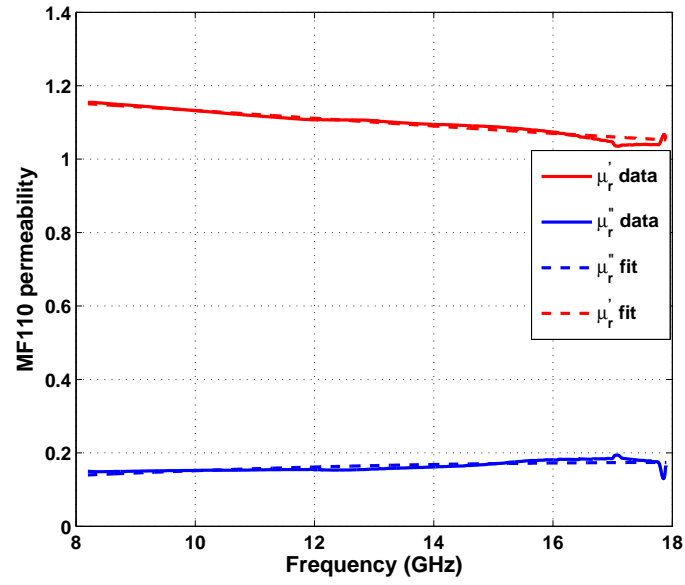


Figure 2.9: MF110 permeability: Measured data and 5 pole Debye fit

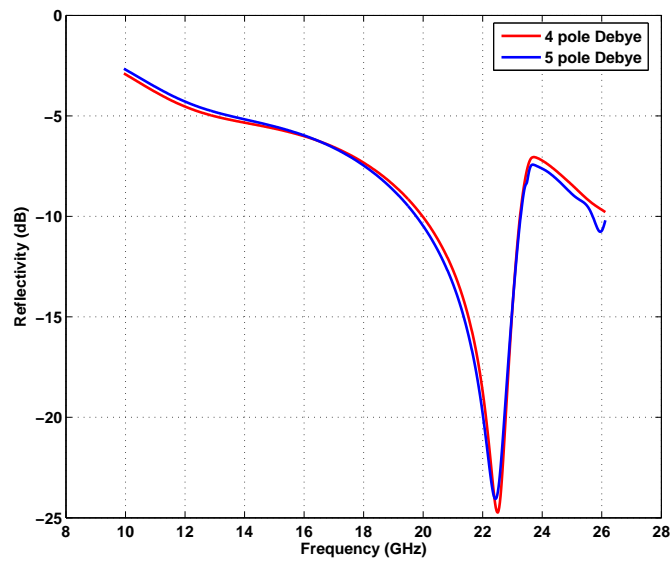


Figure 2.10: Reflectivity spectrum of 0.5'' base, 1:1 pyramid with 1 mm MF112 coating

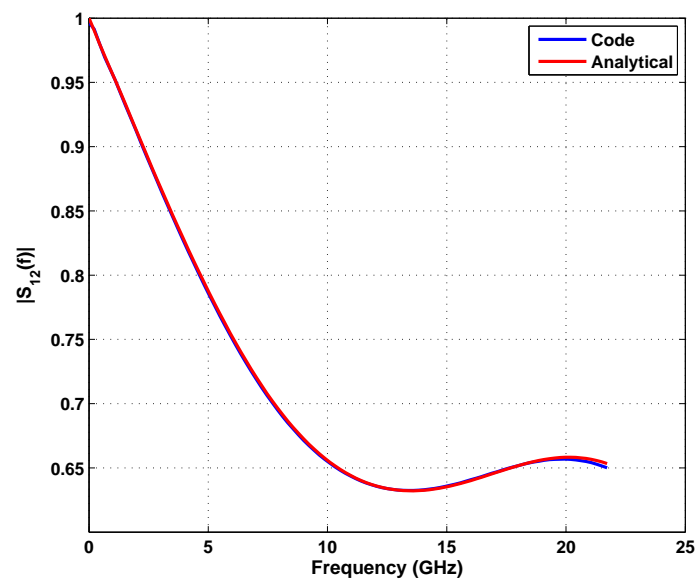


Figure 2.11: Numerical validation of the code

Chapter 3

Results and Discussion

This chapter contains the results obtained from the FDTD code. Results are validated using commercial HFSS software and custom Geometric Optics (GO) code. Commonly used radiometer calibration references, or targets, are finite arrays of square metallic pyramids with a thin coating of microwave absorbing material. Such structures are designed to absorb incident plane waves across a broad range of frequencies, although in practice appear electrically flat and specular at low enough frequencies where the depth $h \ll \lambda$ and exhibit geometrical optics reflection at high enough frequencies where the period $\Lambda \gg \lambda$. Depending on the ratio of height to depth, coating thickness, and specific geometry of the pyramids a broad absorbing band in between these extremes can be tailored. The target geometries studied include square pyramids, circular pyramids and truncated square pyramids. The cross-sectional view of either the square or circular pyramid is given in Fig. 3.1. In order to assess the impact of material property variations on the emissivity spectrum a means of determining the uncertainty on the calculated target reflectivity is developed based on a procedure using the unscented transform [28]. Using this procedure the propagation of error from material parameters is efficiently tracked through the model to the resulting reflectivity product. Stability and convergence issues are also discussed.

3.1 Total reflectivity formulation

Consider a TEM plane wave propagating along $+y$ direction incident on the pyramidal structure. The wave is linearly polarized along z -direction. In order to get the reflectivity, two simu-

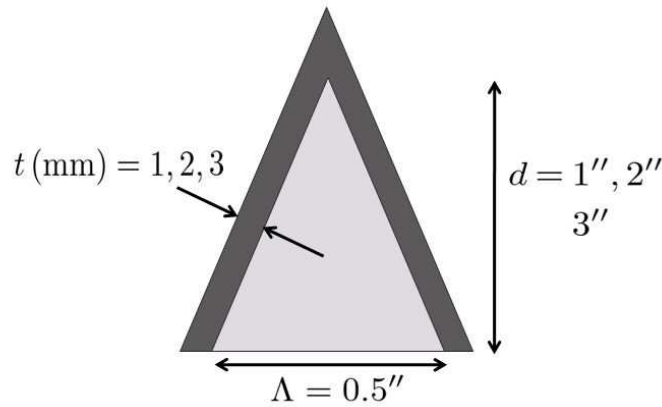


Figure 3.1: 2D cross section of calibration target

lations are performed : incident field simulation (without the scattering structure) and total field simulation (with the scattering structure). The incident electric field intensity can be denoted by $\mathcal{E}_z^i(y; t) = g(t - \frac{y}{c})$, where $g(t - \frac{y}{c})$ represents a transient travelling wave propagating in $+y$ direction. In our study, we used a modulated Gaussian pulse excitation. However $g(\cdot)$ can be any other energy signal. Let $y = 0$ be the observation plane, i.e. the plane where the field values are sampled. Therefore the sampled field is $\mathcal{E}_z^i(y = 0; t) = g(t)$. By defining the Fourier transform, $FT\{g(t)\} \equiv G(f) = |G(f)|e^{j\theta(f)}$, the electric field intensity vector can be represented as

$$\mathcal{E}_z^i(y; t) = 2 \int_0^\infty |G(f)| \cos\left(2\pi ft - 2\pi f \frac{y}{c} + \theta(f)\right) df \quad (3.1)$$

In deriving (22), we have used the time shift property of Fourier transforms, and Hermitian conjugate symmetry of Fourier transforms of real valued signals. The total energy incident normally on an area $\frac{\Lambda^2}{4}$ (m^2), E^i (J) is related to the incident time instantaneous power density $\mathcal{S}_y^i(y = 0; t) = \frac{1}{\eta_o} \mathcal{E}_z^{i2}(y = 0; t)$ (Wm^{-2}) by

$$E^i = \frac{\Lambda^2}{4} \int_{-\infty}^\infty \mathcal{S}_y^i(y = 0; t) dt = \frac{\Lambda^2}{2\eta_o} \int_0^\infty |G(f)|^2 df \quad (3.2)$$

where Λ (m) is the periodicity of the pyramidal base in either x or z direction. It should be noted that in the incident field simulation, the power density is independent of x, z directions.

In the total field simulation, the simulation is carried out with exact settings as that of incident field simulation but with the presence of the scattering structure. The scattered field $\mathcal{E}_x^s, \mathcal{E}_z^s, \mathcal{H}_x^s, \mathcal{H}_z^s$ is obtained by subtracting the incident field from the total field. The total energy scattered back through the area $\frac{\Lambda^2}{4}$, E^s is given by,

$$E^s = - \int_0^{\frac{\Lambda}{2}} \int_0^{\frac{\Lambda}{2}} \int_{-\infty}^{\infty} \mathcal{E}_z^s(x, z; t) \mathcal{H}_x^s(x, z; t) |_{y=0} - \mathcal{E}_x^s(x, z; t) \mathcal{H}_z^s(x, z; t) |_{y=0} dt dx dz \quad (3.3)$$

After some mathematical manipulations E^s can be expressed as,

$$E^s = \int_0^{\infty} E_f^s(f) df$$

$$E_f^s = 2 \int_0^{\frac{\Lambda}{2}} \int_0^{\frac{\Lambda}{2}} \text{Re}\{E_x^s(x, z; f) H_z^{s*}(x, z; f)\} - \text{Re}\{E_z^s(x, z; f) H_x^{s*}(x, z; f)\} dx dz \quad (3.4)$$

The ratio of the reflected energy to the incident energy as a function of frequency, reflectivity $r(f)$ can be obtained as,

$$r(f) = \frac{E_f^s(f)}{\frac{\Lambda^2}{2\eta_0} |G(f)|^2} \quad (3.5)$$

3.2 Reflectivity spectrum of square pyramid array

The reflectivity spectrum of square pyramidal targets in the frequency range [6, 26] GHz is shown in Fig. 3.2. The pyramid base is $\Lambda = 0.5''$ and the aspect ratios $(\frac{\Lambda}{d})$ used are 1 : 1, 1 : 2 and 1 : 4. The coating material is MF112 and the thicknesses used are 1 mm, 2 mm and 3 mm. The simulations were performed with yee cell size of $\frac{\lambda_{min}}{140}$, where λ_{min} corresponds to the free space wavelength at 26 GHz. The FDTD results are compared with results obtained from the commercial FEM software HFSS (see Fig. 3.3). There is good agreement between the FDTD and HFSS results until 23 GHz, thereby confirming the validity of the code and post-processing. HFSS simulations were carried out using wave port excitation, therefore it fails to take into account the higher order Floquet modes other than the fundamental specular mode. For $\Lambda = 0.5''$, 23.6 GHz is the frequency at which the first non-specular Floquet mode starts propagating. It can be noticed that in all the

curves, there is a reflectivity jump at around this frequency. Generally, the 1:4 targets show low reflectivity in the range less than -40 dB. The reflectivity spectrum is characterized by an increase in reflectivity at lower frequencies. This behavior can be attributed to the fact that at lower frequencies, wavelength will be larger thereby the effective thickness of the coating will be reduced considerably. The black vertical line in Fig. 3.2 at 23.6 GHz highlights the reflectivity jump due to the first non-specular Floquet mode. The reflectivity spectrum till 26 GHz as shown in Fig. 3.2 is obtained using measured values of permittivity and permeability. The Debye series model detailed in the last chapter can be used to extrapolate the values of ϵ_r' , ϵ_r'' , μ_r' , μ_r'' for frequencies greater than 26 GHz. The reflectivity spectrum of square pyramid array in the frequency range [6, 200] GHz for 1 mm, 2 mm coating cases are depicted in Fig. 3.4 and for 3 mm case in Fig. 3.5. For 3 mm case, Geometric Optics (GO) based reflectivity spectrum at high frequencies is also shown in Fig. 3.5.

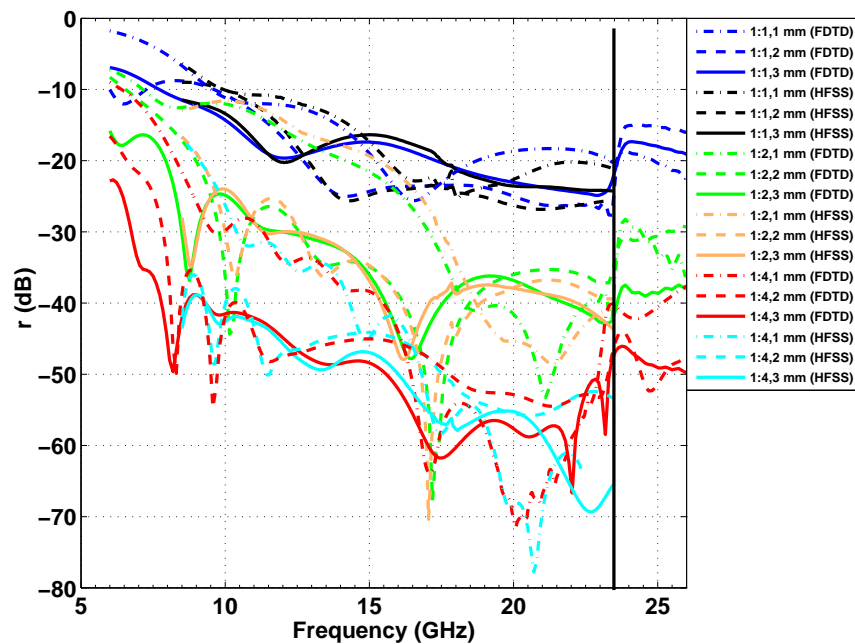


Figure 3.2: Reflectivity of pyramidal targets with MF112 coating for various aspect ratios and coating thicknesses in the frequency range [6,26] GHz.

3.3 Geometrical optics validation

Geometrical optics (GO) based ray tracing was used to evaluate the reflectivities of the targets at high frequencies. The normally incident rays are assumed to have an electric field intensity magnitude of unity. The incident rays will undergo multiple reflections between the pyramidal surfaces before emerging out of the structure. Each reflection will result in an attenuation of the ray magnitude. The ray reflection at the pyramidal surface was taken into account by using Fresnel reflection coefficients for either parallel or perpendicular polarization (depending on the polarization of electric field and which surface the ray strikes). The normal vector to the pyramidal surface depends on the facet on which the ray strikes. In Fig. 3.6, for the case of facet 1, the unit normal vector \hat{n} is given by,

$$\hat{n} = \frac{-\hat{x} + \frac{\Lambda}{2h}\hat{z}}{\sqrt{1 + \frac{\Lambda^2}{4h^2}}} \quad (3.6)$$

where h is the height of the pyramid. Once \hat{n} is known for the point of reflection, the reflection vector \vec{r} (i.e. vector along the direction of reflected ray) can be calculated as follows.

$$\vec{r} = \hat{i} - 2(\hat{n} \cdot \hat{i})\hat{n} \quad (3.7)$$

where \hat{i} is the unit incident vector. Fresnel coefficients are computed for PEC backed MF112 coating. Code for GO reflectivity estimation is listed in appendix C. The GO results are plotted in Fig. 3.5 for the 3 mm coating case. There is good agreement between the FDTD and GO results for frequencies greater than ~ 120 GHz. Hence it can be concluded that to evaluate the pyramid reflectivity at frequencies greater than ~ 120 GHz, GO can be used instead of the computationally expensive dispersive FDTD. The GO method can also be used to estimate the reflectivities at oblique angles. In Figs. 3.4 and 3.5, it can be seen that all the plots exhibit a decaying sinusoidal spectrum at high frequencies. The amplitude of this oscillation is smaller for thicker coatings.

3.4 Floquet mode reflectivity analysis

The frequency domain scattered electric field \vec{E}_{sc} in the case of the doubly periodic scattering structure can be written as

$$\begin{aligned}\vec{E}_{sc} &= \sum_{m=-\infty}^{+\infty} \sum_{n=-\infty}^{+\infty} \vec{E}^{m,n} e^{-jk_x^m x - jk_z^n z} e^{-jk_y^{m,n} y} \\ k_x^m &= \frac{2\pi m}{\Lambda}, \quad k_z^n = \frac{2\pi n}{\Lambda} \\ k_y^{m,n} &= \sqrt{k_o^2 - (k_x^m)^2 - (k_z^n)^2}\end{aligned}\tag{3.8}$$

where (m, n) denote the Floquet mode indices and $\vec{E}^{m,n}$ is the corresponding Floquet mode amplitude. The Floquet mode denoted by (m, n) propagates only when $k_y^{m,n}$ is real, there by resulting in a cutoff frequency for the mode [29]. The cutoff frequency is given by $f_{m,n} = \frac{c}{\Lambda} \sqrt{m^2 + n^2}$. The Floquet mode amplitudes $\vec{E}^{m,n}$ can be calculated by performing the inverse Fourier series of (3.8). A similar procedure can be used to obtain the Floquet mode magnetic field amplitudes $\vec{H}^{m,n}$. Using $\vec{E}^{m,n}$ and $\vec{H}^{m,n}$, the Floquet mode power density can be calculated. The $-y$ component of the Floquet mode power density and the incident power density can be used to calculate the Floquet mode reflectivity $r_{m,n}(f)$. The $r_{m,n}(f)$ spectrum for a pyramid with base $\Lambda = 0.5''$, 1 : 2 aspect ratio and with 2 mm MF112 coating is shown in figure Fig. 3.7. In the figure, r_{tot} represents the total reflectivity estimated using the scattered fields (i.e. fields without performing Floquet decomposition). $\Sigma r_{m,n}$ denotes the sum of reflectivities for indices $-7 < m, n < 7$. $r_{0,0}$ is the specular mode reflectivity with cutoff frequency 0 GHz. It can be seen in Fig. 3.7, that this is the only mode that contributes to the total reflectivity till the onset of the first nonspecular mode at 23.6 GHz. At 23.6 GHz four modes will become propagating modes carrying reflected power at oblique angles. These mode reflectivities are $r_{0,1}, r_{0,-1}, r_{1,0}$ and $r_{-1,0}$. The sum of these identical reflectivities (except for the direction of propagation) is shown as $4 * r_{01}$ in Fig. 3.7.

3.5 Reflectivity spectrum of conical pyramid array

It is of interest to examine structures other than square pyramids, including circular pyramids and truncated square pyramids (i.e., frustra). Such novel structures admit to (respectively) either reduced edge diffraction and more uniform thermal profiles. Accordingly, periodic cone structures and truncated square pyramids are examined for their emissivity spectrum in comparison to regular square pyramids. The reflectivity spectrum of doubly periodic, conical pyramid array is estimated using a previously validated dispersive 3D FDTD code [30]. The pyramid is coated with Emerson-Cummings MF112 trademark material of varying normal thickness t (i.e. thickness along the normal to the cone surface). The base diameter of the cone is $0.5''$ and the ratio of the base diameter to the height of the pyramid is varied as 1:1, 1:2 and 1:4. The center-to-center periodicity of the array is $\Lambda = \frac{0.5''}{\sqrt{2}}$. The reflectivity spectrum in the frequency range [6, 200] GHz is depicted in Figs. (3.8)-(3.10) for $t = 1$ mm, 2 mm and 3 mm coating thickness cases. Further validation of these curves is performed in a manner similar to the procedure in [30]. HFSS is used to compute the normal reflectivity up to 33 GHz, where the first non-specular Floquet mode begins to propagate. The Geometric optics (GO) based high frequency reflectivity approximation is also shown for each case. There is good agreement of $\sim 2 - 3$ dB or better between HFSS and FDTD in most of the cases except for 1:4 pyramids with 1 mm and 3 mm coating thickness. The intercomparison of FDTD with GO results at high frequency is not as good as that of the square pyramid results in [30]. Nevertheless, the GO captures the general reflectivity trend at high frequencies, thus lending credibility to the full wave FDTD solution. It should be remarked that the permittivity and permeability of the MF112 material is available only within the frequency range [6, 26] GHz [30]. Therefore, similar to [30], an extrapolation to higher frequencies using a Debye series was used. An electromagnetic analysis of circular pyramids is reported in [31], but analyzed from the standpoint of the bistatic scattering pattern rather than emissivity spectrum.

A comparison can be made between the calculated reflectivity spectrum of conical pyramids and that of square pyramids as shown in figure 3.11. The periodicity of both the circular and square

pyramid array is $0.5'' \times 0.707$. Only the cases for $t = 2$ mm are compared. For the 1:2 aspect ratio square pyramid, the mean reflectivity in the frequency range [100, 200] GHz is -31.96 dB. On the other hand, for the 1:2, 2 mm conical pyramid case, the mean high frequency reflectivity is -41.86 dB. The mean high frequency reflectivity is estimated over the frequency range where there is an oscillation in the reflectivity spectrum. A similar conclusion can be reached for 1:4 aspect ratio case where the mean reflectivity for square pyramids is -51.48 dB and that of conical pyramids is -64.76 dB. Another noticeable feature is that for conical pyramids, the high frequency reflectivity oscillations are more damped when compared to square pyramids. The standard deviation (std) of r (dB) in the high frequency range for 1:2 square pyramid is 3.76 dB, while for 1:2 circular pyramid it is 2.58 dB. Similarly for 1:4 square pyramid, std is 2.44 dB and for 1:4 circular pyramid it is 1.67 dB. The damping is believed to be due to the broadening of resonant geometrical optics features that would otherwise be caused by specular reflections from flat pyramidal facets. This damping could be a favorable attribute for the construction of broadband targets. At the lowest frequency of 6 GHz the square pyramid reflectivity is lower than that of circular pyramids by ~ 2 dB. Other than these differences, the general reflectivity trends depend more on the coating thickness and aspect ratio than on the pyramid cross-sectional geometry. A solid conclusion that can be reached from figures (3.8)-(3.10) and results in [30] is that irrespective of pyramid cross-section, an aspect ratio of 1:4 or better is essential to achieve broadband reflectivity of -50 dB or less.

In order to ensure the correctness of the FDTD results, a convergence study was carried out for the $0.5''$ base, 1:4, 1 mm MF112 coated circular pyramid by reducing the FDTD grid size in successive simulations. It was found that any grid size less than $\frac{\lambda}{42}$, where λ corresponds to the wavelength in vacuum at 200 GHz, gives accurate results. The results are shown in Fig. 3.19. In addition to this, the distance of the observation plane [30] from the tip of the pyramid was varied and (as expected) the results did not show any difference (Fig. 3.20). Indeed, the observation plane is the virtual plane where the scattered fields are sampled in order to evaluate the reflectivity. Since the scatterer is doubly periodic, the reflectivity should be invariant with respect to the location of this plane. Therefore the only conclusion that can be reached is that for 1:4 circular pyramid cases,

the HFSS results are wrong.

3.6 Reflectivity spectrum of truncated square pyramid array

Due to the preponderance of absorption that occurs near the tips of the pyramids along with the sharp thermal gradient at the tip, it is desirable to truncate the tip so as to lower the location of the emission maximum into a region of more uniform temperature. Such truncation can also occur as the result of tip breakage during the manufacturing process, where sharp tips of composite absorber material can be difficult to mold. Accordingly, the reflectivity spectrum of a truncated pyramidal array is of interest. In order to study the effect of truncation a nominal square pyramidal calibration target array with base of $\Lambda = 0.5''$ and 1:4 aspect ratio was simulated. The pyramid is coated with MF112 absorbent material of thickness, $t = 2$ mm. Figure 3.12 shows the broadband reflectivity in the frequency range [6, 200] GHz for various truncation percentages. The truncation percentage is the height of the pyramid which is removed from the top portion of the untruncated full pyramid as a percentage of the total height of untruncated pyramid. For the 1:4 case with $t = 2$ mm the total height of the untruncated pyramid is $2'' + 16.12$ mm = 66.92 mm. Therefore, a 5% truncation results in removing a pyramidal tip of height 3.34 mm from the untruncated pyramid. The results are validated at high frequencies using GO. Overall there is good agreement between the FDTD and GO solutions in the range $\sim 100 - 200$ GHz, except for the 1 % truncation case where the plateau of the truncated pyramid is small enough so as to behave as a Rayleigh scatterer. In this case the GO model overestimates the scattering from the plateau, leading to an overestimation in reflectivity by up to several dB.

The results in figure (3.12) illustrate the importance of the sharpness of the pyramidal structures. A mere 2% or more truncation results in reflectivity values higher than -50 dB for frequencies greater than ~ 70 GHz. However, truncation does not affect the low frequency reflectivity performance. The reason for this is that the truncated tops behave as Rayleigh scatterer at low enough frequencies. The Rayleigh scattering dependence of $f^4 a^6$, where f is frequency and a is the plateau size favors stronger scattering by the truncated tips only at the higher frequencies. We note that in

no case in Figure 3.12 is the truncation large enough to expose the metallic pyramidal core, although the proximity of the core tip to the incident wave contributes to the tip scattering. Another geometry investigated was the truncated pyramid with spherical top. The geometric details are given in appendix D. It should be noted that spherical top can be fixed only on truncated conical pyramids. For the case of 1:4, 2 mm conical pyramid, the truncation percentage has to be 23.7228 %, for the spherical top to have radius of curvature equal to 2 mm. The reflectivity spectrum of truncated, conical pyramid array of aspect ratio 1:4 and 2 mm MF112 coating is show in Fig. 3.13.

3.7 Target base width scaling

For ISSASI (International Space Station Atmospheric Sounding of Ice) and terahertz atmospheric sounding, the following radiometric frequency bands are of interest: 110 – 118 GHz, 166 – 183 GHz, 325 – 340 GHz, 418 – 424 GHz and 660 – 680 GHz. The plane wave reflectivity spectrum of square pyramid array of base width 0.5'', aspect ratio 1:4 and MF112 coating of 2 mm is given in Fig. 3.4. By scaling the target (i.e. decreasing the dimensions of the nominal pyramid array), we expect to get same reflectivity spectrum at high frequencies. Moreover, FDTD simulation of the nominal target (0.5'', aspect ratio 1:4) is not possible at frequencies higher than 200 GHz, due to the unreasonable memory requirements. In Fig. 3.4, a reflectivity minima of -67 dB can be noticed at 64.6 GHz. In order to shift this minima to 114 GHz (i.e. mid point of the required 110-118 GHz), the base width is scaled as follows, $0.5'' \times 64.6/114 = 0.2833''$. The reflectivity spectrum of this scaled pyramid is shown in Fig. 3.14. From the figure, it can be seen that the minima had moved to 114 GHz. In the FDTD simulation, the Debye series extrapolation of permittivity and permeability using measured data in the frequency range [8, 26] GHz is used. This will not be an accurate model in this high frequency range.

3.8 Unscented transformation sensitivity analysis

The unscented transformation (UT) can be used to find the statistical moments of a nonlinear transformation of a random vector. While increasingly used in extended Kalman filtering, it is

particularly useful when there is no analytical functional form for the transformation, but the values of the function can be calculated at discrete points in the random vector sample space [32]. Let $y = h(\bar{x})$, $\bar{x} \in \mathbb{R}^n$ be a function of the n -dimensional random vector \bar{x} . The mean vector $\bar{\mu}_x$ and autocovariance matrix C_x of \bar{x} are given by

$$\begin{aligned}\bar{\mu}_x &= E[\bar{x}] \\ C_x &= E[(\bar{x} - \bar{\mu}_x)(\bar{x} - \bar{\mu}_x)^T]\end{aligned}\tag{3.9}$$

Using the above statistical information, $2n$ vectors denoted as sigma points are defined. The sigma points $\{\bar{s}^{(i)} | i = 1, 2, \dots, 2n\}$ are calculated using the following expressions.

$$\begin{aligned}\bar{s}^{(i)} &= \bar{\mu}_x + \left(\sqrt{nC_x}\right)_i^T ; i = 1, 2, \dots, n \\ \bar{s}^{(i+n)} &= \bar{\mu}_x - \left(\sqrt{nC_x}\right)_i^T ; i = 1, 2, \dots, n\end{aligned}\tag{3.10}$$

where $\left(\sqrt{nC_x}\right)_i^T$ is the transpose of the i^{th} row of the matrix square root of nC_x . An approximate value for the mean μ_y and variance σ_y^2 of the function $y = h(\bar{x})$ can be calculated as follows.

$$\begin{aligned}\mu_y &\approx \frac{1}{2n} \sum_{i=1}^{2n} h(s^i) \\ \sigma_y^2 &\approx \frac{1}{2n} \sum_{i=1}^{2n} \left(h(s^{(i)}) - \mu_y\right)^2\end{aligned}\tag{3.11}$$

The advantage of the UT is that it can be used to obtain approximate values for statistical moments without resorting to time consuming and often impractical Monte Carlo simulations.

3.9 Uncertainty in material properties

The uncertainty in the real and imaginary parts of the permittivity and permeability of the coating material arises due to two factors: (1) dielectric measurement errors and (2) variations in the composite material's properties from batch to batch. In order to study the effect of this material property variation on the target reflectivity, other parameters such as target geometry, target dimensions, coating thickness etc are assumed to be constant. In that case, the target reflectivity r (dB) is a nonlinear transformation of the four dimensional random vector \bar{x} .

$$r \text{ (dB)} = h(\bar{x}) ; \bar{x} = \left[\varepsilon_r', \varepsilon_r'', \mu_r', \mu_r''\right]^T\tag{3.12}$$

where $\varepsilon_r', \varepsilon_r'', \mu_r', \mu_r''$ are the properties of the dispersive coating material.

In order to perform either a Monte Carlo (MC) simulation or UT, it is assumed that \bar{x} is an Independent and Identically Distributed (IID) n -dimensional Gaussian random vector. Each component of the vector is a Gaussian random variable, which is statistically independent of the remaining elements of the vector. The mean of \bar{x} as a function of frequency is obtained from [24]. Since the random vector \bar{x} is IID, the covariance matrix will be a diagonal matrix, with each diagonal element being the variance of the individual random variable. In order to obtain the variance, it is assumed that the uncertainty bound found in the measurement [24] is equal to 3 times the standard deviation. For instance at 16 GHz, the constitutive properties of MF112 material are given by: $\varepsilon_r' = 5.582, \varepsilon_r'' = 0.147, \mu_r' = 1.106, \mu_r'' = 0.347$. The standard deviations of $\varepsilon_r', \varepsilon_r'', \mu_r', \mu_r''$ are given by $0.36/3, 0.4/3, 0.05/3, 0.15/3$, respectively. The covariance matrix can be obtained by squaring these quantities and placing them in the diagonal elements of the matrix. Hence the covariance matrix at 16 GHz is given by $C_x = \text{diag}(0.0144, 0.0178, 0.0003, 0.0025)$, and independent errors are assumed.

For comparison purposes the mean vector and standard deviation information were also used to drive a MC simulation based upon a large set of Gaussian random variables generated for each material property at 16 GHz. HFSS software was used for the UT and MC calculations, with 3000 random MC vector samples generated. The target simulated was the nominal 0.5" base, 1:4 square pyramid with 2 mm coating. The mean reflectivity and standard deviation obtained from MC analysis are -46.8864 dB and 0.8972 dB, respectively, at 16 GHz. The mean reflectivity and standard deviation obtained by UT simulation are -46.1964 dB and 0.7026 dB respectively. However, the MC simulation of 3000 sample points in HFSS required ~ 27 hours whereas the UT simulation required only 7 minutes. Further confirmation of the utility of the UT method was found by repeating the same validation at 12 GHz. The MC results at this frequency are $-45.3929 \text{ dB} \pm 1.1526 \text{ dB}$ and UT results are $-46.8732 \text{ dB} \pm 1.1477 \text{ dB}$. The reflectivity spectrum along with the uncertainty bounds in the frequency range [8.5, 18] GHz, at an interval of 0.125 GHz is shown in figure 3.15. In electromagnetics, the UT had been applied to uncertainty in antenna design and other related

electromagnetic compatibility problems [28, 33]. As far as we know, this is the first time that the UT has been applied to study the effect of uncertainty in dielectric properties.

3.10 Stability and convergence

In order to ensure stability in 3D FDTD, the Courant Friedrich Levy (CFL) conditions states that $\Delta t \leq \frac{\Delta x}{c\sqrt{3}}$. However even after satisfying this condition, instabilities could arise if the simulation is run for a large number of time steps, as shown in Fig. 3.16. It was found that this late time instability is more profound for 1:1 structures. But for 1:4 structures, large number of time steps did not result in instability. Due to the late time instability and excessive computational time for large number of simulation steps, the simulation should be stopped after reasonable number of steps. If this procedure do not capture all the scattered energy, Prony's extrapolation [34] can be used extrapolate the scattered field time series at each pixel. An example plot of Prony's extrapolation is shown in Fig. 3.17. However it was found that if the simulation is stopped after all the major scattered pulses are sampled, the application of Prony's extrapolation did not made any difference. The effect of late instability on the reflectivity spectrum of 0.5", 1:1, 3 mm MF112 coated square pyramid array is shown in Fig. 3.18. In the figure, if 12000 time steps are used for the simulation, the scattered time series is corrupted resulting in erroneous $r(\text{dB})$. Some of the simulation settings used are given below.

Geometry: 1:1, 0.5" pyramid with 3 mm MF112 coating

Source: Gaussian plane wave with bandwidth 26 GHz

Discretization: $ds = 3e8/26e9/120 = 9.615e-5$ m , $dt = ds/3e8/2 = 0.1602$ ps

Simulation steps: T = 9000

Geometry: 1:4, 0.5" pyramid with 3 mm MF112 coating

Source: Diff Gaussian plane wave with bandwidth [6,200] GHz

Discretization: $ds = 3e8/200e9/28 = 5.3571e-5$ m , $dt = ds/3e8/2 = 89.286$ fs

Simulation steps: T = 16100 or 18000 steps

For 1:4 structures, a discretization better than 1/48 of the wavelength in free space at 200 GHz is

not possible even with 200 cores of HPCS. The number of simulation steps used will not matter, if the number of steps is greater than 18000 or so. The issue of late time instability matters only for 1:1 structures.

3.11 Conclusions

The reflectivity of square pyramids, conical pyramids and truncated square pyramids with MF112 coatings has been studied over a broad range of frequencies commonly used in microwave radiometry. It is concluded that, all other things equal, conical pyramids could be slightly more suitable than square pyramids for constructing broadband targets. However, the reflectivity spectrum is more strongly dependent on pyramidal aspect ratio rather than the specific pyramid cross-sectional geometry. A base to height ratio of 1:4 or better is required to achieve normal reflectivity of less than ~ -50 dB for frequencies from $\sim 20 - 200$ GHz for $\Lambda = 0.5''$ pyramids. The study also explored the effect of sharpness of the pyramidal tips and the use of the unscented transformation to understand the effect of material property uncertainties. Future work includes estimating near field thermal emission from calibration targets and analysis of finite arrays of coated pyramids [35].

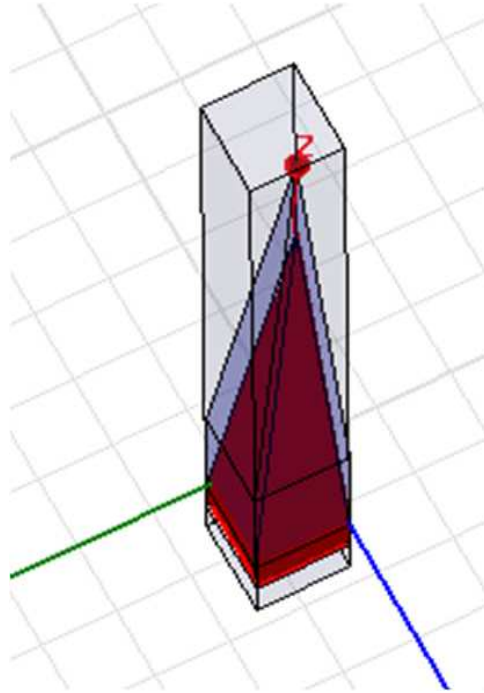


Figure 3.3: HFSS model for square pyramid specular mode reflectivity calculation

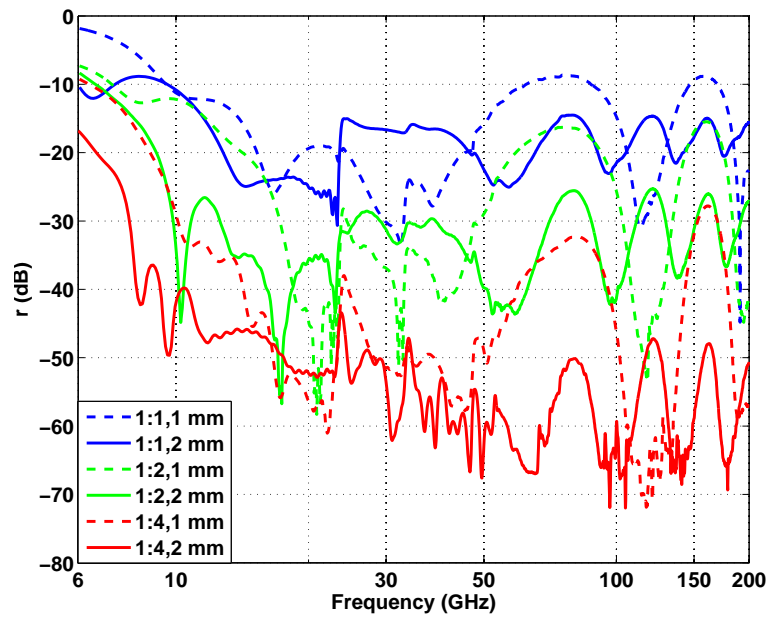


Figure 3.4: Reflectivity of pyramidal targets with MF112 coating for various aspect ratios and coating thicknesses 1 mm,2 mm in the frequency range [6,200] GHz

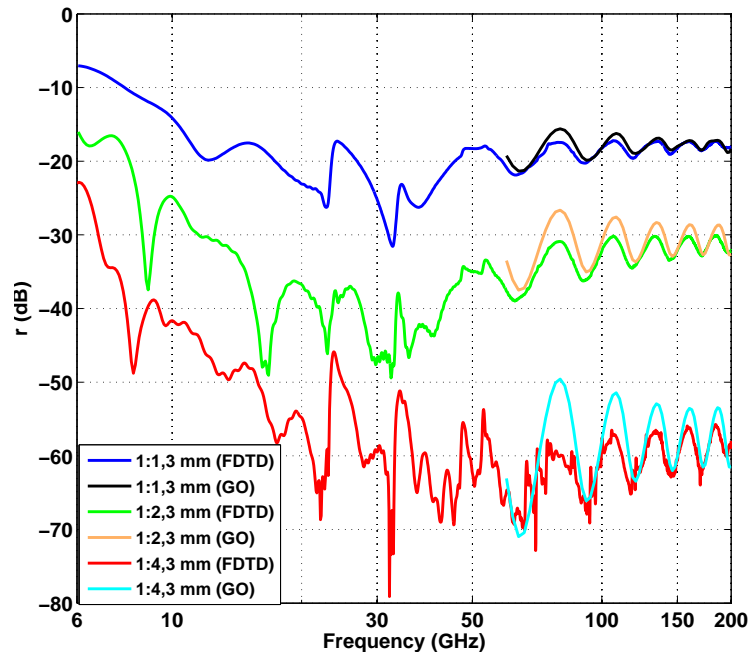


Figure 3.5: Reflectivity of pyramidal targets with MF112 coating for various aspect ratios and coating thickness 3 mm in the frequency range [6,200] GHz. GO validation is also shown for each case.

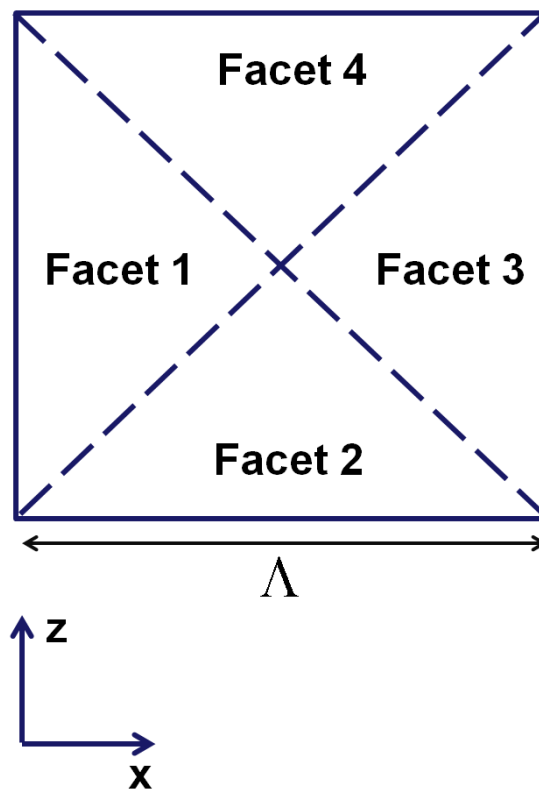


Figure 3.6: Front view of pyramid showing facets for GO modelling

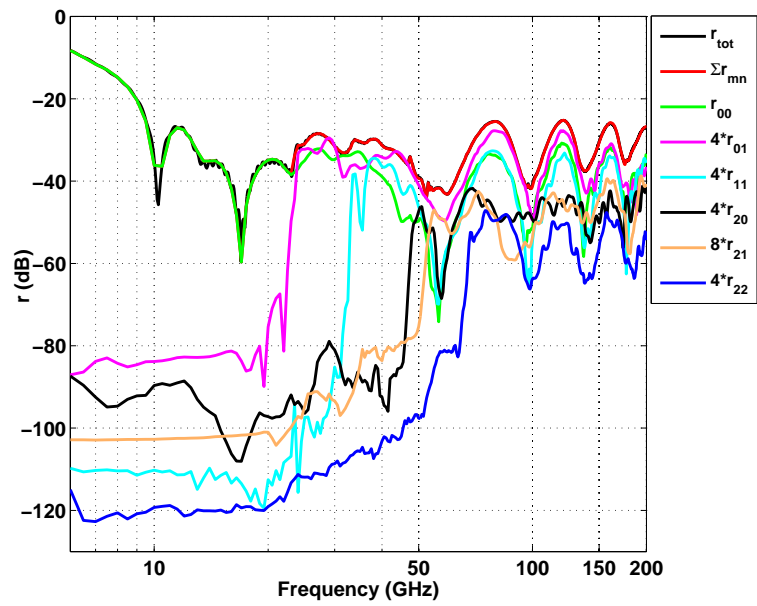


Figure 3.7: Floquet mode reflectivity spectrum for 1:2, 0.5'' base pyramid with 2 mm MF112 coating

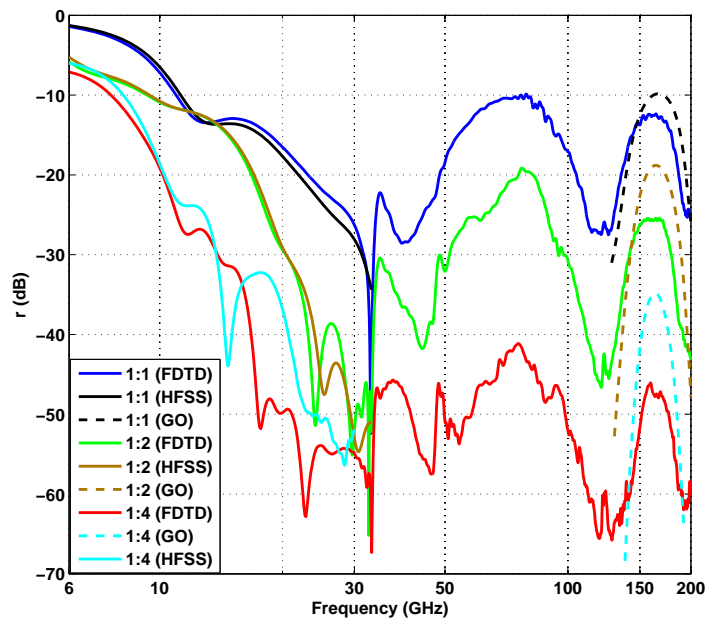


Figure 3.8: Reflectivity spectrum of conical pyramid array with 1 mm of MF112 coating

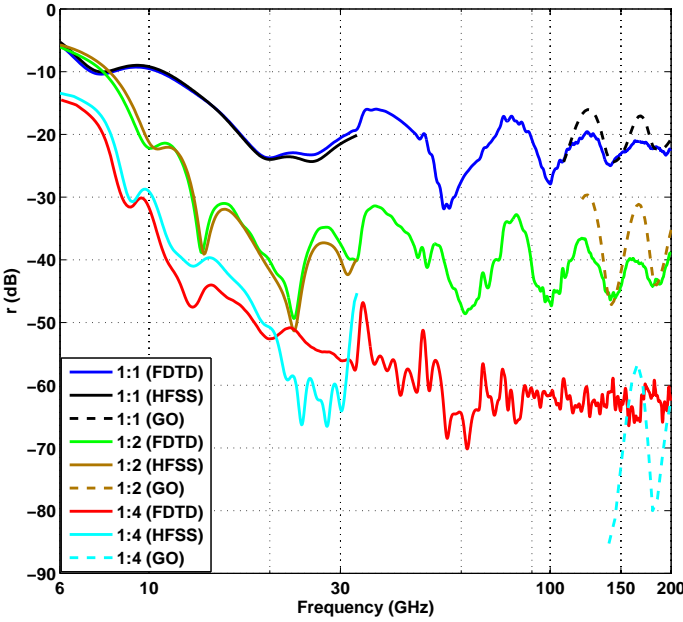


Figure 3.9: Reflectivity spectrum of conical pyramid array with 2 mm of MF112 coating

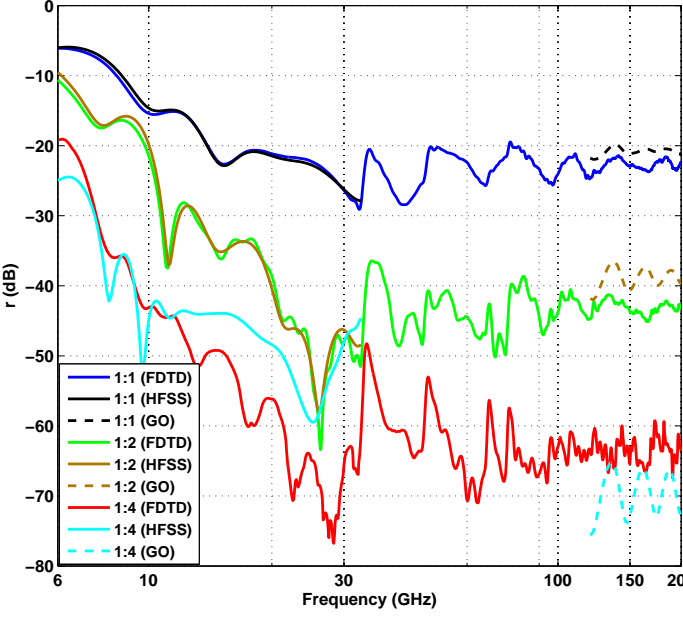


Figure 3.10: Reflectivity spectrum of conical pyramid array with 3 mm of MF112 coating

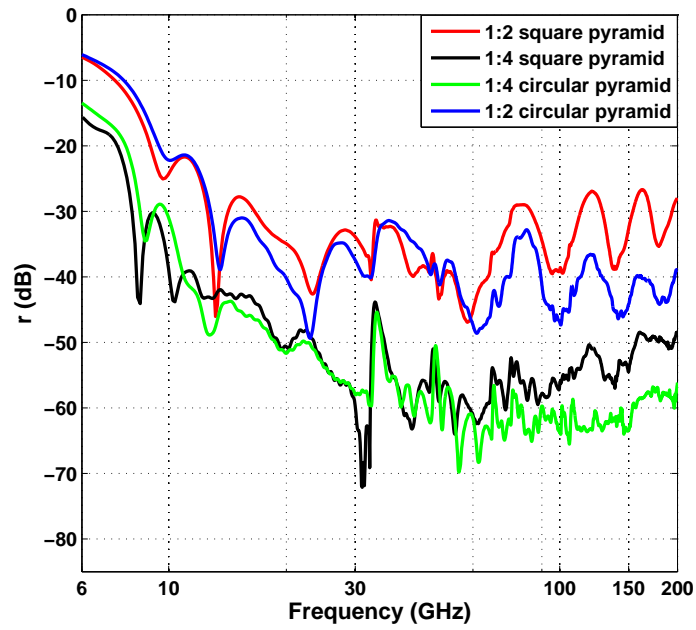


Figure 3.11: Reflectivity spectrum comparison of circular and square pyramids with 2 mm MF112 coating. Periodicity is $\frac{0.5''}{\sqrt{2}}$.

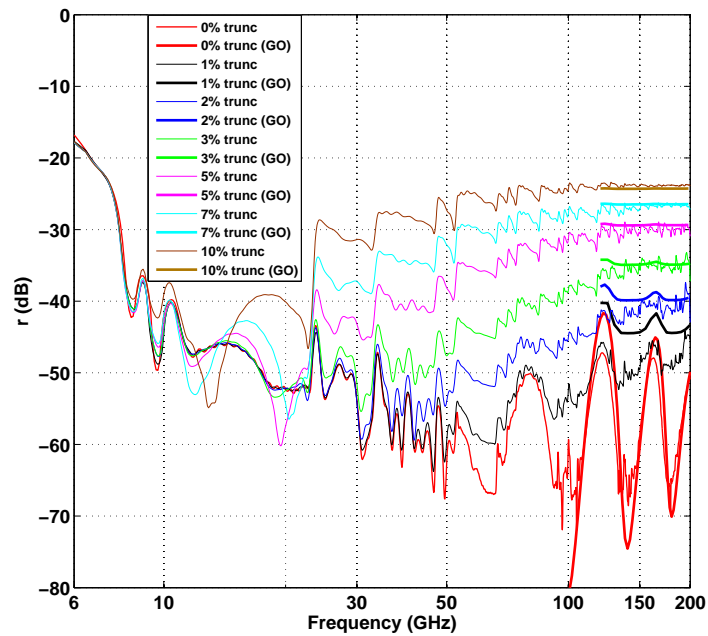


Figure 3.12: Reflectivity spectrum of truncated radiometer calibration targets

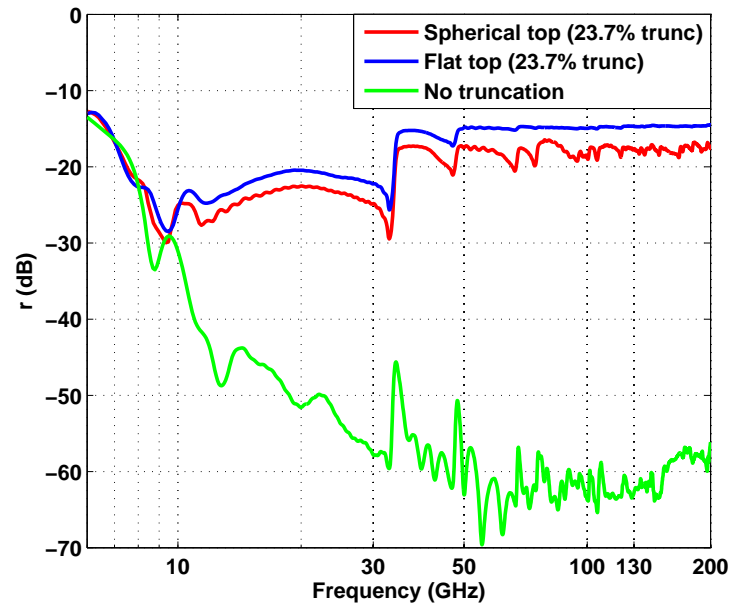


Figure 3.13: Reflectivity spectrum of truncated, conical pyramid array. Aspect ratio of 1:4 and 2 mm MF112 coating.

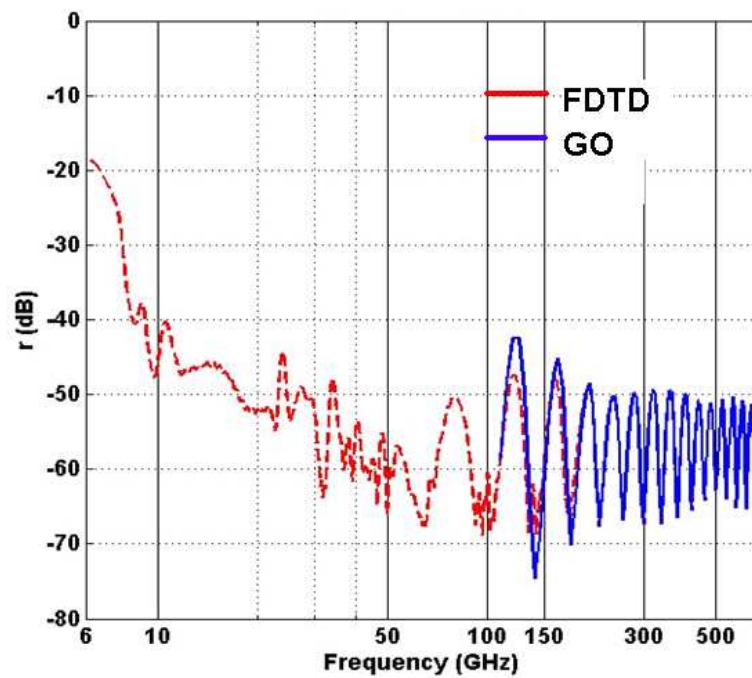


Figure 3.14: Reflectivity spectrum of square pyramid array. Base = $0.2833''$, 1:4 aspect ratio and 2 mm MF112 coating.

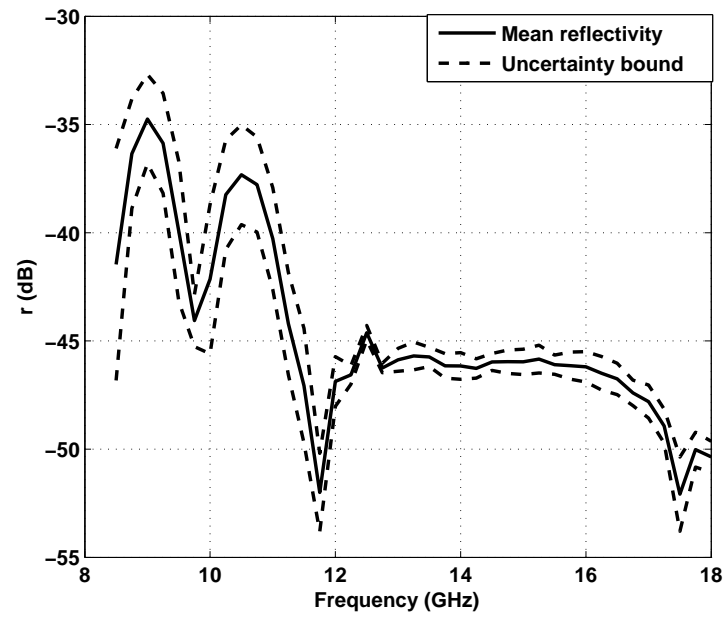


Figure 3.15: Uncertainty bounds in the reflectivity spectrum of 1:4,2 mm square pyramid target with MF112 coating

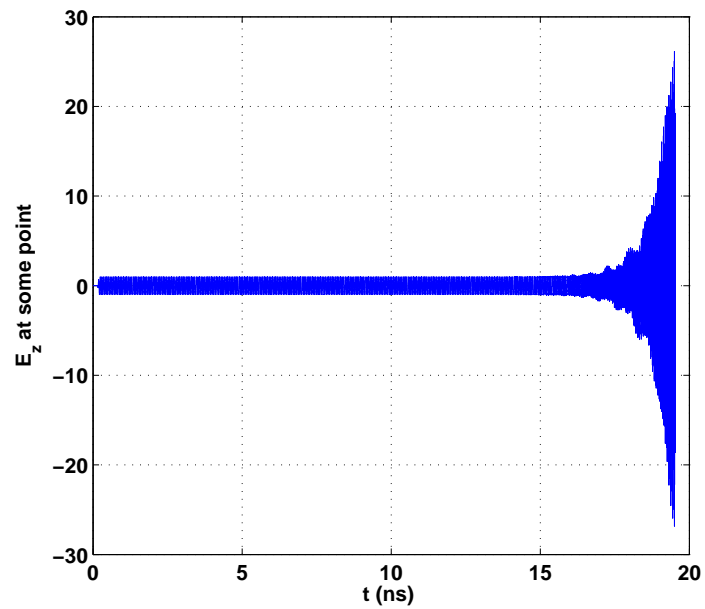


Figure 3.16: Late time instability

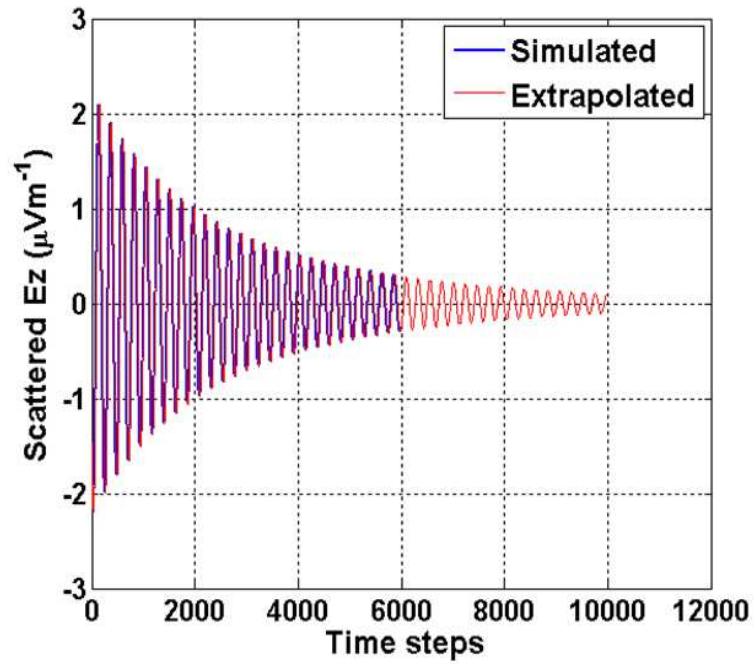


Figure 3.17: Prony extrapolation of scattered field time series

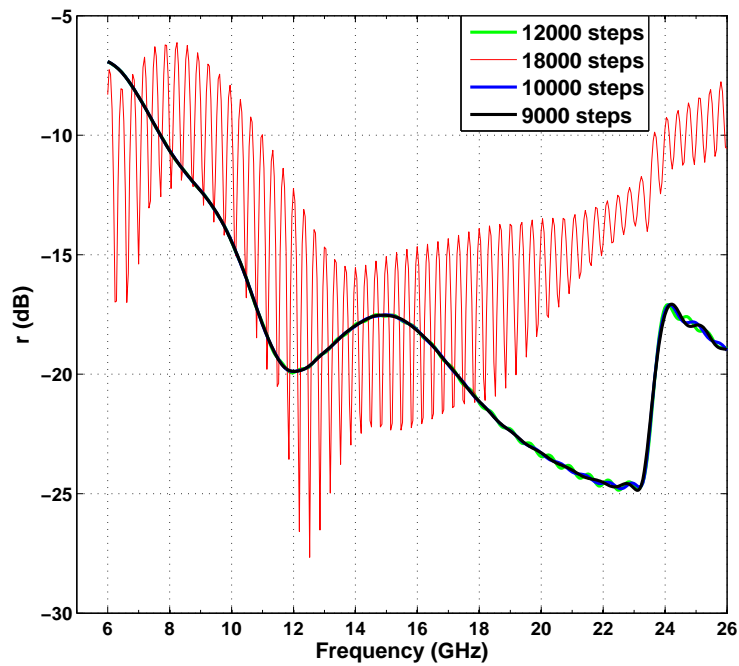


Figure 3.18: Effect of late time instability on reflectivity spectrum

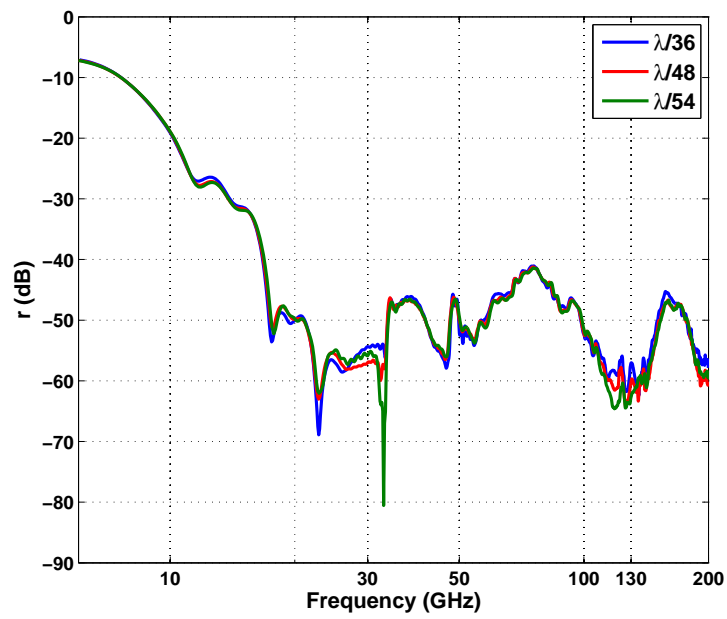


Figure 3.19: Convergence study: $0.5''$ base, 1:4 circular pyramid with 1 mm MF112 coating

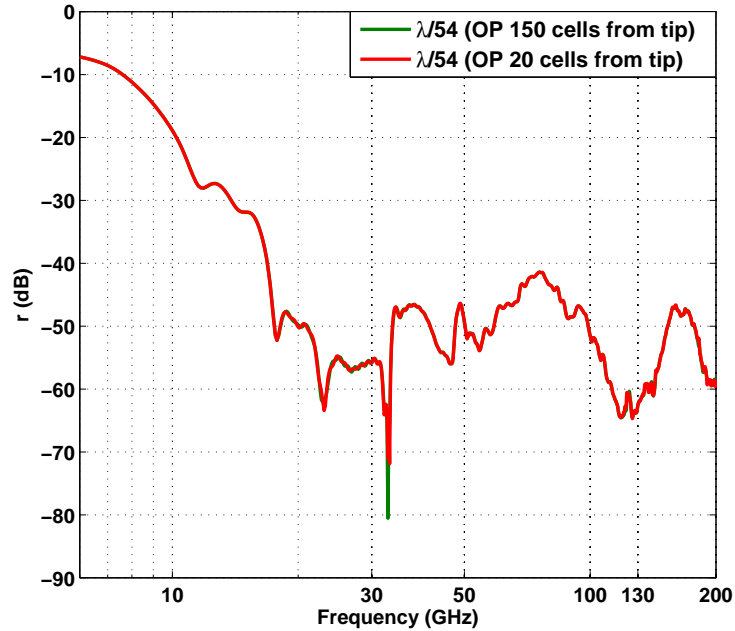


Figure 3.20: Observation plane location : $0.5''$ base, 1:4 circular pyramid with 1 mm MF112 coating

Chapter 4

Transient analysis of dispersive, periodic structures for obliquely incident plane wave using Laguerre Marching-On-In Degree (MoD)

4.1 Introduction

Time domain analysis of dispersive, periodic structures in the case of oblique plane wave incidence is studied in this work. Laguerre Marching-on-in-Degree (MoD) is used for this purpose. Dispersive, periodic structures are important in several applications such as photonic crystals [36], electromagnetic band-gap materials [37] and frequency selective surfaces [38]. Time domain numerical methods are attractive in the sense that a wideband response can be obtained by a single simulation. A FDTD based method for the same problem can be found in [39]. In [39], split-field FDTD [19] with a new set of variables is used. However, it should be remarked that this technique is unstable for incident angles greater than 75° . Conventional dispersive FDTD is limited to dispersive models such as Debye, Lorentz and Drude. On the other hand, by virtue of the Laguerre decomposition, the presented method can simulate general dispersive media. It should also be remarked that, commercial time domain software such as CST Microwave Studio can not perform oblique time domain analysis of periodic structures.

In Laguerre MoD, the transient behaviour of electromagnetic fields is expressed in terms of weighted Laguerre polynomials or Laguerre basis functions [40]. Time domain operations such as time derivative and convolution can be handled in this Laguerre transformation. The Laguerre basis functions are convergent to zero as $t \rightarrow \infty$, there by ensuring unconditionally stability. In Laguerre-FDTD simulations, the CFL stability condition [15] can be circumvented. This will reduce the

simulation time considerably, particularly in the case of dispersive structures. Conventional FDTD simulation of dispersive media is carried out using Piecewise Linear Recursive Convolution (PLRC) [41]. PLRC can be quite time consuming, especially for 3D multiscale, dispersive structures [42]. Laguerre-FDTD simulation of dispersive media can be found in [43]. An alternative formulation based on the wave equation is reported in [44]. In this work, we use the former method. The use of Laguerre-FDTD for the analysis of periodic structures and oblique plane wave incidence is explained in [45]. However, the method is non-dispersive in nature and had been applied only to PEC structures. Laguerre basis functions along with time domain integral equations were used in [46, 47] to analyze transient scattering. A three dimensional implementation of Laguerre-FDTD is reported in [48].

In this work, an one dimensional periodic, electrically dispersive structure is analyzed when a plane wave is incident on it at any arbitrary angle. 2D TM_z polarization is assumed and periodicity is along the y -direction. However, it is straightforward to extend the formulations to 2D TE_z case. In section 2, the Laguerre MoD formulation for periodic, dispersive structure is explained. The Field Transformation Technique (FTM) [49] is used to handle the obliquely incident plane wave on a periodic structure. This is followed by applying the dispersive Laguerre formulation [43] to the field transformed variables. In section 3, the implementation of UPML for the case of dispersive, periodic, Laguerre domain is presented. In section 4, the formulation is numerically validated by estimating the transmission spectrum of a dispersive slab at various angles of incidence and comparing the results with analytical results.

4.2 Laguerre MoD formulation for periodic, dispersive structure

In the case of 2D TM_z polarization, the material properties and the field variables $E_z(x, y; t)$, $H_x(x, y; t)$, $H_y(x, y; t)$ are independent of z direction. Maxwell's equations in time domain reduces to the following set of equations

$$\frac{\partial E_z}{\partial y} = -\mu_o \frac{\partial H_x}{\partial t} \quad (4.1)$$

$$\frac{\partial E_z}{\partial x} = \mu_o \frac{\partial H_y}{\partial t} \quad (4.2)$$

$$\frac{\partial H_y}{\partial x} - \frac{\partial H_x}{\partial y} = \varepsilon_o \frac{\partial}{\partial t} [\varepsilon_r(t) \otimes E_z(t)] + \sigma E_z \quad (4.3)$$

where \otimes denotes convolution integral. In the above equations, spatial dependence of the field variables and constitutive parameters are not explicitly shown. A non-magnetic media is assumed and the permittivity exhibits temporal dispersion. For time domain simulation of periodic structures with oblique plane wave incidence, the Field Transformation Technique (FTM) is used to remove the time shift across the grid. In FTM, $\{E_z, H_x, H_y\}$ are replaced by new variables $\{P_z, Q_x, Q_y\}$ according to the relations,

$$\breve{P}_z = \breve{E}_z \exp(jk_0 \sin \phi y) \quad (4.4)$$

$$\breve{Q}_x = \eta_0 \breve{H}_x \exp(jk_0 \sin \phi y) \quad (4.5)$$

$$\breve{Q}_y = \eta_0 \breve{H}_y \exp(jk_0 \sin \phi y) \quad (4.6)$$

where variables with breve accent are in the frequency domain and y is the direction of periodicity. ϕ is the angle between the incident wave vector and x axis. By substituting (4.4)-(4.6) in frequency domain versions of (4.1)-(4.3), followed by converting the resultant equations into time domain yields the time domain equations for P_z, Q_x, Q_y .

$$-\frac{\partial P_z}{\partial y} + \frac{\sin \phi}{c} \frac{\partial P_z}{\partial t} = \frac{1}{c} \frac{\partial Q_x}{\partial t} \quad (4.7)$$

$$\frac{\partial P_z}{\partial x} = \frac{1}{c} \frac{\partial Q_y}{\partial t} \quad (4.8)$$

$$\frac{\partial Q_y}{\partial x} - \frac{\partial Q_x}{\partial y} + \frac{\sin \phi}{c} \frac{\partial Q_x}{\partial t} = \frac{1}{c} \frac{\partial}{\partial t} [\varepsilon_r(t) \otimes P_z(t)] + \sigma \eta_0 P_z \quad (4.9)$$

In the Laguerre-Mod formulation, the time dependant quantities are replaced by weighted summation of Laguerre basis functions [40],

$$F(x, y; t) = \sum_{q=0}^{\infty} F_q(x, y) \phi_q(st) \quad (4.10)$$

where $F(x, y; t)$ can be either P_z, Q_x, Q_y or ε_r , and $\phi_q(st)$ represents the Laguerre basis function. The Laguerre basis function is given by

$$\phi_q(st) = L_q(st) e^{-\frac{st}{2}} \quad (4.11)$$

where $L_q(st)$ is Laguerre polynomial of degree q and s is the time scaling parameter. By applying (4.10) to equations (4.7)-(4.9), followed by Galerkin testing [40, 43] results in expressions for the q^{th} basis coefficient of the field variables,

$$Q_x^q = -\frac{2c}{s} \frac{\partial P_z^q}{\partial y} + \sin \phi P_z^q + \sum_{\substack{p=0 \\ q>0}}^{q-1} 2 \sin \phi P_z^p - 2Q_x^p \quad (4.12)$$

$$Q_y^q = \frac{2c}{s} \frac{\partial P_z^q}{\partial x} - 2 \sum_{\substack{p=0 \\ q>0}}^{q-1} Q_y^p \quad (4.13)$$

$$P_z^q = \left(\frac{2c}{\varepsilon_r^0 + 2c\eta_0\sigma} \right) \left[\frac{\partial Q_y^q}{\partial x} - \frac{\partial Q_x^q}{\partial y} \right] + \frac{s \sin \phi}{\varepsilon_r^0 + 2c\eta_0\sigma} Q_x^q + \sum_{\substack{p=0 \\ q>0}}^{q-1} \frac{2s \sin \phi}{\varepsilon_r^0 + 2c\eta_0\sigma} Q_x^p - \frac{\varepsilon_r^{q-p} + \varepsilon_r^{q-p-1}}{\varepsilon_r^0 + 2c\eta_0\sigma} P_z^p \quad (4.14)$$

where we have used the following two properties of Laguerre transformation [43, 44],

$$\frac{\partial P_z}{\partial t} = \sum_{q=0}^{\infty} \left[\frac{s}{2} P_z^q + \sum_{\substack{p=0 \\ q>0}}^{q-1} s P_z^p \right] \phi_q(st) \quad (4.15)$$

$$\frac{\partial}{\partial t} [\varepsilon_r(t) \otimes P_z(t)] = \sum_{q=0}^{\infty} \left[\frac{P_z^q \varepsilon_r^0}{2} + \sum_{\substack{p=0 \\ q>0}}^{q-1} \frac{P_z^p}{2} \{ \varepsilon_r^{q-p-1} + \varepsilon_r^{q-p} \} \right] \phi_q(st) \quad (4.16)$$

By substituting (4.12),(4.13) in (4.14), an expression for P_z^q which is amenable to marching-on-in degree can be obtained,

$$\begin{aligned}
& (s \sin^2 \phi - \varepsilon_r^0 - 2c\eta_0\sigma) P_z^q + \frac{4c^2}{s} \frac{\partial^2 P_z^q}{\partial x^2} + \frac{4c^2}{s} \frac{\partial^2 P_z^q}{\partial y^2} - 4c \sin \phi \frac{\partial P_z^q}{\partial y} = \\
& \sum_{\substack{p=0 \\ q>0}}^{q-1} 4c \frac{\partial Q_y^p}{\partial x} + 4c \sin \phi \frac{\partial P_z^p}{\partial y} - 4c \frac{\partial Q_x^p}{\partial y} + (\varepsilon_r^{q-p} + \varepsilon_r^{q-p-1} - 2s \sin^2 \phi) P_z^p
\end{aligned} \tag{4.17}$$

The equation (4.17) is discretized using the conventional 2D FDTD TM_z grid [15] to obtain the discrete equation for software implementation.

$$\begin{aligned}
& \frac{4c^2}{s\Delta x^2} P_z^q|_{i+1,j} + \frac{4c^2}{s\Delta x^2} P_z^q|_{i-1,j} + \left(\frac{4c^2}{s\Delta y^2} - \frac{2c \sin \phi}{\Delta y} \right) P_z^q|_{i,j+1} + \left(\frac{4c^2}{s\Delta y^2} + \frac{2c \sin \phi}{\Delta y} \right) P_z^q|_{i,j-1} \\
& \quad + \left(s \sin^2 \phi - \varepsilon_r^0|_{i,j} - 2c\eta_0\sigma_{i,j} - \frac{8c^2}{s\Delta x^2} - \frac{8c^2}{s\Delta y^2} \right) P_z^q|_{i,j} \\
& = \sum_{\substack{p=0 \\ q>0}}^{q-1} \frac{4c}{\Delta x} [Q_y^p|_{i+1,j} - Q_y^p|_{i,j}] + \frac{2c \sin \phi}{\Delta y} [P_z^p|_{i,j+1} - P_z^p|_{i,j-1}] - \frac{4c}{\Delta y} [Q_x^p|_{i,j+1} - Q_x^p|_{i,j}] \\
& \quad + (\varepsilon_r^{q-p}|_{i,j} + \varepsilon_r^{q-p-1}|_{i,j} - 2s \sin^2 \phi) P_z^p|_{i,j}
\end{aligned} \tag{4.18}$$

where the equation (4.18) along with the UPML boundary condition explained in the next section can be used to build a matrix equation to solve for P_z^q in the entire 2D domain. In (4.18), $P_z|_{i,j}$, $Q_x|_{i,j}$ and $Q_y|_{i,j}$ are located at the center, bottom edge and left edge of the $(i, j)^{th}$ Yee cell. Since the coefficients of P_z^q quantities on the left hand side of (4.18) do not change with each MoD step, the matrix can be decomposed using LU decomposition [50] resulting in faster calculation of P_z^q in each MoD step. For the generation of incident wave, a Total Field/Scattered Field (TF/SF) formulation similar to [45] is used. Once the P_z^q coefficients are obtained, Q_x^q , Q_y^q coefficients in the entire domain are obtained by using the discretized versions of (4.12),(4.13) given as follows.

$$Q_x^q|_{i,j} = \left(\frac{-2c}{s\Delta y} + \frac{\sin \phi}{2} \right) P_z^q|_{i,j} + \left(\frac{2c}{s\Delta y} + \frac{\sin \phi}{2} \right) P_z^q|_{i,j-1} + \sum_{\substack{p=0 \\ q>0}}^{q-1} \sin \phi [P_z^p|_{i,j} + P_z^p|_{i,j-1}] - 2Q_x^p|_{i,j} \tag{4.19}$$

$$Q_y^q|_{i,j} = \frac{2c}{s\Delta x} P_z^q|_{i,j} - \frac{2c}{s\Delta x} P_z^q|_{i-1,j} - 2 \sum_{\substack{p=0 \\ q>0}}^{q-1} Q_y^p|_{i,j} \quad (4.20)$$

4.3 UPML formulation in Laguerre MoD

For UPML slabs on the x-axis boundaries [18, 15], the governing equations can be written as

$$\frac{\partial \check{E}_z}{\partial y} = -j\omega\mu_o s_x^{-1} \check{H}_x \quad (4.21)$$

$$\frac{\partial \check{E}_z}{\partial x} = j\omega\mu_o s_x \check{H}_y \quad (4.22)$$

$$\frac{\partial \check{H}_y}{\partial x} - \frac{\partial \check{H}_x}{\partial y} = j\omega\varepsilon_o s_x \check{E}_z \quad (4.23)$$

where $s_x = 1 + \frac{\sigma_x}{j\omega\varepsilon_o}$. By applying (4.4)-(4.6) to (4.21)-(4.23), the following set of frequency domain equations are obtained.

$$s_x \frac{\partial \check{P}_z}{\partial y} - jk_0 \sin \phi s_x \check{P}_z = -\frac{j\omega}{c} \check{Q}_x \quad (4.24)$$

$$\frac{\partial \check{P}_z}{\partial x} = \frac{j\omega s_x}{c} \check{Q}_y \quad (4.25)$$

$$\frac{\partial \check{Q}_y}{\partial x} - \frac{\partial \check{Q}_x}{\partial y} + jk_0 \sin \phi \check{Q}_x = \frac{j\omega s_x}{c} \check{P}_z \quad (4.26)$$

This is followed by the expansion of s_x and converting the resultant equations to time domain.

The time domain UPML equations for the field transformed variables are as follows.

$$\varepsilon_o \frac{\partial^2 P_z}{\partial y \partial t} + \sigma_x \frac{\partial P_z}{\partial y} - \frac{\varepsilon_o \sin \phi}{c} \frac{\partial^2 P_z}{\partial t^2} = -\frac{\varepsilon_o}{c} \frac{\partial^2 Q_x}{\partial t^2} + \frac{\sigma_x \sin \phi}{c} \frac{\partial P_z}{\partial t} \quad (4.27)$$

$$\frac{\partial P_z}{\partial x} = \frac{1}{c} \frac{\partial Q_y}{\partial t} + \frac{\sigma_x}{c\varepsilon_o} Q_y \quad (4.28)$$

$$\frac{\partial Q_y}{\partial x} - \frac{\partial Q_x}{\partial y} + \frac{\sin \phi}{c} \frac{\partial Q_x}{\partial t} = \frac{1}{c} \frac{\partial P_z}{\partial t} + \frac{\sigma_x}{c\varepsilon_o} P_z \quad (4.29)$$

By applying Laguerre basis function expansion to equations (4.27)-(4.29), we arrive at the spatial differential equations for the Laguerre basis coefficients in the UPML domain.

$$\begin{aligned}
& \left[\frac{s\varepsilon_o}{2} + \sigma_x \right] \frac{\partial P_z^q}{\partial y} + s\varepsilon_o \sum_{\substack{p=0 \\ q>0}}^{q-1} \frac{\partial P_z^p}{\partial y} + \left[\frac{-s^2\varepsilon_o \sin^2 \phi}{4c} - \frac{s\sigma_x \sin \phi}{2c} \right] P_z^q \\
& + \sum_{\substack{p=0 \\ q>0}}^{q-1} \left[\frac{-s^2\varepsilon_o \sin \phi (q-p)}{c} - \frac{s\sigma_x \sin \phi}{c} \right] P_z^p = \frac{-s^2\varepsilon_o}{c} \left[\frac{Q_x^q}{4} + \sum_{\substack{p=0 \\ q>0}}^{q-1} (q-p) Q_x^p \right]
\end{aligned} \tag{4.30}$$

$$\frac{\partial P_z^q}{\partial x} = \left[\frac{s}{2c} + \frac{\sigma_x}{c\varepsilon_o} \right] Q_y^q + \frac{s}{c} \sum_{\substack{p=0 \\ q>0}}^{q-1} Q_y^p \tag{4.31}$$

$$\frac{\partial Q_y^q}{\partial x} - \frac{\partial Q_x^q}{\partial y} + \frac{s \sin \phi}{2c} Q_x^q + \frac{s \sin \phi}{c} \sum_{\substack{p=0 \\ q>0}}^{q-1} Q_x^p = \left[\frac{s}{2c} + \frac{\sigma_x}{c\varepsilon_o} \right] P_z^q + \frac{s}{c} \sum_{\substack{p=0 \\ q>0}}^{q-1} P_z^p \tag{4.32}$$

In the derivation of (4.30) from (4.27), we have used the following second derivative property of Laguerre decomposition.

$$\frac{\partial^2 P_z}{\partial t^2} = s^2 \sum_{q=0}^{\infty} \left[\frac{1}{4} P_z^q + \sum_{\substack{p=0 \\ q>0}}^{q-1} (q-p) P_z^p \right] \phi_q(st) \tag{4.33}$$

The equations (4.30)-(4.32) are discretized on the 2D TM_z Yee cell to obtain the discrete equations given by (4.34)-(4.36).

$$Q_x^p|_{i,j} = A1|_{i,j} P_z^q|_{i,j} + A2|_{i,j} P_z^q|_{i,j-1} + \sum_{\substack{p=0 \\ q>0}}^{q-1} A3^{p,q}|_{i,j} P_z^p|_{i,j} + A4^{p,q}|_{i,j} P_z^p|_{i,j-1} - 4(q-p) Q_x^p|_{i,j} \tag{4.34}$$

$$Q_y^q|_{i,j} = A5|_{i,j} P_z^q|_{i,j} - A5|_{i,j} P_z^q|_{i-1,j} - \frac{s\Delta x}{c} A5|_{i,j} \sum_{\substack{p=0 \\ q>0}}^{q-1} Q_y^p|_{i,j} \tag{4.35}$$

$$\begin{aligned}
P_z^q|_{i,j} &= A6|_{i,j} Q_y^q|_{i+1,j} - A6|_{i,j} Q_y^q|_{i,j} + A7|_{i,j} Q_x^q|_{i,j+1} + A8|_{i,j} Q_x^q|_{i,j} \\
&+ \sum_{\substack{p=0 \\ q>0}}^{q-1} \frac{s \sin \phi \Delta x A6|_{i,j}}{2c} (Q_x^p|_{i,j} + Q_x^p|_{i,j+1}) - \frac{s\Delta x A6|_{i,j}}{c} P_z^p|_{i,j}
\end{aligned} \tag{4.36}$$

$$A1|_{i,j} = \frac{-2c}{s\Delta y} - \frac{4c\sigma_x^{Qx}|_{i,j}}{s^2\varepsilon_o\Delta y} + 0.5 \sin \phi + \frac{\sigma_x^{Qx}|_{i,j} \sin \phi}{s\varepsilon_o} \quad (4.37)$$

$$A2|_{i,j} = \frac{2c}{s\Delta y} + \frac{4c\sigma_x^{Qx}|_{i,j}}{s^2\varepsilon_o\Delta y} + 0.5 \sin \phi + \frac{\sigma_x^{Qx}|_{i,j} \sin \phi}{s\varepsilon_o} \quad (4.38)$$

$$A3^{p,q}|_{i,j} = \frac{-4c}{s\Delta y} + 2 \sin \phi (q - p) + \frac{2\sigma_x^{Qx}|_{i,j} \sin \phi}{s\varepsilon_o} \quad (4.39)$$

$$A4^{p,q}|_{i,j} = \frac{4c}{s\Delta y} + 2 \sin \phi (q - p) + \frac{2\sigma_x^{Qx}|_{i,j} \sin \phi}{s\varepsilon_o} \quad (4.40)$$

$$A5|_{i,j} = \frac{2c\varepsilon_o}{s\varepsilon_o\Delta x + 2\Delta x\sigma_x^{Qy}|_{i,j}}, \quad A6|_{i,j} = \frac{2c\varepsilon_o}{s\varepsilon_o\Delta x + 2\Delta x\sigma_x^{Pz}|_{i,j}} \quad (4.41)$$

$$A7|_{i,j} = \frac{(s \sin \phi \Delta x - 4c) \Delta x A6|_{i,j}}{4c\Delta y}, \quad A8|_{i,j} = \frac{(s \sin \phi \Delta x + 4c) \Delta x A6|_{i,j}}{4c\Delta y} \quad (4.42)$$

It should be noted that in (4.37)-(4.40), $\sigma_x^{Qx}|_{i,j}$ represents the value of σ_x at the position of Q_x vector in the Yee cell denoted by indices (i, j) . The same holds for $\sigma_x^{Qy}|_{i,j}, \sigma_x^{Pz}|_{i,j}$ in (4.41). By substituting (4.34),(4.35) in (4.36), a matrix equation given by (4.43) can be obtained for P_z^q coefficients.

$$\begin{aligned} & (A6|_{i,j}A5|_{i+1,j}) P_z^q|_{i+1,j} + (-A6|_{i,j}A5|_{i+1,j} - A6|_{i,j}A5|_{i,j} + A7|_{i,j}A2|_{i,j+1} + A8|_{i,j}A1|_{i,j} - 1) P_z^q|_{i,j} + \\ & (A6|_{i,j}A5|_{i,j}) P_z^q|_{i-1,j} + (A7|_{i,j}A1|_{i,j+1}) P_z^q|_{i,j+1} + (A8|_{i,j}A2|_{i,j}) P_z^q|_{i,j-1} = \sum_{\substack{p=0 \\ q>0}}^{q-1} \frac{s\Delta x}{c} A6|_{i,j}A5|_{i+1,j} \\ & Q_y^p|_{i+1,j} - \frac{s\Delta x}{c} A6|_{i,j}A5|_{i,j}Q_y^p|_{i,j} - A7|_{i,j}A3^p|_{i,j+1}P_z^p|_{i,j+1} - (A7|_{i,j}A4^p|_{i,j+1} + A8|_{i,j}A3^p|_{i,j} \\ & - \frac{s\Delta x A6|_{i,j}}{c}) P_z^p|_{i,j} - A8|_{i,j}A4^p|_{i,j}P_z^p|_{i,j-1} + \left(4A7|_{i,j}(q-p) - \frac{s \sin \phi \Delta x A6|_{i,j}}{2c} \right) Q_x^p|_{i,j+1} + \\ & \left(4A8|_{i,j}(q-p) - \frac{s \sin \phi \Delta x A6|_{i,j}}{2c} \right) Q_x^p|_{i,j} \end{aligned} \quad (4.43)$$

The equations (4.18),(4.43) are used to construct matrix equation for P_z in the computational domain. Along the y direction, the periodicity condition of $P_z^q|_{i,0} = P_z^q|_{i,Y}$, $Q_x^q|_{i,0} = Q_x^q|_{i,Y}$ is used, where Y is the number of Yee cells along the y direction. The code for this work is show in appendix ???. MATLAB do not have built-in Laguerre polynomial functions. Therefore GSL (GNU Scientific Library) is used to generate the Laguerre coefficients for the source functions.

4.4 Numerical validation

In order to numerically validate the formulations, the transmission spectra S_{12} (dB) of a dispersive slab is estimated at various angles of incidence using this method and the results are compared with analytical results. The slab material is a double pole Debye media. The relative permittivity of the double pole Debye media is given by,

$$\varepsilon_r(\omega) = \varepsilon_\infty + \sum_{p=1}^2 \frac{\varepsilon_{s,p} - \varepsilon_\infty}{1 + j\omega\tau_p} \quad (4.44)$$

where $\varepsilon_\infty = 3$, $\varepsilon_{s,1} = 4$, $\tau_1 = 7 \times 10^{-8}$, $\varepsilon_{s,2} = 4.5$, $\tau_2 = 2 \times 10^{-10}$. The Laguerre decomposition coefficients ε_r^q for (4.44) can be obtained either by using analytical expressions given in [43] or by numerical quadrature of the product of time domain version of (4.44) and the corresponding Laguerre basis function. The spatial discretization is $\Delta x = 24.98 \mu\text{m}$ and a 15 layer UPML is used. The width of the slab is 100 cells along the x-direction. The number of basis functions, $M = 339$ and the simulation duration is $T_f = 1.3374 \text{ ns}$. The scaling factor is set to $s = M/T_f$. A differentiated Gaussian plane wave is used as excitation.

$$f(t) = \frac{2(t_o - t)}{\tau^2} \exp\left[-\frac{(t - t_o)^2}{\tau^2}\right] \quad (4.45)$$

where $\tau = 4.8274 \times 10^{-12}$ and $t_o = 4\tau$. The angle of incidences used are: 0° , 45° , 60° and 75° . The intercomparison of the MoD results with analytical results are shown in figures (4.1)-(4.4). There is good agreement for incident angles 0° , 45° and 60° . For the 75° case, there is a slight mismatch. For most practical problems, the incident angle is almost always less than $\sim 70^\circ$. Since Laguerre MoD uses an entire domain temporal basis function, the accuracy of Laguerre MoD based methods may be inferior to FDTD based methods. However, the validation confirms the correctness of the formulations in both the main grid and UPML, with the added advantage of unconditional stability, less simulation time and ability to handle general dispersive media.

4.5 Conclusions

A novel method for transient electromagnetic analysis of dispersive periodic structures at off-normal angles of incidence is described. By using Laguerre-MoD, unconditional stability is assured. Another contribution of this work is the implementation of UPML in Laguerre MoD using field transformed variables. The developed method can be used to obtain broadband results at incidence angles less than 75° . In comparison to previous FDTD based methods for solving the same problem, this method do not exhibit instability at grazing angles of incidence and can handle general dispersive media. Future work include detailed error analysis and the extension of this method to 3D problems.

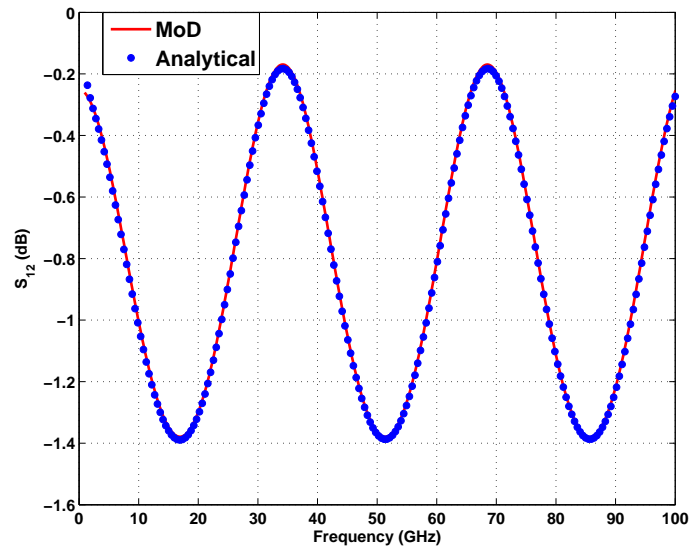


Figure 4.1: Transmission spectrum of dispersive slab at 0° angle of incidence

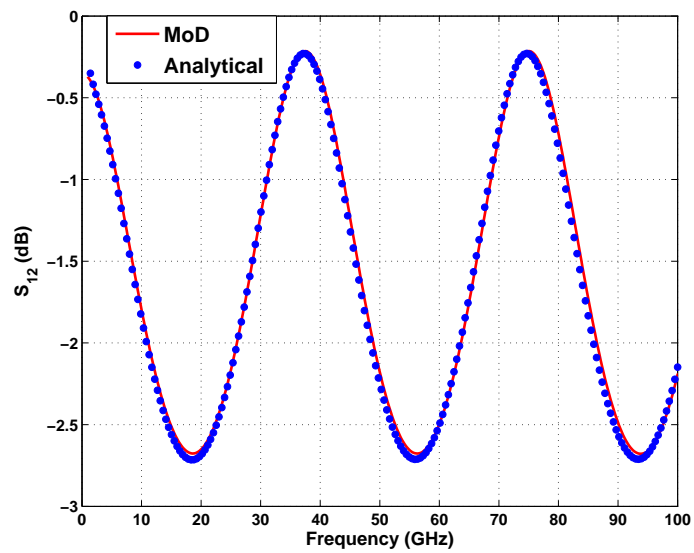


Figure 4.2: Transmission spectrum of dispersive slab at 45° angle of incidence

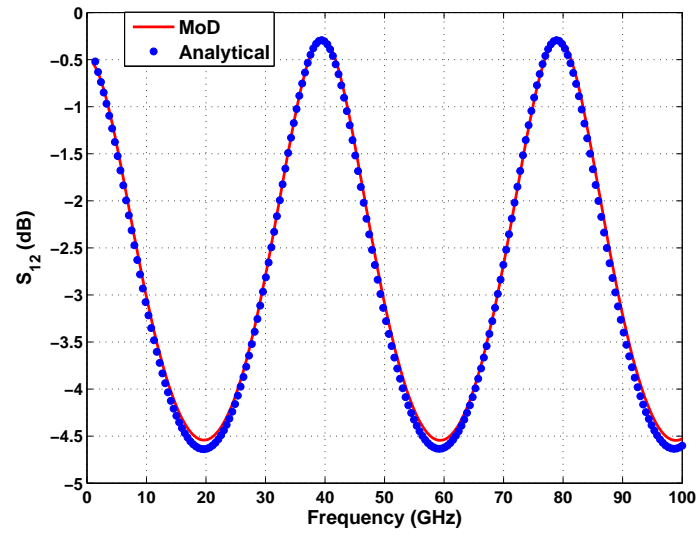


Figure 4.3: Transmission spectrum of dispersive slab at 60° angle of incidence

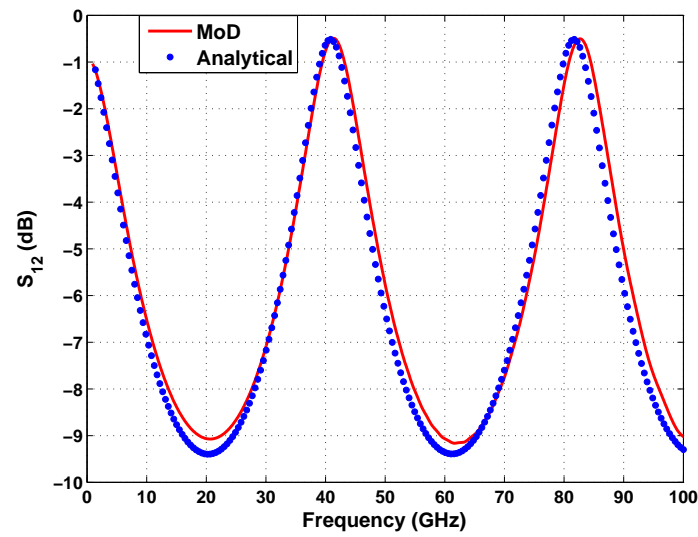


Figure 4.4: Transmission spectrum of dispersive slab at 75° angle of incidence

Chapter 5

Near Field Thermal Emission

If the temperature of a medium is not uniform, the emissivity definition defined by is no longer applicable. In order to calculate thermal emission from a medium with nonuniform temperature profile, Fluctuation Dissipation Theorem (FDT) must be used. FDT gives an expression for the correlation between thermal current densities at a point as a function of temperature, frequency and material properties at that point [51, 52]. Using FDT, Dyadic Green's Function (DGF) can be used to obtain the power density of the fluctuating electromagnetic fields. Thermal emission from simple geometries such as sphere [53], infinite cylinder [54] and layered media [55] had been done mostly for theoretical remote sensing studies. Lately, near field thermal emission using FDT-DGF methodology is applied to radiative heat transfer at nanoscale dimensions [52, 56, 57].

It is not possible to calculate thermal emission from calibration targets of pyramidal geometry using FDT-DGF method, because DGF is not known for such geometries. A stochastic numerical method may be the only solution. The objectives of this chapter are three fold: 1) Thermal emission due to fluctuating magnetic current density sources is not studied well in literature. 2) Calculation of near field thermal emission from simple geometries is essential for the validation of any numerical method, which can for solve thermal emission from arbitrary geometries. A thorough understanding of the theory and some experience is required to do novel work in this area 3) Explore the boundaries between classical radiative transfer theory and electromagnetic wave theory. An approach based on principle of detailed balance is attempted in [10]. This method which may be more simpler than either DGF-FDT or any stochastic numerical method should be revisited once

some solid results are obtained from the FDT-DGF method. Stochastic numerical methods which should be attempted include the Polynomial Chaos based methods such Wiener Chaos Expansion (WCE) [58] or Stochastic Finite Element Method (SFEM) [59]. As a first step, near field thermal emission from an infinite circular cylinder made of MF112 material is calculated using the FDT-DGF method. This is followed by development of a stochastic numerical method for calculation of the near field thermal emission from arbitrarily shaped 2D structures and validating the results with circular cylinder analytical results.

5.1 Fluctuation Dissipation Theorem

FDT for electric and magnetic current densities are given by the following equations.

$$\langle J_j(\vec{r}, \omega) J_k^*(\vec{r}', \omega') \rangle = \frac{\omega \epsilon_o \epsilon_r''}{\pi} \Theta(\omega, T) \delta(\omega - \omega') \delta(\vec{r} - \vec{r}') \delta_{jk} \quad (5.1)$$

$$\langle M_j(\vec{r}, \omega) M_k^*(\vec{r}', \omega') \rangle = \frac{\omega \mu_o \mu_r''}{\pi} \Theta(\omega, T) \delta(\omega - \omega') \delta(\vec{r} - \vec{r}') \delta_{jk} \quad (5.2)$$

$$\Theta(\omega, T) = \frac{\hbar \omega}{\exp\left(\frac{\hbar \omega}{k_B T}\right) - 1} \quad (5.3)$$

where j, k can be either x, y or z , $T(\vec{r})$ is the temperature in Kelvin, k_B is the Boltzmann's constant equivalent to 1.38×10^{-23} J/K, \hbar is the reduced Planck constant and other variables have the usual meaning. As per these equations, the current densities are spatially incoherent and orthogonal current density components are uncorrelated (e.g. J_x, J_y). The electric and magnetic current densities are uncorrelated [60].

$$\langle J_j(\vec{r}, \omega) M_k^*(\vec{r}', \omega') \rangle = 0 \quad (5.4)$$

5.2 Dyadic Green's Function

Dyadic Green Function (DGF) relates a vector source to a vector field. A very clear introduction to DGF is given in first four chapters of [61]. Therefore only important results without proofs are presented in this chapter. However it should be noted that exposure to material in [61] is required to understand this chapter. Let the source electric volume current density be given

by $\vec{J}(\vec{r}) = \frac{1}{i\omega\mu_o} [\delta(\vec{r} - \vec{r}')\hat{x} + \delta(\vec{r} - \vec{r}')\hat{y} + \delta(\vec{r} - \vec{r}')\hat{z}]$. Let $\vec{G}_{ex}(\vec{r}, \vec{r}')$, $\vec{G}_{mx}(\vec{r}, \vec{r}')$ be the electric field intensity and magnetic field intensity generated due to the source $\delta(\vec{r} - \vec{r}')\hat{x}$. Similarly, $\delta(\vec{r} - \vec{r}')\hat{y}$, $\delta(\vec{r} - \vec{r}')\hat{z}$ generates $\vec{G}_{ey}(\vec{r}, \vec{r}')$, $\vec{G}_{my}(\vec{r}, \vec{r}')$ and $\vec{G}_{ez}(\vec{r}, \vec{r}')$, $\vec{G}_{mz}(\vec{r}, \vec{r}')$ respectively. The electric DGF, $\overline{\overline{G}}_e(\vec{r}, \vec{r}')$ and magnetic DGF, $\overline{\overline{G}}_m(\vec{r}, \vec{r}')$ is then given by the following expressions.

$$\overline{\overline{G}}_e(\vec{r}, \vec{r}') = \vec{G}_{ex}(\vec{r}, \vec{r}')\hat{x} + \vec{G}_{ey}(\vec{r}, \vec{r}')\hat{y} + \vec{G}_{ez}(\vec{r}, \vec{r}')\hat{z} \quad (5.5)$$

$$\overline{\overline{G}}_m(\vec{r}, \vec{r}') = i\omega\mu_o [\vec{G}_{mx}(\vec{r}, \vec{r}')\hat{x} + \vec{G}_{my}(\vec{r}, \vec{r}')\hat{y} + \vec{G}_{mz}(\vec{r}, \vec{r}')\hat{z}] \quad (5.6)$$

As per Maxwell's equations, $\{\vec{G}_{ex}, \vec{G}_{ey}, \vec{G}_{ez}\}$ are related to $\{\vec{G}_{mx}, \vec{G}_{my}, \vec{G}_{mz}\}$ through the following equations.

$$\nabla \times \vec{G}_{ex} = i\omega\mu_o \vec{G}_{mx} \quad (5.7)$$

$$\nabla \times \vec{G}_{ey} = i\omega\mu_o \vec{G}_{my} \quad (5.8)$$

$$\nabla \times \vec{G}_{ez} = i\omega\mu_o \vec{G}_{mz} \quad (5.9)$$

$$\nabla \times \vec{G}_{mx} = \delta(\vec{r} - \vec{r}')\hat{x} - i\omega\varepsilon_o \vec{G}_{ex} \quad (5.10)$$

$$\nabla \times \vec{G}_{my} = \delta(\vec{r} - \vec{r}')\hat{y} - i\omega\varepsilon_o \vec{G}_{ey} \quad (5.11)$$

$$\nabla \times \vec{G}_{mz} = \delta(\vec{r} - \vec{r}')\hat{z} - i\omega\varepsilon_o \vec{G}_{ez} \quad (5.12)$$

By using the above equations, a ‘‘Maxwell's equation analogue’’ for DGFs can be obtained.

$$\nabla \times \overline{\overline{G}}_e(\vec{r}; \vec{r}') = \overline{\overline{G}}_m(\vec{r}; \vec{r}') \quad (5.13)$$

$$\nabla \times \overline{\overline{G}}_m(\vec{r}; \vec{r}') = \overline{\overline{I}}\delta(\vec{r} - \vec{r}') + k^2 \overline{\overline{G}}_e(\vec{r}; \vec{r}') \quad (5.14)$$

$$\nabla \cdot \overline{\overline{G}}_e(\vec{r}; \vec{r}') = -\frac{1}{k^2} \nabla \delta(\vec{r} - \vec{r}') \quad (5.15)$$

$$\nabla \cdot \overline{\overline{G}}_m(\vec{r}; \vec{r}') = 0 \quad (5.16)$$

where $\overline{\overline{I}} = \hat{x}\hat{x} + \hat{y}\hat{y} + \hat{z}\hat{z}$ is the unit dyadic. From the above equations, ‘‘Helmholtz equation analogue’’ for DGFs are obtained.

$$\nabla \times \nabla \times \overline{\overline{G}}_e - k^2 \overline{\overline{G}}_e = \overline{\overline{I}}\delta(\vec{r} - \vec{r}') \quad (5.17)$$

$$\nabla \times \nabla \times \overline{\overline{G}}_m - k^2 \overline{\overline{G}}_m = \nabla \times [\overline{\overline{I}}\delta(\vec{r} - \vec{r}')] \quad (5.18)$$

The equations (5.17),(5.17) are quite important in the sense that the derivation of DGF for various simple geometries starts with expressing the dyadic on the right hand side of these equations as an eigen function expansion of Vector Wave Functions (VWF). The electric field intensity $\vec{E}(\vec{r})$ due to an arbitrary source $\vec{J}(\vec{r}')$ can be defined by the principle of superposition.

$$\vec{E}(\vec{r}) = i\omega\mu_o \iiint_V \overline{\overline{G}}_{eo}(\vec{r}; \vec{r}') \cdot \vec{J}(\vec{r}') dv' \quad (5.19)$$

By applying Maxwell's equation to (5.19) and using (5.13), the expression for magnetic field intensity is obtained.

$$\vec{H}(\vec{r}) = \iiint_V \overline{\overline{G}}_{mo}(\vec{r}; \vec{r}') \cdot \vec{J}(\vec{r}') dv' \quad (5.20)$$

where $\overline{\overline{G}}_{eo}(\vec{r}; \vec{r}')$, $\overline{\overline{G}}_{mo}(\vec{r}; \vec{r}')$ are the free space DGFs given by

$$\overline{\overline{G}}_{eo}(\vec{r}; \vec{r}') = \left[\overline{\overline{I}} + \frac{\nabla\nabla}{k^2} \right] g_o(\vec{r}; \vec{r}') \quad (5.21)$$

$$\overline{\overline{G}}_{mo}(\vec{r}; \vec{r}') = \nabla \times \left[\overline{\overline{I}} g_o(\vec{r}; \vec{r}') \right] \quad (5.22)$$

$g_o(\vec{r}; \vec{r}')$ is the scalar free space Green's function, $g_o(\vec{r}; \vec{r}') = \frac{e^{ik|\vec{r}-\vec{r}'|}}{|\vec{r}-\vec{r}'|}$. When magnetic sources are also present, the electric and magnetic field intensities are given as follows.

$$\vec{E}(\vec{r}) = \iiint_V \left[i\omega\mu_o \overline{\overline{G}}_{eo}(\vec{r}; \vec{r}') \cdot \vec{J}(\vec{r}') - \overline{\overline{G}}_{mo}(\vec{r}; \vec{r}') \cdot \vec{M}(\vec{r}') \right] dv' \quad (5.23)$$

$$\vec{H}(\vec{r}) = \iiint_V \left[i\omega\varepsilon_o \overline{\overline{G}}_{eo}(\vec{r}; \vec{r}') \cdot \vec{M}(\vec{r}') + \overline{\overline{G}}_{mo}(\vec{r}; \vec{r}') \cdot \vec{J}(\vec{r}') \right] dv' \quad (5.24)$$

5.3 Formulation of stochastic electromagnetic power density

The quantity of interest in near field thermal emission problems is the stochastic electromagnetic power density given by the following equation.

$$\langle \vec{S}(\vec{r}) \rangle = \frac{1}{2} Re \left\{ \left\langle \vec{E}(\vec{r}) \times \vec{H}^*(\vec{r}) \right\rangle \right\} \quad (5.25)$$

We will first show how an expression for $\langle \vec{S}_z(\vec{r}) \rangle$ is derived. From (5.23),(5.24) expressions for $E_x(\vec{r}), E_y(\vec{r}), H_x^*(\vec{r}), H_y^*(\vec{r})$ relating it to source current densities are obtained.

$$E_x(\vec{r}) = \iiint_V \left[i\omega\mu_o \sum_{l=x,y,z} G_{eo}^{xl}(\vec{r}; \vec{r}') J_l(\vec{r}') - \sum_{n=x,y,z} G_{mo}^{xn}(\vec{r}; \vec{r}') M_n(\vec{r}') \right] dv' \quad (5.26)$$

$$E_y(\vec{r}) = \iiint_V \left[i\omega\mu_o \sum_{l=x,y,z} G_{eo}^{yl}(\vec{r}; \vec{r}') J_l(\vec{r}') - \sum_{n=x,y,z} G_{mo}^{yn}(\vec{r}; \vec{r}') M_n(\vec{r}') \right] dv' \quad (5.27)$$

$$H_x^*(\vec{r}) = \iiint_V \left[-i\omega\varepsilon_o \sum_{l=x,y,z} G_{eo}^{xl*}(\vec{r}; \vec{r}') M_l^*(\vec{r}') + \sum_{n=x,y,z} G_{mo}^{xn*}(\vec{r}; \vec{r}') J_n^*(\vec{r}') \right] dv' \quad (5.28)$$

$$H_y^*(\vec{r}) = \iiint_V \left[-i\omega\varepsilon_o \sum_{l=x,y,z} G_{eo}^{yl*}(\vec{r}; \vec{r}') M_l^*(\vec{r}') + \sum_{n=x,y,z} G_{mo}^{yn*}(\vec{r}; \vec{r}') J_n^*(\vec{r}') \right] dv' \quad (5.29)$$

$$\begin{aligned} \langle E_x(\vec{r})H_y^*(\vec{r}) - E_y(\vec{r})H_x^*(\vec{r}) \rangle &= \sum_{l=x,y,z} \sum_{n=x,y,z} \int_V dv' \int_V dv'' \left[i\omega\mu_o G_{eo}^{xl}(\vec{r}; \vec{r}') G_{mo}^{yn*}(\vec{r}; \vec{r}'') \langle J_l(\vec{r}') J_n^*(\vec{r}'') \rangle \right] \\ &\quad + \left[i\omega\varepsilon_o G_{mo}^{xn}(\vec{r}; \vec{r}') G_{eo}^{yl*}(\vec{r}; \vec{r}'') \langle M_n(\vec{r}') M_l^*(\vec{r}'') \rangle \right] \\ &\quad - \left[i\omega\mu_o G_{eo}^{yl}(\vec{r}; \vec{r}') G_{mo}^{xn*}(\vec{r}; \vec{r}'') \langle J_l(\vec{r}') J_n^*(\vec{r}'') \rangle \right] \\ &\quad - \left[i\omega\varepsilon_o G_{mo}^{yn}(\vec{r}; \vec{r}') G_{eo}^{xl*}(\vec{r}; \vec{r}'') \langle M_n(\vec{r}') M_l^*(\vec{r}'') \rangle \right] \end{aligned} \quad (5.30)$$

In deriving above equation, we have used the property (5.4) resulting in the removal of cross product terms (terms with cross-correlation of electric and magnetic current densities). The components of the DGF matrix are indicated by superscripts along with G_{eo} . For instance, G_{eo}^{yx} relates the field component E_y to J_x . By substituting the FDT expressions (5.1),(5.2) in (5.30), the double summation and double volume integral collapses to single summation over the coordinate directions and single volume integral over the source volume. This is attributed to the sifting property of $\delta(\vec{r}-\vec{r}')$ and δ_{jk} . The expression for $\langle S_z(\vec{r}; \omega) \rangle$ is given by equation (5.33). By inspection, expression for $\langle S_x(\vec{r}; \omega) \rangle$ and $\langle S_y(\vec{r}; \omega) \rangle$ are also obtained.

$$\begin{aligned} \langle S_x(\vec{r}; \omega) \rangle &= \frac{1}{2} Re \left\{ \frac{ik_o^2}{\pi} \sum_{n=x,y,z} \int_V dv' \left[G_{eo}^{yn}(\vec{r}; \vec{r}') G_{mo}^{zn*}(\vec{r}; \vec{r}') - G_{eo}^{zn}(\vec{r}; \vec{r}') G_{mo}^{yn*}(\vec{r}; \vec{r}') \right] \right. \\ &\quad \left. \varepsilon_r''(\vec{r}') \Theta(\omega, T(\vec{r}')) + \left[G_{mo}^{yn}(\vec{r}; \vec{r}') G_{eo}^{zn*}(\vec{r}; \vec{r}') - G_{mo}^{zn}(\vec{r}; \vec{r}') G_{eo}^{yn*}(\vec{r}; \vec{r}') \right] \mu_r''(\vec{r}') \Theta(\omega, T(\vec{r}')) \right\} \end{aligned} \quad (5.31)$$

$$\begin{aligned} \langle S_y(\vec{r}; \omega) \rangle &= \frac{1}{2} Re \left\{ \frac{ik_o^2}{\pi} \sum_{n=x,y,z} \int_V dv' \left[G_{eo}^{zn}(\vec{r}; \vec{r}') G_{mo}^{xn*}(\vec{r}; \vec{r}') - G_{eo}^{xn}(\vec{r}; \vec{r}') G_{mo}^{zn*}(\vec{r}; \vec{r}') \right] \right. \\ &\quad \left. \varepsilon_r''(\vec{r}') \Theta(\omega, T(\vec{r}')) + \left[G_{mo}^{zn}(\vec{r}; \vec{r}') G_{eo}^{xn*}(\vec{r}; \vec{r}') - G_{mo}^{xn}(\vec{r}; \vec{r}') G_{eo}^{zn*}(\vec{r}; \vec{r}') \right] \mu_r''(\vec{r}') \Theta(\omega, T(\vec{r}')) \right\} \end{aligned} \quad (5.32)$$

$$\langle S_z(\vec{r}; \omega) \rangle = \frac{1}{2} Re \left\{ \frac{ik_o^2}{\pi} \sum_{n=x,y,z} \int_V dv' \left[G_{eo}^{xn}(\vec{r}; \vec{r}') G_{mo}^{yn*}(\vec{r}; \vec{r}') - G_{eo}^{yn}(\vec{r}; \vec{r}') G_{mo}^{xn*}(\vec{r}; \vec{r}') \right] \right. \\ \left. \varepsilon_r''(\vec{r}') \Theta(\omega, T(\vec{r}')) + \left[G_{mo}^{xn}(\vec{r}; \vec{r}') G_{eo}^{yn*}(\vec{r}; \vec{r}') - G_{mo}^{yn}(\vec{r}; \vec{r}') G_{eo}^{xn*}(\vec{r}; \vec{r}') \right] \mu_r''(\vec{r}') \Theta(\omega, T(\vec{r}')) \right\} \quad (5.33)$$

5.4 Cylindrical Vector Wave Functions

Vector Wave Functions (VWF) are eigen functions of vector Helmholtz equation [61, 62]. In cylindrical coordinate system, VWFs are given by

$$\bar{M}_n(k_\rho, k_z; \bar{r}) = \nabla \times \hat{z} \psi_n(k_\rho, k_z; \bar{r}) \quad (5.34)$$

$$\bar{N}_n(k_\rho, k_z; \bar{r}) = \frac{1}{k} \nabla \times \nabla \times \hat{z} \psi_n(k_\rho, k_z; \bar{r}) \quad (5.35)$$

$$\bar{L}_n(k_\rho, k_z; \bar{r}) = \nabla \psi_n(k_\rho, k_z; \bar{r}) \quad (5.36)$$

where $\psi_n(k_\rho, k_z; \bar{r})$ is a solution to the scalar wave equation.

$$\nabla^2 \psi_n + k^2 \psi_n = 0 ; k = \sqrt{k_z^2 + k_\rho^2} \quad (5.37)$$

One possible solution to (5.37) is as follows.

$$\psi_n(k_\rho, k_z; \bar{r}) = J_n(k_\rho \rho) e^{+in\phi} e^{+ik_z z} \quad (5.38)$$

where $J_n(k_\rho \rho)$ is Bessel function of first kind. Instead of Bessel function of first kind, Neumann function and Hankel functions can also be solutions. The orthogonality condition for $\psi_n(k_\rho, k_z; \bar{r})$ given by (5.38) can be derived [62, 63] and is given by

$$\int_0^\infty \int_0^{2\pi} \int_{-\infty}^\infty \psi_n(k_\rho, k_z; \bar{r}) \psi_{-n'}(-k'_\rho, -k'_z; \bar{r}) \rho d\rho d\phi dz = (2\pi)^2 \delta_{nn'} \delta(k_z - k'_z) \frac{\delta(k_\rho - k'_\rho)}{k_\rho} \quad (5.39)$$

$\bar{M}_n(k_\rho, k_z; \bar{r})$, $\bar{N}_n(k_\rho, k_z; \bar{r})$ and $\bar{L}_n(k_\rho, k_z; \bar{r})$ satisfies the vector Helmholtz equation given by

$$\nabla \times \nabla \times \vec{F} - k^2 \vec{F} = 0 \quad (5.40)$$

where \vec{F} can be either $\bar{M}_n(k_\rho, k_z; \bar{r})$, $\bar{N}_n(k_\rho, k_z; \bar{r})$ or $\bar{L}_n(k_\rho, k_z; \bar{r})$. \bar{M} , \bar{N} are solenoidal VWFs and \bar{L} is an irrotational VWF. If \bar{M} is electric (magnetic) field, \bar{N} is magnetic (electric) field. By

substituting (5.38) in (5.34) and (5.35), expressions for $\bar{M}_n(k_\rho, k_z; \bar{r})$, $\bar{N}_n(k_\rho, k_z; \bar{r})$ are obtained.

$$\bar{M}_n(k_\rho, k_z; \bar{r}) = \left[\frac{in}{\rho} J_n(k_\rho \rho) \hat{\rho} - k_\rho J'_n(k_\rho \rho) \hat{\phi} \right] e^{in\phi} e^{ik_z z} \quad (5.41)$$

$$\bar{N}_n(k_\rho, k_z; \bar{r}) = \frac{1}{k} \left[ik_z k_\rho J'_n(k_\rho \rho) \hat{\rho} - \frac{nk_z}{\rho} J_n(k_\rho \rho) \hat{\phi} + k_\rho^2 J_n(k_\rho \rho) \hat{z} \right] e^{in\phi} e^{ik_z z} \quad (5.42)$$

where $J'_n(k_\rho \rho) = \frac{dJ_n(k_\rho \rho)}{d\rho}$. Since VWFs are eigen functions of vector wave equation, an arbitrary electric field satisfying vector wave equation can be expressed using eigen function expansion.

$$\begin{aligned} \bar{E}(\bar{r}) = & \sum_{n=-\infty}^{+\infty} \int_{-\infty}^{\infty} dk_z \int_0^{\infty} dk_\rho [a_n(k_\rho, k_z) \bar{M}_n(k_\rho, k_z; \bar{r}) + b_n(k_\rho, k_z) \bar{N}_n(k_\rho, k_z; \bar{r}) \\ & + c_n(k_\rho, k_z) \bar{L}_n(k_\rho, k_z; \bar{r})] \end{aligned} \quad (5.43)$$

the expansion coefficients is obtained by taking the inner product of $\bar{E}(\bar{r})$ with the corresponding VWF and using the orthogonality properties of VWF.

5.4.1 Orthogonality of VWFs

The orthogonality properties of VWFs are derived in several books [64, 62, 61, 63]. Since we will not be using \bar{L}_n , only the orthogonality of \bar{M}_n, \bar{N}_n are stated here.

$$\int_{-\infty}^{\infty} \int_0^{2\pi} \int_0^{\infty} \bar{M}_n(k_\rho, k_z; \bar{r}) \cdot \bar{N}_{n'}(k'_\rho, k'_z; \bar{r}) \rho d\rho d\phi dz = 0 \quad (5.44)$$

$$\int_{-\infty}^{\infty} \int_0^{2\pi} \int_0^{\infty} \bar{M}_n(k_\rho, k_z; \bar{r}) \cdot \bar{M}_{-n'}(-k'_\rho, -k'_z; \bar{r}) \rho d\rho d\phi dz = \quad (5.45)$$

$$(2\pi)^2 k_\rho \delta_{nn'} \delta(k_z - k'_z) \delta(k_\rho - k'_\rho) \quad (5.46)$$

$$\int_{-\infty}^{\infty} \int_0^{2\pi} \int_0^{\infty} \bar{N}_n(k_\rho, k_z; \bar{r}) \cdot \bar{N}_{-n'}(-k'_\rho, -k'_z; \bar{r}) \rho d\rho d\phi dz = \quad (5.47)$$

$$(2\pi)^2 k_\rho \delta_{nn'} \delta(k_z - k'_z) \delta(k_\rho - k'_\rho) \quad (5.48)$$

The above three properties can be derived by substituting (5.41),(5.42) in the left hand side of the above properties and using the following properties of Bessel function of first kind.

$$J_{-n}(x) = (-1)^n J_n(x) \quad (5.49)$$

$$J_n(-x) = (-1)^n J_n(x) \quad (5.50)$$

$$J_{-n}(-x) = J_n(x) \quad (5.51)$$

$$\int_0^\infty J_n(k_\rho \rho) J_n(k'_\rho \rho) \rho d\rho = \frac{\delta(k_\rho - k'_\rho)}{k_\rho} \quad (5.52)$$

$$J_n(x) = \frac{x}{2n} [J_{n-1}(x) + J_{n+1}(x)] \quad (5.53)$$

$$\frac{dJ_n}{dx} = \frac{1}{2} [J_{n-1}(x) - J_{n+1}(x)] \quad (5.54)$$

5.5 DGF for dielectric cylinder

The $\overline{\overline{G}}_{eo}$ in cylindrical coordinate system is given by the following two equations.

$$\overline{\overline{G}}_{eo}(\vec{r}; \vec{r}') = \frac{i}{8\pi} \int_{-\infty}^{\infty} dk_z \sum_{n=-\infty}^{+\infty} \frac{(-1)^n}{k_\rho^2} \left[\bar{M}_n^{(1)}(k_\rho, k_z; \bar{r}) \bar{M}_{-n}(k_\rho, -k_z; \vec{r}') + \bar{N}_n^{(1)}(k_\rho, k_z; \bar{r}) \bar{N}_{-n}(k_\rho, -k_z; \vec{r}') \right] ; \rho > \rho' \quad (5.55)$$

$$\overline{\overline{G}}_{eo}(\vec{r}; \vec{r}') = \frac{i}{8\pi} \int_{-\infty}^{\infty} dk_z \sum_{n=-\infty}^{+\infty} \frac{(-1)^n}{k_\rho^2} \left[\bar{M}_n(k_\rho, k_z; \bar{r}) \bar{M}_{-n}^{(1)}(k_\rho, -k_z; \vec{r}') + \bar{N}_n(k_\rho, k_z; \bar{r}) \bar{N}_{-n}^{(1)}(k_\rho, -k_z; \vec{r}') \right] ; \rho < \rho' \quad (5.56)$$

Superscript (1) denotes that Hankel function of first kind should be used instead of Bessel function of first kind in the definition of the VWFs. For the case of $\rho > \rho'$, the integrand in (5.55) can be written as the following matrix.

$$\begin{bmatrix} (M_{n,\rho}^{(1)} M'_{-n,\rho} + N_{n,\rho}^{(1)} N'_{-n,\rho}) \hat{\rho} \hat{\rho} & (M_{n,\rho}^{(1)} M'_{-n,\phi} + N_{n,\rho}^{(1)} N'_{-n,\phi}) \hat{\rho} \hat{\phi} & N_{n,\rho}^{(1)} N'_{-n,z} \hat{\rho} \hat{z} \\ (M_{n,\phi}^{(1)} M'_{-n,\rho} + N_{n,\phi}^{(1)} N'_{-n,\rho}) \hat{\phi} \hat{\rho} & (M_{n,\phi}^{(1)} M'_{-n,\phi} + N_{n,\phi}^{(1)} N'_{-n,\phi}) \hat{\phi} \hat{\phi} & N_{n,\phi}^{(1)} N'_{-n,z} \hat{\phi} \hat{z} \\ N_{n,z}^{(1)} N'_{-n,\rho} \hat{z} \hat{\rho} & N_{n,z}^{(1)} N'_{-n,\phi} \hat{z} \hat{\phi} & N_{n,z}^{(1)} N'_{-n,z} \hat{z} \hat{z} \end{bmatrix} \quad (5.57)$$

where $M_{n,\rho}^{(1)}$ represents the ρ component of $\bar{M}_n^{(1)}(k_\rho, k_z; \bar{r})$, $N'_{-n,\phi}$ represents the ϕ component of $\bar{N}_{-n}(k_\rho, -k_z; \vec{r}')$.

DGF for dielectric cylinder when source is outside the cylinder is given in [61]. But for thermal emission, we need the DGF when source is inside cylinder. The results for such a DGF is given in [54, 65]. However without deriving it from basic principles, it is not possible to extend it or even apply it for our problem. Let the free space outside a dielectric cylinder of radius a be noted by region 1 and the region inside the cylinder be region 2. By the method of scattering superposition [61]

$$\overline{\overline{G}}_e^{(22)}(\vec{r}; \vec{r}') = \overline{\overline{G}}_{eo}(\vec{r}; \vec{r}') + \overline{\overline{G}}_{es}^{(22)}(\vec{r}; \vec{r}') ; \rho \leq a \quad (5.58)$$

$$\overline{\overline{G}}_e^{(12)}(\vec{r}; \vec{r}') = \overline{\overline{G}}_{es}^{(12)}(\vec{r}; \vec{r}') ; \rho > a \quad (5.59)$$

where the first number in the superscript denotes the media in which the field point \vec{r} is located and the second number in the superscript denotes the media in which the source point \vec{r}' is located. Since in our case, the source is always inside the cylinder (i.e. region 2), the second number of the superscript is always 2. $\overline{\overline{G}}_{eo}(\vec{r}; \vec{r}')$ is given by equations (5.55) and (5.56). The expressions for $\overline{\overline{G}}_{es}^{(22)}(\vec{r}; \vec{r}')$ and $\overline{\overline{G}}_{es}^{(12)}(\vec{r}; \vec{r}')$ are as follows.

$$\begin{aligned} \overline{\overline{G}}_{es}^{(22)}(\vec{r}; \vec{r}') &= \frac{i}{8\pi} \int_{-\infty}^{+\infty} dk_z \sum_{n=-\infty}^{+\infty} \frac{(-1)^n}{\xi^2} [a(n, k_z) \vec{M}_n(\xi, k_z; \vec{r}) \vec{M}_{-n}(\xi, -k_z; \vec{r}') + \\ & b(n, k_z) \vec{N}_n(\xi, k_z; \vec{r}) \vec{M}_{-n}(\xi, -k_z; \vec{r}') + \\ & c(n, k_z) \vec{M}_n(\xi, k_z; \vec{r}) \vec{N}_{-n}(\xi, -k_z; \vec{r}') + \\ & d(n, k_z) \vec{N}_n(\xi, k_z; \vec{r}) \vec{N}_{-n}(\xi, -k_z; \vec{r}')] \end{aligned} \quad (5.60)$$

$$\begin{aligned} \overline{\overline{G}}_{es}^{(12)}(\vec{r}; \vec{r}') &= \frac{i}{8\pi} \int_{-\infty}^{+\infty} dk_z \sum_{n=-\infty}^{+\infty} \frac{(-1)^n}{\eta^2} [e(n, k_z) \vec{M}_n^{(1)}(\eta, k_z; \vec{r}) \vec{M}_{-n}(\eta, -k_z; \vec{r}') + \\ & f(n, k_z) \vec{N}_n^{(1)}(\eta, k_z; \vec{r}) \vec{M}_{-n}(\eta, -k_z; \vec{r}') + \\ & g(n, k_z) \vec{M}_n^{(1)}(\eta, k_z; \vec{r}) \vec{N}_{-n}(\eta, -k_z; \vec{r}') + \\ & h(n, k_z) \vec{N}_n^{(1)}(\eta, k_z; \vec{r}) \vec{N}_{-n}(\eta, -k_z; \vec{r}')] \end{aligned} \quad (5.61)$$

where $\eta = \sqrt{k_1^2 - k_z^2}$, $\xi = \sqrt{k_2^2 - k_z^2}$. The unknown coefficients $\{a, b, c, d, e, f, g, h\}$ are obtained by using the boundary conditions for electric DGF.

$$\hat{\rho} \times \left[\overline{\overline{G}}_{es}^{(12)}(\vec{r}; \vec{r}') \right] = \hat{\rho} \times \left[\overline{\overline{G}}_{eo}(\vec{r}; \vec{r}') + \overline{\overline{G}}_{es}^{(22)}(\vec{r}; \vec{r}') \right] \quad (5.62)$$

$$\hat{\rho} \times \left[\frac{\nabla \times \overline{\overline{G}}_{es}^{(12)}(\vec{r}; \vec{r}')}{\mu_1} \right] = \hat{\rho} \times \left[\frac{\nabla \times \overline{\overline{G}}_{eo}(\vec{r}; \vec{r}') + \nabla \times \overline{\overline{G}}_{es}^{(12)}(\vec{r}; \vec{r}')}{\mu_2} \right] \quad (5.63)$$

These boundary conditions are applied at the boundary of the cylinder i.e. $\vec{r} = (\rho = a, \phi, z)$. When using the above boundary conditions, the expression for $\overline{\overline{G}}_{eo}(\vec{r}; \vec{r}')$ when $\rho > \rho'$ should be used.

This is because all the sources are inside the boundary. The expression is repeated below.

$$\overline{\overline{G}}_{eo}(\vec{r}; \vec{r}') = \frac{i}{8\pi} \int_{-\infty}^{\infty} dk_z \sum_{n=-\infty}^{+\infty} \frac{(-1)^n}{\xi^2} \left[\overline{M}_n^{(1)}(\xi, k_z; \vec{r}) \overline{M}_{-n}(\xi, -k_z; \vec{r}') + \overline{N}_n^{(1)}(\xi, k_z; \vec{r}) \overline{N}_{-n}(\xi, -k_z; \vec{r}') \right]; \quad \rho > \rho' \quad (5.64)$$

The curl of the DGF can be obtained in a straight forward manner using fact that the VWFs M, N is proportional to the curl of N, M respectively. For instance, $\nabla \times \overline{\overline{G}}_{es}^{(12)}(\vec{r}; \vec{r}')$ is given by the following equation.

$$\begin{aligned} \nabla \times \overline{\overline{G}}_{es}^{(12)}(\vec{r}; \vec{r}') = \frac{ik_1}{8\pi} \int_{-\infty}^{+\infty} dk_z \sum_{n=-\infty}^{+\infty} \frac{(-1)^n}{\eta^2} & [e(n, k_z) \vec{N}_n^{(1)}(\eta, k_z; \vec{r}) \vec{M}_{-n}(\eta, -k_z; \vec{r}') + \\ & f(n, k_z) \vec{M}_n^{(1)}(\eta, k_z; \vec{r}) \vec{M}_{-n}(\eta, -k_z; \vec{r}') + \\ & g(n, k_z) \vec{N}_n^{(1)}(\eta, k_z; \vec{r}) \vec{N}_{-n}(\eta, -k_z; \vec{r}') + \\ & h(n, k_z) \vec{M}_n^{(1)}(\eta, k_z; \vec{r}) \vec{N}_{-n}(\eta, -k_z; \vec{r}')] \end{aligned} \quad (5.65)$$

By comparing the above equation with (5.61), the presence of k_1 and the swapping of M, N with N, M can be seen. The coefficients can be obtained by solving the system of equations $Ax = b$ obtained by applying the boundary conditions.

$$A = \begin{bmatrix} -J'_n(\xi a) & \frac{-nJ_n(\xi a)}{a\xi^2} & 0 & 0 & H_n^{(1)'}(\eta a) & \frac{nk_z}{ak_1\eta^2} H_n^{(1)}(\eta a) & 0 & 0 \\ 0 & -\frac{J_n(\xi a)}{k_2} & 0 & 0 & 0 & \frac{H_n^{(1)}(\eta a)}{k_1} & 0 & 0 \\ 0 & 0 & -J'_n(\xi a) & -\frac{nk_z}{ak_2\xi^2} J_n(\xi a) & 0 & 0 & H_n^{(1)'}(\eta a) & \frac{nk_z}{ak_1\eta^2} H_n^{(1)}(\eta a) \\ 0 & 0 & 0 & -\frac{J_n(\xi a)}{k_2} & 0 & 0 & 0 & \frac{H_n^{(1)}(\eta a)}{k_1} \\ \frac{nk_z}{a\mu_{r2}\xi^2} J_n(\xi a) & \frac{k_2}{\mu_{r2}} J'_n(\xi a) & 0 & 0 & \frac{-nk_z}{a\eta^2} H_n^{(1)}(\eta a) & -k_1 H_n^{(1)'}(\eta a) & 0 & 0 \\ \frac{J_n(\xi a)}{\mu_{r2}} & 0 & 0 & 0 & -k_1 H_n^{(1)}(\eta a) & 0 & 0 & 0 \\ 0 & 0 & \frac{-nk_z}{a\mu_{r2}\xi^2} J_n(\xi a) & \frac{-k_2}{\mu_{r2}} J'_n(\xi a) & 0 & 0 & \frac{nk_z}{a\eta^2} H_n^{(1)}(\eta a) & k_1 H_n^{(1)'}(\eta a) \\ 0 & 0 & \frac{J_n(\xi a)}{\mu_{r2}} & 0 & 0 & 0 & -H_n^{(1)}(\eta a) & 0 \end{bmatrix} \quad (5.66)$$

$$x = \begin{bmatrix} a(n, k_z) \\ b(n, k_z) \\ c(n, k_z) \\ d(n, k_z) \\ e(n, k_z) \\ f(n, k_z) \\ g(n, k_z) \\ h(n, k_z) \end{bmatrix} = b = \begin{bmatrix} H_n^{(1)'}(\xi a) \\ 0 \\ \frac{nk_z}{ak_2} H_n^{(1)}(\xi a) \\ \frac{\xi^2}{k_2} H_n^{(1)}(\xi a) \\ -\frac{nk_z}{a\mu_{r2}\xi^2} H_n^{(1)}(\xi a) \\ -\frac{k_2}{\mu_{r2}} H_n^{(1)}(\xi a) \\ \frac{k_2}{\mu_{r2}} H_n^{(1)'}(\xi a) \\ 0 \end{bmatrix} \quad (5.67)$$

This is similar to the matrix equation given in [61], but that is for the case of source outside the cylinder.

Chapter 6

Fast Jacobian Mie Library for Terrestrial Hydrometeors

This work presents an approach for the fast, accurate computation of several useful Mie-based parameters for homogenous, spherical, liquid water and ice hydrometeor distributions over a wide range of frequencies, mean hydrometeor diameters, and physical temperatures as occur in the terrestrial atmosphere. The absorption coefficient, scattering coefficient, backscattering coefficient, and phase asymmetry parameters are cast into functions of three independent variables: frequency, temperature and mean diameter. An exponential drop size distribution with a constant fractional volume of 10^{-6} is used to model polydispersed hydrometeors. The ranges used for frequency, temperature and mean diameter are $[1, 1000]$ GHz, $[-50, +50]^{\circ}$ C and $[0.002, 20]$ mm respectively. The functions are then sampled on a logarithmic grid. Trivariate cubic spline interpolation using non uniform B-splines is then used to efficiently represent these three dimensional functions in a compact library. By using this method, four important criteria are achieved: 1) fast random computability of any of these parameters given the values of frequency, temperature and mean diameter, 2) minimal memory usage by storage of only B-spline coefficients, 3) representation of parameters using well behaved functional forms amenable to analytical differentiation for evaluation of Jacobians or alternatively for higher accuracy, B-spline coefficients calculated using true Jacobian values can be used, and 4) negligibly small and bounded error over the entire domain of the library. These procedures results in considerable acceleration of microwave radiative transfer simulations across a broad frequency spectrum, as demonstrated in calculations for both scattering and non-scattering atmospheres. The methods discussed can also be applied to other geophysical problems

requiring rapid calculation of series-based functions of several independent variables, where the function evaluation is a time consuming process, and maximum error bounds are critical.

6.1 Introduction

Numerical radiative transfer (RT) calculations are essential for understanding and assimilating brightness temperature measurements made at various microwave frequencies and geographical locations. RT model inversions performed using these measurements can yield vertical temperature and water vapor density profiles of the atmosphere, which can be used in numerical weather prediction and climate forecasting [66, 67, 68]. Alternately, brightness temperature measurements can also be directly assimilated into numerical weather models [69]. Efficient numerical weather forecasting applications require particularly fast scattering-based radiative transfer (RT) simulations. One of the processes that imparts a high computational burden for hydrometeor laden atmospheres is the calculation of hydrometeor absorption and scattering coefficients and the phase asymmetry parameter. The excessive computational overhead is a result of the nested summations required in the calculation of the Mie efficiencies and the subsequent numerical integration of the Mie efficiencies over the hydrometeor drop size distribution. The large number of times that such calculations are required in radiative transfer modeling suggests that library look-up techniques can provide significant computational efficiencies provided that library error can be bounded. Reflectivity modeling for meteorological weather radar is similarly well understood [70]. In the Rayleigh regime, the backscattering coefficient is related to the reflectivity factor Z , which in turn depends on the precipitation rate. As a part of this work, fast libraries for liquid and ice hydrometeor backscattering coefficients are also developed.

RT theory describes the interaction of radiation with matter by taking into the consideration the effects of the atmospheric absorption, emission and scattering due to cloud, fog, snow etc on electromagnetic radiation. It has been thoroughly discussed in numerous references [71, 72, 73]. One of the first steps in RT modeling is the computation of the absorption vector, extinction matrix and phase matrix at each point within the medium of interest [66]. For plane parallel atmospheric

models, this step entails calculations at each of many (typically 50-100) vertical levels of the atmosphere. The atmospheric medium consists of gaseous absorbing constituents such as oxygen, water vapor, ozone, and nitrogen. In addition to these gases the atmosphere may also contain suspended or falling liquid or frozen water particles in the troposphere and lower stratosphere. Hydrometeors can absorb, emit, and scatter radiation at microwave frequencies. Hydrometeors can be either rain drops, ice crystals, snowflakes, graupel or hail. They are in general nonspherical in shape. For instance, rain drops are slightly oblate shaped [74, 75]. Ice crystals are either hexagonal or irregular in shape. However for small hydrometeor dimensions, spherical drop assumption is accurate. In this work, we have used the assumption of modelling hydrometeors as either liquid water or solid ice spheres. Furthermore, in this work only homogenous liquid water or ice hydrometeors are considered. In reality, many hydrometeors are a multiphase mixture of air, ice and water [76, 77]. A future extension of this work will deal with the extinction coefficients of nonspherical hydrometeors. T-matrix method instead of Lorentz-Mie theory need to be used for this purpose [78]. The problem of applying an iterative numerical radiative transfer model to hydrometeor - laden atmospheres has been addressed in [66], within which hydrometeors are modeled as dielectric spheres. The analytical solution to the absorption and scattering of electromagnetic waves by a sphere of arbitrary radius, permittivity and permeability was provided by Mie [79, 64, 25], from whose theory the absorption efficiency, scattering efficiency, backscattering efficiency, and phase function asymmetry of a single dielectric sphere can be calculated. However, expressions for the above parameters are in the form of infinite summations, where each term contains spherical Bessel functions requiring software evaluation. Accordingly, doubly nested summations are required to evaluate either the cross-sectional efficiencies or the phase function asymmetry for a single hydrometeor. Owing to hydrometeors of varying radii, clouds are modeled by a polydispersed distribution of hydrometeors. The hydrometeor coefficients of a polydispersed cloud is obtained by the integration of the corresponding efficiencies multiplied by the sphere cross-sectional area over the entire hydrometeor distribution. Numerical quadrature is used to perform this integration, resulting in a third level of nesting. Due to the need for accuracy, the resulting numerical integration often requires many

tens of thousands of elementary calculations for each atmospheric spatial point. Depending on the hydrometeor mean electrical size, this computational burden is comparable to or greater than that of the vertical RT quadrature itself.

This paper presents an efficient approach based on cubic B-spline interpolation for fast, accurate calculation of the Mie hydrometeor coefficients and phase asymmetry parameter for exponential size distributions of terrestrial hydrometeors. B-splines are standard for representing curves and surfaces in computer graphics and computer aided design [80, 81]. Recently, they have been used for volume reconstruction of arbitrarily dimensioned data. For the present Mie application, lookup tables (LUT) for the absorption coefficient, scattering coefficient, backscattering coefficient, and phase matrix asymmetry parameter for both liquid and ice hydrometeor distributions are generated. These LUTs are three dimensional arrays coding the values of these products as a function of the three independent variables of temperature, average hydrometeor size, and frequency over a wide range of these parameters. In total, eight LUTs corresponding to four different products for two types of hydrometeors (liquid and frozen) are generated. Spline interpolation is applied on any of these eight LUTs to evaluate the corresponding products. The method results in considerable acceleration of microwave radiative transfer simulations across a broad frequency spectrum and fast calculation of radar reflectivity for weather radar data assimilation. We demonstrate the effectiveness of this approach by comparing radiative transfer simulations using the B-spline library to the conventional series approach within scattering and non-scattering atmospheres. These inter-comparisons confirm acceptable reconstruction accuracy for most relevant problems in terrestrial radiative transfer and radar studies.

6.2 Mie theory

The electromagnetic absorption and scattering properties of a single sphere are described by the absorption efficiency η_a , scattering efficiency η_s and backscattering efficiency η_b [25, 2]. Let S_i (Wm^{-2}) be the average power density of the electromagnetic wave incident on the sphere, and P_a (W), P_s (W) and P_b (W) be the absorbed, scattered and backscattered power respectively. P_a , P_s

and P_b are related to S_i through the absorption cross section σ_a (m^2), scattering cross section σ_s (m^2) and backscattering cross section σ_b (m^2). They are given by the following relations,

$$\sigma_a = \frac{P_a}{S_i} ; \sigma_s = \frac{P_s}{S_i} ; \sigma_b = \frac{P_b}{S_i} \quad (6.1)$$

The absorption efficiency η_a , scattering efficiency η_s and backscattering efficiency η_b are defined as the ratio of the corresponding electromagnetic cross-sections to the physical cross-section of a sphere of radius a ,

$$\eta_a = \frac{\sigma_a}{\pi a^2} ; \eta_s = \frac{\sigma_s}{\pi a^2} ; \eta_b = \frac{\sigma_b}{\pi a^2} \quad (6.2)$$

The extinction cross-section σ_e and extinction efficiency η_e are similarly given by the sum of the corresponding absorption and scattering quantities,

$$\sigma_e = \sigma_a + \sigma_s ; \eta_e = \eta_a + \eta_s \quad (6.3)$$

The η_e , η_s and η_b for a homogenous dielectric sphere of arbitrary radius and refractive index is given by Mie theory as,

$$\eta_e(x, m) = \frac{2}{x^2} \sum_{n=1}^{\infty} (2n+1) \text{Re} \{a_n + b_n\} \quad (6.4)$$

$$\eta_s(x, m) = \frac{2}{x^2} \sum_{n=1}^{\infty} (2n+1) \{|a_n|^2 + |b_n|^2\} \quad (6.5)$$

$$\eta_b(x, m) = \frac{1}{x^2} \left| \sum_{n=1}^{\infty} (-1)^n (2n+1) (a_n - b_n) \right| \quad (6.6)$$

In (4-6), x is the size parameter given by $x \equiv \frac{2\pi a}{\lambda}$ and a_n, b_n are the Mie coefficients, which are generally complex and calculated as follows,

$$a_n = \frac{m^2 j_n(mx) [x j_n(x)]' - j_n(x) [m x j_n(mx)]'}{m^2 j_n(mx) [x h_n^1(x)]' - h_n^1(x) [m x j_n(mx)]'} \quad (6.7)$$

$$b_n = \frac{j_n(mx) [x j_n(x)]' - j_n(x) [m x j_n(mx)]'}{j_n(mx) [x h_n^1(x)]' - h_n^1(x) [m x j_n(mx)]'} \quad (6.8)$$

where $j_n(x)$, $h_n^1(x)$ are spherical Bessel and Hankel functions of first kind and order n respectively.

In the above equations $m(f, T) \equiv \frac{n_s(f, T)}{n_b(f, T)}$ is the relative complex refractive index of the material of the sphere with respect to the background medium, n_s is the refractive index of the sphere and

n_b is the refractive index of the background medium (usually air). The refractive indices n_s, n_b are both functions of frequency f and temperature T . In these general expressions both the sphere and background are assumed to be non-magnetic. In practice the summations in (7-8) are truncated at a finite number of terms. The maximum number of terms is commonly taken to be the next integer closest to $x + 4x^{\frac{1}{3}} + 2$ [25]. The phase function asymmetry parameter G defines the relative proportion of energy scattered in the forward versus backward directions [66]. The Mie phase function asymmetry for a single spherical scatterer is,

$$G = \frac{4}{x^2 \eta_s(x, m)} \sum_{n=1}^{\infty} \left[\frac{n(n+2)}{n+1} \text{Re} \{a_n^* a_{n+1} + b_n^* b_{n+1}\} + \frac{2n+1}{n(n+1)} \text{Re} \{a_n^* b_n\} \right] \quad (6.9)$$

For $G = 1$, there is only scattering in the forward direction and $G > 0$ denotes a preferential scattering in the forward versus backward direction. Similarly, for $G = -1$ there is scattering only in the backward direction and $G < 0$ denotes a preferential scattering backwards. In (4-6,9), the value of the size parameter x determines the number of significant terms in the series, and as a result the scattering regime of the particle. For electrically small spheres with $x \ll 1$, a single term is usually sufficient. This is the Rayleigh scattering approximation [82]. For electrically large spheres with $x \gg 1$ geometrical optics, physical optics, or ray tracing, approximations can often be used effectively. Nonetheless, in this work the truncated Mie summations are exclusively used without further approximation.

6.3 Look-up table calculation

The radius of hydrometeors varies from $\sim 1\mu\text{m}$ for haze, fog, and small cloud particles up to about $\sim 10\text{ mm}$ for large frozen particles such as graupel, snow and small hail. The statistical characterization of the hydrometeor particle size for a polydispersed cloud is given by a drop size distribution, $n(D)$ [2, 66]. A general functional form of $n(D)$ ($\text{mm}^{-1}\text{m}^{-3}$) is the modified gamma distribution given by,

$$n(D) = N_0 (\Lambda D)^P e^{-(\Lambda D)^Q} \quad (6.10)$$

where $n(D) dD$ is the number of particles per unit volume with diameters in the range $[D, D + dD]$ (mm) and N_0 ($\text{mm}^{-1}\text{m}^{-3}$), Λ (mm^{-1}), P and Q are distribution parameters. By considering $n(D)$ given by (10) as a scaled probability density function, closed form expressions for important statistical quantities such as mean diameter, diameter variance, particle number density, and fractional volume can be derived [2, 66]. For example, the mean diameter $\langle D \rangle$ (mm) and fractional volume of water f_v are given by,

$$\langle D \rangle = \frac{1}{\Lambda} \frac{\Gamma\left(\frac{P+2}{Q}\right)}{\Gamma\left(\frac{P+1}{Q}\right)} \quad (6.11)$$

$$f_v = \frac{10^{-9}\pi N_0}{6\Lambda^4 Q} \Gamma\left(\frac{P+4}{Q}\right) \quad (6.12)$$

where $\Gamma(\cdot)$ is the gamma function. The aggregate absorption, scattering and backscattering coefficients in (Npm^{-1}) can be computed as,

$$\kappa_\alpha(f, T) = \frac{\pi}{4} \int_0^\infty D^2 n(D) \eta_\alpha\left(\frac{\pi D}{\lambda}, m(f, T)\right) dD \quad (6.13)$$

where $\alpha = a, s, b$. Similarly, the aggregate phase function asymmetry $g(f, T)$ for a polydispersion of spherical hydrometeors is given by,

$$g(f, T) = \frac{\int_0^\infty D^2 n(D) \eta_s\left(\frac{\pi D}{\lambda}, m\right) G\left(\frac{\pi D}{\lambda}, m\right) dD}{\int_0^\infty D^2 n(D) \eta_s\left(\frac{\pi D}{\lambda}, m\right) dD} \quad (6.14)$$

Most of the commonly used drop size distributions for precipitation such as Marshall - Palmer (MP), Laws and Parsons, and Sekhon - Srivastava (SS) are of the exponential form [2, 66]. Accordingly, to avoid the problem of cataloguing a four-fold infinity of size distributions we limit this study to exponential distributions for which $P = 0$ and $Q = 1$. Exponential distribution can be used to model major hydrometeor particles such as rain, snow, graupel and hail [83]. In this case $\langle D \rangle = \frac{1}{\Lambda}$. Although the upper limit of integration in (13,14) is infinite, the practical upper limit on the drop diameter is about 6 mm [84]. However, we have used a conservative upper limit of about 15 mean particle diameters due to the exponential decay factor. By $n = 15$, it is noted that the relative error in the integral becomes bounded by 9.6×10^{-4} times the real value, viz.:

$$\frac{\int_0^{n\langle D \rangle} D^2 e^{-\frac{D}{\langle D \rangle}} dD}{\int_0^\infty D^2 e^{-\frac{D}{\langle D \rangle}} dD} = 1 - e^{-n} [0.5n^2 + n + 1] \quad (6.15)$$

A simple empirical sensitivity analysis was performed to confirm the above mentioned upper limit. For 1000 random values of $(f, \langle D \rangle, T)$, κ_b was calculated for liquid hydrometeors for values of n ranging from 5 to 25 in steps of 5. The relative error percentage was calculated for each increment of n . The averages of these error percentages tend to converge to a very small value with each increment. The average percentage errors for the increments 5-10, 10-15, 15-20, 20-25 are 14.5%, 0.31%, 0.023% and 0.021% respectively. This confirms that for $n > 15$, there is hardly any contribution to the coefficient value. In this work, we have used mean diameters ranging from $2 \mu\text{m}$ to 20 mm to cover the range of terrestrial hydrometeors encountered in realistic precipitation models. The constant N_0 for an exponential drop size distribution is a function of $\langle D \rangle$, and can be calculated using equations (11,12). The average fractional volume of liquid or frozen precipitation rarely exceeds 5×10^{-6} . Since N_0 is directly proportional to fractional volume, f_v , a constant value $f_v = 10^{-6}$, corresponding to 1 gm^{-3} of liquid water was used in this work. In this case, $N_0 = \frac{1000}{\pi \langle D \rangle^4}$, where $\langle D \rangle$ is in mm. The coefficients for a different value of fractional volume can be obtained by scaling the results according to the actual density of hydrometeors. Therefore, equations (13,14) reduce to,

$$\kappa_\alpha(f, \langle D \rangle, T) \approx \frac{\pi 10^{-6}}{4} \int_0^{15 \langle D \rangle} D^2 N_0(\langle D \rangle) e^{-\frac{D}{\langle D \rangle}} \eta_\alpha\left(\frac{\pi D}{\lambda}, m\right) dD \quad (6.16)$$

$$g(f, \langle D \rangle, T) \approx \frac{\int_0^{15 \langle D \rangle} D^2 N_0(\langle D \rangle) e^{-\frac{D}{\langle D \rangle}} \eta_s\left(\frac{\pi D}{\lambda}, m\right) G\left(\frac{\pi D}{\lambda}, m\right) dD}{\int_0^{15 \langle D \rangle} D^2 N_0(\langle D \rangle) e^{-\frac{D}{\langle D \rangle}} \eta_s\left(\frac{\pi D}{\lambda}, m\right) dD} \quad (6.17)$$

where D is in mm and $\kappa_\alpha(f, \langle D \rangle, T)$ is in Npm^{-1} . The above products are functions of three independent variables: frequency, temperature, and the mean diameter of the polydispersion. Since the Mie efficiencies are a function of the refractive index of the sphere, the complex dielectric constants of liquid water and ice as a function of frequency and temperature are also implicitly required.

Each product LUT is a three dimensional array that stores the values of $\kappa_a, \kappa_s, \kappa_b, g$ at discrete values of the independent variable triplet $(f, \langle D \rangle, T)$. The ranges used for each independent variable are : $f \in [1, 1000]$ GHz, $\langle D \rangle \in [0.002, 20]$ mm and $T \in [-50, +50]^\circ\text{C}$. For ice hydromete-

ors, $T \in [-50, 0]^\circ\text{C}$ is the temperature range used. Due to the large range of mean diameter and frequency, a logarithmic sampling grid was used for these two variables. Ray's model was used for the dielectric constant of pure water at microwave frequencies [85]. The dielectric constant of ice at microwave frequencies was obtained from Warren [86]. Linear interpolation was used to obtain values of the dielectric constant at frequencies that are not listed in [86]. The Mie efficiencies are calculated using routines provided by Maetzler [87]. These routines are based on Mie formulations in [25], but stable for size parameters up to ~ 1000 . Once the Mie efficiencies $(\eta_a, \eta_s, \eta_b, G)$ and N_0 were calculated, adaptive Simpson's quadrature was used for the numerical evaluation of the distribution integrals (16,17). The surface plots of hydrometeor absorption, scattering, backscattering coefficients and phase asymmetry parameter for both liquid and frozen hydrometeors at $T = 0^\circ\text{C}$ is shown in Fig. (6.6)-(6.6). These plots can be considered as slices from the product LUTs at a constant temperature.

6.4 B-spline interpolation

Spline functions are piecewise polynomials on subintervals that are joined together with prescribed continuity conditions [80]. A spline function of order k consists of piecewise polynomials of maximum degree $k - 1$. Therefore a spline of order 1 is composed of piecewise constants, a spline of order 2 consists of piecewise linear polynomials, etc. A univariate spline function $S(x)$ can be represented in the piecewise polynomial form as,

$$S(x) = P_i(x); x \in [\xi_i, \xi_{i+1}) \quad (6.18)$$

where $\{\xi_i\}_{i=1}^{l+1}$ are a strictly increasing sequence of $l + 1$ break (or tie) points of $S(x)$. A spline function of order k has the following continuity conditions at its breaks.

$$\begin{aligned} P_i(\xi_{i+1}) &= P_{i+1}(\xi_{i+1}); i \in [1, l - 1] \\ P_i^{(n)}(\xi_{i+1}) &= P_{i+1}^{(n)}(\xi_{i+1}); i \in [1, l - 1] \\ &; n = 1, 2, \dots, k - 2 \end{aligned} \quad (6.19)$$

where $P_i^{(n)}(x)$ stands for the n^{th} derivative of $P_i(x)$. The spline interpolation problem can be stated as follows: given the values of a function at break points, $\{g(\xi_i)\}_{i=1}^{l+1}$, the spline function $S(x)$ needs to be determined such that $S(\xi_i) = g(\xi_i); i \in [1, l+1]$. Splines of order 4 (cubic splines) are twice continuously differentiable at the break points and most commonly used in practice. For a cubic spline, each polynomial section would be of degree 3, i.e. $P_i(x) = c_{i3}(x - \xi_i)^3 + c_{i2}(x - \xi_i)^2 + c_{i1}(x - \xi_i) + c_{i0}$. Given the values of the function g at the break points, the continuity conditions, and boundary conditions (usually the values of the first and second derivatives of $S(x)$ at the first and last break points), the coefficients of each piecewise polynomial can be uniquely determined. Simple tridiagonal linear systems of equations are solved to obtain $\{c_{ij}; i \in [1, l], j \in [0, 3]\}$.

An alternate representation of the spline function is known as the B-form representation [80, 81, 88]. This representation is based on the Curry-Schoenberg theorem, which is stated as follows: All the spline functions of order k and break sequence $\{\xi_i\}_{i=1}^{l+1}$ form a linear space denoted by $\Pi_{k,\xi}$. To represent a function using B-splines we choose a strictly non-decreasing sequence of points $\{\tau_i\}_{i=1}^{l+k+1}$ called the knot sequence. The knot sequences need not coincide with the break points. In the B-form representation, the spline function is expressed as a weighted superposition of basis functions called B-splines (or, basis splines). For example, the B-spline of order 1 is given by,

$$B_i^1(x) = \begin{cases} 1 & ; \quad x \in [\tau_i, \tau_{i+1}) \\ 0 & ; \quad \textit{otherwise} \end{cases} \quad (6.20)$$

B-splines of higher order can be determined from lower order B-splines using the Cox-de Boor recurrence relation [80],

$$B_i^k(x) = \left(\frac{x - \tau_i}{\tau_{i+k-1} - \tau_i} \right) B_i^{k-1}(x) + \left(\frac{\tau_{i+k} - x}{\tau_{i+k} - \tau_{i+1}} \right) B_{i+1}^{k-1}(x) \quad (6.21)$$

Using the Cox - de Boor relation, the B-spline of order 4 (or, cubic B-spline) can be obtained and is given by (6.25). The B-splines $B_1^k, B_2^k, \dots, B_{l+1}^k$ defined on the knot sequence $\{\tau_i\}_{i=1}^{l+k+1}$ form the basis for the spline space, $\Pi_{k,\xi}$. It can be shown that the B-form representation of the spline

$$B_i^4(x) = \begin{cases} \frac{(x-\tau_i)^3}{(\tau_{i+3}-\tau_i)(\tau_{i+2}-\tau_i)(\tau_{i+1}-\tau_i)} & ; x \in [\tau_i, \tau_{i+1}) \\ \frac{(x-\tau_i)(x-\tau_i)(\tau_{i+2}-x)}{(\tau_{i+3}-\tau_i)(\tau_{i+2}-\tau_i)(\tau_{i+2}-\tau_{i+1})} + \frac{(x-\tau_i)(\tau_{i+3}-x)(x-\tau_{i+1})}{(\tau_{i+3}-\tau_i)(\tau_{i+3}-\tau_{i+1})(\tau_{i+2}-\tau_{i+1})} \dots & ; x \in [\tau_{i+1}, \tau_{i+2}) \\ \frac{(\tau_{i+4}-x)(x-\tau_{i+1})(\tau_{i+3}-x)}{(\tau_{i+4}-\tau_{i+1})(\tau_{i+3}-\tau_{i+1})(\tau_{i+3}-\tau_{i+2})} + \frac{(\tau_{i+4}-x)(\tau_{i+4}-x)(x-\tau_{i+2})}{(\tau_{i+4}-\tau_{i+1})(\tau_{i+4}-\tau_{i+2})(\tau_{i+3}-\tau_{i+2})} \dots & ; x \in [\tau_{i+2}, \tau_{i+3}) \\ \frac{(x-\tau_i)(x-\tau_{i+3})(x-\tau_{i+3})}{(\tau_{i+3}-\tau_i)(\tau_{i+3}-\tau_{i+1})} \frac{(\tau_{i+3}-\tau_{i+2})}{3} & ; x \in [\tau_{i+3}, \tau_{i+4}) \\ \frac{-(x-\tau_{i+4})}{(\tau_{i+4}-\tau_{i+1})(\tau_{i+4}-\tau_{i+2})(\tau_{i+4}-\tau_{i+3})} & ; x \in [\tau_{i+3}, \tau_{i+4}) \end{cases} \quad (6.25)$$

function $S(x)$ of order k is given by,

$$S(x) = \sum_{i=1}^{l+1} \alpha_i B_i^k(x); x \in [\xi_i, \xi_{i+1}) \quad (6.22)$$

where $\{\alpha_i\}_{i=1}^{l+1}$ are the B-spline coefficients. Importantly, B-splines have local support. Hence the i^{th} B-spline of order k , $B_i^k(x) = 0; x \notin [\tau_i, \tau_{i+k})$. For example, cubic B-splines have support between five successive knots. The local support of B-splines results in computational advantages for the B-form representation over the piecewise polynomial representation of a spline function. A good choice of knot sequence $\{\tau_i\}_{i=1}^{l+5}$ for cubic B-spline interpolation can be determined from the breaks $\{\xi_i\}_{i=1}^{l+1}$ as follows,

$$\begin{aligned} \tau_1 &= \tau_2 = \tau_3 = \tau_4 = \xi_1 \\ \tau_{l+5} &= \tau_{l+4} = \tau_{l+3} = \tau_{l+2} = \xi_{l+1} \\ \tau_i &= \frac{\xi_{i-3} + \xi_{i-2} + \xi_{i-1}}{3} ; 5 \leq i \leq l+1 \end{aligned} \quad (6.23)$$

Extension of spline function theory to multiple variables can be obtained by tensor product construction of univariate B-splines. In this case a trivariate cubic spline function $F(x, y, z)$ is represented in B-form as,

$$F(x, y, z) = \sum_{i=1}^{N_x} \sum_{j=1}^{N_y} \sum_{m=1}^{N_z} \alpha_{ijm} B_i^4(x) B_j^4(y) B_m^4(z) \quad (6.24)$$

In this work, the three dimensional function F can be any of the following eight functions: absorption coefficient, scattering coefficient, backscattering coefficient, or phase asymmetry for liquid water and ice hydrometeors, with the independent variables being frequency, temperature

and mean diameter,

$$F(f, T, \langle D \rangle) = \sum_{i=1}^{N_f} \sum_{j=1}^{N_T} \sum_{m=1}^{N_{\langle D \rangle}} \alpha_{ijm} B_i^A(f) B_j^A(T) B_m^A(\langle D \rangle) \quad (6.26)$$

The α_{ijm} in (26) are the stored Mie B-spline coefficients, and MATLAB Spline toolbox was used for the calculation of these coefficients. The generation of B - spline coefficients is a one time process that does not need to be repeated. The code for reconstructing the Mie products is a straightforward implementation of (26).

6.5 Results and discussion

In this section we discuss the five main aspects of this work - memory and overhead reduction, radiation Jacobian, reconstruction error, computational savings, and radiative transfer simulations. The simulations and related software codes were written in the MATLAB environment.

6.5.1 Memory and Computational Overhead Reduction

To generate the Mie LUTs the mean diameter and frequency ranges were logarithmically gridded with 200 and 60 points, respectively, and the temperature range was gridded linearly with an interval of 2.5°C. The eight normalized Mie products were sampled at these grid points and stored as eight LUTs. The total memory usage of these LUTs is ~ 10.6 MB. The product LUTs are subsequently used for spline interpolation (i.e., piecewise polynomial spline interpolation). The eight product LUTs were converted to eight corresponding B-spline LUTs which contain the B-spline coefficients. From (26), it can be inferred that the size of B-spline LUTs is nearly the same as the size of corresponding product LUTs. The disadvantage of using piecewise polynomial spline interpolation is that the values stored in the product LUTs need to be converted to the piecewise spline polynomial coefficients. This procedure is not localized to a small subset of intervals, thus resulting in the required calculation of all the polynomial coefficients for each interpolation. Hence there is a fixed overhead time required for the evaluation of all the piecewise polynomial coefficients irrespective of the number of product values that need to be interpolated. In the trivariate case, if

the number of values in an individual product LUT is N , the total number of piecewise polynomial coefficients will be $4^3N = 64N$. Therefore in our case, assuming one product LUT is ~ 1.25 MB in size, a RAM usage of 80 MB will be required when performing the piecewise polynomial spline interpolation. This high memory usage also limits the possibility of storing the piecewise polynomial coefficients as LUTs. The fixed overhead and high memory usage thus obviates many of the advantages of conventional splines.

In contrast, B-form interpolation is both localized to a small subset of intervals, requires a large fixed overhead time to calculate the α_{ijm} coefficients, but does not require the temporary storage of large number of spline coefficients. However, when sufficiently large numbers of products needs to be evaluated by interpolation, the spline interpolation has an advantage over B-spline method. This computational advantage is due to the fact that for the spline interpolation, once all the piecewise polynomial coefficients are calculated, the evaluation of these piecewise functions is extremely rapid compared to the three nested summations required for B-splines, as given by (26).

6.5.2 Radiation Jacobian

The radiation Jacobian is defined as the derivative of the radiance field with respect to any electromagnetic parameter of the atmosphere [89]. Therefore, the derivative of any coefficient with respect to (for example) the mean diameter can be evaluated by differentiation of (6.16), (6.17) using Leibnitz rule for differentiation under integral sign. Surface plots of the radiation Jacobian of different Mie products for ice and liquid hydrometeors at $T = 0^\circ\text{C}$ calculated using analytical differentiation are shown in Fig. (6.11)-(6.18). One possible way to evaluate Jacobian is facilitated by analytical differentiation of the cubic B-spline. Therefore, the derivative of any coefficient with respect to (for example) the mean diameter can possibly be evaluated as follows,

$$\frac{dF(f, T, \langle D \rangle)}{d\langle D \rangle} = \sum_{i=1}^{N_f} \sum_{j=1}^{N_T} \sum_{m=1}^{N_{\langle D \rangle}} \alpha_{ijm} B_i^A(f) B_j^A(T) \frac{dB_m^A(\langle D \rangle)}{d\langle D \rangle} \quad (6.27)$$

However, this procedure cannot produce accurate estimates consistently. This is because the B-spline coefficients were calculated using the product coefficients. A better approach is to generate

B-spline coefficients using analytically calculated Jacobian values in the $(f, \langle D \rangle, T)$ grid and then use these B-spline coefficients, β_{ijm} in (6.26). Error analysis was performed by comparing the B-spline evaluated coefficient values with analytically obtained values for 20000 random $(f, \langle D \rangle, T)$ points. This was done for κ_a, κ_s for both liquid and ice hydrometeors. The mean fractional error in all the four cases were of the order of 10^{-4} . The maximum fractional error was less than 0.1 for all the cases except liquid κ_a for which it was 1.8. However, the method given by (27), can be used in a 2D case, where we are only concerned about radiometric frequencies, thereby reducing the 3D LUT to a 2D LUT and hence allowing for much finer discretization along the $\langle D \rangle$ and T axes.

6.5.3 Computational Savings

In this section, the improvement in computational speed using the fast Mie library is discussed. In Fig. 6.1, the logarithmic ratio of the B-spline interpolation time to the exact calculation time using the full Mie series is illustrated for liquid hydrometeor absorption at $T = 0^\circ\text{C}$. This time ratio will be nearly the same for all other products and at any temperature. From the Fig. 6.1, it can be seen that there is considerable speedup when the hydrometeors are large in diameter compared to the wavelength. In this case, the time consuming step of integration over the drop-size distribution is obviated. Usually radiative transfer simulations are performed at the channel frequencies of the remote sensing instrument. In such a case, the B-spline coefficients for only the instrument's channel frequencies need be stored. This reduced storage necessitates only two dimensional interpolation, which is faster than the three dimensional interpolation. Equivalently, for the same amount of memory, in the two dimensional case a finer gridding can be used to provide extreme accuracy.

6.5.4 Reconstruction Error Analysis

In this section, we derive an expression for the maximum error that can be allowed for the reconstructed values of Mie products, and use this to determine the overall library accuracy. Any error in the absorption or scattering coefficient will result in an associated error in the computed

brightness temperature. By using the condition, that the maximum allowed brightness temperature error is bounded by a prescribed value we can derive expressions for the maximum error bound on the coefficients. We use the approach in [90] to derive the absorption coefficient incremental weighting function (IWF) for downwelling radiation. The IWF describes the relationship between infinitesimal variations in any atmospheric parameter and the downwelling brightness temperature. The downwelling brightness temperature observed at height h and zenith angle θ for a non-scattering plane-parallel atmosphere is,

$$\begin{aligned}
T_{DB}(h, \theta, \nu) = & T_B^b(T_{CB}, \nu) \exp \left[- \int_h^\infty \kappa_a^o(z) \sec \theta dz \right] \\
& + \int_h^\infty T_B^b(T(z), \nu) \sec \theta \kappa_a^o(z) \\
& \exp \left[- \int_h^z \kappa_a^o(z') \sec \theta dz' \right] dz
\end{aligned} \tag{6.28}$$

In (28), ν denotes the frequency and T_{CB} , $\kappa_a^o(z)$, $T(z)$ and $T_B^b(\cdot)$ represents the cosmic background temperature, absorption coefficient as a function of altitude, physical temperature as a function of altitude and blackbody brightness temperature function respectively. The downwelling brightness temperature is due to the cosmic background radiation and the thermal emission, both attenuated by the atmospheric absorption. If $\delta\kappa_a(z)$ is the variation in the absorption coefficient profile, the corresponding variation in the observed downwelling brightness temperature, $T_{DB}(h, \theta, \nu)$ denoted by δT_{DB} is given by,

$$\delta T_{DB} = \int_h^\infty W_{\kappa_a}^\downarrow(z, \theta, \nu) \delta\kappa_a(z) dz \tag{6.29}$$

where $W_{\kappa_a}^\downarrow(z, \theta, \nu)$ is the absorption IWF for downwelling brightness temperature. An approximate expression for $W_{\kappa_a}^\downarrow(z, \theta, \nu)$ is derived by substituting $\kappa_a^o(z) + \delta\kappa_a(z)$ in (28) and subtracting the

original expression for $T_{DB}(h, \theta, \nu)$,

$$\begin{aligned}
W_{\kappa_a}^\downarrow(z, \theta, \nu) = & -T_B^b(T_{CB}, \nu) \sec \theta \exp \left[-\int_h^\infty \kappa_a^o(z) \sec \theta dz \right] \\
& + T_B^b(T(z), \nu) \sec \theta \exp \left[-\int_h^z \kappa_a^o(z') \sec \theta dz' \right] \\
& - \sec^2 \theta \int_z^\infty T_B^b(T(z'), \nu) \kappa_a^o(z') dz' \\
& \exp \left[-\int_h^{z'} \kappa_a^o(z'') \sec \theta dz'' \right]
\end{aligned} \tag{6.30}$$

By applying the following assumptions to (30), the IWF can be simplified: 1) the observation point is assumed to be on the ground i.e., $h = 0$. 2) $\kappa_a(z) = 0; z > H$, where $H = 8$ km is the atmospheric scale height. 3) $\kappa_a^o(z) = \kappa_a^o$ i.e. a constant atmospheric absorption coefficient profile is assumed, and 4) the thermodynamic temperature, $T(z) = T$ is constant. The simplified IWF then becomes,

$$\begin{aligned}
W_{\kappa_a}^\downarrow(z, \theta, \nu) = & \sec \theta \exp[-\kappa_a^o \sec \theta H] \\
& \left(T_B^b(T, \nu) - T_B^b(T_{CB}, \nu) \right)
\end{aligned} \tag{6.31}$$

The simplified expression for δT_{DB} is obtained by substituting (31) in (29),

$$\begin{aligned}
\delta T_{DB} = & \delta \kappa_a H \sec \theta \exp[-\kappa_a^o \sec \theta H] \\
& \left(T_B^b(T, \nu) - T_B^b(T_{CB}, \nu) \right)
\end{aligned} \tag{6.32}$$

Since we are concerned about the maximum possible value of the brightness temperature deviation, $|\delta T_{DB}|_{max}$, (32) is maximized by choosing an extreme atmospheric temperature of $T = 325$ K. In this case, $|\delta T_{DB}|_{max}$ becomes,

$$|\delta T_{DB}|_{max} = 2.56 \times 10^6 \delta \kappa_a \sec \theta \exp[-\kappa_a^o \sec \theta H] \tag{6.33}$$

Constraining the maximum brightness temperature error by 10 mK yields,

$$|\delta T_{DB}|_{max} \leq 0.01K \Rightarrow \frac{\delta \kappa_o}{\kappa_a^o} \leq \frac{3.9 \times 10^{-9}}{\kappa_a^o \sec \theta \exp[-\kappa_a^o \sec \theta H]} \tag{6.34}$$

For a constant κ_a^o , the expression on the right side of (34) can be minimized with respect to θ , thus resulting in an expression for maximum allowable fractional error in the reconstructed value of the absorption coefficient,

$$\left| \frac{\delta \kappa_a}{\kappa_a^o} \right|_{max} = \begin{cases} 8.48 \times 10^{-5} & ; \kappa_a^o < \frac{1}{H} \\ \frac{3.9 \times 10^{-9} \exp \kappa_a^o H}{\kappa_a^o} & ; \kappa_a^o > \frac{1}{H} \end{cases} \quad (6.35)$$

It should be noted that the assumptions we have used to derive this expression are conservative, and not normally encountered in practice.

The model in (35) can be used to evaluate the accuracy of the spline reconstructed absorption coefficient values. In Fig. 6.2, the fractional error in reconstructed values of liquid and ice hydrometeor absorption are plotted against the corresponding absorption coefficients for 2000 random values of $(f, \langle D \rangle, T)$ and fractional volume. The maximum allowable fractional error in the absorption coefficient for brightness temperature errors less than 0.01 K and 0.1 K are also plotted. It can be seen that for the prescribed level of library discretization the liquid absorption coefficient fractional error is always well below the 0.01 K error bound. However the ice absorption coefficient fractional error is higher than the water absorption coefficient, but still smaller than $\sim 0.1K$. This error is attributed to the ice dielectric model that was used in this work [86], which has discontinuities in its derivatives. The reconstruction error for ice hydrometeors can be reduced further by either finer sampling or by smoothing the ice dielectric constant model before calculating the ice extinction coefficients.

6.5.5 Radiative Transfer Simulations

In this section, the results of RT simulations performed to verify the accuracy of the developed library is presented. These results confirm the applicability of the library for RT computations. The atmosphere used for the RT simulations was the 1976 version of U.S. Standard Atmosphere, with water vapor density in each level corresponding to 50% of the saturation vapor density at the level pressure and temperature. Surface reflectivity is computed at a particular frequency by assuming an ocean surface with salinity 3.5% and using the Ray model [85] and Klein and Swift

model [91] for dielectric constant and conductivity respectively. The base atmosphere was modified by inserting liquid and ice hydrometeors over 1 – 10 km [66]. The simulations were carried out in the frequency range [1, 1000] GHz in steps of 1 GHz.

In the first simulation, multiple scattering was ignored by setting the extinction coefficient of each level to the sum of absorption coefficient and scattering coefficient. The relative difference in the top of the atmosphere brightness temperature for a downward looking radiometer was obtained as a function of frequency. The relative difference corresponds to the difference between the cases when real Mie series value and spline interpolated values of extinction coefficients were used. The maximum and the mean value for this relative difference are $1.15 \times 10^{-3}\%$ and $3 \times 10^{-5}\%$ respectively. In the second RT simulation, multiple scattering was taken into account by using Henyey-Greenstein phase function and a scattering based RT model [66]. The maximum and mean value of the relative difference are $9.72 \times 10^{-2}\%$ and $7.21 \times 10^{-3}\%$ respectively.

6.6 Conclusions

In this work, the absorption coefficient, scattering coefficient, backscattering coefficient, and phase asymmetry parameter of both liquid and ice spherical, homogenous hydrometeors as a function of frequency, temperature and mean diameter of the hydrometeor distribution is represented in a piecewise functional form using trivariate cubic B-splines. By using this method, it was possible to achieve significant computation time reduction for calculating the extinction parameters and phase asymmetry parameter, especially for large hydrometeors and at high microwave frequencies. Furthermore, the reconstruction error that is caused by the spline interpolation is negligible enough to preclude any adverse impact on the accuracy of radiative transfer simulations for most relevant terrestrial applications. The memory requirement for this fast library is around 10.6 MB for all eight products. The library further supports evaluation of the radiation Jacobian by either the rapid analytical differentiation of the B-spline basis functions or for higher accuracy, B-spline coefficients can be calculated by using true Jacobian values. The reconstruction time, memory usage can be further decreased with improvement in accuracy by storing the B-spline coefficients only

at frequencies of interest where radiative transfer simulation is required. The cubic B-spline based approximation method can be applied to other geophysical problems, where function evaluation is a time consuming process and reconstruction accuracy is critical. Future work will include applying these techniques to nonspherical or even multi-phase hydrometeors.

Acknowledgment

The authors are grateful to Prof. Gregory Beylkin of University of Colorado, Boulder for valuable suggestions regarding B-splines and Prof. Christian Maetzler for providing the code to calculate Mie efficiencies. The authors would also like to thank Dr. Bjorn Lambrigsten of NASA Jet Propulsion Laboratory for his support of this study. This work was funded by award number 1358415 from the NASA Jet Propulsion Laboratory.

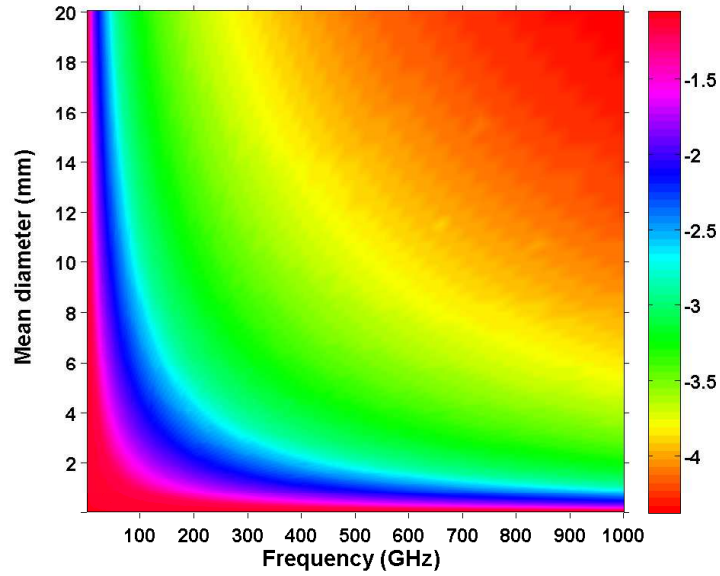


Figure 6.1: Logarithmic ratio of the calculation time for B-spline interpolation to that for exact Mie series calculation of polydispersed liquid hydrometeor absorption coefficients. An exponential drop-size distribution, temperature $T = 0^\circ\text{C}$ and fractional volume $f = 10^{-6}$ are assumed

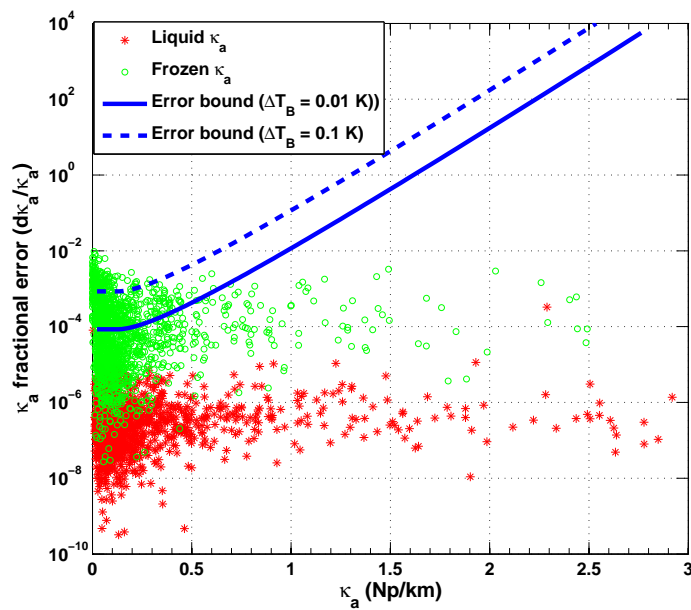


Figure 6.2: Fractional error in reconstructed values of liquid and ice hydrometeor absorption coefficient vs. liquid and ice hydrometeor absorption values. The maximum allowable error bounds for $T_{DB} = 0.01\text{K}$ and 0.1K are shown.

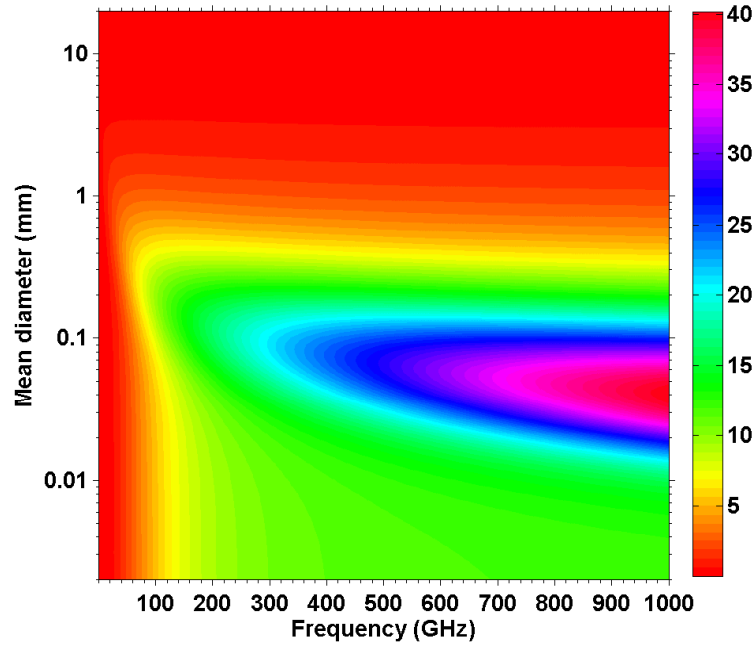


Figure 6.3: Liquid hydrometeor κ_a (dB/km) vs. $(f, \langle D \rangle)$ at $T = 0^\circ C$

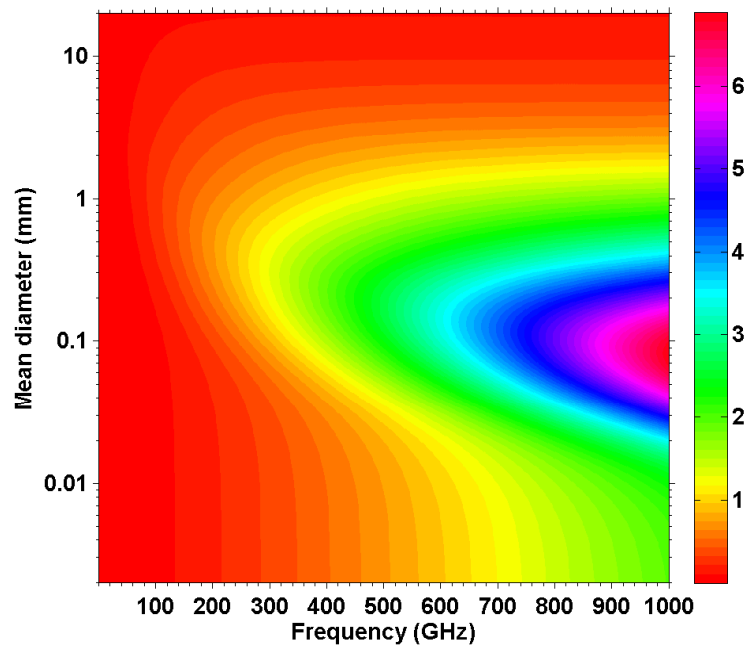


Figure 6.4: Ice hydrometeor κ_a (dB/km) vs. $(f, \langle D \rangle)$ at $T = 0^\circ C$

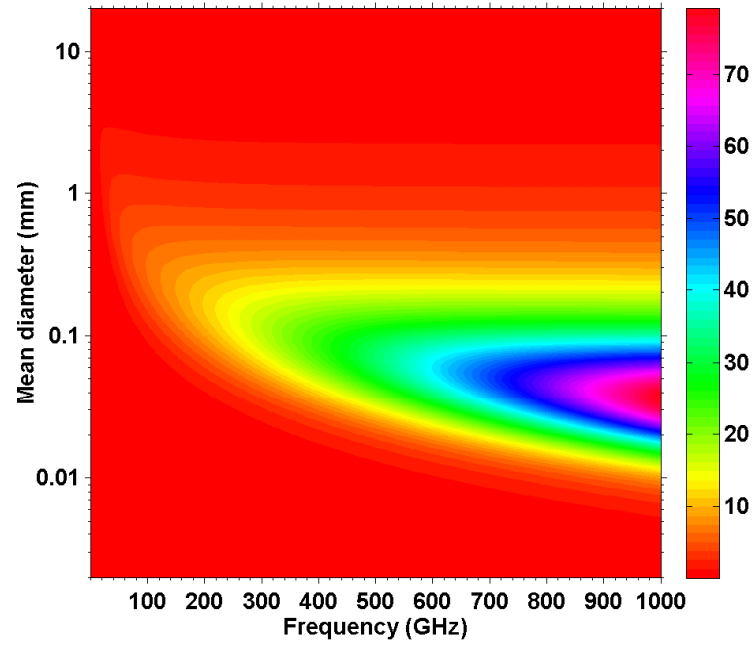


Figure 6.5: Liquid hydrometeor κ_s (dB/km) vs. $(f, \langle D \rangle)$ at $T = 0^\circ C$

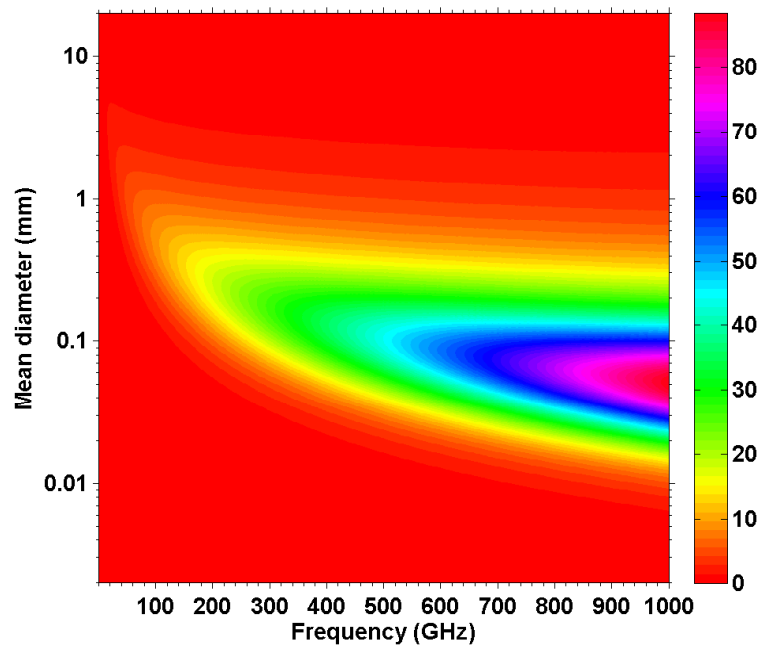


Figure 6.6: Ice hydrometeor κ_s (dB/km) vs. $(f, \langle D \rangle)$ at $T = 0^\circ C$

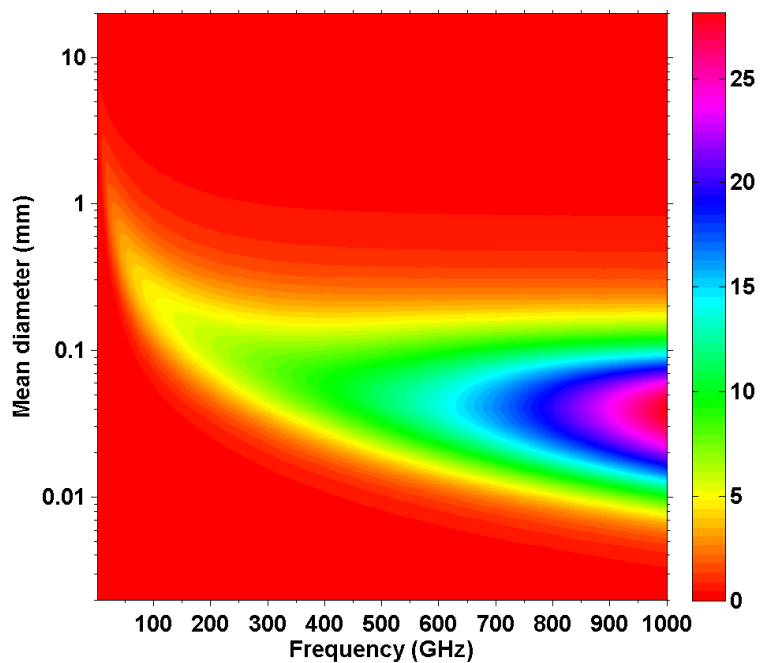


Figure 6.7: Liquid hydrometeor κ_b (dB/km) vs. $(f, \langle D \rangle)$ at $T = 0^\circ C$

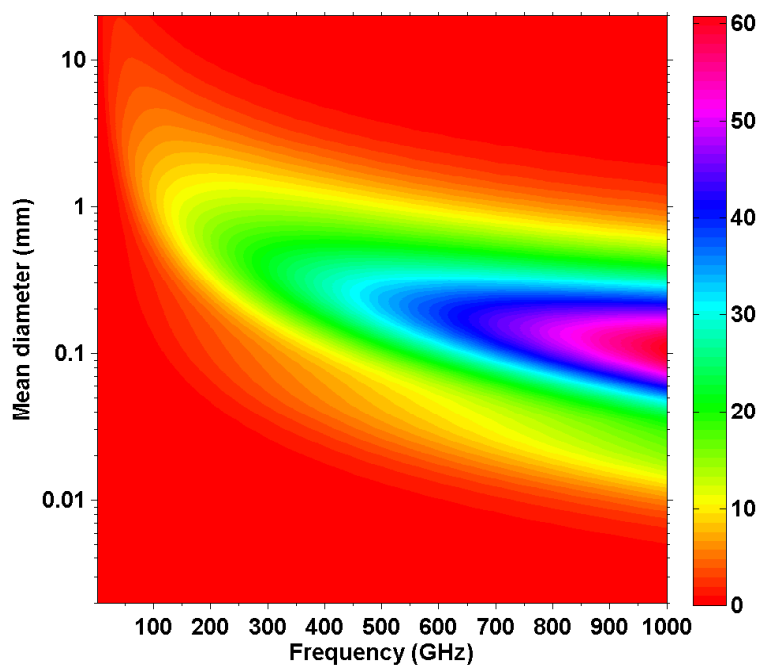


Figure 6.8: Ice hydrometeor κ_b (dB/km) vs. $(f, \langle D \rangle)$ at $T = 0^\circ C$

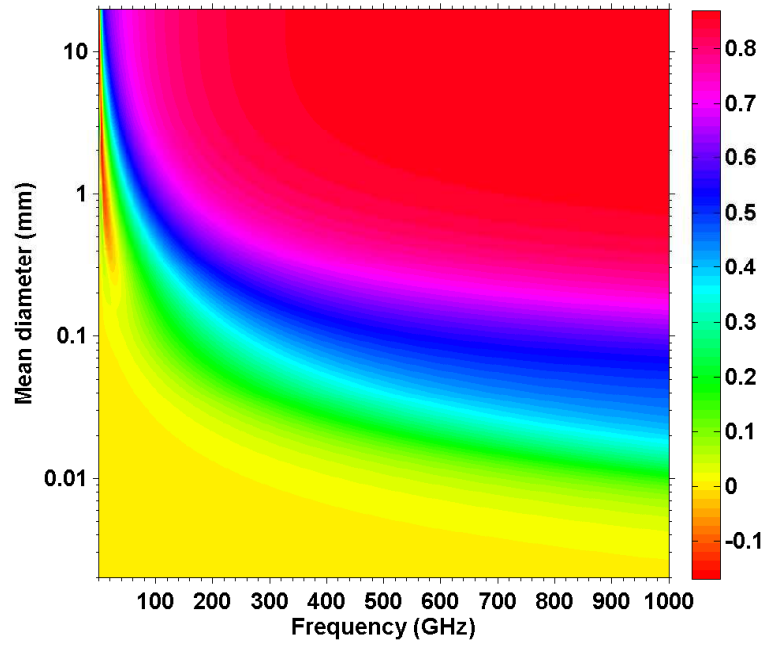


Figure 6.9: Liquid hydrometeor g vs. $(f, \langle D \rangle)$ at $T = 0^\circ\text{C}$

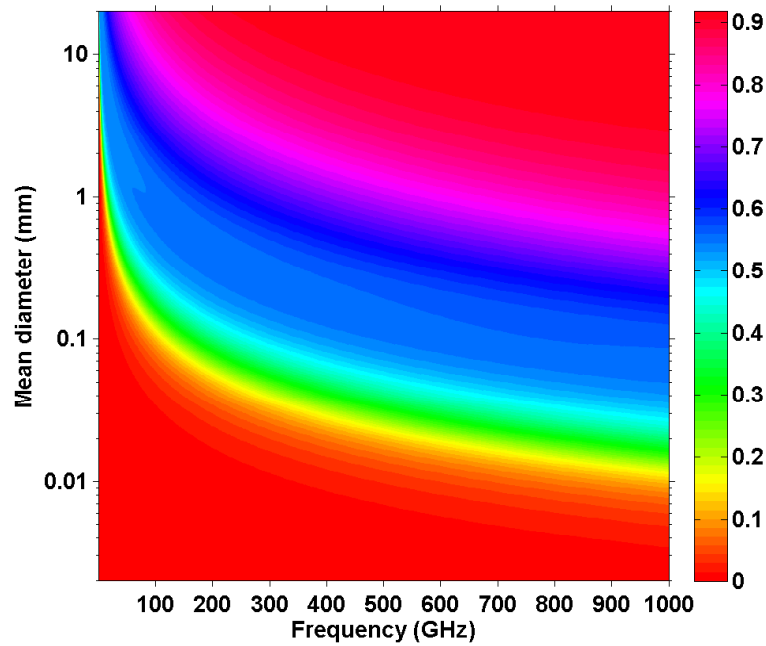


Figure 6.10: Ice hydrometeor g vs. $(f, \langle D \rangle)$ at $T = 0^\circ\text{C}$

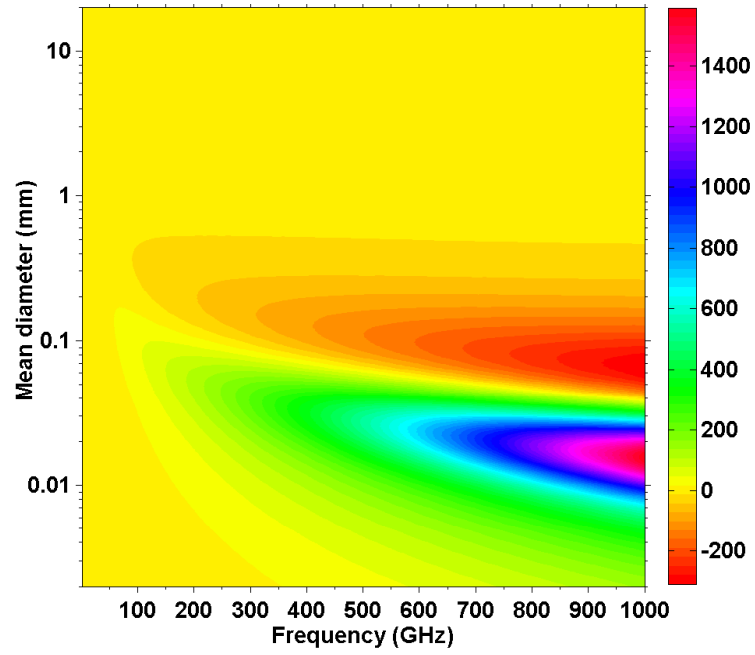


Figure 6.11: Liquid hydrometeor $\frac{d\kappa_a}{d\langle D \rangle}$ vs. $(f, \langle D \rangle)$ at $T = 0^\circ\text{C}$

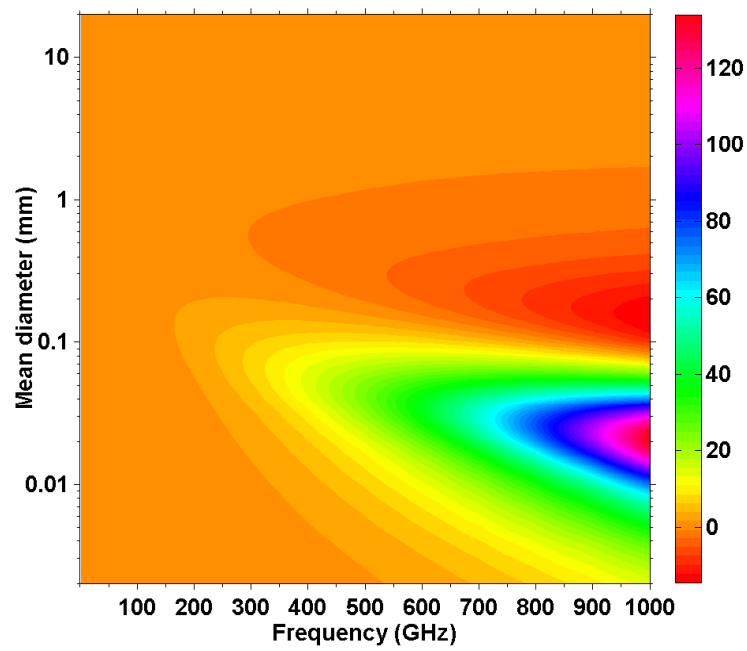


Figure 6.12: Ice hydrometeor $\frac{d\kappa_a}{d\langle D \rangle}$ vs. $(f, \langle D \rangle)$ at $T = 0^\circ\text{C}$

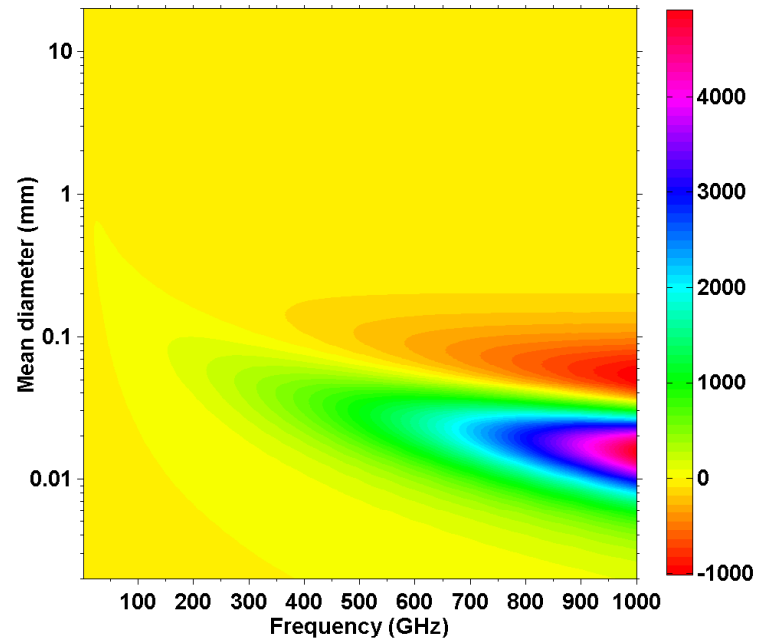


Figure 6.13: Liquid hydrometeor $\frac{d\kappa_s}{d\langle D \rangle}$ vs. $(f, \langle D \rangle)$ at $T = 0^\circ\text{C}$

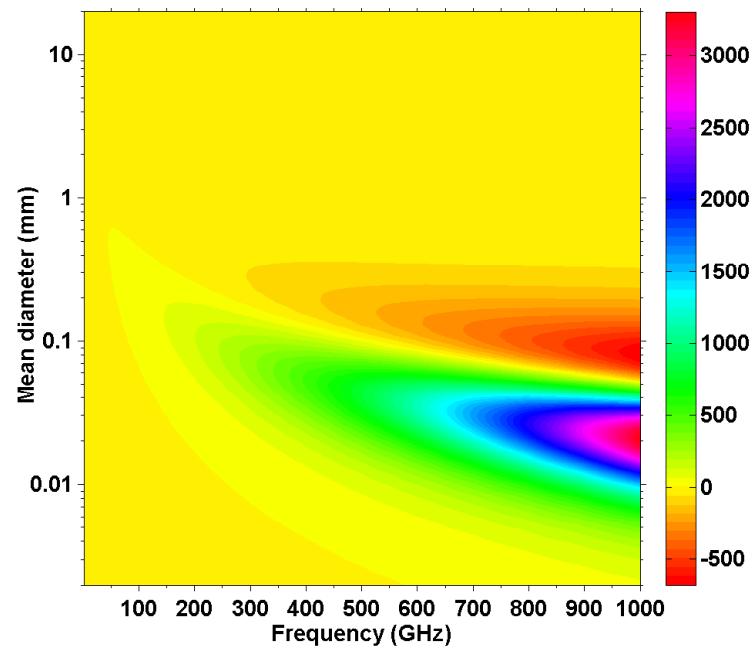


Figure 6.14: Ice hydrometeor $\frac{d\kappa_s}{d\langle D \rangle}$ vs. $(f, \langle D \rangle)$ at $T = 0^\circ\text{C}$

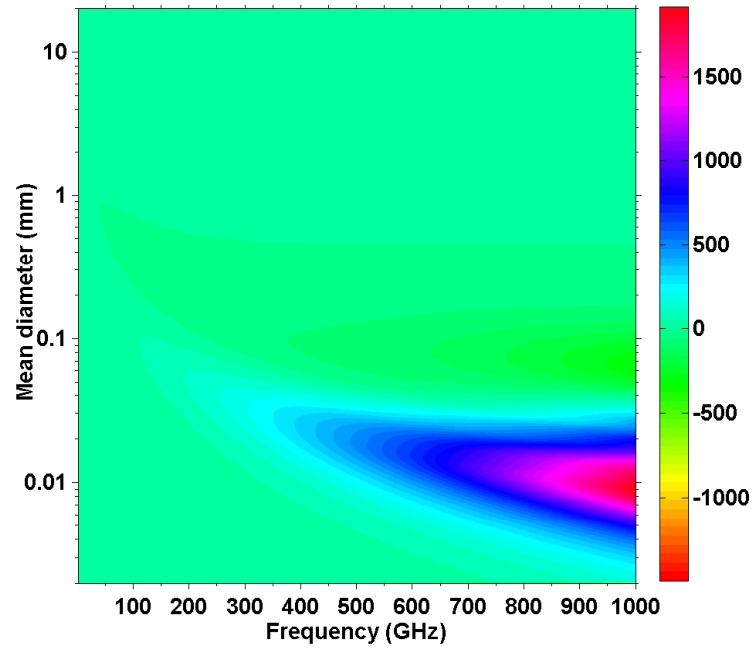


Figure 6.15: Liquid hydrometeor $\frac{d\kappa_b}{d\langle D \rangle}$ vs. $(f, \langle D \rangle)$ at $T = 0^\circ\text{C}$

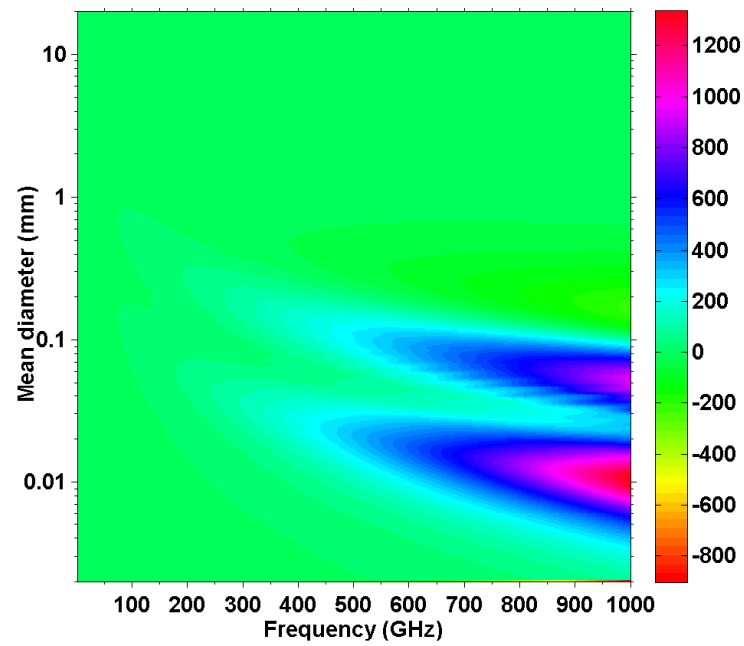


Figure 6.16: Ice hydrometeor $\frac{d\kappa_b}{d\langle D \rangle}$ vs. $(f, \langle D \rangle)$ at $T = 0^\circ\text{C}$

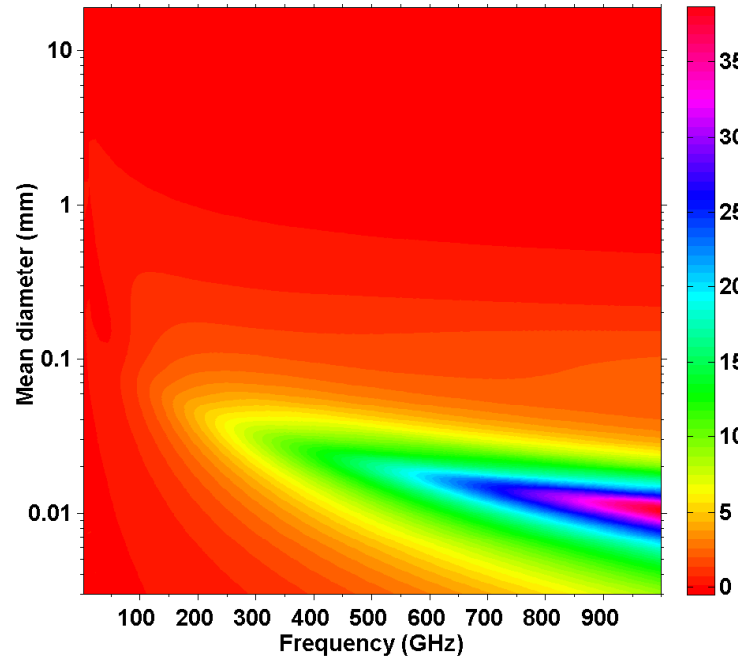


Figure 6.17: Liquid hydrometeor $\frac{dg}{d\langle D \rangle}$ vs. $(f, \langle D \rangle)$ at $T = 0^\circ\text{C}$

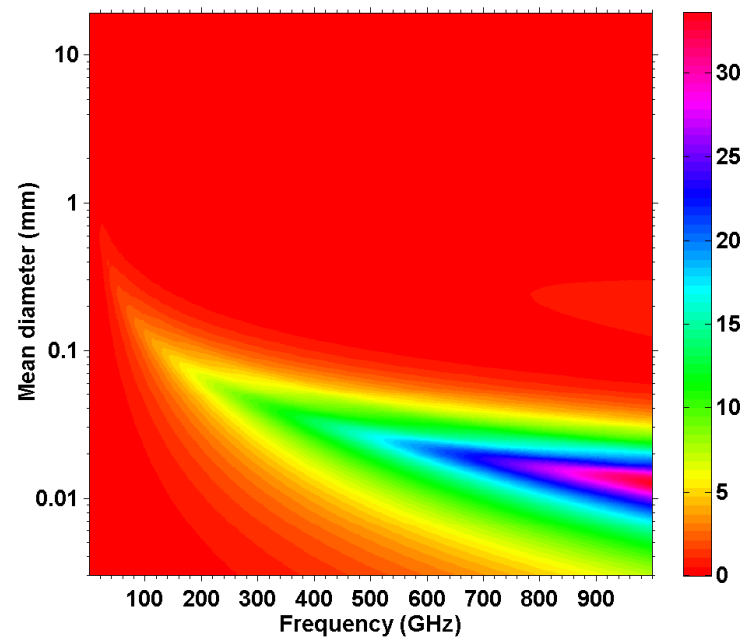


Figure 6.18: Ice hydrometeor $\frac{d\kappa_a}{d\langle D \rangle}$ vs. $(f, \langle D \rangle)$ at $T = 0^\circ\text{C}$

Chapter 7

Conclusions and Future work

7.1 Conclusions

This thesis is a “hybrid thesis” rather than a monolithic one. The central theme of this thesis is the full wave electromagnetic **analysis** of radiometer calibration targets. The originality of the work comes from the fact that a doubly dispersive 3D FDTD code capable of being run on a distributed processor system was developed from scratch. The developed code was well validated and reflectivity spectrum of a wide variety of calibration target geometries, aspect ratios and coating thicknesses were obtained by using the custom code. The reflectivity spectrum was validated using HFSS commercial software and asymptotic GO technique. This resulted in the first full wave electromagnetic analysis of calibration targets published in a peer reviewed journal. This work supercedes the previous work of [10], where only 2D wedge shaped structures were analyzed. The 2D targets were made of homogenous material and the variation of constitutive parameters as a function of frequency was not taken into account. In this work the aluminum core is also taken into account and measured values of $\varepsilon(f), \mu(f)$ in the range [8, 26] GHz are used. For the results outside this frequency range, a Debye series extrapolation is used. From a conceptual point of view, the reflectivity spectrum of all the cases exhibit a general trend. At low frequencies, the wavelength is large resulting in the corrugated surface appearing “flat” to incident wave. Hence the reflectivity is quite high, because it is similar to a plane wave incident on a thin dispersive coating on a PEC ground plane. This occurs at frequencies where the Rayleigh criterion for smooth surface is satisfied (i.e. $f < \frac{c}{8H}$, where H is the pyramid height). This is the reason why the low frequency

reflectivity is essentially same for different target cross-sections (square, circular, truncated etc). As the frequency of the incident plane wave is increased, there is a sharp increase in reflectivity at the point where the first non-specular Floquet mode starts propagating. At high frequencies, the GO behavior dominates and the reflectivity oscillations arise from the standing wave in the coating. Further contributions include analysis of alternate structures such as conical targets, truncated pyramids and truncated conical pyramids with spherical top.

The near field thermal emission from calibration targets (which is measured by the antennas during radiometer calibration) is a difficult problem from a numerical/analytical perspective. Some guidelines along this direction is given in the thesis in chapter 5 and this chapter. Such a work if done could supercede this thesis. The two other contributions in this thesis ($\sim 50\%$) are given in chapters 4 and 6.

In order to compare the quality of this work with the similar studies done in China, we refer the reader to few conference papers [1, 92]. A reflectivity spectrum copied from [1] is shown in Fig. 7.1. These works [1, 92] are flawed due to several reasons as listed below.

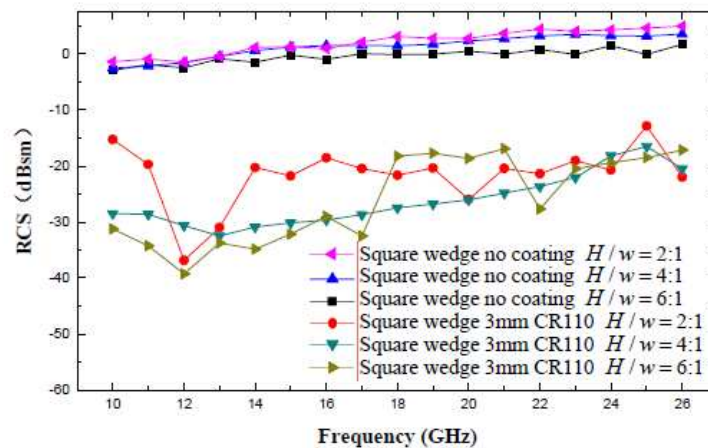


Figure 7.1: Reflectivity spectrum as shown in [1]

- (1) The authors claim to have used FDTD with subgridding method to analyse this problem.

But from the paper, it is obvious that they have used some commercial software package

(most likely CST Microwave Studio). In order to make readers believe that they have used subgridding, they have copied and pasted the details of subgridding from [93, 15] into their conference papers. Also the figure depicting subgridding is copied and pasted. Subgridding as given in [93, 15] is a very complex procedure which includes 3D spatial interpolation and time interpolation between successive FDTD updation. It is not trivial to implement it in a 3D environment. Moreover, the subgridding in [93, 15] is done for boundary surfaces parallel to the coordinate planes, which is not in the case for pyramids.

- (2) FDTD is a time domain method, but they have not mentioned anything about dispersive FDTD which is essential for handling the dispersive coating. A table is given showing the electrical properties of the CR110 and CR112 material. But the data is given in a piecewise constant format. Since the sources used in FDTD simulations are of finite duration, the frequency domain content of the signals will not be confined to a single frequency. Hence dispersive FDTD is required for dispersive materials. Non-dispersive FDTD can be used only if the constitutive parameters do not vary across the frequency spectrum of the source signal.
- (3) The results shown in these papers are not validated with an independent method, which is essential to confirm the accuracy of the results. An erroneous feature that can be observed in Fig. 7.1 is the reflectivity going above 0 dB for the pyramids with no coating.
- (4) In Fig. 7.1, it is obvious that they have solved the problem at discrete frequencies (shown by markers) and joined the discrete results with straight lines. This is characteristic of frequency domain methods such as FEM and is contradictory to the authors claim of using FDTD. The shapes of these curves are of a “zig-zag” nature. However, in our work, the reflectivity spectrum for various aspect ratios and coating thicknesses exhibit a general trend.

7.2 Future work

From a numerical/theoretical perspective, the future work in this problem include the following investigations.

- (1) Measurement of complex relative permittivity and permeability of ECCOSORB[™] materials such as MF-110, MF-112, MF-114 and MF-124 for frequencies greater than 26 GHz. The Debye series based extrapolation is not a reliable method, considering the fact these materials are composite materials.
- (2) Measurement of specific heat capacity and conductivity of ECCOSORB[™] materials. The ECCOSORB MF series material datasheet gives the following data: the density $\rho = 1.6 \times 10^3 - 4.9 \times 10^3 \text{ Kgm}^{-3}$ and thermal conductivity $k \approx 1.2552 \text{ Wm}^{-1}\text{K}^{-1}$.
- (3) Use of commercial CEM softwares such as HFSS, FEKO, CST and COMSOL. These softwares may be more faster than custom dispersive FDTD code and may give oblique plane wave reflectivity. However the 3D FDTD code developed as part of thesis is a very reliable analysis and validation tool, which can be used along with these standard CEM softwares. The importance of the custom code is manifested in estimating the reflectivity spectrum of 1:4 aspect ratio conical pyramids, where there was considerable discrepancy between the FDTD and HFSS results. By performing a convergence study, the correctness of the FDTD results were confirmed.
- (4) Analysis of finite array of square pyramids should be attempted. In this thesis, PEC/PMC boundary conditions are used to simulate an infinite array, which is only an approximation to the real scenario. One possible technique to handle finite array is to use Characteristic Basis Function Method (CBFM) which can solve electrically large scattering problems [94, 95, 96]. CBFM is a relatively new technique that reduces the number of unknowns and hence the size of MoM matrix. It is a “physics based method”, where MoM basis functions are specially constructed to fit the problem geometry by incorporating the physics of the

problem into their generation. However this should be attempted only after verifying the size of the largest finite array FEKO can simulate (preferably on a multicore system), thus making sure whether FEKO can satisfy our requirements. Typically, MoM is used for solving scattering from moderate-size objects in terms of the wavelength.

- (5) Use of COMSOL multiphysics software for solving the heat equation for the periodic square pyramid array with suitable thermal boundary conditions.
- (6) Development of a stochastic numerical method to estimate near field thermal emission from structures of arbitrary geometry and temperature profile. Temperature profile is obtained by the COMSOL heat equation solution. The numerical method may be either WCE (Wiener Chaos Expansion) or a weighting function based method [10]. Even if such a method is developed, the accuracy of estimating the near field brightness temperature is dependent on how accurately we know the pointwise temperature distribution inside the target. The uncertainty in our knowledge of the temperature distribution affects the accuracy of the estimated brightness temperature.
- (7) One of the difficulty in using the FDT-DGF method outlined in chapter 5 for near field thermal emission is the fact that DGF can be derived only for certain simple geometries. Obtaining DGF from FDTD is a not a practical task and had never been done before, because each FDTD simulation will give just the 3 components among the 9 components of the DGF for fixed source and observation position!. The number of simulations can be reduced by coding the sources. Due to the linearity of Maxwell's equations and assuming a nonlinear media, sources of different frequencies do not result in harmonic generation. Hence we can use sources of different frequencies at different source points. For example, assume the observation point \vec{r} is fixed. n sources are defined by $S_n(\vec{r}'_n; f_n)$, where \vec{r}'_n is the source location and f_n its frequency. Let the sources be directed along x direction. By recording the vector field time series at observation point \vec{r} and performing a spectral estimation procedure, the three DGF components $\left\{ G_e^{xx}(\vec{r}, \vec{r}'_n; f_n), G_e^{yx}(\vec{r}, \vec{r}'_n; f_n), G_e^{zx}(\vec{r}, \vec{r}'_n; f_n) \right\}$ for various \vec{r}'_n at f_n

can be obtained. Suppose we want to find $\{G_e^{xx}(\vec{r}, \vec{r}'_n; f_n), G_e^{yx}(\vec{r}, \vec{r}'_n; f_n), G_e^{zx}(\vec{r}, \vec{r}'_n; f_l)\}$, where $f_l = \{f_1, f_2, \dots, f_n\}$ using FDTD without source coding will take n^2 simulations, one the other hand by using source coding it will take n simulations. The obvious bottleneck is that when have reduced the number of simulations by n , the DGF components obtained are at different frequencies given by list f_l . Furthermore, large number of sources in FDTD (without any frequency overlap) may be difficult. Gaussian modulated sinusoids have minimum overlap if their center frequencies are sufficiently apart.

7.2.1 Heat Diffusion Equation

The heat diffusion equation is given by [97]

$$\frac{\partial}{\partial x} \left(k \frac{\partial T}{\partial x} \right) + \frac{\partial}{\partial y} \left(k \frac{\partial T}{\partial y} \right) + \frac{\partial}{\partial z} \left(k \frac{\partial T}{\partial z} \right) + \dot{q} = \rho c_p \frac{\partial T}{\partial t} \quad (7.1)$$

where $T(\vec{r}, t)$ is the temperature, $k(\vec{r})$ ($\text{Wm}^{-1}\text{K}^{-1}$) is the thermal conductivity, $\rho(\vec{r})$ is the density and $c_p(\vec{r})$ is the specific heat capacity of the material. $\dot{q}(\vec{r})$ (Wm^{-3}) is the heat rate per unit volume (heat source). Assuming steady state conditions and no internal heat source, the heat diffusion equation simplifies to the following equation.

$$\frac{\partial}{\partial x} \left(k \frac{\partial T}{\partial x} \right) + \frac{\partial}{\partial y} \left(k \frac{\partial T}{\partial y} \right) + \frac{\partial}{\partial z} \left(k \frac{\partial T}{\partial z} \right) = 0 \quad (7.2)$$

The steady state temperature in the calibration target array is obtained by numerically solving the above equation subjected to any of the following boundary conditions [97].

- (1) Constant surface temperature: Boundary surface is held at a constant temperature, T_s
- (2) Finite heat flux: $-k \frac{\partial T}{\partial n} |_s = q_s''$
- (3) Adiabatic or insulated surface: $\frac{\partial T}{\partial n} |_s = 0$
- (4) Convection boundary condition: $-k \frac{\partial T}{\partial n} |_s = h [T_\infty - T_s]$
- (5) Periodic boundary condition

where h is the convection heat transfer coefficient. The value of h depends on number of factors such as surface geometry, nature of fluid motion etc. Its exact value will not be known. For free convection from a surface to a gaseous fluid, $h \in [2, 25] \text{ Wm}^{-2}\text{K}^{-1}$ [97]. T_∞ is the temperature of the fluid in contact with the surface. $\frac{\partial T}{\partial n}$ is the normal derivative of temperature on the boundary surface.

Bibliography

- [1] N. Feng and W. Wei. The optimization design for microwave wide band blackbody calibration target. ICMMT 2008 proceedings, 2010.
- [2] Fawwaz T. Ulaby, R.K. Moore, and A. K. Fung. Microwave remote sensing Active and Passive Vol I : Microwave remote sensing fundamentals and radiometry. Addison-Wesley publishing company, 1981.
- [3] J. Randa, A. E. Cox, and D. K. Walker. Proposal for development of a national microwave brightness temperature standard. Proc. SPIE, 6301, September 2006.
- [4] E.G. Njoku, T.J. Jackson, V. Lakshmi, T.K. Chan, and S.V. Nghiem. Soil moisture retrieval from amsr-e. Geoscience and Remote Sensing, IEEE Transactions on, 41(2):215 – 229, feb. 2003.
- [5] F.J. Wentz, D.K. Smith, C.A. Mears, and C.L. Gentemann. Advanced algorithms for quikscat and seawinds/amsr. In Geoscience and Remote Sensing Symposium, 2001. IGARSS '01. IEEE 2001 International, volume 3, pages 1079 –1081 vol.3, 2001.
- [6] D. B. Kunkee, S. D. Swadley, G. A. Poe, Y. Hong, and M. F. Werner. Special sensor microwave imager sounder (ssmis) radiometric calibration anomalies part i: Identification and characterization. Geoscience and Remote Sensing, IEEE Transactions on, 46(4), April 2008.
- [7] E.M. Twarog, W.E. Purdy, P.W. Gaiser, K.H. Cheung, and B.E. Kelm. Windsat on-orbit warm load calibration. Geoscience and Remote Sensing, IEEE Transactions on, 44(3):516 – 529, march 2006.
- [8] S.W. Bidwell, G.M. Flaming, J.F. Durning, and E.A. Smith. The global precipitation measurement (gpm) microwave imager (gmi) instrument: role, performance, and status. In Geoscience and Remote Sensing Symposium, 2005. IGARSS '05. Proceedings. 2005 IEEE International, volume 1, page 4 pp., july 2005.
- [9] D. M. Jackson. Calibration of Millimeter-Wave Radiometers with Application to Clear-Air Remote Sensing of the Atmosphere. PhD thesis, Georgia Institute of Technology, Atlanta, GA, 1999.
- [10] D. M. Jackson and A. J. Gasiewski. Electromagnetic and thermal analyses of radiometer calibration targets. Proc. IGARSS., pages 2827–2829, July 2000.

- [11] M. G. Moharam and T. K. Gaylord. Diffraction analysis of dielectric surface-relief gratings. J. Opt. Soc. Am., 72:1385–1392, October 1982.
- [12] J. T. Johnson, R. T. Shin, and J. A. Kong. Scattering and thermal emission from a two dimensional periodic surface. Progress in Electromagnetics Research, 17, January 1997.
- [13] O. M. Bucci and G. Franceschetti. Scattering from wedge-tapered absorbers. IEEE Trans. Antennas Propagat., 19, January 1971.
- [14] K. S. Yee. Numerical solution of initial boundary value problems involving maxwell's equations in isotropic media. IEEE Trans. Antennas. Propag, 14:302–307, may 1966.
- [15] Allen Taflove and Susan C. Hagness. Computational electrodynamics : The Finite Difference Time Domain method. Artech-House, Norwood,Massachusetts, third edition, 2005.
- [16] A. Elsherbeni and V. Demir. The Finite-Difference Time-Domain Method for Electromagnetics with MATLAB Simulations. SciTech Publishing, Rayleigh,NC, 2009.
- [17] U. S. Inan and R. A. Marshall. Numerical Electromagnetics: The FDTD Method. Cambridge University Press, New York, 2011.
- [18] S. D. Gedney. An anisotropic perfectly matched layer-absorbing medium for the truncation of fdtd lattices. IEEE Trans. Antennas Propagat., 44:1630–1639, 1996.
- [19] J. A. Roden, S. D. Gedney, M. P. Kesler, J. G. Maloney, and P. H. Harms. Time-domain analysis of periodic structures at oblique incidence:orthogonal and nonorthogonal fdtd implementations. IEEE Trans. Antennas Propagat., 46:420–427, 1998.
- [20] R. Garg. Analytical and computational methods in electromagnetics. Artech-House, first edition, 2008.
- [21] W. Yu, R. Mittra, T. Su, Y. Liu, and X. Yang. Parallel Finite-Difference-Time-Domain Method. Artech-House, 2006.
- [22] R. H. Landau, M. J. Paez, and C. C. Bordeianu. Computational Physics. WILEY-VCH, second edition, 2007.
- [23] P. S. Pacheco. An introduction to parallel programming. Elsevier, Burlington,MA, 2011.
- [24] A. E. Cox and M. D. Janezic. Preliminary studies of electromagnetic properties of microwave absorbing materials used in calibration targets. Denver, CO, August 2006. IEEE International Geoscience and Remote Sensing Symposium.
- [25] C. F. Bohren and D. R. Huffman. Absorption and Scattering of Light by Small Particles. Wiley-VCH, second edition, 2004.
- [26] J. Clegg and M. P. Robinson. A genetic algorithm used to fit debye functions to the dielectric properties of tissues. Evolutionary Computation (CEC), 2010 IEEE Congress on, pages 1–8, July 2010.
- [27] Yahya Rahmat-Samii and Eric Michielssen. Electromagnetic Optimization by Genetic Algorithms. John Wiley and Sons, 1999.

- [28] L.R.A.X. de Menezes, A.J.M. Soares, F.C. Silva, M.A.B. Terada, and D. Correia. A new procedure for assessing the sensitivity of antennas using the unscented transform. Antennas and Propagation, IEEE Transactions on, 58(3):988 –993, march 2010.
- [29] Jean Van Bladel. Electromagnetic fields. Wiley-Interscience, second edition, 2007.
- [30] S. Sandeep and A. Gasiewski. Electromagnetic analysis of radiometer calibration targets using dispersive 3d fdtd. Antennas and Propagation, IEEE Transactions on, (99), 2012.
- [31] M. Jin, M. Bai, W. Y. Chen, J. K. He, and J. G. Miao. Scattering from periodic cone structure array. Progress in Electromagnetics Research, 7(7), 1997.
- [32] D. Simon. Optimal State Estimation: Kalman, H infinity and Nonlinear approaches. Wiley-Interscience, 2006.
- [33] R.S. Edwards, A.C. Marvin, and S.J. Porter. Uncertainty analyses in the finite-difference time-domain method. Electromagnetic Compatibility, IEEE Transactions on, 52(1):155 –163, feb. 2010.
- [34] W. L. Ko and R. Mittra. A combination of fd-td and prony’s methods for analyzing microwave integrated circuits. IEEE Trans. Microwave Theory Tech., 39:2176 – 2181, 1991.
- [35] J. Wang, Y. Yang, J. Miao, and Y. Chen. Emissivity calculation for a finite circular array of pyramidal absorbers based on kirchhoffs law of thermal radiation. IEEE Trans. Antennas Propagat., 58(99), April 2010.
- [36] J. D. Joannopoulos, S. G. Johnson, J. N. Winn, and R. D. Meade. Photonic Crystals: Molding the Flow of Light. Dover Publishing, New York, 1989.
- [37] F. Yang and Y. R. Samii. Electromagnetic band gap structures in antenna engineering. Cambridge Press, New York, 2009.
- [38] B. A. Munk. Frequency Selective Surfaces: Theory and Design. Wiley, 2000.
- [39] F. I. Baida and A. Belkhir. Split-field fdtd method for oblique incidence study of periodic dispersive metallic structures. Opt. Lett., 34:2453–2455, 2009.
- [40] Young-Seek Chung, T.K. Sarkar, Baek Ho Jung, and M. Salazar-Palma. An unconditionally stable scheme for the finite-difference time-domain method. Microwave Theory and Techniques, IEEE Transactions on, 51(3):697 – 704, mar 2003.
- [41] D. F. Kelley and R. J. Luebbers. Piecewise linear recursive convolution for dispersive media using fdtd. IEEE Trans. Antennas Propagat., 44:792 – 797, 1996.
- [42] S. Sandeep and A. J. Gasiewski. Electromagnetic analysis of radiometer calibration targets using dispersive 3d fdtd. IEEE Trans. Antennas. Propag., 60(6):2821 – 2828, jun 2012.
- [43] B. H. Jung, Z. Mei, and T. K. Sarkar. Transient wave propagation in a general dispersive media using the laguerre functions in a marching-on-in-degree (mod) methodology. Progress In Electromagnetics Research, 118:135–149, 2011.

- [44] Myunghyun Ha and M. Swaminathan. A laguerre-fdtd formulation for frequency-dependent dispersive materials. Microwave and Wireless Components Letters, IEEE, 21(5):225 –227, may 2011.
- [45] Zhao-Yang Cai, Bin Chen, Qin Yin, and Run Xiong. The wlp-fdtd method for periodic structures with oblique incident wave. Antennas and Propagation, IEEE Transactions on, 59(10):3780 –3785, oct. 2011.
- [46] B. H. Jung, Y. S. Chung, and T. K. Sarkar. Time-domain efm, mfe and cfie formulations using laguerre polynomials as temporal basis functions for the analysis of transient scattering from arbitrary shaped conducting structures. Progress In Electromagnetics Research, 39:1–45, 2003.
- [47] Y. Shi and J. M. Jin. A time-domain volume integral equation and its marching-on-in-degree solution for analysis of dispersive dielectric objects. IEEE Trans. Antennas. Propag., 59(3):969–978, mar 2011.
- [48] Y. T. Duan, B. Chen, D. G. Fang, and B. H. Zhou. Efficient implementation for 3-d laguerre-based finite-difference time-domain method. IEEE Trans. Microwave Theory Tech., 59(1):56–64, jan 2011.
- [49] M. E. Veysoglu, R. T. Shin, and J. A. Kong. A finite-difference time-domain analysis of wave scattering from periodic surfaces: Oblique incidence case. J. Electromag. Waves Appl, 7:1595 – 1607, 1993.
- [50] R. L. Burden and J. D. Faires. Numerical Analysis. eighth edition, 2005.
- [51] S. M. Rytov, Y. A. Kravtsov, and V. I. Tatarski. Principles of Statistical Radiophysics, volume 3. 1987.
- [52] Mathieu Francoeur and M. Pinar Meng. Role of fluctuational electrodynamics in near-field radiative heat transfer. Journal of Quantitative Spectroscopy and Radiative Transfer, 109(2):280 – 293, 2008.
- [53] G. W. Kattawar and M. Eisner. Radiation from a homogeneous isothermal sphere. Appl. Opt., 9(12):2685–2690, Dec 1970.
- [54] N. K. Uzunoglu, P. G. Cottis, and P. S. Papakonstantinou. Analysis of thermal radiation from an inhomogenous cylindrical human body model. IEEE Trans. Microwave Theory Tech., 35(8), Aug 1987.
- [55] L. Tsang, J. A. Kong, and K. H. Ding. Scattering of electromagnetic waves. Wiley, 2000.
- [56] A. Narayanaswamy and G. Chen. Thermal near-field radiative transfer between two spheres. eprint arXiv:0909.0765, September 2009.
- [57] Nanorod near-field radiative heat exchange analysis. Journal of Quantitative Spectroscopy and Radiative Transfer, 112(3):412 – 419, 2011.
- [58] Majid Badieirostami, Ali Adibi, Hao-Min Zhou, and Shui-Nee Chow. Model for efficient simulation of spatially incoherent light using the wiener chaos expansion method. Opt. Lett., 32(21):3188–3190, Nov 2007.

- [59] R. G. Ghanem and P. D. Spanos. Stochastic Finite Elements: A Spectral Approach. Dover Civil and Mechanical Engineering, 2003.
- [60] W. ECKHARDT. First and second fluctuation-dissipation-theorem in electromagnetic fluctuation theory. OPTICS COMMUNICATIONS, 41(5), may 1982.
- [61] C. T. Tai. Dyadic Green Functions in Electromagnetic Theory. IEEE Press series on electromagnetic wave theory, second edition.
- [62] R. E. Collin. Field Theory of Guided Waves. IEEE Press, Piscataway,NJ, 1990.
- [63] W. C. Chew. Waves and Fields in Inhomogenous Media. IEEE Press series on electromagnetic wave theory, 1995.
- [64] J. A. Stratton. Electromagnetic theory. IEEE Press series on electromagnetic wave theory, 2007.
- [65] N. K. Uzunoglu. Scattering from inhomogeneities inside a fiber waveguide. J. Opt. Soc. Am., 71(3), Mar 1981.
- [66] M. A. Janssen. Atmospheric Remote Sensing by Microwave Radiometry, chapter 3, pages 91 – 139. Wiley, New york, 1993.
- [67] F. Solheim, J. R. Goodwin, E. R. Westwater, Y. Han, S. J. Keihm, K. Marsh, and R. Ware. Radiometric profiling of temperature, water vapor and cloud liquid water using various inversion methods. Radio Science, 33:393 – 404, 1998.
- [68] C. D. Rogers. Inverse methods for atmospheric sounding: Theory and Practice. World Scientific Publishing Co, 2000.
- [69] E. Kalnay. Atmospheric modeling, Data Assimilation and Predictability. Cambridge University Press, 2009.
- [70] H. Sauvageot. Radar Meteorology. Artech House, Norwood, MA, 1992.
- [71] S. Chandrasekhar. Radiative Transfer. Dover, 1960.
- [72] G. E. Thomas and K. Stamnes. Radiative Transfer in the Atmosphere and Ocean. Cambridge University Press, 1999.
- [73] K. N. Liou. An Introduction to Atmospheric Radiation. Academic, New York, 1980.
- [74] K. V. Beard and C. Chuang. A new model for the equilibrium shapes of raindrops. J. Atmos. Sci., 44:1509–1524, 1987.
- [75] K. Aydin, T. A. Seliga, and V. N. Bringi. Differential radar scattering properties of model hail and mixed-phase hydrometeors. Radio Science, 19:58–66, 1984.
- [76] G. Botta, K. Aydin, and J. Verlinde. Modeling of microwave scattering from cloud ice crystal aggregates and melting aggregates: A new approach. IEEE Trans. Geosci. Remote Sensing, 7, 2010.
- [77] G. W. Petty and W. Huang. Microwave backscatter and extinction by soft ice spheres and complex snow aggregates. J. Atmos. Sci, 67:769–787, 2010.

- [78] M. I. Mishchenko, J. W. Hovenier, and L. D. Travis. Light Scattering by Nonspherical Particles: Theory, Measurement and Applications. Academic Press, 2000.
- [79] G. Mie. Beitrge zur optik trber medien, speziell kolloidaler metallungen. Ann. Phys., 330:377 – 445, 1908.
- [80] C. de Boor. A Practical Guide to Splines. Springer - Verilag, 2001.
- [81] D. F. Rogers. An Introduction to NURBS : with historical perspective. Morgan Kaufmann, 2001.
- [82] M. A. Karam, D.M. LeVine, Y.M.M. Antar, and A. Stogryn. Improvement of the rayleigh approximation for scattering from a small scatterer. IEEE Trans. Antennas Propagat., 43:681 – 688, July 1995.
- [83] P. Bauer, L. Schanz, R. Bennartz, and P. Schlüssel. Outlook for combined tmi-virs algorithms for trmm: Lessons from the pip and aip projects. J. Atmos. Sci., 55:1714–1729, 1998.
- [84] E. Villermaux and B. Bossa. Single-drop fragmentation determines size distribution of raindrops. Nature Physics, 5:697 – 702, July 2009.
- [85] P. S. Ray. Broadband complex refractive indices of ice and water. Appl. Opt., 11:1836 – 1844, 1972.
- [86] S. G. Warren. Optical constants of ice from the ultraviolet to the microwave. Appl. Opt., 23:1206–1225, 1984.
- [87] C. Matzler. Matlab functions for mie scattering and absorption. Research report no. 2002-08, Institut fr Angewandte Physik, Bern, Switzerland, 2002.
- [88] D. Kincaid and W. Cheney. Numerical Analysis: Mathematics of Scientific Computing. American Mathematical Society, Providence, RI, third edition, 2002.
- [89] A.G. Voronovich, A.J. Gasiewski, and B. Weber. A fast multistream scattering-based jacobian for microwave radiance assimilation. IEEE Trans. Geosci. Remote Sensing, 42(8):1749 – 1761, August 2004.
- [90] M. Klein and A. J. Gasiewski. Nadir sensitivity of passive millimeter and submillimeter wave channels to clear air temperature and water vapor variations. Journal of Geophysical Research, 105:17481–17511, July 2000.
- [91] L. A. Klein and C. T. Swift. An improved model for the dielectric constant of sea water at microwave frequencies. IEEE Trans. Antennas Propagat., 25:104–111, 1977.
- [92] N. Feng, W. Wei, and H. Peikang. The systematic optimization designs for the microwave wide band blackbody calibration target’s electromagnetic and thermal characteristics. URSI General Assembly 2008, 2008.
- [93] Three-dimensional subgridding algorithm for fdtd. IEEE Trans. Antennas Propagat., pages 422–429, March 1997.

- [94] E. Lucente, A. Monorchio, and R. Mittra. An iteration-free mom approach based on excitation independent characteristic basis functions for solving large multiscale electromagnetic scattering problems. IEEE Trans. Antennas Propagat., 56(4), Apr 2008.
- [95] E. Lucente, G. Tiberi, A. Monorchio, G. Manara, and R. Mittra. The characteristic basis function method (cbfm): A numerically efficient strategy for solving large electromagnetic scattering problems. Turk J Elec Engin, 16(1), 2008.
- [96] K. Xiao, F. Zhao, S. L. Chai, and J. J. Mao. Scattering analysis of periodic arrays using combined cbf/p-fft method. Progress In Electromagnetics Research, 115:131–146, 2011.
- [97] Frank P. Incropera and David P. DeWitt. Fundamentals of heat and mass transfer. John Wiley & Sons, fifth edition, 2002.
- [98] D. F. Smith, B. L. Weber, S. Sandeep, and A. J. Gasiewski. An anisotropic ocean surface emissivity model based on windsat polarimetric brightness observations - joem. URSI - National Radio Science Meeting, January 2010.
- [99] K. S. Kunz and R. J. Luebbers. Finite Difference Time Domain Method for Electromagnetics. CRC, Boca Raton, Florida, 1993.
- [100] B. H. Jung and T. K. Sarkar. Solving time domain helmholtz wave equation with mod-fdm. Progress In Electromagnetics Research, 79:339–352, 2008.

Appendix A

3D dispersive FDTD code

```
/* FDTD code for broadband electromagnetic analysis of electric
and magnetic dispersive periodic structures
- 3D
- UPML on y-axis boundaries
- PBC/SBC on x,z-axis boundaries
- Electric,Magnetic Dispersive
- Parallel FDTD

1) E,D vectors on yee cell edge centres and H,B vectors
on Yee cell face centres.
Ex[i + 0.5][j][k], Ey[i][j + 0.5][k], Ez[i][j][k + 0.5]
Dx[i + 0.5][j][k], Dy[i][j + 0.5][k], Dz[i][j][k + 0.5]
Hx[i][j + 0.5][k + 0.5], Hy[i + 0.5][j][k + 0.5], Hz[i + 0.5][j + 0.5][k]
Bx[i][j + 0.5][k + 0.5], By[i + 0.5][j][k + 0.5], Bz[i + 0.5][j + 0.5][k]

2) UPML field components      : Ex,Ey,Ez,Dx,Dy,Dz,Hx,Hy,Hz,Bx,By,Bz
Main grid field components : Ex,Ey,Ez,Hx,Hy,Hz

3) UPML slabs just on ymin and ymax
PBC/SBC on xmin,xmax,zmin,zmax

4) C1 constants defined only for UPML
K1 constants defined only for maingrid
RA only for maingrid

5) Field components on UPML-problem space boundary are calculated with
UPML update equations

6) PML0 - PML on ymin boundary (rank 1)
PML1 - PML on ymax boundary (rank 2)
*/

#include "mpi.h"
#include "iostream.h"
#include "math.h"
#include "stdlib.h"
#include "fstream.h"
#include "Defs.h"
#include "Matrix.h"
#include "AuxFuncs.h"
#include "complex.h"
#include "fft.h"

#define PL 12 //Number of PML layers.
int PSX; //Number of yee cells in problem space along x-direction
int PSY; //Number of yee cells in problem space along y-direction
int PSZ; //Number of yee cells in problem space along z-direction
int XCELLS; //Total number of yee cells along x-direction
```

```

int YCELLS;      //Total number of yee cells along y-direction
int ZCELLS;      //Total number of yee cells along z-direction
int OP;
int SP = PL + 25;
double dx,dy,dz;

//Switch between PBC or SBC
const bool SBC = true;
//Switch between incident field and total field simulation
bool INCSIM = true;
//Source excitation type
const int source = DIFFGAUSSIAN;
bool POSTPROC = false;

//Structure dimension
//mp      : base/height of the pyramid (PBC)
//dbase   : Number of yee cells for the base
//basewidth in cm
//aircells : Number of air cells behind the metal base
double mp = 0.25;
const uint dbase = 4;
uint coatthck = 1; //Thickness in mm
uint coating;
const int aircells = 5;
double basewidth = 1.27;
uint pyrtpyidx;
//Parallelization
int yeePerProc;
int NProcs;

// Matrices
MatPtr3 Dx,Dy,Dz,Bx,By,Bz,Ex,Ey,Ez,Hx,Hy,Hz;
MatPtr3 Dxo,Dyo,Dzo;
MatPtr3 Bxo,Byo,Bzo;
MatPtr3 C1Dx,C2Dx;
MatPtr3 C1Bx,C2Bx;
MatPtr3 C2Ey,C3Ey,C1Ez,C2Ez;
MatPtr3 C2Hy,C3Hy,C1Hz,C2Hz;
MatPtr3 K1Ex,K2Ex,K1Ey,K2Ey,K1Ez,K2Ez;
MatPtr3 K1Hx,K2Hx,K1Hy,K2Hy,K1Hz,K2Hz;
MatPtr4 RAEy,RAEz,RAHx,RAHy,RAHz;

// Material matrix
Umat MediaFullDomain;

// Function prototypes
void CreateAllMatrices(int rank);
void DeleteAllMatrices(int rank);
void FillUpdateEqnConstantMatrices(double dx,double sigmas,double d,
                                   double m,double dt,int rank);

void InitMaterialMatrix();
uint AddMetalPyr(double dx,uint material);
uint AddCoating(double dx,uint material);
void ConvToSBC(int rank);
double GetEpsinf(int xidx,int yidx,int zidx);
double GetSigma(int xidx,int yidx,int zidx);
double GetMuinf(int xidx,int yidx,int zidx);
double GetXmDebye(int xidx,int yidx,int zidx,int p,double dt,uint pole);
double GetXimDebye(int xidx,int yidx,int zidx,int p,double dt,uint pole);
double GetXeDebye(int xidx,int yidx,int zidx,int p,double dt,uint pole);
double GetXieDebye(int xidx,int yidx,int zidx,int p,double dt,uint pole);
double GetTaumu(uint media,uint pole);
double GetTaueps(uint media,uint pole);
uint Round(double);
inline bool IsDispersive(uint media) {return (media == MF112 ||
                                             media == MF110 || media == MF114); }
void TimeAlignHfield(double* field,uint sz);

```

```

void TimeAlignHfield(complex* field,uint sz);
double GetFieldVal(uint xidx,uint yidx,uint zidx,uint fieldComp);

int main(int argc, char* argv[])
{
    //Input argument to switch between incident and total field
    //simulation
    if(argc > 1) {
        if(!strcmp(argv[1],"t") || !strcmp(argv[1],"T"))
            INCSIM = false;
        else if(!strcmp(argv[1],"i") || !strcmp(argv[1],"I"))
            INCSIM = true;
        else if(!strcmp(argv[1],"p") || !strcmp(argv[1],"P")) {
            POSTPROC = true;
            INCSIM = false;
        }
        coatthck = strtod(argv[2],'\0');
        mp = strtod(argv[3],'\0');
    }
    //Output frequencies
    int NumofOutFreq = 389;
    double OutFreqs [389];
    int outfreqcnt = 0;
    for(double outfr = 6;outfr <= 200;outfr += 0.5) {
        OutFreqs[outfreqcnt++] = outfr*1e9;
    }
    //Initialize MPI
    int rank;
    MPI_Status status;
    MPI_Init(&argc,&argv);
    MPI_Comm_rank(MPI_COMM_WORLD,&rank);
    MPI_Comm_size(MPI_COMM_WORLD,&NProcs);

    //T - Number of time steps
    //i,j,k - x,y,z direction yee cell index
    //n - Temporal index
    //pidx - Debye pole index
    //time - real time in seconds
    int T = 19000;
    int i,j,k,n,pidx;
    int ii,jj,kk;
    int mpidx;
    double time = 0;
    int SPrank,SPidx;
    int OPrank,OPidx;

    double RAExtot,Exo,RAEztot,Ezo,RAEytot,Eyo,
    RAHxtot,Hxo,Hyo,RAHytot,Hzo,RAHztot;
    double DXeEx0,DXieEx0,CEx,DXeEz0,DXieEz0,
    CEz,DXeEy0,DXieEy0,CEy;
    bool dispcond;

    ofstream outEz,outEy,outEx;
    ofstream outHx,outHy,outHz;
    ofstream outMedia;

    //Initiliazations
    //C - Courant number
    //CFL condition : dt < dx.C/c
    //fs - sinusoidal source frequency
    double dt,f,C,tau,to,spd;
    double fs;
    double fc,Df;
    double fl,fu,Tb;
    uint invC = 2;spd = 28;
    C = 1/(double)(invC);

```

```

if(source == GAUSSIAN) {
    f = 26e9;
    tau = sqrt(2.3)/pi/f;
    to = 4*tau;
    dx = c/f/spd;
    dy = dx;dz = dx;
    dt = dz*C/c;
}
else if(source == MODGAUSSIAN) {
    //fc - center frequency
    //Df - BW
    Df = 153e9;
    fc = 147e9;
    tau = 2/pi/(Df);
    dx = c/(fc + Df)/spd;
    dy = dx;dz = dx;
    dt = dz*C/c;
    to = 4*tau;
}
else if(source == EXPRAMPSSINE) {
    fs = 30e9;
    dx = c/fs/spd;
    dy = dx;dz = dx;
    dt = dz*C/c;
}
else if(source == DIFFGAUSSIAN) {
    fl = 6e9;
    fu = 200e9;
    Tb = (1/pi)*sqrt(log(fu/fl)/(fu*fu - fl*fl));
    to = 3.2*Tb;
    dx = c/200e9/spd;
    dy = dx;dz = dx;
    dt = dz*C/c;
}

//Number of cells for coating
coating = Round(sqrt(1+pow(2/mp,2))*coatthck*1e-3/dy);
//Determine the number of cells for the base (full base)
PSX = Round(basewidth*1e-2/dx);
//Make PSX even
if((PSX%2)){
    PSX = PSX + 1;
}
PSZ = PSX;
//Rounded up basewidth (cm)
basewidth = PSX*dx*100;
XCELLS = PSX;ZCELLS = PSZ;
PSY = Round((basewidth/mp)*1e-2/dx) + coating + 200 + dbase
+ aircells;
//Number of yee cells per processor in problem space
yeePerProc = (int)ceil(double(PSY)/double(NProcs-3));
PSY = yeePerProc * (NProcs - 3);
YCELLS = PSY + (2 * PL);

// Polynomial grading (UPML)
double m = 3.5;
double sigmas = -log(exp(-16))*(m+1)/(2*120*pi*dx*PL);
double d = PL*dx;

if(!POSTPROC) {
    CreateAllMatrices(rank);
    InitMaterialMatrix();
    pyrtoptidx = AddMetalPyr(dx,AL);
    pyrtoptidx = AddCoating(dx,MF112);
    FillUpdateEqnConstantMatrices(dx,sigmas,d,m,dt,rank);
    OP = pyrtoptidx - 150;
    //OP = PL+10;
}

```

```

if(INCSIM) {
    //Remove the scatterer for incident field simulation
    InitMaterialMatrix();
}
FillUpdateEqnConstantMatrices(dx,sigmao,d,m,dt,rank);
}
if(SBC) {
    if(!POSTPROC)
        ConvToSBC(rank);
    XCELLS = Round(XCELLS/2);
    ZCELLS = Round(ZCELLS/2);
}

//rank 0 is not used
//Find rank and rankidx for SP,OP
int flag = 0;
while(!flag && !POSTPROC) {
    for(int ridx = 1;ridx <= NProcs - 1;ridx++) {
        int ymin,ymax;
        if(ridx == 1) {
            ymin = 0 ; ymax = PL;
        }
        else if(ridx == 2) {
            ymin = YCELLS + 1 - PL ; ymax = YCELLS + 1;
        }
        else if(ridx == NProcs - 1) {
            ymin = PL + (ridx - 3)*yeePerProc + 1;
            ymax = PL + (ridx - 3)*yeePerProc + yeePerProc - 1;
        }
        else {
            ymin = PL + (ridx - 3)*yeePerProc + 1;
            ymax = PL + (ridx - 3)*yeePerProc + yeePerProc;
        }
        if(SP >= ymin && SP <= ymax) {
            SPrank = ridx;
            SPidx = SP - ymin;
        }
        if(OP >= ymin && OP <= ymax) {
            OPrank = ridx;
            OPidx = OP - ymin;
        }
    }
    //NProcs - 1 ignored for this case
    if(OPidx == yeePerProc - 1) {
        OP = OP - 1;
        flag = 0;
    }
    else {
        flag = 1;
    }
}

//Output files
if(rank == OPrank && !POSTPROC) {
    if(!INCSIM) {
        outEz.open("/pan1/projects/awmra/Ez.dat",ios::out);
        outEx.open("/pan1/projects/awmra/Ex.dat",ios::out);
        outEy.open("/pan1/projects/awmra/Ey.dat",ios::out);
        outHx.open("/pan1/projects/awmra/Hx.dat",ios::out);
        outHz.open("/pan1/projects/awmra/Hz.dat",ios::out);
        outHy.open("/pan1/projects/awmra/Hy.dat",ios::out);
        outMedia.open("/pan1/projects/awmra/Media.dat",ios::out);
    }
    else {
        outEz.open("/pan1/projects/awmra/Ezinc.dat",ios::out);
    }
}

```

```

        outHx.open("/pan1/projects/awmra/Hxinc.dat",ios::out);
    }
}
//Write to Media.txt
/*for(i = 0;i < XCELLS;i++) {
    for(j = 0;j < YCELLS;j++) {
        for(k = 0;k < ZCELLS;k++) {
            outMedia<<MediaFullDomain[i][j][k]<<endl;
        }
    }
}*/

if(rank == 0 && !POSTPROC) {
    cout<<"-----FDTD 3D simulation-----\n";
    if(INCSIM)
        cout<<"Incident field simulation"<<endl;
    else
        cout<<"Total field simulation"<<endl;
    if(source == EXPRAMPSINE)
        cout<<"Sinusoidal excitation frequency = "<<fs/1e9<<" GHz"<<endl;
        cout<<"ds = lambda/"<<spd<<" = "<<dx*1000<<" mm"<<endl;
    cout<<"dt = "<<dt*1e12<<" ps"<<endl;
    cout<<"Number of Yee cells along x/z direction = "<<XCELLS<<endl;
    cout<<"Number of Yee cells along y direction = "<<YCELLS<<endl;
    cout<<endl;
    cout<<"Pyramid base width = "<<basewidth<<" cm"<<endl;
    cout<<"Pyramid height = "<<basewidth/mp<<" cm"<<endl;
    cout<<endl;
    //cout<<"Source plane location : "<<SP - PL<<" yee cells from the
    PML-problem space boundary"<<endl;
    //cout<<"Observation plane location : 2 yee cells away from the pyramid tip"<<endl;
    cout<<"Coating thickness : "<<coatthck<<" mm"<<endl;
    cout<<"Number of cells in coating : "<<coating<<endl;
    cout<<endl;
    cout<<"Source plane location : "<<SP<<endl;
    cout<<"Observation plane location : "<<OP<<endl;
    cout<<"Source plane rank : "<<SPrank<<endl;
    cout<<"Source plane index : "<<SPidx<<endl;
    cout<<"Observation plane rank : "<<OPrank<<endl;
    cout<<"Observation plane index : "<<OPidx<<endl;
    cout<<"Total number of time steps : "<<T<<endl;
    if(SBC) cout<<"Boundary condition : PEC/PMC"<<endl;
    else cout<<"Boundary condition : Periodic Boundary Condition (PBC)"<<endl;
    if(source == GAUSSIAN) {
        cout<<"Source excitation : Gaussian"<<endl;
        cout<<"tau/dt = "<<tau/dt<<endl;
        cout<<"to/dt = "<<to/dt<<endl;
    }
    else if(source == EXPRAMPSINE) {
        cout<<"Source excitation : Exp ramped sine"<<endl;
    }
    else if(source == MODGAUSSIAN) {
        cout<<"Source excitation : Mod Gaussian"<<endl;
        cout<<"tau/dt = "<<tau/dt<<endl;
        cout<<"to/dt = "<<to/dt<<endl;
    }
}

//-----FDTD update loop starts here-----
//Temp variables to hold previous field values and field differential values.
double dHx,dHy,dHz;
double dEx,dEy,dEz;

//Boundary field matrices
MatPtr2 Hzb,Hxb,Ezb,Exb,Ezb1,Exb1;

if(POSTPROC) {

```

```

goto pproc;
}

//Create boundary field matrices
if(rank == 1) {
  CreateMatrix(Hzb,XCELLS,ZCELLS + 1);
  CreateMatrix(Hxb,XCELLS + 1,ZCELLS);
}
if(rank == 2) {
  CreateMatrix(Hzb,XCELLS,ZCELLS + 1);
  CreateMatrix(Hxb,XCELLS + 1,ZCELLS);
}
if(rank >=3 && rank <= NProcs - 2) {
  CreateMatrix(Hzb,XCELLS,ZCELLS + 1);
  CreateMatrix(Hxb,XCELLS + 1,ZCELLS);
  CreateMatrix(Ezb,XCELLS + 1,ZCELLS);
  CreateMatrix(Exb,XCELLS,ZCELLS + 1);
}
if(rank == NProcs - 1) {
  CreateMatrix(Ezb,XCELLS + 1,ZCELLS);
  CreateMatrix(Ezb1,XCELLS + 1,ZCELLS);
  CreateMatrix(Exb,XCELLS,ZCELLS + 1);
  CreateMatrix(Exb1,XCELLS,ZCELLS + 1);
}

//PMLO (rank1)
if(rank == 1) {
  for(n = 0;n < T;n++) {
    cout<<n<<endl;
    // Dx update (Dx at n)
    for(i = 0;i < XCELLS;i++) {
      for(j = 0;j < PL + 1;j++) {
        for(k = 0;k < ZCELLS + 1;k++) {
          //Dxo = Dx at n - 1
          Dxo[i][j][k] = Dx[i][j][k];

          //PEC
          if(j == 0) {
            Dx[i][j][k] = 0;
          }

          //PBC on zmin
          else if(k == 0) {
            if(!SBC) {
              if(j == PL)
                dHz = (Hzb[i][k] - Hz[i][j-1][k])/dy;
              else
                dHz = (Hz[i][j][k] - Hz[i][j-1][k])/dy;
              dHy = (Hy[i][j][k] - Hy[i][j][ZCELLS-1])/dz;

              Dx[i][j][k] = C1Dx[i][j][k]*Dx[i][j][k] + C2Dx[i][j][k]*(dHz - dHy);
            }
            else {
              Dx[i][j][k] = 0;
            }
          }

          //PBC on zmax
          else if(k == ZCELLS) {
            if(!SBC) {
              Dx[i][j][k] = Dx[i][j][0];
            }
            else {
              Dx[i][j][k] = 0;
            }
          }
        }
      }
    }
  }
}

```

```

    if(j == PL)
        dHz = (Hzb[i][k] - Hz[i][j-1][k])/dy;
    else
        dHz = (Hz[i][j][k] - Hz[i][j-1][k])/dy;
    dHy = (Hy[i][j][k] - Hy[i][j][k-1])/dz;

    Dx[i][j][k] = C1Dx[i][j][k]*Dx[i][j][k] + C2Dx[i][j][k]*(dHz - dHy);
}
}
}

//Ex update (Ex at n)
for(i = 0; i < XCELLS; i++) {
    for(j = 0; j < PL + 1; j++) {
        for(k = 0; k < ZCELLS + 1; k++) {
            Ex[i][j][k] = Ex[i][j][k] + (1/epso)*(Dx[i][j][k] - Dxo[i][j][k]);
        }
    }
}

//Dy update at n
for(i = 0; i < XCELLS + 1; i++) {
    for(j = 0; j < PL; j++) {
        for(k = 0; k < ZCELLS + 1; k++) {
            //Dyo = Dy at n - 1
            Dyo[i][j][k] = Dy[i][j][k];

            // BC on corners
            if(i == 0 && k == 0) {
                if(!SBC) {
                    dHz = (Hz[i][j][k] - Hz[XCELLS-1][j][k])/dx;
                    dHx = (Hx[i][j][k] - Hx[i][j][ZCELLS-1])/dz;

                    Dy[i][j][k] = Dy[i][j][k] + dt*(dHx - dHz);
                }
                else {
                    Dy[i][j][k] = 0;
                }
            }
            // PBC on corners
            else if((i == 0 && k == ZCELLS) || (i == XCELLS && k == ZCELLS)
                || (i == XCELLS && k == 0)) {
                if(!SBC) {
                    Dy[i][j][k] = Dy[0][j][0];
                }
                else {
                    Dy[i][j][k] = 0;
                }
            }
            // BC on xmin
            else if(i == 0) {
                if(!SBC) {
                    dHz = (Hz[i][j][k] - Hz[XCELLS-1][j][k])/dx;
                    dHx = (Hx[i][j][k] - Hx[i][j][k-1])/dz;

                    Dy[i][j][k] = Dy[i][j][k] + dt*(dHx - dHz);
                }
                else {
                    dHz = 2*(Hz[i][j][k])/dx;
                    dHx = (Hx[i][j][k] - Hx[i][j][k-1])/dz;

                    Dy[i][j][k] = Dy[i][j][k] + dt*(dHx - dHz);
                }
            }
            // BC on xmax
            else if(i == XCELLS) {

```

```

    if(!SBC) {
        Dy[i][j][k] = Dy[0][j][k];
    }
    else {
        dHz = -2*(Hz[XCELLS-1][j][k])/dx;
        dHx = (Hx[i][j][k] - Hx[i][j][k-1])/dz;

        Dy[i][j][k] = Dy[i][j][k] + dt*(dHx - dHz);
    }
}
// BC on zmin
else if(k == 0) {
    if(!SBC) {
        dHz = (Hz[i][j][k] - Hz[i-1][j][k])/dx;
        dHx = (Hx[i][j][k] - Hx[i][j][ZCELLS-1])/dz;

        Dy[i][j][k] = Dy[i][j][k] + dt*(dHx - dHz);
    }
    else {
        Dy[i][j][k] = 0;
    }
}
// BC on zmax
else if(k == ZCELLS) {
    if(!SBC) {
        Dy[i][j][k] = Dy[i][j][0];
    }
    else {
        Dy[i][j][k] = 0;
    }
}
else {
    dHx = (Hx[i][j][k] - Hx[i][j][k-1])/dz;
    dHz = (Hz[i][j][k] - Hz[i-1][j][k])/dx;

    Dy[i][j][k] = Dy[i][j][k] + dt*(dHx - dHz);
}
}
}
}

//Ey update (Ey at n)
for(j = 0;j < PL;j++) {
    for(i = 0;i < XCELLS + 1;i++) {
        for(k = 0;k < ZCELLS + 1;k++) {
            Ey[i][j][k] = Ey[i][j][k] + C2Ey[i][j][k]*Dy[i][j][k]
                - C3Ey[i][j][k]*Dyo[i][j][k];
        }
    }
}

//Dz update
for(i = 0;i < XCELLS + 1;i++) {
    for(j = 0;j < (PL + 1);j++) {
        for(k = 0;k < ZCELLS;k++) {

            //Dzo = Dz at n - 1
            Dzo[i][j][k] = Dz[i][j][k];

            // PEC
            if(j == 0) {
                Dz[i][j][k] = 0;
            }
            // BC on xmin
            else if(i == 0) {
                if(!SBC) {
                    dHy = (Hy[i][j][k] - Hy[XCELLS-1][j][k])/dx;

```

```

    if(j == PL)
        dHx = (Hxb[i][k] - Hx[i][j-1][k])/dy;
    else
        dHx = (Hx[i][j][k] - Hx[i][j-1][k])/dy;

    Dz[i][j][k] = Dz[i][j][k] + dt*(dHy - dHx);
}
else {
    dHy = 2*(Hy[i][j][k])/dx;
    if(j == PL)
        dHx = (Hxb[i][k] - Hx[i][j-1][k])/dy;
    else
        dHx = (Hx[i][j][k] - Hx[i][j-1][k])/dy;

    Dz[i][j][k] = Dz[i][j][k] + dt*(dHy - dHx);
}
}
// BC on xmax
else if(i == XCELLS) {
    if(!SBC) {
        Dz[i][j][k] = Dz[0][j][k];
    }
    else {
        dHy = -2*(Hy[XCELLS-1][j][k])/dx;
        if(j == PL)
            dHx = (Hxb[i][k] - Hx[i][j-1][k])/dy;
        else
            dHx = (Hx[i][j][k] - Hx[i][j-1][k])/dy;

        Dz[i][j][k] = Dz[i][j][k] + dt*(dHy - dHx);
    }
}
else {
    dHy = (Hy[i][j][k] - Hy[i-1][j][k])/dx;
    if(j == PL)
        dHx = (Hxb[i][k] - Hx[i][j-1][k])/dy;
    else
        dHx = (Hx[i][j][k] - Hx[i][j-1][k])/dy;

    Dz[i][j][k] = Dz[i][j][k] + dt*(dHy - dHx);
}
}
}
//Ez update (Ez at n)
for(j = 0; j < PL + 1; j++) {
    for(i = 0; i < XCELLS + 1; i++) {
        for(k = 0; k < ZCELLS; k++) {
            Ez[i][j][k] = C1Ez[i][j][k]*Ez[i][j][k] + C2Ez[i][j][j]*
                (Dz[i][j][k] - Dzo[i][j][k]);
        }
    }
}

//Send Ex,Ez to rank 3 proc
for(mpidx = 0; mpidx < XCELLS; mpidx++) {
    MPI_Send(&Ex[mpidx][PL][0], ZCELLS + 1, MPI_DOUBLE, rank + 2, 1*10+3*1+0,
        MPI_COMM_WORLD);
}
for(mpidx = 0; mpidx < XCELLS + 1; mpidx++) {
    MPI_Send(&Ez[mpidx][PL][0], ZCELLS, MPI_DOUBLE, rank + 2, 1*10+3*1+1,
        MPI_COMM_WORLD);
}

//B,H updates
time = time + 0.5*dt;

```

```

//Bx update (Bx at n + 0.5)
for(i = 0; i < XCELLS + 1; i++) {
  for(j = 0; j < PL; j++) {
    for(k = 0; k < ZCELLS; k++) {

      //Bxo = Bx at n - 0.5
      Bxo[i][j][k] = Bx[i][j][k];

      dEz = (Ez[i][j+1][k] - Ez[i][j][k])/dy;
      dEy = (Ey[i][j][k+1] - Ey[i][j][k])/dz;

      Bx[i][j][k] = C1Bx[i][j][k]*Bx[i][j][k] - C2Bx[i][j][k]*(dEz - dEy);
    }
  }
}

//Hx update (Hx at n + 0.5)
for(j = 0; j < PL; j++) {
  for(i = 0; i < XCELLS + 1; i++) {
    for(k = 0; k < ZCELLS; k++) {
      if(i == XCELLS && !SBC) {Hx[i][j][k] = Hx[0][j][k];}
      else {
        Hx[i][j][k] = Hx[i][j][k] + (1/muo)*(Bx[i][j][k] - Bxo[i][j][k]);
      }
    }
  }
}

//By update
for(i = 0; i < XCELLS; i++) {
  for(j = 0; j < PL + 1; j++) {
    for(k = 0; k < ZCELLS; k++) {
      //Byo = By at n - 0.5
      Byo[i][j][k] = By[i][j][k];

      dEx = (Ex[i][j][k+1] - Ex[i][j][k])/dz;
      dEz = (Ez[i+1][j][k] - Ez[i][j][k])/dx;

      By[i][j][k] = By[i][j][k] - dt*(dEx - dEz);
    }
  }
}

//Hy update
for(i = 0; i < XCELLS; i++) {
  for(j = 0; j < PL + 1; j++) {
    for(k = 0; k < ZCELLS; k++) {
      Hy[i][j][k] = Hy[i][j][k] + C2Hy[i][j][k]*By[i][j][k] -
        C3Hy[i][j][k]*Byo[i][j][k];
    }
  }
}

//Bz update (Bz at n + 0.5)
for(i = 0; i < XCELLS; i++) {
  for(j = 0; j < PL; j++) {
    for(k = 0; k < ZCELLS + 1; k++) {
      //Bzo = Bz at n - 0.5
      Bzo[i][j][k] = Bz[i][j][k];

      dEy = (Ey[i+1][j][k] - Ey[i][j][k])/dx;
      dEx = (Ex[i][j+1][k] - Ex[i][j][k])/dy;
    }
  }
}

```

```

//Hz update (Hz at n + 0.5)
for(i = 0;i < XCELLS;i++) {
  for(j = 0;j < PL;j++) {
    for(k = 0;k < ZCELLS + 1;k++) {
      Hz[i][j][k] = C1Hz[i][j][k]*Hz[i][j][k] + C2Hz[i][j][k]
        *(Bz[i][j][k] - Bzo[i][j][k]);
    }
  }
}

for(mpidx = 0;mpidx < XCELLS + 1;mpidx++) {
  MPI_Recv(&Hxb[mpidx][0],ZCELLS,MPI_DOUBLE,3,3*10+1*1+0,MPI_COMM_WORLD,
    &status);
}

for(mpidx = 0;mpidx < XCELLS;mpidx++) {
  MPI_Recv(&Hzb[mpidx][0],ZCELLS + 1,MPI_DOUBLE,3,3*10+1*1+1,MPI_COMM_WORLD,
    &status);
}

time = time + 0.5*dt;

} //n
} //rank1

//PML1 (rank2)
if(rank == 2) {
  for(n = 0;n < T;n++) {
    // Dx update (Dx at n)
    for(i = 0;i < XCELLS;i++) {
      for(j = 0;j < (PL + 1);j++) {
        for(k = 0;k < ZCELLS + 1;k++) {
          //Dxo = Dx at n - 1
          Dxo[i][j][k] = Dx[i][j][k];

          // PEC
          if(j == PL) {
            Dx[i][j][k] = 0;
          }
          // PBC on zmin
          else if(k == 0) {
            if(!SBC) {
              if(j == 0)
                dHz = (Hz[i][j][k] - Hzb[i][k])/dy;
              else
                dHz = (Hz[i][j][k] - Hz[i][j-1][k])/dy;
              dHy = (Hy[i][j][k] - Hy[i][j][ZCELLS-1])/dz;

              Dx[i][j][k] = C1Dx[i][j][k]*Dx[i][j][k] + C2Dx[i][j][k]*(dHz - dHy);
            }
            else {
              Dx[i][j][k] = 0;
            }
          }
          //PBC on zmax
          else if(k == ZCELLS) {
            if(!SBC) {
              Dx[i][j][k] = Dx[i][j][0];
            }
            else {
              Dx[i][j][k] = 0;
            }
          }
          else {
            if(j == 0)
              dHz = (Hz[i][j][k] - Hzb[i][k])/dy;
            else

```

```

    dHz = (Hz[i][j][k] - Hz[i][j-1][k])/dy;
    dHy = (Hy[i][j][k] - Hy[i][j][k-1])/dz;

    Dx[i][j][k] = C1Dx[i][j][k]*Dx[i][j][k] + C2Dx[i][j][k]*(dHz - dHy);
  }
}
}
//Ex update at n
for(j = 0;j < PL + 1;j++) {
  for(i = 0;i < XCELLS;i++) {
    for(k = 0;k < ZCELLS + 1;k++) {
      Ex[i][j][k] = Ex[i][j][k] + (1/eps0)*(Dx[i][j][k] - Dx0[i][j][k]);
    }
  }
}
//Dy update at n
for(i = 0;i < XCELLS + 1;i++) {
  for(j = 0;j < PL;j++) {
    for(k = 0;k < ZCELLS + 1;k++) {
      //Dy0 = Dy at n - 1
      Dy0[i][j][k] = Dy[i][j][k];

      // BC on corners
      if(i == 0 && k == 0) {
        if(!SBC) {
          dHz = (Hz[i][j][k] - Hz[XCELLS-1][j][k])/dx;
          dHx = (Hx[i][j][k] - Hx[i][j][ZCELLS-1])/dz;

          Dy[i][j][k] = Dy[i][j][k] + dt*(dHx - dHz);
        }
        else {
          Dy[i][j][k] = 0;
        }
      }
      // PBC on corners
      else if((i == 0 && k == ZCELLS) || (i == XCELLS && k == ZCELLS)
              || (i == XCELLS && k == 0)) {
        if(!SBC) {
          Dy[i][j][k] = Dy[0][j][0];
        }
        else {
          Dy[i][j][k] = 0;
        }
      }
      // BC on xmin
      else if(i == 0) {
        if(!SBC) {
          dHz = (Hz[i][j][k] - Hz[XCELLS-1][j][k])/dx;
          dHx = (Hx[i][j][k] - Hx[i][j][k-1])/dz;

          Dy[i][j][k] = Dy[i][j][k] + dt*(dHx - dHz);
        }
        else {
          dHz = 2*(Hz[i][j][k])/dx;
          dHx = (Hx[i][j][k] - Hx[i][j][k-1])/dz;

          Dy[i][j][k] = Dy[i][j][k] + dt*(dHx - dHz);
        }
      }
      // BC on xmax
      else if(i == XCELLS) {
        if(!SBC) {
          Dy[i][j][k] = Dy[0][j][k];
        }
        else {
          dHz = -2*(Hz[XCELLS-1][j][k])/dx;

```

```

    dHx = (Hx[i][j][k] - Hx[i][j][k-1])/dz;

    Dy[i][j][k] = Dy[i][j][k] + dt*(dHx - dHz);
}
}
// BC on zmin
else if(k == 0) {
    if(!SBC) {
        dHz = (Hz[i][j][k] - Hz[i-1][j][k])/dx;
        dHx = (Hx[i][j][k] - Hx[i][j][ZCELLS-1])/dz;

        Dy[i][j][k] = Dy[i][j][k] + dt*(dHx - dHz);
    }
    else {
        Dy[i][j][k] = 0;
    }
}
// BC on zmax
else if(k == ZCELLS) {
    if(!SBC) {
        Dy[i][j][k] = Dy[i][j][0];
    }
    else {
        Dy[i][j][k] = 0;
    }
}
else {
    dHx = (Hx[i][j][k] - Hx[i][j][k-1])/dz;
    dHz = (Hz[i][j][k] - Hz[i-1][j][k])/dx;

    Dy[i][j][k] = Dy[i][j][k] + dt*(dHx - dHz);
}
}
}
//Ey update at n
for(i = 0; i < XCELLS + 1; i++) {
    for(j = 0; j < PL; j++) {
        for(k = 0; k < ZCELLS + 1; k++) {
            Ey[i][j][k] = Ey[i][j][k] + C2Ey[i][j][k]*Dy[i][j][k]
                - C3Ey[i][j][k]*Dyo[i][j][k];
        }
    }
}
//Dz update
for(i = 0; i < XCELLS + 1; i++) {
    for(j = 0; j < (PL + 1); j++) {
        for(k = 0; k < ZCELLS; k++) {

            //Dzo = Dz at n - 1
            Dzo[i][j][k] = Dz[i][j][k];

            // PEC
            if(j == PL) {
                Dz[i][j][k] = 0;
            }
            // BC on xmin
            else if(i == 0) {
                if(!SBC) {
                    dHy = (Hy[i][j][k] - Hy[XCELLS-1][j][k])/dx;
                    if(j == 0)
                        dHx = (Hx[i][j][k] - Hxb[i][k])/dy;
                    else
                        dHx = (Hx[i][j][k] - Hx[i][j-1][k])/dy;

                    Dz[i][j][k] = Dz[i][j][k] + dt*(dHy - dHx);
                }
            }
        }
    }
}

```

```

else {
    dHy = 2*(Hy[i][j][k])/dx;
    if(j == 0)
        dHx = (Hx[i][j][k] - Hxb[i][k])/dy;
    else
        dHx = (Hx[i][j][k] - Hx[i][j-1][k])/dy;

    Dz[i][j][k] = Dz[i][j][k] + dt*(dHy - dHx);
}
}
// BC on xmax
else if(i == XCELLS) {
    if(!SBC) {
        Dz[i][j][k] = Dz[0][j][k];
    }
    else {
        dHy = -2*(Hy[XCELLS-1][j][k])/dx;
        if(j == 0)
            dHx = (Hx[i][j][k] - Hxb[i][k])/dy;
        else
            dHx = (Hx[i][j][k] - Hx[i][j-1][k])/dy;

        Dz[i][j][k] = Dz[i][j][k] + dt*(dHy - dHx);
    }
}
else {
    dHy = (Hy[i][j][k] - Hy[i-1][j][k])/dx;
    if(j == 0)
        dHx = (Hx[i][j][k] - Hxb[i][k])/dy;
    else
        dHx = (Hx[i][j][k] - Hx[i][j-1][k])/dy;

    Dz[i][j][k] = Dz[i][j][k] + dt*(dHy - dHx);
}
}
}
}
//Ez update
for(i = 0; i < XCELLS + 1; i++) {
    for(j = 0; j < (PL + 1); j++) {
        for(k = 0; k < ZCELLS; k++) {
            Ez[i][j][k] = C1Ez[i][j][k]*Ez[i][j][k] + C2Ez[i][j][k]*
                (Dz[i][j][k] - Dzo[i][j][k]);
        }
    }
}

//Send Ex,Ez to rank 'NProcs - 1'
for(mpidx = 0; mpidx < XCELLS; mpidx++) {
    MPI_Send(&Ex[mpidx][0][0], ZCELLS + 1, MPI_DOUBLE, NProcs - 1, 2*10+(NProcs-1)*1+0,
        MPI_COMM_WORLD);
}
for(mpidx = 0; mpidx < XCELLS + 1; mpidx++) {
    MPI_Send(&Ez[mpidx][0][0], ZCELLS, MPI_DOUBLE, NProcs - 1, 2*10+(NProcs-1)*1+1,
        MPI_COMM_WORLD);
}

time = time + 0.5*dt;

//Bx update
for(i = 0; i < XCELLS + 1; i++) {
    for(j = 0; j < PL; j++) {
        for(k = 0; k < ZCELLS; k++) {
            //Bxo = Bx at n - 0.5
            Bxo[i][j][k] = Bx[i][j][k];
        }
    }
}

```

```

    dEz = (Ez[i][j+1][k] - Ez[i][j][k])/dy;
    dEy = (Ey[i][j][k+1] - Ey[i][j][k])/dz;

    Bx[i][j][k] = C1Bx[i][j][k]*Bx[i][j][k] - C2Bx[i][j][k]*(dEz - dEy);
  }
}

//Hx update
for(i = 0; i < XCELLS + 1; i++) {
  for(j = 0; j < PL; j++) {
    for(k = 0; k < ZCELLS; k++) {
      if(i == XCELLS && !SBC) {Hx[i][j][k] = Hx[0][j][k];}
      else {
        Hx[i][j][k] = Hx[i][j][k] + (1/muo)*(Bx[i][j][k] - Bxo[i][j][k]);
      }
    }
  }
}

//By update (By at n + 0.5)
for(i = 0; i < XCELLS; i++) {
  for(j = 0; j < PL + 1; j++) {
    for(k = 0; k < ZCELLS; k++) {
      //Byo = By at n - 0.5
      Byo[i][j][k] = By[i][j][k];

      dEx = (Ex[i][j][k+1] - Ex[i][j][k])/dz;
      dEz = (Ez[i+1][j][k] - Ez[i][j][k])/dx;

      By[i][j][k] = By[i][j][k] - dt*(dEx - dEz);
    }
  }
}

//Hy update (Hy at n + 0.5)
for(i = 0; i < XCELLS; i++) {
  for(j = 0; j < PL + 1; j++) {
    for(k = 0; k < ZCELLS; k++) {
      Hy[i][j][k] = Hy[i][j][k] + C2Hy[i][j][k]*By[i][j][k] -
        C3Hy[i][j][k]*Byo[i][j][k];
    }
  }
}

//Bz update (Bz at n + 0.5)
for(i = 0; i < XCELLS; i++) {
  for(j = 0; j < PL; j++) {
    for(k = 0; k < ZCELLS + 1; k++) {
      //Bzo = Bz at n - 0.5
      Bzo[i][j][k] = Bz[i][j][k];

      dEy = (Ey[i+1][j][k] - Ey[i][j][k])/dx;
      dEx = (Ex[i][j+1][k] - Ex[i][j][k])/dy;

      Bz[i][j][k] = Bz[i][j][k] - dt*(dEy - dEx);
    }
  }
}

//Hz update (Hz at n + 0.5)
for(i = 0; i < XCELLS; i++) {
  for(j = 0; j < PL; j++) {
    for(k = 0; k < ZCELLS + 1; k++) {
      Hz[i][j][k] = C1Hz[i][j][k]*Hz[i][j][k] + C2Hz[i][j][k]
        *(Bz[i][j][k] - Bzo[i][j][k]);
    }
  }
}

```

```

}
}

//Recv Hxb,Hzb
for(mpidx = 0;mpidx < XCELLS + 1;mpidx++) {
  MPI_Recv(&Hxb[mpidx][0],ZCELLS,MPI_DOUBLE,NProcs - 1,
    (NProcs-1)*10+(rank*1)+0,MPI_COMM_WORLD,&status);
}
for(mpidx = 0;mpidx < XCELLS;mpidx++) {
  MPI_Recv(&Hzb[mpidx][0],ZCELLS + 1,MPI_DOUBLE,NProcs - 1,
    (NProcs-1)*10+(rank*1)+1,MPI_COMM_WORLD,&status);
}

time = time + 0.5*dt;

} //n
} //rank2

if(rank >=3 && rank <= NProcs - 2) {
  for(n = 0;n < T;n++) {
    //Ex main grid update equations
    for(i = 0;i < XCELLS;i++) {
      for(j = 0;j < yeePerProc;j++) {
        for(k = 0;k < ZCELLS + 1;k++) {
          Exo      = Ex[i][j][k];
          RAExtot  = 0;
          dispcond = true;
          for(pidx = 1;pidx <= MAXPOLESEPS;pidx++) {
            RAExtot = RAExtot + RAEx[i][j][k][pidx-1];
          }

          if(k == 0) {
            if(!SBC) {
              if(j == yeePerProc - 1)
                dHz = (Hzb[i][k] - Hz[i][j][k])/dy;
              else
                dHz = (Hz[i][j+1][k] - Hz[i][j][k])/dy;
                dHy = (Hy[i][j][k] - Hy[i][j][ZCELLS-1])/dz;
                Ex[i][j][k] = (dt/(epso*K1Ex[i][j][k]))*(dHz - dHy)
                  + (K2Ex[i][j][k]/K1Ex[i][j][k])*Ex[i][j][k] +
                  RAExtot/K1Ex[i][j][k];
            }
            else {
              Ex[i][j][k] = 0;
            }
          }
          //PBC on zmax
          else if(k == ZCELLS) {
            if(!SBC) {
              Ex[i][j][k] = Ex[i][j][0];
            }
            else {
              Ex[i][j][k] = 0;
            }
            dispcond = false;
          }
          else {
            if(j == yeePerProc - 1)
              dHz = (Hzb[i][k] - Hz[i][j][k])/dy;
            else
              dHz = (Hz[i][j+1][k] - Hz[i][j][k])/dy;
              dHy = (Hy[i][j][k] - Hy[i][j][k-1])/dz;
              Ex[i][j][k] = (dt/(epso*K1Ex[i][j][k]))*(dHz - dHy)
                + (K2Ex[i][j][k]/K1Ex[i][j][k])*Ex[i][j][k] +
                RAExtot/K1Ex[i][j][k];
          }
        }
      }
    }
  }
}

```

```

    int rankoff = (rank - 3)*yeePerProc + 1;
    //Update RAEx for the next update
    if(k > ZCELLS/2 && !SBC) { kk = k - 1; }
    else { kk = k;}
    //dispcnd will be false for k = ZCELLS
    dispcnd = dispcnd && IsDispersive(MediaFullDomain[i][j+PL+rankoff][kk]);
    if(dispcnd) {
        for(pidx = 1;pidx <= MAXPOLESEPS;pidx++) {
            DXeEx0 = GetXeDebye(i,j+PL+rankoff,kk,0,dt,pidx) -
            GetXeDebye(i,j+PL+rankoff,kk,1,dt,pidx);
            DXieEx0 = GetXieDebye(i,j+PL+rankoff,kk,0,dt,pidx) -
            GetXieDebye(i,j+PL+rankoff,kk,1,dt,pidx);
            CEEx = exp(-dt/ GetTaueps(MediaFullDomain[i][j+PL+rankoff][kk],pidx));

            RAEx[i][j][k][pidx-1] = DXeEx0*Ex[i][j][k] + DXieEx0*(Exo - Ex[i][j][k]) +
            CEEx*RAEx[i][j][k][pidx-1];
        }
    }
}
}
}

//Ey main grid update equations
for(i = 0;i < XCELLS + 1;i++) {
    for(j = 0;j < yeePerProc;j++) {
        for(k = 0;k < ZCELLS + 1;k++) {
            Eyo = Ey[i][j][k];
            RAEytot = 0;
            dispcnd = true;
            for(pidx = 1;pidx <= MAXPOLESEPS;pidx++) {
                RAEytot = RAEytot + RAEy[i][j][k][pidx-1];
            }

            if(i == 0 && k == 0) {
                if(!SBC) {
                    dHx = (Hx[i][j][k] - Hx[i][j][ZCELLS-1])/dz;
                    dHz = (Hz[i][j][k] - Hz[XCELLS-1][j][k])/dx;
                    Ey[i][j][k] = (dt/(epso*K1Ey[i][j][k]))*(dHx - dHz) +
                    (K2Ey[i][j][k]/K1Ey[i][j][k])*Ey[i][j][k] +
                    RAEytot/K1Ey[i][j][k];
                }
                else {
                    Ey[i][j][k] = 0;
                }
            }
            else if((i == 0 && k == ZCELLS) || (i == XCELLS && k == 0)
            || (i == XCELLS && k == ZCELLS)) {
                if(!SBC) {
                    Ey[i][j][k] = Ey[0][j][0];
                }
                else {
                    Ey[i][j][k] = 0;
                }
                dispcnd = false;
            }
            else if(i == 0) {
                if(!SBC) {
                    dHx = (Hx[i][j][k] - Hx[i][j][k-1])/dz;
                    dHz = (Hz[i][j][k] - Hz[XCELLS-1][j][k])/dx;
                    Ey[i][j][k] = (dt/(epso*K1Ey[i][j][k]))*(dHx - dHz) +
                    (K2Ey[i][j][k]/K1Ey[i][j][k])*Ey[i][j][k] +
                    RAEytot/K1Ey[i][j][k];
                }
                else {
                    dHx = (Hx[i][j][k] - Hx[i][j][k-1])/dz;
                    dHz = 2*(Hz[i][j][k])/dx;
                }
            }
        }
    }
}
}

```

```

Ey[i][j][k] = (dt/(epso*K1Ey[i][j][k]))*(dHx - dHz) +
(K2Ey[i][j][k]/K1Ey[i][j][k])*Ey[i][j][k] +
RAEytot/K1Ey[i][j][k];
}
}
else if(i == XCELLS) {
if(!SBC) {
Ey[i][j][k] = Ey[0][j][k];
dispcnd = false;
}
else {
dHx = (Hx[i][j][k] - Hx[i][j][k-1])/dz;
dHz = -2*(Hz[XCELLS-1][j][k])/dx;
Ey[i][j][k] = (dt/(epso*K1Ey[i][j][k]))*(dHx - dHz) +
(K2Ey[i][j][k]/K1Ey[i][j][k])*Ey[i][j][k] +
RAEytot/K1Ey[i][j][k];
}
}
else if(k == 0) {
if(!SBC) {
dHx = (Hx[i][j][k] - Hx[i][j][ZCELLS-1])/dz;
dHz = (Hz[i][j][k] - Hz[i-1][j][k])/dx;
Ey[i][j][k] = (dt/(epso*K1Ey[i][j][k]))*(dHx - dHz) +
(K2Ey[i][j][k]/K1Ey[i][j][k])*Ey[i][j][k] +
RAEytot/K1Ey[i][j][k];
}
else {
Ey[i][j][k] = 0;
}
}
else if(k == ZCELLS) {
if(!SBC) {
Ey[i][j][k] = Ey[i][j][0];
}
else {
Ey[i][j][k] = 0;
}
dispcnd = false;
}
else {
dHx = (Hx[i][j][k] - Hx[i][j][k-1])/dz;
dHz = (Hz[i][j][k] - Hz[i-1][j][k])/dx;
Ey[i][j][k] = (dt/(epso*K1Ey[i][j][k]))*(dHx - dHz) +
(K2Ey[i][j][k]/K1Ey[i][j][k])*Ey[i][j][k] +
RAEytot/K1Ey[i][j][k];
}
}

//Update RAEy for the next update
if(i > XCELLS/2 && !SBC) { ii = i - 1;}
else { ii = i; }
if(k > ZCELLS/2 && !SBC) { kk = k - 1;}
else { kk = k; }
int rankoff = (rank - 3)*yeePerProc;
dispcnd = dispcnd && IsDispersive(MediaFullDomain[ii][j+PL+rankoff][kk]);
if(dispcnd) {
for(pidx = 1;pidx <= MAXPOLESEPS;pidx++) {
DXeEy0 = GetXeDebye(ii,j+PL+rankoff,kk,0,dt,pidx)-
GetXeDebye(ii,j+PL+rankoff,kk,1,dt,pidx);
DXieEy0 = GetXieDebye(ii,j+PL+rankoff,kk,0,dt,pidx)-
GetXieDebye(ii,j+PL+rankoff,kk,1,dt,pidx);
CEy = exp(-dt/ GetTaueps(MediaFullDomain[ii][j+PL+rankoff][kk],pidx));
RAEy[i][j][k][pidx-1] = DXeEy0*Ey[i][j][k] + DXieEy0*(Eyo - Ey[i][j][k]) +
CEy*RAEy[i][j][k][pidx-1];
}
}
}
}
}
}

```

```

}

//Ez update
for(i = 0; i < XCELLS + 1; i++) {
  for(j = 0; j < yeePerProc; j++) {
    for(k = 0; k < ZCELLS; k++) {
      Ezo = Ez[i][j][k];
      RAEztot = 0;
      dispcnd = true;
      for(pidx = 1; pidx <= MAXPOLESEPS; pidx++) {
        RAEztot = RAEztot + RAEz[i][j][k][pidx-1];
      }

      if(i == 0) {
        if(!SBC) {
          dHy = (Hy[i][j][k] - Hy[XCELLS-1][j][k])/dx;
          if(j == yeePerProc - 1)
            dHx = (Hxb[i][k] - Hx[i][j][k])/dy;
          else
            dHx = (Hx[i][j+1][k] - Hx[i][j][k])/dy;

          Ez[i][j][k] = (dt/(epso*K1Ez[i][j][k]))*(dHy - dHx) +
            (K2Ez[i][j][k]/K1Ez[i][j][k])*Ez[i][j][k] +
            RAEztot/K1Ez[i][j][k];
        }
        else {
          dHy = 2*(Hy[i][j][k])/dx;
          if(j == yeePerProc - 1)
            dHx = (Hxb[i][k] - Hx[i][j][k])/dy;
          else
            dHx = (Hx[i][j+1][k] - Hx[i][j][k])/dy;

          Ez[i][j][k] = (dt/(epso*K1Ez[i][j][k]))*(dHy - dHx) +
            (K2Ez[i][j][k]/K1Ez[i][j][k])*Ez[i][j][k] +
            RAEztot/K1Ez[i][j][k];
        }
      }
      else if(i == XCELLS) {
        if(!SBC) {
          Ez[i][j][k] = Ez[0][j][k];
          dispcnd = false;
        }
        else {
          dHy = -2*(Hy[XCELLS-1][j][k])/dx;
          if(j == yeePerProc - 1)
            dHx = (Hxb[i][k] - Hx[i][j][k])/dy;
          else
            dHx = (Hx[i][j+1][k] - Hx[i][j][k])/dy;

          Ez[i][j][k] = (dt/(epso*K1Ez[i][j][k]))*(dHy - dHx) +
            (K2Ez[i][j][k]/K1Ez[i][j][k])*Ez[i][j][k] +
            RAEztot/K1Ez[i][j][k];
        }
      }
      else {
        dHy = (Hy[i][j][k] - Hy[i-1][j][k])/dx;
        if(j == yeePerProc - 1)
          dHx = (Hxb[i][k] - Hx[i][j][k])/dy;
        else
          dHx = (Hx[i][j+1][k] - Hx[i][j][k])/dy;

        Ez[i][j][k] = (dt/(epso*K1Ez[i][j][k]))*(dHy - dHx) +
          (K2Ez[i][j][k]/K1Ez[i][j][k])*Ez[i][j][k] +
          RAEztot/K1Ez[i][j][k];
      }
    }
  }
}

//Update RAEz for next update

```

```

if(i > XCELLS/2 && !SBC) { ii = i - 1;}
else { ii = i; }
int rankoff = (rank - 3)*yeePerProc + 1;
dispcnd = dispcnd && IsDispersive(MediaFullDomain[ii][j+PL+rankoff][k]);
if(dispcnd) {
  for(pidx = 1;pidx <= MAXPOLESEPS;pidx++) {
    DXeEz0 = GetXeDebye(ii,j+PL+rankoff,k,0,dt,pidx)
    - GetXeDebye(ii,j+PL+rankoff,k,1,dt,pidx);
    DXieEz0 = GetXieDebye(ii,j+PL+rankoff,k,0,dt,pidx)
    - GetXieDebye(ii,j+PL+rankoff,k,1,dt,pidx);
    CEz = exp(-dt / GetTaueps(MediaFullDomain[ii][j+PL+rankoff][k],pidx));

    RAEz[i][j][k][pidx-1] = DXeEz0*Ez[i][j][k] + DXieEz0*(Ezo - Ez[i][j][k]) +
    CEz*RAEz[i][j][k][pidx-1];
  }
}
}
}

if(rank == 3) {
  //Recv Ez,Ex
  for(mpidx = 0;mpidx < XCELLS;mpidx++) {
    MPI_Recv(&Exb[mpidx][0],ZCELLS + 1,MPI_DOUBLE,rank - 2,1*10+3*1+0,
    MPI_COMM_WORLD,&status);
  }
  for(mpidx = 0;mpidx < XCELLS + 1;mpidx++) {
    MPI_Recv(&Ezb[mpidx][0],ZCELLS,MPI_DOUBLE,rank - 2,1*10+3*1+1,
    MPI_COMM_WORLD,&status);
  }
}
else {
  //Recv Ez,Ex
  for(mpidx = 0;mpidx < XCELLS;mpidx++) {
    MPI_Recv(&Exb[mpidx][0],ZCELLS + 1,MPI_DOUBLE,rank - 1,(rank - 1)*10
    +(rank*1)+0,MPI_COMM_WORLD,&status);
  }
  for(mpidx = 0;mpidx < XCELLS + 1;mpidx++) {
    MPI_Recv(&Ezb[mpidx][0],ZCELLS,MPI_DOUBLE,rank - 1,(rank - 1)*10
    +(rank*1)+1,MPI_COMM_WORLD,&status);
  }
}

//Send Ex,Ez to rank+1 proc
for(mpidx = 0;mpidx < XCELLS;mpidx++) {
  MPI_Send(&Ex[mpidx][yeePerProc-1][0],ZCELLS + 1,MPI_DOUBLE,rank + 1,
  rank*10+(rank + 1)*1+0,MPI_COMM_WORLD);
}
for(mpidx = 0;mpidx < XCELLS + 1;mpidx++) {
  MPI_Send(&Ez[mpidx][yeePerProc-1][0],ZCELLS,MPI_DOUBLE,rank + 1,
  rank*10+(rank + 1)+1,MPI_COMM_WORLD);
}

//Source excitation
if(rank == SPrank) {
  for(int is = 0 ; is < XCELLS + 1;is++) {
    for(int ks = 0;ks < ZCELLS;ks++) {
      if(source == EXPRAMPSINE) {
        if(n <= 960)
          Ez[is][SPidx][ks] = Ez[is][SPidx][ks] + exp(-1*pow((time-960*dt)/(200*dt),2)) *
          sin(2*pi*time*fs);
        else
          Ez[is][SPidx][ks] = Ez[is][SPidx][ks] + sin(2*pi*time*fs);
      }
      else if(source == GAUSSIAN) {
        Ez[is][SPidx][ks] = Ez[is][SPidx][ks] + exp(-1*pow((time-to)/(tau),2));
      }
    }
  }
}

```

```

else if(source == MODGAUSSIAN) {
    Ez[is][SPidx][ks] = Ez[is][SPidx][ks] +
        exp(-1*pow((time-to)/(tau),2))*cos(2*pi*time*fc);
}
else if(source == DIFFGAUSSIAN) {
    Ez[is][SPidx][ks] = Ez[is][SPidx][ks] +
        sqrt(2*e)*((time - 2*to)/Tb)*exp(-1*pow((time - 2*to)/Tb,2));
}
}
}
}

if(INCSIM) {
    if(rank == OPrank) {
        outEz<<Ez[Round(XCELLS/2)][OPidx][Round(ZCELLS/2)]<<endl;
        outHx<<(Hx[Round(XCELLS/2)][OPidx][Round(ZCELLS/2)] +
            Hx[Round(XCELLS/2)][OPidx+1][Round(ZCELLS/2)])/2<<endl;
    }
}

//n1 - First index,n2 - Last index for writing data to .dat file
int n1 = 0;
int n2 = T;
//Ez - total field
if(n >= n1 && n <= n2 && rank == OPrank && !INCSIM){
    for(int xidx = 0;xidx < XCELLS + 1;xidx++){
        for(int zidx = 0;zidx < ZCELLS + 1;zidx++){

            double val;
            if(zidx == 0){
                val = Ez[xidx][OPidx][zidx];
            }
            else if(zidx == ZCELLS){
                val = Ez[xidx][OPidx][zidx -1];
            }
            else{
                val = (Ez[xidx][OPidx][zidx] + Ez[xidx][OPidx][zidx-1])/2;
            }

            outEz<<val<<endl;
        }
    }
}

//Ey - total field
/*if(n >= n1 && n <= n2 && rank == OPrank && !INCSIM){
    for(int xidx = 0;xidx < XCELLS + 1;xidx++){
        for(int zidx = 0;zidx < ZCELLS + 1;zidx++){
            double val;
            val = (Ey[xidx][OPidx][zidx] + Ey[xidx][OPidx-1][zidx])/2;

            outEy<<val<<endl;
        }
    }
}*/

//Hx - total field
if(n >= n1 && n <= n2 && rank == OPrank && !INCSIM){
    for(int xidx = 0;xidx < XCELLS + 1;xidx++){
        for(int zidx = 0;zidx < ZCELLS + 1;zidx++){
            double val;
            if(zidx == 0) {
                val = (Hx[xidx][OPidx][zidx] + Hx[xidx][OPidx+1][zidx])/2;
            }
            else if(zidx == ZCELLS){
                val = (Hx[xidx][OPidx][zidx-1] + Hx[xidx][OPidx+1][zidx-1])/2;
            }
        }
    }
}

```

```

        else{
            val = (Hx[xidx][OPidx][zidx] + Hx[xidx][OPidx+1][zidx]
+ Hx[xidx][OPidx][zidx-1] + Hx[xidx][OPidx+1][zidx-1])/4;
        }
        outHx<<val<<endl;
    }
}
}

//Hz - total field
if(n >= n1 && n <= n2 && rank == OPrank && !INCSIM){
for(int xidx = 0;xidx < XCELLS + 1;xidx++){
for(int zidx = 0;zidx < ZCELLS + 1;zidx++){
    double val;
    if(xidx == 0 || xidx == XCELLS || zidx == 0 || zidx == ZCELLS){
        val = 0;
    }
    else{
        val = (Hz[xidx][OPidx][zidx] + Hz[xidx-1][OPidx][zidx]
+ Hz[xidx][OPidx+1][zidx] + Hz[xidx-1][OPidx+1][zidx])/4;
    }
    outHz<<val<<endl;
}
}
}

//Hy
/*if(n >= n1 && n <= n2 && rank == OPrank && !INCSIM){
for(int xidx = 0;xidx < XCELLS + 1;xidx++){
for(int zidx = 0;zidx < ZCELLS + 1;zidx++){
    double val;
    if(xidx == 0 || xidx == XCELLS) {
        val = 0;
    }
    else if(zidx == 0) {
        val = (Hy[xidx-1][OPidx][zidx] + Hy[xidx][OPidx][zidx])/2;
    }
    else if(zidx == ZCELLS) {
        val = (Hy[xidx-1][OPidx][zidx-1] + Hy[xidx][OPidx][zidx-1])/2;
    }
    else {
        val = (Hy[xidx-1][OPidx][zidx-1] + Hy[xidx][OPidx][zidx-1] +
+ Hy[xidx][OPidx][zidx] + Hy[xidx-1][OPidx][zidx])/4;
    }

    outHy<<val<<endl;
}
}
}
*/

//Ex
if(n >= n1 && n <= n2 && rank == OPrank && !INCSIM){
for(int xidx = 0;xidx < XCELLS + 1;xidx++){
for(int zidx = 0;zidx < ZCELLS + 1;zidx++){
    double val;
    if(xidx == 0 || zidx == 0 || xidx == XCELLS || zidx == ZCELLS){
        val = 0;
    }
    else{
        val = (Ex[xidx][OPidx][zidx] + Ex[xidx-1][OPidx][zidx])/2;
    }
    outEx<<val<<endl;
}
}
}
}

```

```

time = time + 0.5*dt;

//Hx update
for(i = 0;i < XCELLS + 1;i++) {
  for(j = 0;j < yeePerProc;j++) {
    for(k = 0;k < ZCELLS;k++) {
      // Hx update in main grid
      Hxo = Hx[i][j][k];
      dEy = (Ey[i][j][k+1] - Ey[i][j][k])/dz;
      if(j == 0)
        dEz = (Ez[i][j][k] - Ezb[i][k])/dy;
      else
        dEz = (Ez[i][j][k] - Ez[i][j-1][k])/dy;

      RAHxtot = 0;
      for(pidx = 1;pidx <= MAXPOLESMU;pidx++) {
        RAHxtot = RAHxtot + RAHx[i][j][k][pidx-1];
      }

      if(i == XCELLS && !SBC) {
        Hx[i][j][k] = Hx[0][j][k];
      }
      else {
        Hx[i][j][k] = (dt/(muo*K1Hx[i][j][k]))*(dEy - dEz)
          + (K2Hx[i][j][k]/K1Hx[i][j][k])*Hx[i][j][k]
          + RAHxtot/K1Hx[i][j][k];
      }

      //Update RAHx for the next update of Hx
      double DXmHx0 = 0,DXimHx0 = 0,CHx;
      bool dispcond = false;
      if((i > XCELLS/2 && !SBC)) {
        ii = i - 1;
      }
      else {
        ii = i;
      }
      int rankoff = (rank - 3) * yeePerProc;
      dispcond = IsDispersive(MediaFullDomain[ii][j+rankoff+PL][k]);
      if(dispcond) {
        for(pidx = 1;pidx <= MAXPOLESMU;pidx++) {
          DXmHx0 = GetXmDebye(ii,j+rankoff+PL,k,0,dt,pidx)
            - GetXmDebye(ii,j+rankoff+PL,k,1,dt,pidx);
          DXimHx0 = GetXimDebye(ii,j+rankoff+PL,k,0,dt,pidx)
            - GetXimDebye(ii,j+rankoff+PL,k,1,dt,pidx);
          CHx = exp(-dt/ GetTauMu(MediaFullDomain[ii][j+rankoff+PL][k],pidx));

          RAHx[i][j][k][pidx-1] = DXmHx0*Hx[i][j][k] + DXimHx0*(Hxo - Hx[i][j][k]) +
            CHx*RAHx[i][j][k][pidx-1];
        }
      }
    }
  }
}

//Hy update (n + 0.5)
for(i = 0;i < XCELLS;i++) {
  for(j = 0;j < yeePerProc;j++) {
    for(k = 0;k < ZCELLS;k++) {
      //Hy update in main grid
      Hyo = Hy[i][j][k];
      dEz = (Ez[i+1][j][k] - Ez[i][j][k])/dx;
      dEx = (Ex[i][j][k+1] - Ex[i][j][k])/dz;

      RAHytot = 0;
      for(pidx = 1;pidx <= MAXPOLESMU;pidx++) {

```

```

    RAHytot = RAHytot + RAHy[i][j][k][pidx-1];
}
Hy[i][j][k] = (dt/(muo*K1Hy[i][j][k]))*(dEz - dEx)
+ (K2Hy[i][j][k]/K1Hy[i][j][k])*Hy[i][j][k]
+ RAHytot/K1Hy[i][j][k];

// Update RAHy for the next update of Hy
dispcnd = false;
double DXmHy0,DXimHy0,CHy;
int rankoff = (rank - 3)*yeePerProc + 1;
dispcnd = IsDispersive(MediaFullDomain[i][j+PL+rankoff][k]);
if(dispcnd) {
for(pidx = 1;pidx <= MAXPOLESMU;pidx++) {
DXmHy0 = GetXmDebye(i,j+PL+rankoff,k,0,dt,pidx)
- GetXmDebye(i,j+PL+rankoff,k,1,dt,pidx);
DXimHy0 = GetXimDebye(i,j+PL+rankoff,k,0,dt,pidx)
- GetXimDebye(i,j+PL+rankoff,k,1,dt,pidx) ;
CHy = exp(-dt/GetTauMu(MediaFullDomain[i][j+PL+rankoff][k],pidx));

RAHy[i][j][k][pidx-1] = DXmHy0*Hy[i][j][k] + DXimHy0*(Hyo - Hy[i][j][k])
+ CHy*RAHy[i][j][k][pidx-1];
}
}
}
}

//Hz update (at n + 0.5)
for(j = 0;j < yeePerProc;j++) {
for(i = 0;i < XCELLS;i++) {
for(k = 0;k < ZCELLS + 1;k++) {
//Hz update in main grid
Hzo = Hz[i][j][k];
if(j == 0)
dEx = (Ex[i][j][k] - Exb[i][k])/dy;
else
dEx = (Ex[i][j][k] - Ex[i][j-1][k])/dy;
dEy = (Ey[i+1][j][k] - Ey[i][j][k])/dx;

RAHztot = 0;
for(pidx = 1;pidx <= MAXPOLESMU;pidx++) {
RAHztot = RAHztot + RAHz[i][j][k][pidx-1];
}
Hz[i][j][k] = (dt/(muo*K1Hz[i][j][k]))*(dEx - dEy) +
(K2Hz[i][j][k]/K1Hz[i][j][k])*Hz[i][j][k]
+ RAHztot/K1Hz[i][j][k];

//Update RAHz for the next update of Hz
double DXmHz0,DXimHz0,CHz;
dispcnd = false;
if(k > ZCELLS/2 && !SBC) { kk = k - 1;}
else { kk = k;}
int rankoff = (rank - 3)*yeePerProc;
dispcnd = IsDispersive(MediaFullDomain[i][j+PL+rankoff][kk]);
if(dispcnd) {
for(pidx = 1;pidx <= MAXPOLESMU;pidx++) {
DXmHz0 = GetXmDebye(i,j+PL+rankoff,kk,0,dt,pidx)
- GetXmDebye(i,j+PL+rankoff,kk,1,dt,pidx);
DXimHz0 = GetXimDebye(i,j+PL+rankoff,kk,0,dt,pidx)
- GetXimDebye(i,j+PL+rankoff,kk,1,dt,pidx);
CHz = exp(-dt/GetTauMu(MediaFullDomain[i][j+PL+rankoff][kk],pidx));
RAHz[i][j][k][pidx-1] = DXmHz0*Hz[i][j][k] + DXimHz0*(Hzo - Hz[i][j][k])
+ CHz*RAHz[i][j][k][pidx-1];
}
}
}
}
}
}

```

```

}

//Send Hxb,Hzb
if(rank == 3) {
  for(mpidx = 0;mpidx < XCELLS + 1;mpidx++) {
    MPI_Send(&Hx[mpidx][0][0],ZCELLS,MPI_DOUBLE,1,
      rank*10+(1*1)+0,MPI_COMM_WORLD);
  }
  for(mpidx = 0;mpidx < XCELLS;mpidx++) {
    MPI_Send(&Hz[mpidx][0][0],ZCELLS + 1,MPI_DOUBLE,1,
      rank*10+(1*1)+1,MPI_COMM_WORLD);
  }
}
else {
  for(mpidx = 0;mpidx < XCELLS + 1;mpidx++) {
    MPI_Send(&Hx[mpidx][0][0],ZCELLS,MPI_DOUBLE,rank - 1,
      rank*10+((rank-1)*1)+0,MPI_COMM_WORLD);
  }
  for(mpidx = 0;mpidx < XCELLS;mpidx++) {
    MPI_Send(&Hz[mpidx][0][0],ZCELLS + 1,MPI_DOUBLE,rank - 1,
      rank*10+((rank-1)*1)+1,MPI_COMM_WORLD);
  }
}
//Recv Hxb,Hzb
for(mpidx = 0;mpidx < XCELLS + 1;mpidx++) {
  MPI_Recv(&Hxb[mpidx][0],ZCELLS,MPI_DOUBLE,rank + 1,
    (rank+1)*10+(rank*1)+0,MPI_COMM_WORLD,&status);
}
for(mpidx = 0;mpidx < XCELLS;mpidx++) {
  MPI_Recv(&Hzb[mpidx][0],ZCELLS + 1,MPI_DOUBLE,rank + 1,
    (rank+1)*10+(rank*1)+1,MPI_COMM_WORLD,&status);
}

time = time + 0.5*dt;
} //n
} //rank >=3 && rank <= NProcs - 2

if(rank == NProcs - 1) {
  for(n = 0;n < T;n++) {
    // Ex main grid update equations
    for(i = 0;i < XCELLS;i++) {
      for(j = 0;j < yeePerProc - 1;j++) {
        for(k = 0;k < ZCELLS + 1;k++) {
          Exo = Ex[i][j][k];
          RAExtot = 0;
          dispcond = true;
          for(pidx = 1;pidx <= MAXPOLESEPS;pidx++) {
            RAExtot = RAExtot + RAEx[i][j][k][pidx-1];
          }

          if(k == 0) {
            if(!SBC) {
              dHz = (Hz[i][j+1][k] - Hz[i][j][k])/dy;
              dHy = (Hy[i][j][k] - Hy[i][j][ZCELLS-1])/dz;
              Ex[i][j][k] = (dt/(epso*K1Ex[i][j][k]))*(dHz - dHy)
                + (K2Ex[i][j][k]/K1Ex[i][j][k])*Ex[i][j][k] +
                RAExtot/K1Ex[i][j][k];
            }
            else {
              Ex[i][j][k] = 0;
            }
          }
        }
      }
    }
    //PBC on zmax
    else if(k == ZCELLS) {
      if(!SBC) {
        Ex[i][j][k] = Ex[i][j][0];
      }
    }
  }
}

```

```

else {
    Ex[i][j][k] = 0;
}
dispscond = false;
}
else {
    dHz = (Hz[i][j+1][k] - Hz[i][j][k])/dy;
    dHy = (Hy[i][j][k] - Hy[i][j][k-1])/dz;
    Ex[i][j][k] = (dt/(epso*K1Ex[i][j][k]))*(dHz - dHy)
        + (K2Ex[i][j][k]/K1Ex[i][j][k])*Ex[i][j][k] +
        RAEExtot/K1Ex[i][j][k];
}

int rankoff = (rank - 3)*yeePerProc + 1;
//Update RAEEx for the next update
if(k > ZCELLS/2 && !SBC) { kk = k - 1; }
else { kk = k;}
//dispscond will be false for k = ZCELLS
dispscond = dispscond && IsDispersive(MediaFullDomain[i][j+PL+rankoff][kk]);
if(dispscond) {
    for(pidx = 1;pidx <= MAXPOLESEPS;pidx++) {
        DXeEx0 = GetXeDebye(i,j+PL+rankoff,kk,0,dt,pidx)
            - GetXeDebye(i,j+PL+rankoff,kk,1,dt,pidx);
        DXieEx0 = GetXieDebye(i,j+PL+rankoff,kk,0,dt,pidx)
            - GetXieDebye(i,j+PL+rankoff,kk,1,dt,pidx);
        CEx = exp(-dt/ GetTaueps(MediaFullDomain[i][j+PL+rankoff][kk],pidx));

        RAEEx[i][j][k][pidx-1] = DXeEx0*Ex[i][j][k] + DXieEx0*(Exo - Ex[i][j][k]) +
            CEx*RAEEx[i][j][k][pidx-1];
    }
}
}
}
}

//Ey main grid update equations
for(i = 0;i < XCELLS + 1;i++) {
    for(j = 0;j < yeePerProc;j++) {
        for(k = 0;k < ZCELLS + 1;k++) {
            Eyo = Ey[i][j][k];
            RAEytot = 0;
            dispscond = true;
            for(pidx = 1;pidx <= MAXPOLESEPS;pidx++) {
                RAEytot = RAEytot + RAEy[i][j][k][pidx-1];
            }

            if(i == 0 && k == 0) {
                if(!SBC) {
                    dHx = (Hx[i][j][k] - Hx[i][j][ZCELLS-1])/dz;
                    dHz = (Hz[i][j][k] - Hz[XCELLS-1][j][k])/dx;
                    Ey[i][j][k] = (dt/(epso*K1Ey[i][j][k]))*(dHx - dHz) +
                        (K2Ey[i][j][k]/K1Ey[i][j][k])*Ey[i][j][k] +
                        RAEytot/K1Ey[i][j][k];
                }
                else {
                    Ey[i][j][k] = 0;
                }
            }
        }
    }
    else if((i == 0 && k == ZCELLS) || (i == XCELLS && k == 0)
        || (i == XCELLS && k == ZCELLS)) {
        if(!SBC) {
            Ey[i][j][k] = Ey[0][j][0];
        }
        else {
            Ey[i][j][k] = 0;
        }
    }
    dispscond = false;
}

```

```

}
else if(i == 0) {
  if(!SBC) {
    dHx = (Hx[i][j][k] - Hx[i][j][k-1])/dz;
    dHz = (Hz[i][j][k] - Hz[XCELLS-1][j][k])/dx;
    Ey[i][j][k] = (dt/(epso*K1Ey[i][j][k]))*(dHx - dHz) +
      (K2Ey[i][j][k]/K1Ey[i][j][k])*Ey[i][j][k] +
      RAEytot/K1Ey[i][j][k];
  }
  else {
    dHx = (Hx[i][j][k] - Hx[i][j][k-1])/dz;
    dHz = 2*(Hz[i][j][k])/dx;
    Ey[i][j][k] = (dt/(epso*K1Ey[i][j][k]))*(dHx - dHz) +
      (K2Ey[i][j][k]/K1Ey[i][j][k])*Ey[i][j][k] +
      RAEytot/K1Ey[i][j][k];
  }
}
else if(i == XCELLS) {
  if(!SBC) {
    Ey[i][j][k] = Ey[0][j][k];
    dispcond = false;
  }
  else {
    dHx = (Hx[i][j][k] - Hx[i][j][k-1])/dz;
    dHz = -2*(Hz[XCELLS-1][j][k])/dx;
    Ey[i][j][k] = (dt/(epso*K1Ey[i][j][k]))*(dHx - dHz) +
      (K2Ey[i][j][k]/K1Ey[i][j][k])*Ey[i][j][k] +
      RAEytot/K1Ey[i][j][k];
  }
}
else if(k == 0) {
  if(!SBC) {
    dHx = (Hx[i][j][k] - Hx[i][j][ZCELLS-1])/dz;
    dHz = (Hz[i][j][k] - Hz[i-1][j][k])/dx;
    Ey[i][j][k] = (dt/(epso*K1Ey[i][j][k]))*(dHx - dHz) +
      (K2Ey[i][j][k]/K1Ey[i][j][k])*Ey[i][j][k] +
      RAEytot/K1Ey[i][j][k];
  }
  else {
    Ey[i][j][k] = 0;
  }
}
else if(k == ZCELLS) {
  if(!SBC) {
    Ey[i][j][k] = Ey[i][j][0];
  }
  else {
    Ey[i][j][k] = 0;
  }
  dispcond = false;
}
else {
  dHx = (Hx[i][j][k] - Hx[i][j][k-1])/dz;
  dHz = (Hz[i][j][k] - Hz[i-1][j][k])/dx;
  Ey[i][j][k] = (dt/(epso*K1Ey[i][j][k]))*(dHx - dHz) +
    (K2Ey[i][j][k]/K1Ey[i][j][k])*Ey[i][j][k] +
    RAEytot/K1Ey[i][j][k];
}

//Update RAEy for the next update
if(i > XCELLS/2 && !SBC) { ii = i - 1;}
else { ii = i; }
if(k > ZCELLS/2 && !SBC) { kk = k - 1;}
else { kk = k; }
int rankoff = (rank - 3)*yeePerProc;
dispcond = dispcond && IsDispersive(MediaFullDomain[ii][j+PL+rankoff][kk]);
if(dispcond) {

```

```

for(pidx = 1;pidx <= MAXPOLESEPS;pidx++) {
  DXeEy0 = GetXeDebye(ii,j+PL+rankoff,kk,0,dt,pidx)
  -GetXeDebye(ii,j+PL+rankoff,kk,1,dt,pidx);
  DXieEy0 = GetXieDebye(ii,j+PL+rankoff,kk,0,dt,pidx)
  -GetXieDebye(ii,j+PL+rankoff,kk,1,dt,pidx);
  CEy = exp(-dt/ GetTaueps(MediaFullDomain[ii][j+PL+rankoff][kk],pidx));
  RAEy[i][j][k][pidx-1] = DXeEy0*Ey[i][j][k] + DXieEy0*(Eyo - Ey[i][j][k]) +
  CEy*RAEy[i][j][k][pidx-1];
}
}
}
}

//Ez update
for(i = 0;i < XCELLS + 1;i++) {
  for(j = 0;j < yeePerProc - 1;j++) {
    for(k = 0;k < ZCELLS;k++) {
      Ezo = Ez[i][j][k];
      RAEztot = 0;
      dispcond = true;
      for(pidx = 1;pidx <= MAXPOLESEPS;pidx++) {
        RAEztot = RAEztot + RAEz[i][j][k][pidx-1];
      }

      if(i == 0) {
        if(!SBC) {
          dHy = (Hy[i][j][k] - Hy[XCELLS-1][j][k])/dx;
          dHx = (Hx[i][j+1][k] - Hx[i][j][k])/dy;

          Ez[i][j][k] = (dt/(epso*K1Ez[i][j][k]))*(dHy - dHx) +
            (K2Ez[i][j][k]/K1Ez[i][j][k])*Ez[i][j][k] +
            RAEztot/K1Ez[i][j][k];
        }
        else {
          dHy = 2*(Hy[i][j][k])/dx;
          dHx = (Hx[i][j+1][k] - Hx[i][j][k])/dy;

          Ez[i][j][k] = (dt/(epso*K1Ez[i][j][k]))*(dHy - dHx) +
            (K2Ez[i][j][k]/K1Ez[i][j][k])*Ez[i][j][k] +
            RAEztot/K1Ez[i][j][k];
        }
      }
      else if(i == XCELLS) {
        if(!SBC) {
          Ez[i][j][k] = Ez[0][j][k];
          dispcond = false;
        }
        else {
          dHy = -2*(Hy[XCELLS-1][j][k])/dx;
          dHx = (Hx[i][j+1][k] - Hx[i][j][k])/dy;

          Ez[i][j][k] = (dt/(epso*K1Ez[i][j][k]))*(dHy - dHx) +
            (K2Ez[i][j][k]/K1Ez[i][j][k])*Ez[i][j][k] +
            RAEztot/K1Ez[i][j][k];
        }
      }
      else {
        dHy = (Hy[i][j][k] - Hy[i-1][j][k])/dx;
        dHx = (Hx[i][j+1][k] - Hx[i][j][k])/dy;

        Ez[i][j][k] = (dt/(epso*K1Ez[i][j][k]))*(dHy - dHx) +
          (K2Ez[i][j][k]/K1Ez[i][j][k])*Ez[i][j][k] +
          RAEztot/K1Ez[i][j][k];
      }
    }
  }
}

//Update RAEz for next update

```

```

if(i > XCELLS/2 && !SBC) { ii = i - 1;}
else { ii = i; }
int rankoff = (rank - 3)*yeePerProc + 1;
dispcnd = dispcnd && IsDispersive(MediaFullDomain[ii][j+PL+rankoff][k]);
if(dispcnd) {
  for(pidx = 1;pidx <= MAXPOLESEPS;pidx++) {
    DXeEz0 = GetXeDebye(ii,j+PL+rankoff,k,0,dt,pidx)
    - GetXeDebye(ii,j+PL+rankoff,k,1,dt,pidx);
    DXieEz0 = GetXieDebye(ii,j+PL+rankoff,k,0,dt,pidx)
    - GetXieDebye(ii,j+PL+rankoff,k,1,dt,pidx);
    CEz = exp(-dt / GetTaueps(MediaFullDomain[ii][j+PL+rankoff][k],pidx));

    RAEz[i][j][k][pidx-1] = DXeEz0*Ez[i][j][k] + DXieEz0*(Ezo - Ez[i][j][k]) +
    CEz*RAEz[i][j][k][pidx-1];
  }
}
}
}

//Recv Ez,Ex
for(mpidx = 0;mpidx < XCELLS;mpidx++) {
  MPI_Recv(&Exb[mpidx][0],ZCELLS + 1,MPI_DOUBLE,rank - 1,
  (rank-1)*10+(rank*1)+0,MPI_COMM_WORLD,&status);
}
for(mpidx = 0;mpidx < XCELLS + 1;mpidx++) {
  MPI_Recv(&Ezb[mpidx][0],ZCELLS,MPI_DOUBLE,rank - 1,
  (rank-1)*10+(rank*1)+1,MPI_COMM_WORLD,&status);
}

//Recv Ezb1,Exb1
for(mpidx = 0;mpidx < XCELLS;mpidx++) {
  MPI_Recv(&Exb1[mpidx][0],ZCELLS + 1,MPI_DOUBLE,2,
  2*10+(NProcs-1)*1+0,MPI_COMM_WORLD,&status);
}
for(mpidx = 0;mpidx < XCELLS + 1;mpidx++) {
  MPI_Recv(&Ezb1[mpidx][0],ZCELLS,MPI_DOUBLE,2,
  2*10+(NProcs-1)*1+1,MPI_COMM_WORLD,&status);
}

time = time + 0.5*dt;

//Hx update
for(i = 0;i < XCELLS + 1;i++) {
  for(j = 0;j < yeePerProc;j++) {
    for(k = 0;k < ZCELLS;k++) {
      // Hx update in main grid
      Hxo = Hx[i][j][k];
      dEy = (Ey[i][j][k+1] - Ey[i][j][k])/dz;
      if(j == 0)
        dEz = (Ez[i][j][k] - Ezb[i][k])/dy;
      else if(j == yeePerProc - 1)
        dEz = (Ezb1[i][k] - Ez[i][j-1][k])/dy;
      else
        dEz = (Ez[i][j][k] - Ez[i][j-1][k])/dy;

      RAHxtot = 0;
      for(pidx = 1;pidx <= MAXPOLESMU;pidx++) {
        RAHxtot = RAHxtot + RAHx[i][j][k][pidx-1];
      }

      if(i == XCELLS && !SBC) {
        Hx[i][j][k] = Hx[0][j][k];
      }
      else {
        Hx[i][j][k] = (dt/(muo*K1Hx[i][j][k]))*(dEy - dEz)
        + (K2Hx[i][j][k]/K1Hx[i][j][k])*Hx[i][j][k]

```

```

    + RAHxtot/K1Hx[i][j][k];
}

//Update RAHx for the next update of Hx
double DXmHx0 = 0,DXimHx0 = 0,CHx;
bool dispcond = false;
if((i > XCELLS/2 && !SBC)) {
    ii = i - 1;
}
else {
    ii = i;
}
int rankoff = (rank - 3)*yeePerProc;
dispcond = IsDispersive(MediaFullDomain[ii][j+PL+rankoff][k]);
if(dispcond) {
    for(pidx = 1;pidx <= MAXPOLESMU;pidx++) {
        DXmHx0 = GetXmDebye(ii,j+PL+rankoff,k,0,dt,pidx)
        - GetXmDebye(ii,j+PL+rankoff,k,1,dt,pidx);
        DXimHx0 = GetXimDebye(ii,j+PL+rankoff,k,0,dt,pidx)
        - GetXimDebye(ii,j+PL+rankoff,k,1,dt,pidx);
        CHx = exp(-dt/ GetTauMu(MediaFullDomain[ii][j+PL+rankoff][k],pidx));
        RAHx[i][j][k][pidx-1] = DXmHx0*Hx[i][j][k] + DXimHx0*(Hxo - Hx[i][j][k]) +
        CHx*RAHx[i][j][k][pidx-1];
    }
}
}
}
}

//Hy update
for(i = 0;i < XCELLS;i++) {
    for(j = 0;j < yeePerProc - 1;j++) {
        for(k = 0;k < ZCELLS;k++) {
            // Hy update in main grid
            Hyo = Hy[i][j][k];
            dEz = (Ez[i+1][j][k] - Ez[i][j][k])/dx;
            dEx = (Ex[i][j][k+1] - Ex[i][j][k])/dz;

            RAHytot = 0;
            for(pidx = 1;pidx <= MAXPOLESMU;pidx++) {
                RAHytot = RAHytot + RAHy[i][j][k][pidx-1];
            }
            Hy[i][j][k] = (dt/(muo*K1Hy[i][j][k]))*(dEz - dEx)
                + (K2Hy[i][j][k]/K1Hy[i][j][k])*Hyo + RAHytot/K1Hy[i][j][k];

            //Update RAHy for the next update of Hy
            dispcond = false;
            double DXmHy0,DXimHy0,CHy;
            int rankoff = (rank - 3)*yeePerProc + 1;
            dispcond = IsDispersive(MediaFullDomain[i][j+PL+rankoff][k]);
            if(dispcond) {
                for(pidx = 1;pidx <= MAXPOLESMU;pidx++) {
                    DXmHy0 = GetXmDebye(i,j+PL+rankoff,k,0,dt,pidx)
                    - GetXmDebye(i,j+PL+rankoff,k,1,dt,pidx);
                    DXimHy0 = GetXimDebye(i,j+PL+rankoff,k,0,dt,pidx)
                    - GetXimDebye(i,j+PL+rankoff,k,1,dt,pidx);
                    CHy = exp(-dt/GetTauMu(MediaFullDomain[i][j+PL+rankoff][k],pidx));
                    RAHy[i][j][k][pidx-1] = DXmHy0*Hyo + DXimHy0*(Hyo - Hy[i][j][k])
                    + CHy*RAHy[i][j][k][pidx-1];
                }
            }
        }
    }
}
}
}
}

```

```

//Hz update
for(i = 0;i < XCELLS;i++) {
  for(j = 0;j < yeePerProc;j++) {
    for(k = 0;k < ZCELLS + 1;k++) {
      // Hz update in main grid
      Hzo = Hz[i][j][k];

      if(j == 0)
        dEx = (Ex[i][j][k] - Exb[i][k])/dy;
      else if(j == yeePerProc - 1)
        dEx = (Exb1[i][k] - Ex[i][j-1][k])/dy;
      else
        dEx = (Ex[i][j][k] - Ex[i][j-1][k])/dy;
      dEy = (Ey[i+1][j][k] - Ey[i][j][k])/dx;

      RAHztot = 0;
      for(pidx = 1;pidx <= MAXPOLESMU;pidx++) {
        RAHztot = RAHztot + RAHz[i][j][k][pidx-1];
      }

      Hz[i][j][k] = (dt/(muo*K1Hz[i][j][k]))*(dEx - dEy) +
        (K2Hz[i][j][k]/K1Hz[i][j][k])*Hz[i][j][k]
        + RAHztot/K1Hz[i][j][k];

      //Update RAHz for the next update of Hz
      double DXmHz0,DXimHz0,CHz;
      dispcond = false;
      if(k > ZCELLS/2 && !SBC) { kk = k - 1;}
      else { kk = k;}
      int rankoff = (rank - 3)*yeePerProc;
      dispcond = IsDispersive(MediaFullDomain[i][j+PL+rankoff][kk]);
      if(dispcond) {
        for(pidx = 1;pidx <= MAXPOLESMU;pidx++) {
          DXmHz0 = GetXmDebye(i,j+PL+rankoff,kk,0,dt,pidx)
            - GetXmDebye(i,j+PL+rankoff,kk,1,dt,pidx);
          DXimHz0 = GetXimDebye(i,j+PL+rankoff,kk,0,dt,pidx)
            - GetXimDebye(i,j+PL+rankoff,kk,1,dt,pidx);
          CHz = exp(-dt/GetTauMu(MediaFullDomain[i][j+PL+rankoff][kk],pidx));
          RAHz[i][j][k][pidx-1] = DXmHz0*Hz[i][j][k] + DXimHz0*(Hzo - Hz[i][j][k])
            +CHz*RAHz[i][j][k][pidx-1];
        }
      }
    }
  }
}

//Send Hx,Hz to rank 2
for(mpidx = 0;mpidx < XCELLS + 1;mpidx++) {
  MPI_Send(&Hx[mpidx][yeePerProc-1][0],ZCELLS,MPI_DOUBLE,2,
    rank*10+(2*1)+0,MPI_COMM_WORLD);
}
for(mpidx = 0;mpidx < XCELLS;mpidx++) {
  MPI_Send(&Hz[mpidx][yeePerProc-1][0],ZCELLS + 1,MPI_DOUBLE,2,
    rank*10+(2*1)+1,MPI_COMM_WORLD);
}

//Send Hx,Hz to rank 'NProcs - 2'
for(mpidx = 0;mpidx < XCELLS + 1;mpidx++) {
  MPI_Send(&Hx[mpidx][0][0],ZCELLS,MPI_DOUBLE,NProcs - 2,
    rank*10+(NProcs - 2)+0,MPI_COMM_WORLD);
}
for(mpidx = 0;mpidx < XCELLS;mpidx++) {
  MPI_Send(&Hz[mpidx][0][0],ZCELLS + 1,MPI_DOUBLE,NProcs - 2,
    rank*10+(NProcs - 2)+1,MPI_COMM_WORLD);
}

```

```

time = time + 0.5*dt;

} //n
} // rank = NProcs - 1

//Delete the boundary field matrices
if(rank == 1) {
  DeleteMatrix(Hzb,XCELLS,ZCELLS + 1);
  DeleteMatrix(Hxb,XCELLS + 1,ZCELLS);
}
if(rank == 2) {
  DeleteMatrix(Hzb,XCELLS,ZCELLS + 1);
  DeleteMatrix(Hxb,XCELLS + 1,ZCELLS);
}
if(rank >=3 && rank <= NProcs - 2) {
  DeleteMatrix(Hzb,XCELLS,ZCELLS + 1);
  DeleteMatrix(Hxb,XCELLS + 1,ZCELLS);
  DeleteMatrix(Ezb,XCELLS + 1,ZCELLS);
  DeleteMatrix(Exb,XCELLS,ZCELLS + 1);
}
if(rank == NProcs - 1) {
  DeleteMatrix(Ezb,XCELLS + 1,ZCELLS);
  DeleteMatrix(Ezb1,XCELLS + 1,ZCELLS);
  DeleteMatrix(Exb,XCELLS,ZCELLS + 1);
  DeleteMatrix(Exb1,XCELLS,ZCELLS + 1);
}

DeleteAllMatrices(rank);
if(rank == 0Prank) {
  if(!INCSIM) {
    outEz.close();
    outEy.close();
    outEx.close();
    outHx.close();
    outHz.close();
  }
  else {
    outEz.close();
    outHx.close();
  }
}

pproc:
MPI_Finalize();
//-----
//Postprocessing
if(!INCSIM && !rank) {
  cout<<"Postprocessing..."<<endl;
  ifstream Ezf,Eyf,Exf,Hxf,Hzf,Hyf,Ezincf,Hxincf;
  int idx;
  char str[200];
  CmplxPtr3 Ezsfr,Eysfr,Exsfr,Hzsfr,Hxsfr,Hysfr,S;
  double f1 = 6e9;
  double f2 = 200e9;
  cout<<"Postprocessing : f1 = "<<f1<<endl;
  cout<<"Postprocessing : f2 = "<<f2<<endl;

  //Get the incident field data
  Ezincf.open("/pan1/projects/awmra/Ezinc.dat",ios::in);
  Hxincf.open("/pan1/projects/awmra/Hxinc.dat",ios::in);
  double* Ezinc;
  double* Hxinc;
  Ezinc = new double[T];
  Hxinc = new double[T];

  //Read Exinc,Hxinc data files
  idx = 0;

```

```

while(!Ezincf.eof()) {
    Ezincf.getline(str,200);
    Ezinc[idx] = strtod(str,'\0');
    idx++;
}
idx = 0;
while(!Hxincf.eof()) {
    Hxincf.getline(str,200);
    Hxinc[idx] = strtod(str,'\0');
    idx++;
}
cout<<"Read Ezinc,Hxinc"<<endl;

//Frequency points
uint Nres = pow(2,17) - T;
double df = (1/dt)/(T+Nres);
uint N1 = (uint)Round(f1/df);
uint N2 = (uint)Round(f2/df);

cout<<"Creating freq domain field matrices"<<endl;
//Frequency domain complex fields
CreateMatrix(Ezsfr,ZCELLS + 1,XCELLS + 1,N2 - N1 + 1);
CreateMatrix(Exsfr,ZCELLS + 1,XCELLS + 1,N2 - N1 + 1);
//CreateMatrix(Eysfr,ZCELLS + 1,XCELLS + 1,N2 - N1 + 1);
CreateMatrix(Hzsfr,ZCELLS + 1,XCELLS + 1,N2 - N1 + 1);
CreateMatrix(Hxsfr,ZCELLS + 1,XCELLS + 1,N2 - N1 + 1);
//CreateMatrix(Hysfr,ZCELLS + 1,XCELLS + 1,N2 - N1 + 1);

//Ez
complex* Eztpxl = new complex[T+Nres];
complex* Ezfrpxl = new complex[T+Nres];
double* Ezdata = new double[(XCELLS + 1)*(ZCELLS + 1)*T];
Ezf.open("/pan1/projects/awmra/Ez.dat",ios::in);
idx = 0;
while(!Ezf.eof()) {
    Ezf.getline(str,200);
    Ezdata[idx++] = strtod(str,'\0');
}
for(int i = 0;i < XCELLS + 1;i++) {
    for(int k = 0;k < ZCELLS + 1;k++) {
        int offset = i*(ZCELLS + 1) + k;
        for(int q = 0;q < T;q++) {
            Eztpxl[q] = complex(Ezdata[offset + q*(XCELLS + 1)*(ZCELLS + 1)] - Ezinc[q],0);
        }
        CFFT::Forward(&Eztpxl[0],&Ezfrpxl[0],T+Nres);
        for(int q = 0;q < N2 - N1 + 1;q++) {
            Ezsfr[k][i][q] = Ezfrpxl[q + N1];
        }
    }
}
delete [] Eztpxl; delete [] Ezfrpxl; delete [] Ezdata;
Ezf.close();
cout<<"Filled Ezsfr matrix"<<endl;

//Ey
/*complex* Eytpxl = new complex[T+Nres];
complex* Eyfrpxl = new complex[T+Nres];
double* Eydata = new double[(XCELLS + 1)*(ZCELLS + 1)*T];
Eyf.open("/pan1/projects/awmra/Ey.dat",ios::in);
idx = 0;
while(!Eyf.eof()) {
    Eyf.getline(str,200);
    Eydata[idx++] = strtod(str,'\0');
}
for(int i = 0;i < XCELLS + 1;i++) {
    for(int k = 0;k < ZCELLS + 1;k++) {
        int offset = i*(ZCELLS + 1) + k;

```

```

for(int q = 0;q < T;q++) {
  Eytpxl[q] = complex(Eydata[offset + q*(XCELLS + 1)*(ZCELLS + 1)],0);
}
CFFT::Forward(&Eytpxl[0],&Eyfrpxl[0],T+Nres);
for(int q = 0;q < N2 - N1 + 1;q++) {
  Eysfr[k][i][q] = Eyfrpxl[q + N1];
}
}
}
delete [] Eytpxl; delete [] Eyfrpxl; delete [] Eydata;
Eyf.close();*/

//Ex
complex* Extpxl = new complex[T+Nres];
complex* Exfrpxl = new complex[T+Nres];
double* Exdata = new double[(XCELLS + 1)*(ZCELLS + 1)*T];
Exf.open("/pan1/projects/awmra/Ex.dat",ios::in);
idx = 0;
while(!Exf.eof()) {
  Exf.getline(str,200);
  Exdata[idx++] = strtod(str,'\0');
}
for(int i = 0;i < XCELLS + 1;i++) {
  for(int k = 0;k < ZCELLS + 1;k++) {
    int offset = i*(ZCELLS + 1) + k;
    for(int q = 0;q < T;q++) {
      Extpxl[q] = complex(Exdata[offset + q*(XCELLS + 1)*(ZCELLS + 1)],0);
    }
    CFFT::Forward(&Extpxl[0],&Exfrpxl[0],T+Nres);
    for(int q = 0;q < N2 - N1 + 1;q++) {
      Exsfr[k][i][q] = Exfrpxl[q + N1];
    }
  }
}
delete [] Extpxl; delete [] Exfrpxl; delete [] Exdata;
Exf.close();
cout<<"Filled Exsfr matrix"<<endl;

//Hz
complex* Hztpxl = new complex[T+Nres];
complex* Hzfrpxl = new complex[T+Nres];
double* Hzdata = new double[(XCELLS + 1)*(ZCELLS + 1)*T];
Hzf.open("/pan1/projects/awmra/Hz.dat",ios::in);
idx = 0;
while(!Hzf.eof()) {
  Hzf.getline(str,200);
  Hzdata[idx++] = strtod(str,'\0');
}
for(int i = 0;i < XCELLS + 1;i++) {
  for(int k = 0;k < ZCELLS + 1;k++) {
    int offset = i*(ZCELLS + 1) + k;
    for(int q = 0;q < T;q++) {
      Hztpxl[q] = complex(Hzdata[offset + q*(XCELLS + 1)*(ZCELLS + 1)],0);
    }
    TimeAlignHfield(&Hztpxl[0],T + Nres);
    CFFT::Forward(&Hztpxl[0],&Hzfrpxl[0],T+Nres);
    for(int q = 0;q < N2 - N1 + 1;q++) {
      Hzsfr[k][i][q] = Hzfrpxl[q + N1];
    }
  }
}
delete [] Hztpxl; delete [] Hzfrpxl; delete [] Hzdata;
Hzf.close();
cout<<"Filled Hzsfr matrix"<<endl;

//Hy

```

```

/*complex* Hytpxl    = new complex[T+Nres];
complex* Hyfrpxl    = new complex[T+Nres];
double* Hydata      = new double[(XCELLS + 1)*(ZCELLS + 1)*T];
Hyf.open("/pan1/projects/awmra/Hy.dat",ios::in);
idx = 0;
while(!Hyf.eof()) {
    Hyf.getline(str,200);
    Hydata[idx++] = strtod(str,'\0');
}
for(int i = 0;i < XCELLS + 1;i++) {
    for(int k = 0;k < ZCELLS + 1;k++) {
        int offset = i*(ZCELLS + 1) + k;
        for(int q = 0;q < T;q++) {
            Hytpxl[q] = complex(Hydata[offset + q*(XCELLS + 1)*(ZCELLS + 1)],0);
        }
        TimeAlignHfield(&Hytpxl[0],T + Nres);
        CFFT::Forward(&Hytpxl[0],&Hyfrpxl[0],T+Nres);
        for(int q = 0;q < N2 - N1 + 1;q++) {
            Hysfr[k][i][q] = Hyfrpxl[q + N1];
        }
    }
}
delete [] Hytpxl; delete [] Hyfrpxl; delete [] Hydata;
Hyf.close();*/

//Hx
complex* Hxtpxl    = new complex[T+Nres];
complex* Hxfrpxl    = new complex[T+Nres];
double* Hxdata      = new double[(XCELLS + 1)*(ZCELLS + 1)*T];
Hxf.open("/pan1/projects/awmra/Hx.dat",ios::in);
idx = 0;
while(!Hxf.eof()) {
    Hxf.getline(str,200);
    Hxdata[idx++] = strtod(str,'\0');
}
for(int i = 0;i < XCELLS + 1;i++) {
    for(int k = 0;k < ZCELLS + 1;k++) {
        int offset = i*(ZCELLS + 1) + k;
        for(int q = 0;q < T;q++) {
            Hxtpxl[q] = complex(Hxdata[offset + q*(XCELLS + 1)*(ZCELLS + 1)] - Hxinc[q],0);
        }
        TimeAlignHfield(&Hxtpxl[0],T + Nres);
        CFFT::Forward(&Hxtpxl[0],&Hxfrpxl[0],T+Nres);
        for(int q = 0;q < N2 - N1 + 1;q++) {
            Hxsfr[k][i][q] = Hxfrpxl[q + N1];
        }
    }
}
delete [] Hxtpxl; delete [] Hxfrpxl; delete [] Hxdata;
Hxf.close();
cout<<"Filled Hxsfr matrix"<<endl;

//Write time average power spectral density to output file
ofstream Sout;
Sout.open("Sout.dat",ios::out);
Sout<<XCELLS + 1<<endl;
Sout<<ZCELLS + 1<<endl;
Sout<<N2 - N1 + 1<<endl;
Sout<<dx<<endl;
Sout<<dt<<endl;
Sout<<df<<endl;
//Calculate time average power spectral density
CreateMatrix(S,ZCELLS + 1,XCELLS + 1,N2 - N1 + 1);
for(int i = 0;i < XCELLS + 1;i++) {
    for(int k = 0;k < ZCELLS + 1;k++) {
        for(int q = 0;q < N2 - N1 + 1;q++) {
            S[k][i][q] = complex(((Exsfr[k][i][q]*(Hzsfr[k][i][q].conjugate()))).re()) -

```

```

        ((Ezsfr[k][i][q]*(Hxsfr[k][i][q].conjugate())).re()),0);
        Sout<<2*(S[k][i][q].re())<<endl;
    }
}
Sout.close();
cout<<"Created Sout.dat"<<endl;

//Write the Ezinc magnitude (freq domain) to file
ofstream Ezincmagf;
Ezincmagf.open("Ezincmagf.dat",ios::out);
//Incident field
complex* Ezinct      = new complex[T+Nres];
complex* Ezincfr     = new complex[T+Nres];
for(int q = 0;q < T;q++) {
    Ezinct[q] = complex(Ezinc[q],0);
}
CFFT::Forward(&Ezinct[0],&Ezincfr[0],T+Nres);
for(int q = 0;q < N2 - N1 + 1;q++) {
    Ezincmagf<<sqrt(Ezincfr[q+N1].norm())<<endl;
}
delete [] Ezinct; delete [] Ezincfr;
Ezincmagf.close();
cout<<"Created Ezincmagf.dat"<<endl;

//Write the list of frequencies
ofstream Flist;
Flist.open("Flist.dat",ios::out);
for(int q = 0;q < N2 - N1 + 1;q++) {
    Flist<<(q + N1)/dt/(T+Nres)<<endl;
}
Flist.close();
cout<<"Created Flist.dat"<<endl;

/*cout<<"Floquet mode analysis"<<endl;
ofstream EzFloquet,ExFloquet,EyFloquet;
ofstream HzFloquet,HxFloquet,HyFloquet;
ExFloquet.open("ExFloquet.dat",ios::out);
EyFloquet.open("EyFloquet.dat",ios::out);
EzFloquet.open("EzFloquet.dat",ios::out);
HxFloquet.open("HxFloquet.dat",ios::out);
HyFloquet.open("HyFloquet.dat",ios::out);
HzFloquet.open("HzFloquet.dat",ios::out);

for(int j = 0;j < NumofOutFreq;j++) {
    int qf;
    double radiometFreq = OutFreqs[j];
    for(int q = 0;q < N2 - N1 + 1;q++) {
        if(((q + N1)/dt/(T+Nres)) > radiometFreq) {
            double diff1 = fabs(((double)(q + N1 - 1))/dt/((double)(T+Nres)) - radiometFreq);
            double diff2 = fabs(((double)(q + N1))/dt/((double)(T+Nres)) - radiometFreq);
            if(diff1 < diff2) {
                qf = q - 1;
                break;
            }
            else {
                qf = q;
                break;
            }
        }
    }
}
for(int i = 0;i < XCELLS + 1;i++) {
    for(int k = 0;k < ZCELLS + 1;k++) {
        ExFloquet<<Exsfr[k][i][qf].re()<<endl;
        EyFloquet<<Eysfr[k][i][qf].re()<<endl;
        EzFloquet<<Ezsfr[k][i][qf].re()<<endl;
    }
}

```

```

    ExFloquet<<Exsfr[k][i][qf].im()<<endl;
    EyFloquet<<Eysfr[k][i][qf].im()<<endl;
    EzFloquet<<Ezsfr[k][i][qf].im()<<endl;

    HxFloquet<<Hxsfr[k][i][qf].re()<<endl;
    HyFloquet<<Hysfr[k][i][qf].re()<<endl;
    HzFloquet<<Hzsfr[k][i][qf].re()<<endl;
    HxFloquet<<Hxsfr[k][i][qf].im()<<endl;
    HyFloquet<<Hysfr[k][i][qf].im()<<endl;
    HzFloquet<<Hzsfr[k][i][qf].im()<<endl;
}
}

ExFloquet.close();EyFloquet.close();
EzFloquet.close();
HxFloquet.close();HyFloquet.close();
HzFloquet.close();
*/
cout<<"Finished"<<endl;

delete [] Ezinc;
delete [] Hxinc;
Ezincf.close();
Hxincf.close();
DeleteMatrix(Ezsfr,ZCELLS + 1,XCELLS + 1,N2 - N1 + 1);
DeleteMatrix(Exsfr,ZCELLS + 1,XCELLS + 1,N2 - N1 + 1);
DeleteMatrix(Hzsfr,ZCELLS + 1,XCELLS + 1,N2 - N1 + 1);
DeleteMatrix(Hxsfr,ZCELLS + 1,XCELLS + 1,N2 - N1 + 1);
//DeleteMatrix(Hysfr,ZCELLS + 1,XCELLS + 1,N2 - N1 + 1);
//DeleteMatrix(Eysfr,ZCELLS + 1,XCELLS + 1,N2 - N1 + 1);
DeleteMatrix(S,ZCELLS + 1,XCELLS + 1,N2 - N1 + 1);
}

return 0;
}

//-----
void TimeAlignHfield(double* field,uint sz) {
for(int idx = 0;idx < sz;idx++) {
if(idx != 0 && idx != sz - 1) {
field[idx] = 0.5*(field[idx] + field[idx + 1]);
}
}
}
void TimeAlignHfield(complex* field,uint sz) {
for(int idx = 0;idx < sz;idx++) {
if(idx != 0 && idx != sz - 1) {
field[idx] = 0.5*(field[idx] + field[idx + 1]);
}
}
}

//Range of xidx:[0,PSX],zidx:[0,PSZ],yidx:[0,PSY]
double GetFieldVal(uint xidx,uint yidx,uint zidx,uint fieldComp)
{
double val;
if(fieldComp == Exc) {
if(xidx == 0 || zidx == 0 || xidx == PSX || zidx == PSZ){
val = 0;
}
else {
val = (Ex[xidx][yidx+PL][zidx] + Ex[xidx-1][yidx+PL][zidx])/2;
}
}
}
}

```

```

else if(fieldComp == Eyc) {
    if(yidx == 0 || yidx == PSY)
        val = Ey[xidx][PL+yidx][zidx];
    else
        val = (Ey[xidx][PL+yidx][zidx] + Ey[xidx][PL+yidx-1][zidx])/2;
}
else if(fieldComp == Ezc) {
    if(zidx == 0)
        val = Ez[xidx][PL+yidx][zidx];
    else if(zidx == PSZ)
        val = Ez[xidx][PL+yidx][zidx - 1];
    else
        val = (Ez[xidx][PL+yidx][zidx] + Ez[xidx][PL+yidx][zidx-1])/2;
}
else if(fieldComp == Hxc) {
    if(zidx == 0)
        val = (Hx[xidx][PL+yidx][zidx] + Hx[xidx][PL+yidx-1][zidx])/2;
    else if(zidx == ZCELLS)
        val = (Hx[xidx][PL+yidx][zidx-1] + Hx[xidx][PL+yidx-1][zidx-1])/2;
    else
        val = (Hx[xidx][PL+yidx][zidx] + Hx[xidx][PL+yidx-1][zidx]
            + Hx[xidx][PL+yidx][zidx-1] + Hx[xidx][PL+yidx-1][zidx-1])/4;
}
else if(fieldComp == Hyc) {
}

return val;
}

void InitMaterialMatrix()
{
for(int i = 0; i < XCELLS; i++) {
    for(int j = 0; j < YCELLS; j++) {
        for(int k = 0; k < ZCELLS; k++) {
            if(j < PL || j > PL + PSY - 1) {
                MediaFullDomain[i][j][k] = PML;
            }
            else if(j >= 50 && j <= 75) {
                //MediaFullDomain[i][j][k] = MF112;
            }
            else if(j >= 93 && j <= 95 && i >= 10 && i <= 20 && k >= 10 && k <= 20) {
                //MediaFullDomain[i][j][k] = MF112;
            }

            else {
                MediaFullDomain[i][j][k] = AIR;
            }
        }
    }
}
}

uint AddMetalPyr(double dx, uint material)
{
//PL + PSY - 1 : AIR
//Base : PL + PSY - 2, ..., PL + PSY - 2 - dbase + 1
for(int i = 0; i < XCELLS; i++) {
    for(int j = PL + PSY - aircells - dbase; j <= PL + PSY - 1 - aircells; j++) {
        for(int k = 0; k < ZCELLS; k++) {
            MediaFullDomain[i][j][k] = material;
        }
    }
}

double z, d, w;
int j, hw, yidx;
d = (basewidth/mp)*1e-2;

```

```

j   = PL + PSY - aircells - dbase - 1;
z   = (PL + PSY - aircells - dbase - 1 - j)*dx;
w   = basewidth*1e-2 * (1 - z/d);
hw  = Round(w/2/dx);
yidx = PL + PSY - aircells - dbase - 1;

do {
  for(int xidx = PSX/2 - hw;xidx <= PSX / 2 + hw - 1;xidx++) {
    for(int zidx = PSX/2 - hw;zidx <= PSX / 2 + hw - 1;zidx++) {
      MediaFullDomain[xidx][yidx][zidx] = material;
    }
  }

  yidx = yidx - 1;
  j--;
  z = (PL + PSY - aircells - dbase - 1 - j)*dx;
  w = basewidth*1e-2 * (1 - z/d);
  hw = Round(w/2/dx);
}
while (hw>=1);

return yidx + 1;
}

//Add absorbent coating
uint AddCoating(double dx,uint material)
{
  uint pyrtoptyidxtmp = PL + PSY;

  for(int i = 0;i < XCELLS;i++) {
    for(int k = 0;k < ZCELLS;k++) {
      for(int j = PL;j < PL + PSY - 1;j++) {
        if(MediaFullDomain[i][j][k] == AL || MediaFullDomain[i][j][k] == PEC) {
          //Add the coating
          for(uint c = j - 1;c >= j - coating;c--) {
            MediaFullDomain[i][c][k] = material;
            if(c < pyrtoptyidxtmp) {
              pyrtoptyidxtmp = c;
            }
          }
          break;
        }
      }
    }
  }

  return pyrtoptyidxtmp;
}

void FillUpdateEqnConstantMatrices(double dx, double sigmao,double d,double m,
                                   double dt,int rank)
{
  double Dx_sigmay,Bx_sigmay;
  double Ey_sigmay,Ez_sigmay;
  double Hy_sigmay,Hx_sigmay;
  int i,ii,kk;

  //UPML coefficients
  if(rank == 1 || rank == 2) {
    //C1Dx,C2Dx
    for(i = 0;i < XCELLS; i++) {
      for(int j = 0;j < PL + 1; j++) {
        for(int k = 0;k < ZCELLS + 1; k++) {
          //Dx_sigmay
          if(rank == 1)

```

```

    Dx_sigmay = sigmao * pow((PL-j)*dx/d,m);
else
    Dx_sigmay = sigmao * pow(j*dx/d,m);

//C1Dx,C2Dx
C1Dx[i][j][k] = (2 * epso - Dx_sigmay * dt)
    /(2 * epso + Dx_sigmay * dt);
C2Dx[i][j][k] = (2 * epso * dt)
    /(2 * epso + Dx_sigmay * dt);
}
}
}

//C2Ey,C3Ey
for(i = 0;i < XCELLS + 1; i++) {
for(int j = 0;j < PL; j++) {
for(int k = 0;k < ZCELLS + 1; k++) {
//Ey_sigmay
if(rank == 1)
    Ey_sigmay = sigmao * pow((PL-j-0.5)*dx/d,m);
else
    Ey_sigmay = sigmao * pow((j+0.5)*dx/d,m);

//C2Ey,C3Ey
C2Ey[i][j][k] = (2 * epso + Ey_sigmay * dt)
    /((2 * epso)
    * epso);
C3Ey[i][j][k] = (2 * epso - Ey_sigmay * dt)
    /((2 * epso)
    * epso);

}
}
}

//C1Ez,C2Ez
for(i = 0;i < XCELLS + 1; i++) {
for(int j = 0;j < (PL + 1); j++) {
for(int k = 0;k < ZCELLS; k++) {
//Ez_ky,Ez_sigmay
if(rank == 1)
    Ez_sigmay = sigmao * pow((PL-j)*dx/d,m);
else
    Ez_sigmay = sigmao * pow(j*dx/d,m);

//C1Ez,C2Ez
C1Ez[i][j][k] = (2 * epso - Ez_sigmay * dt)
    /(2 * epso + Ez_sigmay * dt);
C2Ez[i][j][k] = (2 * epso)
    /((2 * epso + Ez_sigmay * dt)
    * epso);
}
}
}

//C1Bx,C2Bx
for(i = 0;i < XCELLS + 1;i++) {
for(int j = 0;j < PL;j++) {
for(int k = 0;k < ZCELLS;k++) {
//Bx_ky,Bx_sigmay
if(rank == 1)
    Bx_sigmay = sigmao * pow((PL-j-0.5)*dx/d,m);
else
    Bx_sigmay = sigmao * pow((j+0.5)*dx/d,m);

//C1Bx,C2Bx
C1Bx[i][j][k] = (2 * epso - Bx_sigmay * dt)

```

```

        /(2 * eps0 + Bx_sigmay * dt);
C2Bx[i][j][k] = (2 * eps0 * dt)
        /(2 * eps0 + Bx_sigmay * dt);

    }
}

//C2Hy,C3Hy
for(i = 0;i < XCELLS;i++) {
for(int j = 0;j < PL + 1;j++) {
for(int k = 0;k < ZCELLS;k++) {
if(rank == 1)
Hy_sigmay = sigmao * pow((PL-j)*dx/d,m);
else
Hy_sigmay = sigmao * pow(j*dx/d,m);

//C2Hy,C3Hy
C2Hy[i][j][k] = (2 * eps0 + Hy_sigmay * dt)
    /((2 * eps0)
    * muo );
C3Hy[i][j][k] = (2 * eps0 - Hy_sigmay * dt)
    /((2 * eps0)
    * muo );
}
}
}

//C2Hz,C1Hz
for(i = 0;i < XCELLS;i++) {
for(int j = 0;j < PL;j++) {
for(int k = 0;k < ZCELLS + 1;k++) {
//Hz_ky,Hx_sigmay
if(rank == 1)
Hz_sigmay = sigmao * pow((PL-j-0.5)*dx/d,m);
else
Hz_sigmay = sigmao * pow((j+0.5)*dx/d,m);

//C2Hz,C1Hz
C2Hz[i][j][k] = (2 * eps0)
    /((2 * eps0 + Hz_sigmay * dt)
    * muo );
C1Hz[i][j][k] = (2 * eps0 - Hz_sigmay * dt)
    /(2* eps0 + Hz_sigmay * dt);
}
}
}

}

if(rank == 0 || rank == 1 || rank == 2)
return;

//rank 3 .. rank NProcs-1 : Processors for problem space domain
//rank3 adjacent to PML0
int jmax,rankoff;

//K1Ex,K2Ex
if(rank == NProcs - 1)
jmax = yeePerProc - 1;
else
jmax = yeePerProc;
rankoff = (rank - 3)*yeePerProc;
double epsinfEx,sigmaEx,XeEx0,XieEx0;
for(i = 0;i < XCELLS;i++) {

```

```

for(int j = 0;j < jmax;j++) {
  for(int k = 0;k < ZCELLS + 1;k++) {
    if(k <= ZCELLS/2) {
      kk = k;
    }
    else {
      kk = k - 1;
    }

    sigmaEx = GetSigma(i,j+PL+rankoff,kk);
    epsinfEx = GetEpsinf(i,j+PL+rankoff,kk);
    XeEx0 = GetXeDebye(i,j+PL+rankoff,kk,0,dt,0);
    XieEx0 = GetXieDebye(i,j+PL+rankoff,kk,0,dt,0);

    K1Ex[i][j][k] = epsinfEx + XeEx0 - XieEx0 + (sigmaEx*dt/2/eps0);
    K2Ex[i][j][k] = epsinfEx - XieEx0 - (sigmaEx*dt/2/eps0);
  }
}
//K1Ey,K2Ey
jmax = yeePerProc;
rankoff = (rank - 3)*yeePerProc;
double epsinfEy,sigmaEy,XeEy0,XieEy0;
for(i = 0;i < XCELLS + 1;i++) {
  for(int j = 0;j < yeePerProc;j++) {
    for(int k = 0;k < ZCELLS + 1;k++) {
      if(k > ZCELLS/2) {
        kk = k - 1;
      }
      else {
        kk = k;
      }
      if(i > XCELLS/2) {
        ii = i - 1;
      }
      else {
        ii = i;
      }
      epsinfEy = GetEpsinf(ii,j+PL+rankoff,kk);
      sigmaEy = GetSigma(ii,j+PL+rankoff,kk);
      XeEy0 = GetXeDebye(ii,j+PL+rankoff,kk,0,dt,0);
      XieEy0 = GetXieDebye(ii,j+PL+rankoff,kk,0,dt,0);

      K1Ey[i][j][k] = epsinfEy + XeEy0 - XieEy0 + (sigmaEy*dt/2/eps0);
      K2Ey[i][j][k] = epsinfEy - XieEy0 - (sigmaEy*dt/2/eps0);
    }
  }
}
//K1Ez,K2Ez
if(rank == NProcs - 1)
  jmax = yeePerProc - 1;
else
  jmax = yeePerProc;
rankoff = (rank - 3)*yeePerProc;
double epsinfEz,sigmaEz,XeEz0,XieEz0;
for(i = 0;i < XCELLS + 1;i++) {
  for(int j = 0;j < jmax;j++) {
    for(int k = 0;k < ZCELLS;k++) {
      if(i > XCELLS/2) {
        ii = i - 1;
      }
      else {
        ii = i;
      }
      epsinfEz = GetEpsinf(ii,j+PL+rankoff,k);
      sigmaEz = GetSigma(ii,j+PL+rankoff,k);
      XeEz0 = GetXeDebye(ii,j+PL+rankoff,k,0,dt,0);

```

```

XieEz0 = GetXieDebye(ii,j+PL+rankoff,k,0,dt,0);

K1Ez[i][j][k] = epsinfEz + XeEz0 - XieEz0 + (sigmaEz*dt/2/epso);
K2Ez[i][j][k] = epsinfEz - XieEz0 - (sigmaEz*dt/2/epso);
}
}
//K1Hx,K2Hx
jmax = yeePerProc;
rankoff = (rank - 3)*yeePerProc;
for(i = 0;i < XCELLS + 1;i++) {
for(int j = 0;j < jmax;j++) {
for(int k = 0;k < ZCELLS;k++) {
double MuinfHx,XmHx0,XimHx0;
if(i == XCELLS) {
ii = 0;
}
else if(i > XCELLS/2) {
ii = i - 1;
}
else {
ii = i;
}
MuinfHx = GetMuinf(ii,j+PL+rankoff,k);
XmHx0 = GetXmDebye(ii,j+PL+rankoff,k,0,dt,0);
XimHx0 = GetXimDebye(ii,j+PL+rankoff,k,0,dt,0);

K1Hx[i][j][k] = MuinfHx + XmHx0 - XimHx0;
K2Hx[i][j][k] = MuinfHx - XimHx0;
}
}
}
//K1Hy,K2Hy
//Note : Only PSY - 2 Hy's inside the problem space
if(rank == NProcs - 1)
jmax = yeePerProc - 1;
else
jmax = yeePerProc;
rankoff = (rank - 3)*yeePerProc;
for(i = 0;i < XCELLS;i++) {
for(int j = 0;j < jmax;j++) {
for(int k = 0;k < ZCELLS;k++) {
double MuinfHy,XmHy0,XimHy0;
MuinfHy = GetMuinf(i,j+PL+1+rankoff,k);
XmHy0 = GetXmDebye(i,j+PL+1+rankoff,k,0,dt,0);
XimHy0 = GetXimDebye(i,j+PL+1+rankoff,k,0,dt,0);

K1Hy[i][j][k] = MuinfHy + XmHy0 - XimHy0;
K2Hy[i][j][k] = MuinfHy - XimHy0;
}
}
}
//K1Hz,K2Hz
jmax = yeePerProc;
rankoff = (rank - 3)*yeePerProc;
for(i = 0;i < XCELLS;i++) {
for(int j = 0;j < jmax;j++) {
for(int k = 0;k < ZCELLS + 1;k++) {
double MuinfHz,XmHz0,XimHz0;
if(k == ZCELLS) {
kk = 0;
}
else if(k > ZCELLS/2) {
kk = k - 1;
}
else {
kk = k;
}
}
}
}

```

```

    }
    MuinfHz = GetMuinf(i,j+PL+rankoff,kk);
    XmHz0   = GetXmDebye(i,j+PL+rankoff,kk,0,dt,0);
    XimHz0  = GetXimDebye(i,j+PL+rankoff,kk,0,dt,0);

    K1Hz[i][j][k] = MuinfHz + XmHz0 - XimHz0;
    K2Hz[i][j][k] = MuinfHz - XimHz0;
  }
}
}
}
}

```

```

// Get the value of muinf (relative permeability)
// in the main grid cell
double GetMuinf(int xidx,int yidx,int zidx)
{
  int xmax,ymax,zmax;
  if(!SBC) {
    xmax = 2*XCELLS - 1;
    ymax = 2*YCELLS - 1;
    zmax = 2*ZCELLS - 1;
  }
  else {
    xmax = XCELLS;
    ymax = YCELLS;
    zmax = ZCELLS;
  }
  if((xidx >= 0 && xidx <= xmax) &&
      (yidx >= 0 && yidx <= ymax) &&
      (zidx >= 0 && zidx <= zmax)) {

    switch(MediaFullDomain[xidx][yidx][zidx]) {
      case AIR: case PML: case PEC: case AL:
      case PYREX:
        return 1.0;
        break;
      case MF110:
        return MF110Debyemur[1];
        break;
      case MF112:
        return MF112Debyemur[1];
        break;
      case MF114:
        return MF114Debyemur[1];
        break;
      default:
        return 1.0;
        break;
    }
  }
  else {
    cout<<"GetMuinf() : Error in indices"<<endl;
    return 1.0;
  }
}

```

```

// Get the value of epsinf (relative permittivity)
// in the main grid cell
double GetEpsinf(int xidx,int yidx,int zidx)
{
  int xmax,ymax,zmax;
  if(!SBC) {
    xmax = 2*XCELLS - 1;
    ymax = 2*YCELLS - 1;
    zmax = 2*ZCELLS - 1;
  }

```

```

}
else {
    xmax = XCELLS;
    ymax = YCELLS;
    zmax = ZCELLS;
}
if((xidx >= 0 && xidx <= xmax) &&
    (yidx >= 0 && yidx <= ymax) &&
    (zidx >= 0 && zidx <= zmax)) {

    switch(MediaFullDomain[xidx][yidx][zidx]) {
    case AIR: case PML: case PEC: case AL:
        return 1.0;
        break;
    case PYREX:
        return 4.2;
        break;
    case MF110:
        return MF110Debyemur[1];
        break;
    case MF112:
        return MF112Debyeepsr[1];
        break;
    case MF114:
        return MF114Debyeepsr[1];
        break;
    default:
        return 1.0;
        break;
    }
}
else {
    cout<<xidx<<endl;
    cout<<zidx<<endl;
    cout<<yidx<<endl;
    cout<<"GetEpsinf() : Error in indices"<<endl;
    return 1.0;
}
}

// Get the value of sigma (electical conductivity)
// in the main grid cell
double GetSigma(int xidx,int yidx,int zidx)
{
    int xmax,ymax,zmax;
    if(!SBC) {
        xmax = 2*XCELLS - 1;
        ymax = 2*YCELLS - 1;
        zmax = 2*ZCELLS - 1;
    }
    else {
        xmax = XCELLS;
        ymax = YCELLS;
        zmax = ZCELLS;
    }
    if((xidx >= 0 && xidx <= xmax) &&
        (yidx >= 0 && yidx <= ymax) &&
        (zidx >= 0 && zidx <= zmax)) {

        switch(MediaFullDomain[xidx][yidx][zidx]) {
        case AIR: case PYREX:
            return 0.0;
            break;
        case PML:
            cout<<"GetSigma() : PML conductivity error"<<endl;
            return 0.0;
            break;

```

```

case PEC:
    return PECsigma;
    break;
case AL:
    return ALsigma;
    break;
default:
    return 0.0;
    break;
}
}
else {
    cout<<"GetSigma() : Error in indices"<<endl;
    return 1.0;
}
}

//pole = [1,MAXPOLESEPS]
//pole = 0 -- total
double GetXeDebye(int xidx,int yidx,int zidx,int p,double dt,uint pole)
{
    int xmax,ymax,zmax;
    if(!SBC) {
        xmax = 2*XCELLS - 1;
        ymax = 2*YCELLS - 1;
        zmax = 2*ZCELLS - 1;
    }
    else {
        xmax = XCELLS;
        ymax = YCELLS;
        zmax = ZCELLS;
    }
    if((xidx >= 0 && xidx <= xmax) &&
        (yidx >= 0 && yidx <= ymax) &&
        (zidx >= 0 && zidx <= zmax)) {

        double Xe = 0,deltaeps,taueps;
        uint pidx;

        switch(MediaFullDomain[xidx][yidx][zidx]) {
        case AIR: case PML: case PEC: case AL:
        case PYREX:
            return 0.0;
            break;
        case MF110:
            Xe = 0;
            if(pole > MF110Debyeepsr[0]) {
                cout<<"GetXeDebye :: Pole index error."<<endl;
                return 0.0;
            }
            else if(pole == 0) {
                for(pidx = 1;pidx <= MF110Debyeepsr[0];pidx++) {
                    deltaeps = MF110Debyeepsr[2*pidx];
                    taueps = MF110Debyeepsr[2*pidx + 1];
                    Xe = Xe + deltaeps*(exp(-p*dt/taueps)-
                        exp(-(p+1)*dt/taueps));
                }
            }
            else {
                deltaeps = MF110Debyeepsr[2*pole];
                taueps = MF110Debyeepsr[2*pole + 1];
                Xe = deltaeps*(exp(-p*dt/taueps)- exp(-(p+1)*dt/taueps));
            }
            return Xe;
            break;
        case MF112:
            Xe = 0;

```

```

if(pole > MF112Debyeepsr[0]) {
    cout<<"GetXeDebye :: Pole index error."<<endl;
    return 0.0;
}
else if(pole == 0) {
    for(pidx = 1;pidx <= MF112Debyeepsr[0];pidx++) {
        deltaeps = MF112Debyeepsr[2*pidx];
        taueps   = MF112Debyeepsr[2*pidx + 1];
        Xe = Xe + deltaeps*(exp(-p*dt/taueps)-
            exp(-(p+1)*dt/taueps));
    }
}
else {
    deltaeps = MF112Debyeepsr[2*pole];
    taueps   = MF112Debyeepsr[2*pole + 1];
    Xe      = deltaeps*(exp(-p*dt/taueps)- exp(-(p+1)*dt/taueps));
}
return Xe;
break;
case MF114:
    Xe = 0;
    if(pole > MF114Debyeepsr[0]) {
        cout<<"GetXeDebye :: Pole index error."<<endl;
        return 0.0;
    }
    else if(pole == 0) {
        for(pidx = 1;pidx <= MF114Debyeepsr[0];pidx++) {
            deltaeps = MF114Debyeepsr[2*pidx];
            taueps   = MF114Debyeepsr[2*pidx + 1];
            Xe = Xe + deltaeps*(exp(-p*dt/taueps)-
                exp(-(p+1)*dt/taueps));
        }
    }
    else {
        deltaeps = MF114Debyeepsr[2*pole];
        taueps   = MF114Debyeepsr[2*pole + 1];
        Xe      = deltaeps*(exp(-p*dt/taueps)- exp(-(p+1)*dt/taueps));
    }
    return Xe;
    break;
default:
    return 0.0;
    break;
}
}
else {
    cout<<"GetXeDebye() : Error in indices"<<endl;
    return 0.0;
}
}

//pole - [1,MAXPOLESUMU]
//pole = 0 -- total
double GetXmDebye(int xidx,int yidx,int zidx,int p,double dt,uint pole)
{
    int xmax,ymax,zmax;
    if(!SBC) {
        xmax = 2*XCELLS - 1;
        ymax = 2*YCELLS - 1;
        zmax = 2*ZCELLS - 1;
    }
    else {
        xmax = XCELLS;
        ymax = YCELLS;
        zmax = ZCELLS;
    }
}
if((xidx >= 0 && xidx <= xmax) &&

```

```

(yidx >= 0 && yidx <= ymax) &&
(zidx >= 0 && zidx <= zmax)) {

double Xm = 0,deltamu,taumu;
uint pidx;

switch(MediaFullDomain[xidx][yidx][zidx]) {
case AIR: case PML: case PEC: case AL:
case PYREX:
return 0.0;
break;
case MF110:
Xm = 0;
if(pole > MF110Debyemur[0]) {
cout<<"GetXmDebye :: Pole index error."<<endl;
return 0.0;
}
else if(pole == 0) {
for(pidx = 1;pidx <= MF110Debyemur[0];pidx++) {
deltamu = MF110Debyemur[2*pidx];
taumu = MF110Debyemur[2*pidx + 1];
Xm = Xm + deltamu*(exp(-p*dt/taumu)-
exp(-(p+1)*dt/taumu));
}
}
else {
deltamu = MF110Debyemur[2*pole];
taumu = MF110Debyemur[2*pole + 1];
Xm = deltamu*(exp(-p*dt/taumu)- exp(-(p+1)*dt/taumu));
}
return Xm;
break;
case MF112:
Xm = 0;
if(pole > MF112Debyemur[0]) {
cout<<"GetXmDebye :: Pole index error."<<endl;
return 0.0;
}
else if(pole == 0) {
for(pidx = 1;pidx <= MF112Debyemur[0];pidx++) {
deltamu = MF112Debyemur[2*pidx];
taumu = MF112Debyemur[2*pidx + 1];
Xm = Xm + deltamu*(exp(-p*dt/taumu)-
exp(-(p+1)*dt/taumu));
}
}
else {
deltamu = MF112Debyemur[2*pole];
taumu = MF112Debyemur[2*pole + 1];
Xm = deltamu*(exp(-p*dt/taumu)- exp(-(p+1)*dt/taumu));
}
return Xm;
break;
case MF114:
Xm = 0;
if(pole > MF114Debyemur[0]) {
cout<<"GetXmDebye :: Pole index error."<<endl;
return 0.0;
}
else if(pole == 0) {
for(pidx = 1;pidx <= MF114Debyemur[0];pidx++) {
deltamu = MF114Debyemur[2*pidx];
taumu = MF114Debyemur[2*pidx + 1];
Xm = Xm + deltamu*(exp(-p*dt/taumu)-
exp(-(p+1)*dt/taumu));
}
}
}
}

```

```

else {
    deltamu = MF114Debyemur[2*pole];
    taumu   = MF114Debyemur[2*pole + 1];
    Xm      = deltamu*(exp(-p*dt/taumu)- exp(-(p+1)*dt/taumu));
}
return Xm;
break;
default:
    return 0.0;
    break;
}
}
else {
    cout<<"GetXmDebye() : Error in indices"<<endl;
    return 0.0;
}
}

//Returns the pth Xim for the given spatial indices.
//pole = 0. Returns the sum of the contribution due to each pole.
//Otherwise returns the pole contribution
//pth Xim for the dth pole = deltamu*exp(-p*dt/taumu)*
(taumu/dt - (taumu/dt + 1)*exp(-dt/taumu))
//pole - [1,MAXPOLESMU]
double GetXieDebye(int xidx,int yidx,int zidx,int p,double dt,uint pole)
{
    int xmax,ymax,zmax;
    if(!SBC) {
        xmax = 2*XCELLS - 1;
        ymax = 2*YCELLS - 1;
        zmax = 2*ZCELLS - 1;
    }
    else {
        xmax = XCELLS;
        ymax = YCELLS;
        zmax = ZCELLS;
    }
    if((xidx >= 0 && xidx <= xmax) &&
        (yidx >= 0 && yidx <= ymax) &&
        (zidx >= 0 && zidx <= zmax)) {

        double Xie = 0,deltaeps,taueps;
        uint pidx;

        switch(MediaFullDomain[xidx][yidx][zidx]) {
        case AIR: case PML: case PEC: case AL:
        case PYREX:
            return 0.0;
            break;
        case MF110:
            Xie = 0;
            if(pole > MF110Debyeepsr[0]) {
                cout<<"GetXieDebye :: Pole index error."<<endl;
                return 0.0;
            }
            else if(pole == 0) {
                for(pidx = 1;pidx <= MF110Debyeepsr[0];pidx++) {
                    deltaeps = MF110Debyeepsr[2*pidx];
                    taueps   = MF110Debyeepsr[2*pidx + 1];
                    Xie = Xie + deltaeps*exp(-p*dt/taueps)*(taueps/dt -
                        (taueps/dt + 1)*exp(-dt/taueps));
                }
            }
            else {
                deltaeps = MF110Debyeepsr[2*pole];
                taueps   = MF110Debyeepsr[2*pole + 1];
                Xie      = deltaeps*exp(-p*dt/taueps)*(taueps/dt -

```

```

    (taueps/dt + 1)*exp(-dt/taueps));
}
return Xie;
break;
case MF112:
Xie = 0;
if(pole > MF112Debyeepsr[0]) {
    cout<<"GetXieDebye :: Pole index error."<<endl;
    return 0.0;
}
else if(pole == 0) {
    for(pidx = 1;pidx <= MF112Debyeepsr[0];pidx++) {
        deltaeps = MF112Debyeepsr[2*pidx];
        taueps = MF112Debyeepsr[2*pidx + 1];
        Xie = Xie + deltaeps*exp(-p*dt/taueps)*
            (taueps/dt - (taueps/dt + 1)*exp(-dt/taueps));
    }
}
else {
    deltaeps = MF112Debyeepsr[2*pole];
    taueps = MF112Debyeepsr[2*pole + 1];
    Xie = deltaeps*exp(-p*dt/taueps)*
        (taueps/dt - (taueps/dt + 1)*exp(-dt/taueps));
}
return Xie;
break;
case MF114:
Xie = 0;
if(pole > MF114Debyeepsr[0]) {
    cout<<"GetXieDebye :: Pole index error."<<endl;
    return 0.0;
}
else if(pole == 0) {
    for(pidx = 1;pidx <= MF114Debyeepsr[0];pidx++) {
        deltaeps = MF114Debyeepsr[2*pidx];
        taueps = MF114Debyeepsr[2*pidx + 1];
        Xie = Xie + deltaeps*exp(-p*dt/taueps)*
            (taueps/dt - (taueps/dt + 1)*exp(-dt/taueps));
    }
}
else {
    deltaeps = MF114Debyeepsr[2*pole];
    taueps = MF114Debyeepsr[2*pole + 1];
    Xie = deltaeps*exp(-p*dt/taueps)*
        (taueps/dt - (taueps/dt + 1)*exp(-dt/taueps));
}
return Xie;
break;
default:
    return 0.0;
    break;
}
}
else {
    cout<<"GetXieDebye() : Error in indices"<<endl;
    return 0.0;
}
}

//Returns the pth Xim for the given spatial indices.
//pole = 0. Returns the sum of the contribution due to each pole.
//0otherwise returns the pole contribution
//pth Xim for the dth pole = deltamu*exp(-p*dt/taumu)
*(taumu/dt - (taumu/dt + 1)*exp(-dt/taumu))
//pole - [1,MAXPOLESMU]
double GetXimDebye(int xidx,int yidx,int zidx,int p,double dt,uint pole)
{

```

```

int xmax,ymax,zmax;
if(!SBC) {
    xmax = 2*XCELLS - 1;
    ymax = 2*YCELLS - 1;
    zmax = 2*ZCELLS - 1;
}
else {
    xmax = XCELLS;
    ymax = YCELLS;
    zmax = ZCELLS;
}
if((xidx >= 0 && xidx <= xmax) &&
    (yidx >= 0 && yidx <= ymax) &&
    (zidx >= 0 && zidx <= zmax)) {

    double Xim = 0,deltamu,taumu;
    uint pidx;

    switch(MediaFullDomain[xidx][yidx][zidx]) {
    case AIR: case PML: case PEC: case AL:
    case PYREX:
        return 0.0;
        break;
    case MF110:
        Xim = 0;
        if(pole > MF110Debyemur[0]) {
            cout<<"GetXimDebye :: Pole index error."<<endl;
            return 0.0;
        }
        else if(pole == 0) {
            for(pidx = 1;pidx <= MF110Debyemur[0];pidx++) {
                deltamumu = MF110Debyemur[2*pidx];
                taumu = MF110Debyemur[2*pidx + 1];
                Xim = Xim + deltamumu*exp(-p*dt/taumu)*(taumu/dt -
                    (taumu/dt + 1)*exp(-dt/taumu));
            }
        }
        else {
            deltamumu = MF110Debyemur[2*pole];
            taumu = MF110Debyemur[2*pole + 1];
            Xim = deltamumu*exp(-p*dt/taumu)*(taumu/dt -
                (taumu/dt + 1)*exp(-dt/taumu));
        }
        return Xim;
        break;
    case MF112:
        Xim = 0;
        if(pole > MF112Debyemur[0]) {
            cout<<"GetXimDebye :: Pole index error."<<endl;
            return 0.0;
        }
        else if(pole == 0) {
            for(pidx = 1;pidx <= MF112Debyemur[0];pidx++) {
                deltamumu = MF112Debyemur[2*pidx];
                taumu = MF112Debyemur[2*pidx + 1];
                Xim = Xim + deltamumu*exp(-p*dt/taumu)
                    *(taumu/dt - (taumu/dt + 1)*exp(-dt/taumu));
            }
        }
        else {
            deltamumu = MF112Debyemur[2*pole];
            taumu = MF112Debyemur[2*pole + 1];
            Xim = deltamumu*exp(-p*dt/taumu)
                *(taumu/dt - (taumu/dt + 1)*exp(-dt/taumu));
        }
        return Xim;
        break;
    }
}

```

```

case MF114:
  Xim = 0;
  if(pole > MF114Debyemur[0]) {
    cout<<"GetXimDebye :: Pole index error."<<endl;
    return 0.0;
  }
  else if(pole == 0) {
    for(pidx = 1;pidx <= MF114Debyemur[0];pidx++) {
      deltamu = MF114Debyemur[2*pidx];
      taumu = MF114Debyemur[2*pidx + 1];
      Xim = Xim + deltamu*exp(-p*dt/taumu)*(taumu/dt
        - (taumu/dt + 1)*exp(-dt/taumu));
    }
  }
  else {
    deltamu = MF114Debyemur[2*pole];
    taumu = MF114Debyemur[2*pole + 1];
    Xim = deltamu*exp(-p*dt/taumu)*(taumu/dt
      - (taumu/dt + 1)*exp(-dt/taumu));
  }
  return Xim;
  break;
default:
  return 0.0;
  break;
}
}
else {
  cout<<"GetXimDebye() : Error in indices"<<endl;
  return 0.0;
}
}

double GetTauMu(uint media,uint pole)
{
  if(!(pole >=1 && pole <= MAXPOLESMU)) {
    cout<<"GetTauMu :: Pole index error"<<endl;
    return 0;
  }
  switch(media) {
  case MF112:
    return MF112Debyemur[2*pole+1];
    break;
  case MF110:
    return MF110Debyemur[2*pole+1];
    break;
  case MF114:
    return MF114Debyemur[2*pole+1];
    break;
  default:
    return 0;
  }
}

double GetTauEps(uint media,uint pole)
{
  if(!(pole >=1 && pole <= MAXPOLESEPS)) {
    cout<<"GetTauEps :: Pole index error"<<endl;
    return 0;
  }
  switch(media) {
  case MF112:
    return MF112Debyeepsr[2*pole+1];
    break;
  case MF110:
    return MF110Debyeepsr[2*pole+1];
    break;
  }
}

```

```

case MF114:
    return MF114Debyeepsr[2*pole+1];
    break;

default:
    return 0;
}
}

// Create all the matrices used in the program
void CreateAllMatrices(int rank)
{
    int XCELLSP,ZCELLSP;
    XCELLSP = XCELLS;
    ZCELLSP = ZCELLS;

    //-----
    //Field matrices
    if(SBC) {
        XCELLS = Round(XCELLS/2);
        ZCELLS = Round(ZCELLS/2);
    }
    //Rank1 = PML0
    //Rank2 = PML1
    if(rank == 1 || rank == 2) {
        CreateMatrix(Ex,XCELLS,PL + 1,ZCELLS + 1);
        CreateMatrix(Ey,XCELLS + 1,PL,ZCELLS + 1);
        CreateMatrix(Ez,XCELLS + 1,PL + 1,ZCELLS);
        CreateMatrix(Dx,XCELLS,PL + 1,ZCELLS + 1);
        CreateMatrix(Dy,XCELLS + 1,PL,ZCELLS + 1);
        CreateMatrix(Dz,XCELLS + 1,PL + 1,ZCELLS);
        CreateMatrix(Dxo,XCELLS,PL + 1,ZCELLS + 1);
        CreateMatrix(Dyo,XCELLS + 1,PL,ZCELLS + 1);
        CreateMatrix(Dzo,XCELLS + 1,PL + 1,ZCELLS);
        CreateMatrix(Hx,XCELLS + 1,PL,ZCELLS);
        CreateMatrix(Hy,XCELLS,PL + 1,ZCELLS);
        CreateMatrix(Hz,XCELLS,PL,ZCELLS + 1);
        CreateMatrix(Bx,XCELLS + 1,PL,ZCELLS);
        CreateMatrix(By,XCELLS,PL + 1,ZCELLS);
        CreateMatrix(Bz,XCELLS,PL,ZCELLS + 1);
        CreateMatrix(Bxo,XCELLS + 1,PL,ZCELLS);
        CreateMatrix(Byo,XCELLS,PL + 1,ZCELLS);
        CreateMatrix(Bzo,XCELLS,PL,ZCELLS + 1);
    }
    else if(rank != 0) {
        //Non-PML domains
        //Rank3 .. Rank(NProcs-1)
        //Rank3 adjacent to PML0 (ymin PML)
        //Rank(NProcs-1) adjacent to PML1
        if(rank != NProcs - 1) {
            CreateMatrix(Ex,XCELLS,yeePerProc,ZCELLS + 1);
            CreateMatrix(Ez,XCELLS + 1,yeePerProc,ZCELLS);
            CreateMatrix(Hy,XCELLS,yeePerProc,ZCELLS);
        }
        else {
            CreateMatrix(Ex,XCELLS,yeePerProc - 1,ZCELLS + 1);
            CreateMatrix(Ez,XCELLS + 1,yeePerProc - 1,ZCELLS);
            CreateMatrix(Hy,XCELLS,yeePerProc - 1,ZCELLS);
        }
        CreateMatrix(Ey,XCELLS + 1,yeePerProc,ZCELLS + 1);
        CreateMatrix(Hx,XCELLS + 1,yeePerProc,ZCELLS);
        CreateMatrix(Hz,XCELLS,yeePerProc,ZCELLS + 1);
    }
}

//-----
//Coefficient matrices are first filled in PBC condition
//and then split for the SBC case

```

```

if(SBC) {
  XCELLS = XCELLSP;
  ZCELLS = ZCELLSP;
}
//UPML coefficients
if(rank == 1 || rank == 2) {
  CreateMatrix(C1Dx,XCELLS,PL + 1,ZCELLS + 1);
  CreateMatrix(C2Dx,XCELLS,PL + 1,ZCELLS + 1);
  CreateMatrix(C1Bx,XCELLS + 1,PL,ZCELLS);
  CreateMatrix(C2Bx,XCELLS + 1,PL,ZCELLS);
  CreateMatrix(C2Ey,XCELLS + 1,PL,ZCELLS + 1);
  CreateMatrix(C3Ey,XCELLS + 1,PL,ZCELLS + 1);
  CreateMatrix(C1Ez,XCELLS + 1,PL + 1,ZCELLS);
  CreateMatrix(C2Ez,XCELLS + 1,PL + 1,ZCELLS);
  CreateMatrix(C2Hy,XCELLS,PL + 1,ZCELLS);
  CreateMatrix(C3Hy,XCELLS,PL + 1,ZCELLS);
  CreateMatrix(C1Hz,XCELLS,PL,ZCELLS + 1);
  CreateMatrix(C2Hz,XCELLS,PL,ZCELLS + 1);
}
//PLRC coefficients
if(rank != 0 && rank != 1 && rank != 2) {
  //Non PML domains
  //Rank3 .. Rank(NProcs-1)
  //Rank3 adjacent to PML0 (ymin PML)
  //Rank(NProcs-1) adjacent to PML1
  if(rank != NProcs - 1) {
    CreateMatrix(K1Ex,XCELLS,yeePerProc,ZCELLS + 1);
    CreateMatrix(K2Ex,XCELLS,yeePerProc,ZCELLS + 1);
    CreateMatrix(K1Ez,XCELLS + 1,yeePerProc,ZCELLS);
    CreateMatrix(K2Ez,XCELLS + 1,yeePerProc,ZCELLS);
    CreateMatrix(K1Hy,XCELLS,yeePerProc,ZCELLS);
    CreateMatrix(K2Hy,XCELLS,yeePerProc,ZCELLS);

    CreateMatrix(RAEx,XCELLS,yeePerProc,ZCELLS + 1,MAXPOLESEPS);
    CreateMatrix(RAEz,XCELLS + 1,yeePerProc,ZCELLS,MAXPOLESEPS);
    CreateMatrix(RAHy,XCELLS,yeePerProc,ZCELLS,MAXPOLESMU);
  }
  else {
    CreateMatrix(K1Ex,XCELLS,yeePerProc - 1,ZCELLS + 1);
    CreateMatrix(K2Ex,XCELLS,yeePerProc - 1,ZCELLS + 1);
    CreateMatrix(K1Ez,XCELLS + 1,yeePerProc - 1,ZCELLS);
    CreateMatrix(K2Ez,XCELLS + 1,yeePerProc - 1,ZCELLS);
    CreateMatrix(K1Hy,XCELLS,yeePerProc - 1,ZCELLS);
    CreateMatrix(K2Hy,XCELLS,yeePerProc - 1,ZCELLS);

    CreateMatrix(RAEx,XCELLS,yeePerProc - 1,ZCELLS + 1,MAXPOLESEPS);
    CreateMatrix(RAEz,XCELLS + 1,yeePerProc - 1,ZCELLS,MAXPOLESEPS);
    CreateMatrix(RAHy,XCELLS,yeePerProc - 1,ZCELLS,MAXPOLESMU);
  }
  CreateMatrix(K1Ey,XCELLS + 1,yeePerProc,ZCELLS + 1);
  CreateMatrix(K2Ey,XCELLS + 1,yeePerProc,ZCELLS + 1);
  CreateMatrix(K1Hx,XCELLS + 1,yeePerProc,ZCELLS);
  CreateMatrix(K2Hx,XCELLS + 1,yeePerProc,ZCELLS);
  CreateMatrix(K1Hz,XCELLS,yeePerProc,ZCELLS + 1);
  CreateMatrix(K2Hz,XCELLS,yeePerProc,ZCELLS + 1);

  CreateMatrix(RAEy,XCELLS + 1,yeePerProc,ZCELLS + 1,MAXPOLESEPS);
  CreateMatrix(RAHx,XCELLS + 1,yeePerProc,ZCELLS,MAXPOLESMU);
  CreateMatrix(RAHz,XCELLS,yeePerProc,ZCELLS + 1,MAXPOLESMU);
}

//-----
//Media matrix
/*if(rank == 1 || rank == 2) {
  CreateMatrix(Media,XCELLS,PL,ZCELLS);
}
else if(rank != 0) {

```

```

    CreateMatrix(Media,XCELLS,yeePerProc,ZCELLS);
}*/

//MediaFullDomain is for all the processors
CreateMatrix(MediaFullDomain,XCELLS,YCELLS,ZCELLS);
}

// Delete all the matrices used in the program
void DeleteAllMatrices(int rank)
{
    //Rank1 = PML0
    //Rank2 = PML1
    if(rank == 1 || rank == 2) {
        DeleteMatrix(Ex,XCELLS,PL + 1,ZCELLS + 1);
        DeleteMatrix(Ey,XCELLS + 1,PL,ZCELLS + 1);
        DeleteMatrix(Ez,XCELLS + 1,PL + 1,ZCELLS);
        DeleteMatrix(Dx,XCELLS,PL + 1,ZCELLS + 1);
        DeleteMatrix(Dy,XCELLS + 1,PL,ZCELLS + 1);
        DeleteMatrix(Dz,XCELLS + 1,PL + 1,ZCELLS);
        DeleteMatrix(Dxo,XCELLS,PL + 1,ZCELLS + 1);
        DeleteMatrix(Dyo,XCELLS + 1,PL,ZCELLS + 1);
        DeleteMatrix(Dzo,XCELLS + 1,PL + 1,ZCELLS);
        DeleteMatrix(Hx,XCELLS + 1,PL,ZCELLS);
        DeleteMatrix(Hy,XCELLS,PL + 1,ZCELLS);
        DeleteMatrix(Hz,XCELLS,PL,ZCELLS + 1);
        DeleteMatrix(Bx,XCELLS + 1,PL,ZCELLS);
        DeleteMatrix(By,XCELLS,PL + 1,ZCELLS);
        DeleteMatrix(Bz,XCELLS,PL,ZCELLS + 1);
        DeleteMatrix(Bxo,XCELLS + 1,PL,ZCELLS);
        DeleteMatrix(Byo,XCELLS,PL + 1,ZCELLS);
        DeleteMatrix(Bzo,XCELLS,PL,ZCELLS + 1);
    }
    else if(rank != 0) {
        //Non-PML domains
        //Rank3 .. Rank(NProcs-1)
        //Rank3 adjacent to PML0 (ymin PML)
        //Rank(NProcs-1) adjacent to PML1
        if(rank != NProcs - 1) {
            DeleteMatrix(Ex,XCELLS,yeePerProc,ZCELLS + 1);
            DeleteMatrix(Ez,XCELLS + 1,yeePerProc,ZCELLS);
            DeleteMatrix(Hy,XCELLS,yeePerProc,ZCELLS);
        }
        else {
            DeleteMatrix(Ex,XCELLS,yeePerProc - 1,ZCELLS + 1);
            DeleteMatrix(Ez,XCELLS + 1,yeePerProc - 1,ZCELLS);
            DeleteMatrix(Hy,XCELLS,yeePerProc - 1,ZCELLS);
        }
        DeleteMatrix(Ey,XCELLS + 1,yeePerProc,ZCELLS + 1);
        DeleteMatrix(Hx,XCELLS + 1,yeePerProc,ZCELLS);
        DeleteMatrix(Hz,XCELLS,yeePerProc,ZCELLS + 1);
    }

    //UPML coefficients
    if(rank == 1 || rank == 2) {
        DeleteMatrix(C1Dx,XCELLS,PL + 1,ZCELLS + 1);
        DeleteMatrix(C2Dx,XCELLS,PL + 1,ZCELLS + 1);
        DeleteMatrix(C1Bx,XCELLS + 1,PL,ZCELLS);
        DeleteMatrix(C2Bx,XCELLS + 1,PL,ZCELLS);
        DeleteMatrix(C2Ey,XCELLS + 1,PL,ZCELLS + 1);
        DeleteMatrix(C3Ey,XCELLS + 1,PL,ZCELLS + 1);
        DeleteMatrix(C1Ez,XCELLS + 1,PL + 1,ZCELLS);
        DeleteMatrix(C2Ez,XCELLS + 1,PL + 1,ZCELLS);
        DeleteMatrix(C2Hy,XCELLS,PL + 1,ZCELLS);
        DeleteMatrix(C3Hy,XCELLS,PL + 1,ZCELLS);
        DeleteMatrix(C1Hz,XCELLS,PL,ZCELLS + 1);
        DeleteMatrix(C2Hz,XCELLS,PL,ZCELLS + 1);
    }
}

```

```

//PLRC coefficients
if(rank != 0 && rank != 1 && rank != 2) {
  //Non PML domains
  //Rank3 .. Rank(NProcs-1)
  //Rank3 adjacent to PML0 (ymin PML)
  //Rank(NProcs-1) adjacent to PML1
  if(rank != NProcs - 1) {
    DeleteMatrix(K1Ex,XCELLS,yeePerProc,ZCELLS + 1);
    DeleteMatrix(K2Ex,XCELLS,yeePerProc,ZCELLS + 1);
    DeleteMatrix(K1Ez,XCELLS + 1,yeePerProc,ZCELLS);
    DeleteMatrix(K2Ez,XCELLS + 1,yeePerProc,ZCELLS);
    DeleteMatrix(K1Hy,XCELLS,yeePerProc,ZCELLS);
    DeleteMatrix(K2Hy,XCELLS,yeePerProc,ZCELLS);

    DeleteMatrix(RAEx,XCELLS,yeePerProc,ZCELLS + 1,MAXPOLESEPS);
    DeleteMatrix(RAEz,XCELLS + 1,yeePerProc,ZCELLS,MAXPOLESEPS);
    DeleteMatrix(RAHy,XCELLS,yeePerProc,ZCELLS,MAXPOLESMU);
  }
  else {
    DeleteMatrix(K1Ex,XCELLS,yeePerProc - 1,ZCELLS + 1);
    DeleteMatrix(K2Ex,XCELLS,yeePerProc - 1,ZCELLS + 1);
    DeleteMatrix(K1Ez,XCELLS + 1,yeePerProc - 1,ZCELLS);
    DeleteMatrix(K2Ez,XCELLS + 1,yeePerProc - 1,ZCELLS);
    DeleteMatrix(K1Hy,XCELLS,yeePerProc - 1,ZCELLS);
    DeleteMatrix(K2Hy,XCELLS,yeePerProc - 1,ZCELLS);

    DeleteMatrix(RAEx,XCELLS,yeePerProc - 1,ZCELLS + 1,MAXPOLESEPS);
    DeleteMatrix(RAEz,XCELLS + 1,yeePerProc - 1,ZCELLS,MAXPOLESEPS);
    DeleteMatrix(RAHy,XCELLS,yeePerProc - 1,ZCELLS,MAXPOLESMU);
  }
  DeleteMatrix(K1Ey,XCELLS + 1,yeePerProc,ZCELLS + 1);
  DeleteMatrix(K2Ey,XCELLS + 1,yeePerProc,ZCELLS + 1);
  DeleteMatrix(K1Hx,XCELLS + 1,yeePerProc,ZCELLS);
  DeleteMatrix(K2Hx,XCELLS + 1,yeePerProc,ZCELLS);
  DeleteMatrix(K1Hz,XCELLS,yeePerProc,ZCELLS + 1);
  DeleteMatrix(K2Hz,XCELLS,yeePerProc,ZCELLS + 1);

  DeleteMatrix(RAEy,XCELLS + 1,yeePerProc,ZCELLS + 1,MAXPOLESEPS);
  DeleteMatrix(RAHx,XCELLS + 1,yeePerProc,ZCELLS,MAXPOLESMU);
  DeleteMatrix(RAHz,XCELLS,yeePerProc,ZCELLS + 1,MAXPOLESMU);
}
}

void ConvToSBC(int rank) {
  int XCELLSP,ZCELLSP;
  XCELLSP = XCELLS;
  ZCELLSP = ZCELLS;
  XCELLS = Round(XCELLS/2);
  ZCELLS = Round(ZCELLS/2);

  //Copy the UPML coefficients
  if(rank == 1 || rank == 2) {
    CopyMatrix(C1Dx,XCELLS,PL + 1,ZCELLS + 1,XCELLSP,PL + 1,ZCELLSP + 1);
    CopyMatrix(C2Dx,XCELLS,PL + 1,ZCELLS + 1,XCELLSP,PL + 1,ZCELLSP + 1);
    CopyMatrix(C1Bx,XCELLS + 1,PL,ZCELLS,XCELLSP + 1,PL,ZCELLSP);
    CopyMatrix(C2Bx,XCELLS + 1,PL,ZCELLS,XCELLSP + 1,PL,ZCELLSP);
    CopyMatrix(C2Ey,XCELLS + 1,PL,ZCELLS + 1,XCELLSP + 1,PL,ZCELLSP + 1);
    CopyMatrix(C3Ey,XCELLS + 1,PL,ZCELLS + 1,XCELLSP + 1,PL,ZCELLSP + 1);
    CopyMatrix(C1Ez,XCELLS + 1,PL + 1,ZCELLS,XCELLSP + 1,PL + 1,ZCELLSP);
    CopyMatrix(C2Ez,XCELLS + 1,PL + 1,ZCELLS,XCELLSP + 1,PL + 1,ZCELLSP);
    CopyMatrix(C2Hy,XCELLS,PL + 1,ZCELLS,XCELLSP,PL + 1,ZCELLSP);
    CopyMatrix(C3Hy,XCELLS,PL + 1,ZCELLS,XCELLSP,PL + 1,ZCELLSP);
    CopyMatrix(C1Hz,XCELLS,PL,ZCELLS + 1,XCELLSP,PL,ZCELLSP + 1);
    CopyMatrix(C2Hz,XCELLS,PL,ZCELLS + 1,XCELLSP,PL,ZCELLSP + 1);
  }
}

```

```

if(rank != 0 && rank != 1 && rank != 2) {
  if(rank != NProcs-1) {
    CopyMatrix(K1Ex,XCELLS,yeePerProc,ZCELLS + 1,XCELLSP,yeePerProc,ZCELLSP + 1);
    CopyMatrix(K2Ex,XCELLS,yeePerProc,ZCELLS + 1,XCELLSP,yeePerProc,ZCELLSP + 1);
    CopyMatrix(K1Ez,XCELLS + 1,yeePerProc,ZCELLS,XCELLSP + 1,yeePerProc,ZCELLSP);
    CopyMatrix(K2Ez,XCELLS + 1,yeePerProc,ZCELLS,XCELLSP + 1,yeePerProc,ZCELLSP);
    CopyMatrix(K1Hy,XCELLS,yeePerProc,ZCELLS,XCELLSP,yeePerProc,ZCELLSP);
    CopyMatrix(K2Hy,XCELLS,yeePerProc,ZCELLS,XCELLSP,yeePerProc,ZCELLSP);

    CopyMatrix(RAEx,XCELLS,yeePerProc,ZCELLS + 1,MAXPOLESEPS,
      XCELLSP,yeePerProc,ZCELLSP + 1,MAXPOLESEPS);
    CopyMatrix(RAEz,XCELLS + 1,yeePerProc,ZCELLS,MAXPOLESEPS,
      XCELLSP + 1,yeePerProc,ZCELLSP,MAXPOLESEPS);
    CopyMatrix(RAHy,XCELLS,yeePerProc,ZCELLS,MAXPOLESMU,
      XCELLSP,yeePerProc,ZCELLSP,MAXPOLESMU);
  }
  else {
    CopyMatrix(K1Ex,XCELLS,yeePerProc - 1,ZCELLS + 1,XCELLSP,yeePerProc - 1,ZCELLSP + 1);
    CopyMatrix(K2Ex,XCELLS,yeePerProc - 1,ZCELLS + 1,XCELLSP,yeePerProc - 1,ZCELLSP + 1);
    CopyMatrix(K1Ez,XCELLS + 1,yeePerProc - 1,ZCELLS,XCELLSP + 1,yeePerProc - 1,ZCELLSP);
    CopyMatrix(K2Ez,XCELLS + 1,yeePerProc - 1,ZCELLS,XCELLSP + 1,yeePerProc - 1,ZCELLSP);
    CopyMatrix(K1Hy,XCELLS,yeePerProc - 1,ZCELLS,XCELLSP,yeePerProc - 1,ZCELLSP);
    CopyMatrix(K2Hy,XCELLS,yeePerProc - 1,ZCELLS,XCELLSP,yeePerProc - 1,ZCELLSP);

    CopyMatrix(RAEx,XCELLS,yeePerProc - 1,ZCELLS + 1,MAXPOLESEPS,
      XCELLSP,yeePerProc - 1,ZCELLSP + 1,MAXPOLESEPS);
    CopyMatrix(RAEz,XCELLS + 1,yeePerProc - 1,ZCELLS,MAXPOLESEPS,
      XCELLSP + 1,yeePerProc - 1,ZCELLSP,MAXPOLESEPS);
    CopyMatrix(RAHy,XCELLS,yeePerProc - 1,ZCELLS,MAXPOLESMU,
      XCELLSP,yeePerProc - 1,ZCELLSP,MAXPOLESMU);
  }

  CopyMatrix(K1Ey,XCELLS + 1,yeePerProc,ZCELLS + 1,XCELLSP + 1,yeePerProc,ZCELLSP + 1);
  CopyMatrix(K2Ey,XCELLS + 1,yeePerProc,ZCELLS + 1,XCELLSP + 1,yeePerProc,ZCELLSP + 1);
  CopyMatrix(K1Hx,XCELLS + 1,yeePerProc,ZCELLS,XCELLSP + 1,yeePerProc,ZCELLSP);
  CopyMatrix(K2Hx,XCELLS + 1,yeePerProc,ZCELLS,XCELLSP + 1,yeePerProc,ZCELLSP);
  CopyMatrix(K1Hz,XCELLS,yeePerProc,ZCELLS + 1,XCELLSP,yeePerProc,ZCELLSP + 1);
  CopyMatrix(K2Hz,XCELLS,yeePerProc,ZCELLS + 1,XCELLSP,yeePerProc,ZCELLSP + 1);

  CopyMatrix(RAEy,XCELLS + 1,yeePerProc,ZCELLS + 1,MAXPOLESEPS,
    XCELLSP + 1,yeePerProc,ZCELLSP + 1,MAXPOLESEPS);
  CopyMatrix(RAHx,XCELLS + 1,yeePerProc,ZCELLS,MAXPOLESMU,
    XCELLSP + 1,yeePerProc,ZCELLSP,MAXPOLESMU);
  CopyMatrix(RAHz,XCELLS,yeePerProc,ZCELLS + 1,MAXPOLESMU,
    XCELLSP,yeePerProc,ZCELLSP + 1,MAXPOLESMU);
}

XCELLS = XCELLSP;
ZCELLS = ZCELLSP;
}

```

Appendix B

Genetic algorithm Debye series fitting code

```
% Genetic algorithm based Debye-series fitting (4pole) for mu/eps

% Random initial condition (GA is not dependent on this)
xo = [1.001023455843576e+001,...
      2.770914027513712e+001,...
      2.712774278667365e-009,...
      2.999846048253153e+001,...
      8.597467505694346e-008,...
      2.993848406191331e+001,...
      2.813650593172032e-008,...
      2.996133584411322e+001,...
      5.716714775731167e-008];

gaopts = gaoptimset(@ga);
% Four iterations of GA
for i = 1 : 4
    gaopts = gaoptimset(gaopts,'PopInitRange',[-50 ; 100],...
        'Generations',4e4,'StallGenLimit',3e4,'MutationFcn',...
        @mutationadaptfeasible,'InitialPopulation',xo,...
        'CrossoverFcn',@crossoverheuristic,'PlotFcns',@gplotbestf,'TolFun',1e-8);

% The first set is the minimum and the second set maximum
[x fval] = ga(@gafitfunc,9,[],[],[],[],...
    [0 0 3e-11 0 3e-11 0 3e-11 0 3e-11 ],...
    [200 100 1e-5 100 1e-5 100 1e-5 100 1e-5 ],[],gaopts);

x'
xo = x;
end

-----
function [fitval] = gafitfunc(x)

A = x(1);de1 = x(2);t1 = x(3);
de2 = x(4);t2 = x(5);
de3 = x(6);t3 = x(7);
de4 = x(8);t4 = x(9);
de5 = x(10);t5 = x(11);

f = linspace(8.25e9,12.35e9,3e3);
w = 2*pi*f;

epsr = GetEpsr(f/1e9);
epstrm = A + de1./(1+sqrt(-1)*w*t1) + de2./(1+sqrt(-1)*w*t2) + de3./(1+sqrt(-1)*w*t3) + ...
    de4./(1+sqrt(-1)*w*t4) + de5./(1+sqrt(-1)*w*t5);
fitval = sum(abs(epsr - epstrm).^2);

-----
```

```
function [epsr] = GetEpsr(freq)
% Get the measured data at frequency 'freq'

% Measured data and frequency points
global fr;
global mf114eps;

epsr = [];
epsr = zeros(1,length(freq));

epsr = interp1(fr,mf114eps,freq,'cubic');
```

Appendix C

Periodic surface reflectivity using Geometric Optics (GO)

```
function [Pi,Pr] = GO(fr,t,eps1,mu1,tr)

% fr      - Frequency (Hz)
% t       - Coating thickness (m)
% eps1,mu1- Relative, imaginary part > 0
% base    - Base dimension
% asp_rat - Aspect ratio
% h       - Height
% ds      - Ray incremental
% dx      - Source plane discretization interval
% SP      - Source plane
% Pi      - Incident power

% 0.5 inch base
base    = 0.5*2.54e-2;
asp_rat = 4;
h       = asp_rat * base;
ds      = base / 300;
dx      = base / 200;
SP      = (asp_rat+1)*base;
ko      = 2*pi*fr*sqrt(pi*4e7*8.85e-12);
etao    = sqrt(pi*4e7/8.85e-12);
Pi      = 0;
m       = t*sqrt(1+(2*h/base)^2);

% inipos - Initial position of the ray,
% inipos(row,col,1) - xini of the ray (row,col)
% inipos(row,col,2) - yini of the ray (row,col)
% If the ray is hitting the edge the values will be 'nan'
% ray_mode(row,col) --> 1 (TE) , ray_mode(row,col) --> 0 (TM)
% ray_mode(row,col) --> nan (ray hitting edge)
cplx_amp = ones(numel([dx : dx : base]),numel([dx : dx : base]));
ray_mode = zeros(numel([dx : dx : base]),numel([dx : dx : base]));
inipos   = zeros(numel([dx : dx : base]),numel([dx : dx : base]),2);
finpos   = zeros(numel([dx : dx : base]),numel([dx : dx : base]),3);
S_ave    = zeros(numel([dx : dx : base]),numel([dx : dx : base]));

row = 1;
col = 1;

for xini = [dx : dx : base]
    row = 1;
    for yini = [dx : dx : base]

        Pi = Pi + (1/2/etao)*dx*dx;
        % Initial position of the ray
        inipos(row,col,1) = xini;
        inipos(row,col,2) = yini;
```

```

[z,r] = SurfaceHeightPyr(xini,yini,base,asp_rat,t,tr);
% ray_mode and cplx_amp
if r == 1 || r == 2
    % TE
    ray_mode(row,col) = 1;
    cplx_amp(row,col) = 1;
elseif r == 3 || r == 4 || r == 5
    % TM
    ray_mode(row,col) = 0;
    cplx_amp(row,col) = 1/etao;
end

% ray_pts - Points for plotting
% ray_pos - Current position of ray
% s - Unit vector along propagation direction
ray_pts = [xini;yini;SP];
ray_pos = [xini;yini;SP];
s = [0;0;-1];

cnt = 1;
while 1
    ray_pos_p = ray_pos;
    ray_pos = ray_pos + ds*s;
    cplx_amp(row,col) = cplx_amp(row,col) * exp(-1i*ko*ds);
    if ray_pos(3) > SP
        % Ray has reached SP
        ray_pos = 0.5*(ray_pos_p + ray_pos);
        ray_pts = [ray_pts ray_pos];
        cplx_amp(row,col) = cplx_amp(row,col) * exp(1i*0.5*ko*ds);
        finpos(row,col,1) = ray_pos(1) ; finpos(row,col,2) = ray_pos(2);
        finpos(row,col,3) = ray_pos(3);
        if ray_mode(row,col) == 1
            % TE
            S_ave(row,col) = (0.5/etao)*(abs(cplx_amp(row,col))^2)*dot(s,[0;0;1]);
        elseif ray_mode(row,col) == 0
            % TM
            S_ave(row,col) = (0.5*etao)*(abs(cplx_amp(row,col))^2)*dot(s,[0;0;1]);
        end
        break;
    else
        [zs,r] = SurfaceHeightPyr(ray_pos(1),ray_pos(2),base,asp_rat,t,tr);
        if ray_pos(3) < zs
            ray_pos = 0.5*(ray_pos_p + ray_pos);
            cplx_amp(row,col) = cplx_amp(row,col) * exp(1i*0.5*ko*ds);
            ray_pts = [ray_pts ray_pos];
            [n,r] = SurfaceNormalPyr(ray_pos(1),ray_pos(2),base,asp_rat,t,tr);
            if ray_mode(row,col) == 1
                % TE
                if r == 5
                    [R] = TE_singlelayer_PECback(fr,eps1,mu1,t*10,acos(dot(-s,n)));
                else
                    [R] = TE_singlelayer_PECback(fr,eps1,mu1,t,acos(dot(-s,n)));
                end
                cplx_amp(row,col) = cplx_amp(row,col) * R;
            elseif ray_mode(row,col) == 0
                % TM
                if r == 5
                    [R] = TM_singlelayer_PECback(fr,eps1,mu1,t*10,acos(dot(-s,n)));
                else
                    [R] = TM_singlelayer_PECback(fr,eps1,mu1,t,acos(dot(-s,n)));
                end
                cplx_amp(row,col) = cplx_amp(row,col) * R;
            end
            end
            re = 2*n*dot(-s,n) + s;
            re = re/norm(re);
            s = re;
        end
    end
end

```

```

        end
    end
    if ray_pos(3) < 0
        disp('Something is wrong');
        ray_pos(3);
    end
    cnt = cnt + 1;
    if cnt > 2e4
        disp('Ray taking too long to come back to SP');
        break;
    end
end

%     plot3(ray_pts(1,2:size(ray_pts,2)),ray_pts(2,2:size(ray_pts,2)),ray_pts(3,2:size(ray_pts,2)),'r');
%     hold on;
%     plot3(ray_pts(1,1:2),ray_pts(2,1:2),ray_pts(3,1:2),'g');
%     grid on;
    row = row + 1;
end
col = col + 1;
end

row = 1;col = 1;
S_ave_tot = 0;
for xini = [dx : dx : base]
    row = 1;
    for yini = [dx : dx : base]
        if(~isnan(S_ave(row,col)))
            S_ave_tot = S_ave_tot + S_ave(row,col);
        end
        row = row + 1;
    end
    col = col + 1;
end
Pr = S_ave_tot * dx * dx;

-----
function [z,r] = SurfaceHeightPyr(x,y,base,asp_rat,t,tr)
% Surface height z = f(x,y)

% Transform x,y to the unit cell
if x > base || x < 0
    if x > 0
        x = x - floor(x/base)*base;
    else
        x = base - (abs(x) - floor(abs(x)/base)*base);
    end
end
if y > base || y < 0
    if y > 0
        y = y - floor(y/base)*base;
    else
        y = base - (abs(y) - floor(abs(y)/base)*base);
    end
end

h = asp_rat * base;
m = t*sqrt(1+(2*asp_rat)^2);
p = (tr/100)*(h+m);
b = p/2/asp_rat;

if (x > (0.5*base - b) && (x < (0.5*base + b)) && ...
    (y > (0.5*base - b) && (y < (0.5*base + b)))
    % region 5 - Top face
    z = h + m - p;
    r = 5;
elseif (x < 0.5*base) && (y >= x) && (y <= (-x + base))

```

```

    % Region 1
    z = 2*h*x/base + m;
    r = 1;
elseif (x > 0.5*base) && (y <= x) && (y >= (-x + base))
    % Region 2
    z = 2*h*(base - x)/base + m;
    r = 2;
elseif (y < 0.5*base) && (x >= y) && (x <= base - y)
    % Region 3
    z = 2*h*y/base + m;
    r = 3;
elseif (y > 0.5*base) && (x >= base - y) && (x <= y)
    % Region 4
    z = 2*h*(base - y)/base + m;
    r = 4;
end

-----

function [n,r] = SurfaceNormalPyr(x,y,base,asp_rat,t,tr)
% Surface normal : Depends on the facet

if x > base || x < 0
    if x > 0
        x = x - floor(x/base)*base;
    else
        x = base - (abs(x) - floor(abs(x)/base)*base);
    end
end
if y > base || y < 0
    if y > 0
        y = y - floor(y/base)*base;
    else
        y = base - (abs(y) - floor(abs(y)/base)*base);
    end
end

h = asp_rat * base;
mag_n = sqrt(1 + (base^2)/4/(h^2));
m = t*sqrt(1+(2*asp_rat)^2);
p = (tr/100)*(h+m);
b = p/2/asp_rat;

if (x > (0.5*base - b)) && (x < (0.5*base + b)) && ...
    (y > (0.5*base - b)) && (y < (0.5*base + b))
    % region 5 - Top face
    n = [0;0;1];
    r = 5;
elseif (x < 0.5*base) && (y >= x) && (y <= (-x + base))
    % Region 1
    n = [-1;0;base/2/h]./mag_n;
    r = 1;
elseif (x > 0.5*base) && (y <= x) && (y >= (-x + base))
    % Region 2
    n = [1;0;base/2/h]./mag_n;
    r = 2;
elseif (y < 0.5*base) && (x >= y) && (x <= base - y)
    % Region 3
    n = [0;-1;base/2/h]./mag_n;
    r = 3;
elseif (y > 0.5*base) && (x >= base - y) && (x <= y)
    % Region 4
    n = [0;1;base/2/h]./mag_n;
    r = 4;
end

-----

function [R] = TE_singlelayer_PECback(f,eps1,mu1,d,th)

```

```

% f - Frequency (Hz)
% eps1 - Relative epsilon (imaginary part > 0)
% m12 - Relative mu (imaginary part > 0)
% d - Thickness (m)
% th - In radians

muo = 4*pi*1e-7;
epso = 8.85e-12;
ko = 2*pi*f*sqrt(muo*epso);
k1 = 2*pi*f*sqrt(muo*epso*eps1*mu1);
kx = ko*sin(th);
kz = sqrt(ko^2 - kx.^2);
kz1 = (sqrt(k1^2 - kx.^2));

m = -1i*tan(kz1*d).*(kz*mu1*muo)./(kz1*muo);
R = (m - 1)./(m + 1);

-----
function [R] = TM_singlelayer_PECback(f,eps1,mu1,d,th)

% f - Frequency (Hz)
% eps2 - Relative epsilon (imaginary part > 0)
% mu2 - Relative mu (imaginary part > 0)
% d - Thickness (m)
% th - In radians

muo = 4*pi*1e-7;
epso = 8.85e-12;
ko = 2*pi*f*sqrt(muo*epso);
k1 = 2*pi*f*sqrt(muo*epso*eps1*mu1);

% Complex angle of refraction in thin layer
th1 = asin(ko * sin(th) ./ k1);
R1 = exp(-2*1i*d*k1*cos(th1));

m = ((R1 + 1)./(R1 - 1)).*(ko*eps1*epso*cos(th))./(k1*epso*cos(th1));
R = (m - 1)./(m + 1);

```

Appendix D

Truncated pyramid geometry

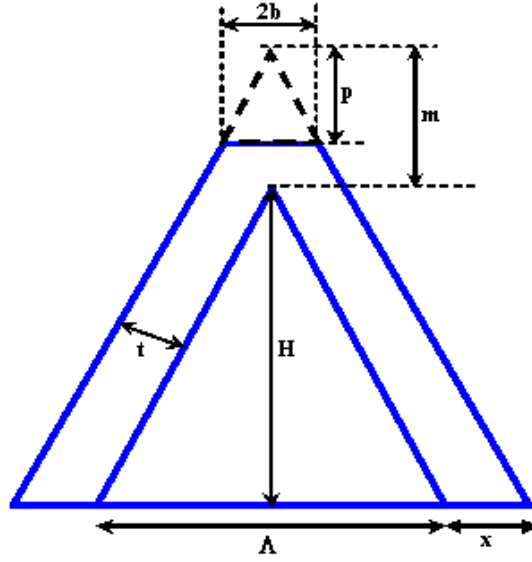


Figure D.1: Truncated pyramid geometry

$$\begin{aligned}
 m &= t \sqrt{1 + \left(\frac{2H}{\Lambda}\right)^2} \\
 x &= (H + m) \frac{\Lambda}{2H} - \frac{\Lambda}{2} \\
 p &= \frac{tr}{100} (H + m) ; \text{ } tr \text{ is the truncation percentage} \\
 b &= \frac{p\Lambda}{2H}
 \end{aligned}
 \tag{D.1}$$

In order to fit a spherical cap on a truncated pyramid, the slope of the tangent of the circle has to be equal to the slope of the face of the pyramid (see figure below). θ_c is fixed by the aspect ratio of the pyramid. The second degree of freedom is either the truncation percentage tr or radius of curvature of the spherical cap. If tr is given, then r_c can be calculated. On the other hand if r_c is given, tr can be calculated.

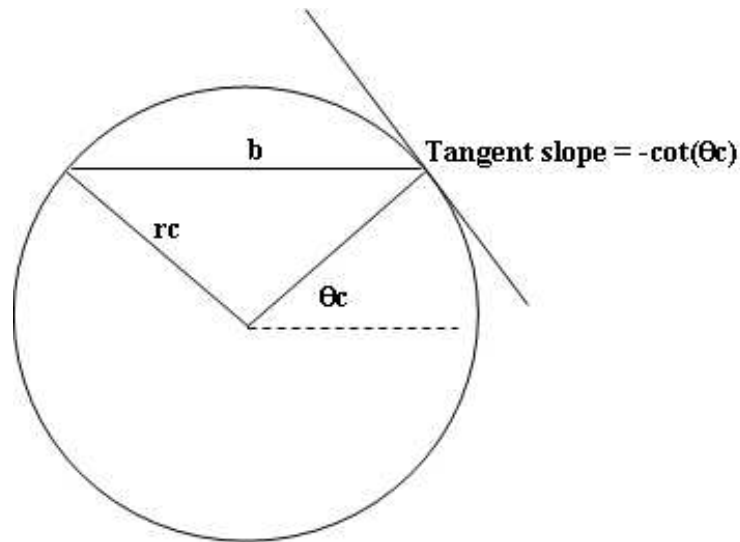


Figure D.2: Spherical cap

$$\theta_c = \cot^{-1} \left(\frac{2H}{\Lambda} \right) \quad (D.2)$$

$$r_c = b \cdot \sec(\theta_c)$$

For the case of 1:4 pyramid and $r_c = t$, $\theta_c = 7.125^\circ$. $b = 0.9923t$, $p = 7.9382t$.

$$tr = \frac{793.82t}{H + \sqrt{65}t} \quad (D.3)$$

For $t = 2$ mm, $tr = 23.7228$ %.

For spherical cap truncation, the following two conclusions can be reached.

1) If you want a “good spherical top” (not a one which is nearly flat), the truncation percentage has to be significant, resulting in high reflectivity. For example, as derived above if the radius of

curvature of the spherical cap is $r_c = t = 2$ mm, the truncation percentage for 1:4 pyramid is given by $tr = 23.7228$ %. Truncation percentage of $tr = 23.7228$ % means most of the tip coating is removed.

2) If the truncation percentage is not large enough, the radius of curvature r_c will be large and it will be nearly a flat truncated top. The reflectivity spectrum of flat truncated square pyramids with various truncation ratios are given in chapter 3.

Appendix E

Laguerre MoD code

```
//C++ code for Laguerre coefficient generation and post processing
//Run before and after the MATLAB main code
-----

#ifndef __AUXFUNCS_H__
#define __AUXFUNCS_H__

struct GaussianPulse {
    double to;
    double tau;
};

double GaussianPulseVal(GaussianPulse* pulse,double t);
double DebyeRelaxation(double* data,int len,double t);

#endif

-----

#include "AuxFuncs.h"
#include <cmath>

double GaussianPulseVal(GaussianPulse* pulse,double t) {
    //return exp(-pow((t-pulse->to)/pulse->tau,2));

    return exp(-pow((t-pulse->to)/pulse->tau,2))*(-1/pulse->tau/pulse->tau)
        *2*(t-pulse->to);
}

double DebyeRelaxation(double data[],int len,double t) {
    int p = (int)((len - 1)/2);
    double epsinf = data[0];
    double sum = 0;
    for(int pole = 0;pole < p;pole++) {
        sum += ((data[2*pole+1] - epsinf)/data[2*pole+2])*exp(-t/data[2*pole+2]);
    }

    return sum;
}

-----

#include <stdio.h>
#include <cmath>
#include <iostream>
#include <fstream>
#include <gsl/gsl_sf_laguerre.h>
#include <gsl/gsl_vector.h>
#include <gsl/gsl_const.h>
#include <gsl/gsl_matrix.h>
```

```

#include <gsl/gsl_permutation.h>
#include <gsl/gsl_linalg.h>
#include "AuxFuncs.h"

using namespace std;

double LaguerreBasis(int n,double st);

//Fundamental constants
double pi = 3.14159;
double c = 2.99792458e8;
double muo = 4*pi*1e-7;
double epso = 8.85e-12;
double etao = sqrt(muo/epso);

int main() {
    //BW : sqrt(2.3)/pi/tau
    //HWTM (Half Width Tenth Maximum) : 1.517*tau
    //to : Time shift of the Gaussian pulse
    //Tf : Simulation stop time
    //M : Total number of Laguerre basis functions
    //double fc = 1000e9;
    double fBW = 100e9;
    double tau = sqrt(2.3)/pi/fBW;
    double to = 4*tau;
    double Tf = to + 180*1.517*tau;
    double M = ceil(2*(fBW)*Tf + 1) + 80;
    double dx = c/(fBW)/120;
    double t = 0;
    //s x Tf = 9 x M
    double s = 1*M/Tf;

    //double debdata[] = {2,3,1e-10,3.8,1e-11};
    cout.precision(20);
    cout<<"M = "<<M<<endl;
    cout<<"Tf = "<<Tf<<endl;
    cout<<"s = "<<s<<endl;
    cout<<"dx = "<<dx<<endl;

    int IL = 20;

    double phi = 60*pi/180;
    //Source
    //TF/SF boundary is located at 'iL'th column Pz
    //x = 0 is at the PEC behind the UPML
    //So TF/SF boundary is at (iL - 0.5)*dx from x = 0
    //We need Pz_{iL-1,j}
    GaussianPulse PzPulse,QyPulse,PzPulse_1;
    PzPulse.to = to + (IL - 1.5)*dx*cos(phi)/c;
    PzPulse.tau = tau;
    PzPulse_1.to = to + (IL - 0.5)*dx*cos(phi)/c;
    PzPulse_1.tau = tau;
    QyPulse.to = to + (IL - 1)*dx*cos(phi)/c;
    QyPulse.tau = tau;
    gsl_matrix* Pz_inc_p = gsl_matrix_calloc(M,1);
    gsl_matrix* Pz_inc_p1 = gsl_matrix_calloc(M,1);
    gsl_matrix* Qy_inc_p = gsl_matrix_calloc(M,1);
    gsl_matrix* debCoeffs = gsl_matrix_calloc(M,1);
    int panels = 1e4;
    double dst = s*Tf/panels;
    double st1,st2,st3;
    double csum,csum1,csum2,csum3;
    //Calculate Pz_inc_p, Qy_inc_p
    for(int n = 0;n < M;n++) {
        csum = 0;csum1 = 0;csum2 = 0;csum3 = 0;
        for(int p = 0;p < panels/2;p++) {
            st1 = 2*p*dst;

```

```

    st2 = (2*p+1)*dst;
    st3 = (2*p+2)*dst;
    //Simpson's quadrature
    csum += dst*(GaussianPulseVal(&PzPulse,st1/s)*LaguerreBasis(n,st1) +
        4*GaussianPulseVal(&PzPulse,st2/s)*LaguerreBasis(n,st2) +
        GaussianPulseVal(&PzPulse,st3/s)*LaguerreBasis(n,st3))/3;
    csum1 += -cos(phi)*dst*(GaussianPulseVal(&QyPulse,st1/s)*LaguerreBasis(n,st1) +
        4*GaussianPulseVal(&QyPulse,st2/s)*LaguerreBasis(n,st2) +
        GaussianPulseVal(&QyPulse,st3/s)*LaguerreBasis(n,st3))/3;
    csum2 += dst*(GaussianPulseVal(&PzPulse_1,st1/s)*LaguerreBasis(n,st1) +
        4*GaussianPulseVal(&PzPulse_1,st2/s)*LaguerreBasis(n,st2) +
        GaussianPulseVal(&PzPulse_1,st3/s)*LaguerreBasis(n,st3))/3;
    /*csum3 += dst*(DebyeRelaxation(debdata,5,st1/s)*LaguerreBasis(n,st1) +
        4*DebyeRelaxation(debdata,5,st2/s)*LaguerreBasis(n,st2) +
        DebyeRelaxation(debdata,5,st3/s)*LaguerreBasis(n,st3))/3;*/
}
gsl_matrix_set(Pz_inc_p,n,0,csum);
gsl_matrix_set(Pz_inc_p1,n,0,csum2);
gsl_matrix_set(Qy_inc_p,n,0,csum1);
//gsl_matrix_set(debCoeffs,n,0,csum3);
}

ofstream Pzq;
ofstream Qyq;
ofstream Pzq1;
ofstream debs;
Pzq.open("Pzq.dat",ios::out);
Pzq1.open("Pzq1.dat",ios::out);
Qyq.open("Qyq.dat",ios::out);
Pzq.precision(25);
Pzq1.precision(25);
Qyq.precision(25);
//debs.open("deb.dat",ios::out);
for(int n = 0;n < M;n++) {
    Pzq<<gsl_matrix_get(Pz_inc_p,n,0)<<endl;
    Pzq1<<gsl_matrix_get(Pz_inc_p1,n,0)<<endl;
    Qyq<<gsl_matrix_get(Qy_inc_p,n,0)<<endl;
    //debs<<gsl_matrix_get(debCoeffs,n,0)<<endl;
}
Pzq.close();
Pzq1.close();
Qyq.close();
//debs.close();

double* coeffs = new double[(int)M];
FILE* f;
f= fopen("Pzmatlabout.dat","r");
char a[100];
for(int n = 0;n < M;n++) {
    fscanf(f,"%s \n",a);
    coeffs[n] = atof(a);
}
fclose(f);

ofstream Pzcppout;
Pzcppout.open("Pzcppout.dat",ios::out);
Pzcppout.precision(20);
for(double time = 0;time < Tf;time += Tf/3e4) {
    double val = 0;
    for(int n = 0;n < M;n++) {
        val += coeffs[n]*LaguerreBasis(n,s*time);
    }
    //Pz<<GaussianPulseVal(&PzPulse,time)<<endl;
    Pzcppout<<val<<endl;
}
Pzcppout.close();

```

```

    return 0;
}

// \phi_p(st) = exp(-0.5*st)*L_{p}(st)
double LaguerreBasis(int n,double st) {
    return gsl_sf_laguerre_n(n,0,st) * exp(-0.5*st);
}

```

MATLAB Laguerre MoD main code

```

pi    = 3.14159;
c     = 2.99792458e8;
muo   = 4*pi*1e-7;
epso  = 8.85e-12;
etao  = sqrt(muo/epso);

%BW : sqrt(2.3)/pi/tau
%HWTM (Half Width Tenth Maximum) : 1.517*tau
%to : Time shift of the Gaussian pulse
%Tf : Simulation stop time
%M : Total number of Laguerre basis functions
% fc  = 500e9;
fBW   = 100e9;
tau   = sqrt(2.3)/pi/fBW;
to    = 4*tau;
Tf    = to + 180*1.517*tau;
M     = ceil(2*(fBW)*Tf + 1) + 80;
dx    = c/(fBW)/120;
s     = 1*M/Tf;

% Materials
VACUUM = 0;
UPML   = 1;
MED1   = 3;
PEC    = 2;
VacuumEpsDebye = [1];
Med1EpsDebye   = [3,4,7e-8,4.5,2e-10];
% Med1EpsDebye = [3];

PL      = 17;
XCELLS_PS = 200;
XCELLS   = XCELLS_PS + 2*PL;
YCELLS   = 20;
IL       = 30;

load Pzq.dat;
load Qyq.dat;load Pzq1.dat;
Pzinc   = Pzq;
Qyinc   = Qyq;
Pzinc1  = Pzq1;
clear Pzq;
clear Qyq;clear Pzq1;

phi = 60*pi/180;

A      = zeros(XCELLS*YCELLS,XCELLS*YCELLS);
Media  = zeros(YCELLS,XCELLS);
Sigma  = zeros(YCELLS,XCELLS);
Pz     = zeros(YCELLS,XCELLS,M);
Qy     = zeros(YCELLS,XCELLS+1,M);
Qx     = zeros(YCELLS,XCELLS,M);

Media(:,1:PL)           = UPML;
Media(:,XCELLS_PS+PL+1:XCELLS) = UPML;
% Media(:,35:135) = MED1;

```

```

% Media(:,66:70) = PEC;

for row = 1 : YCELLS
    for col = 1 : XCELLS
        if Media(row,col) == PEC
            Sigma(row,col) = 1e8;
        else
            Sigma(row,col) = 0;
        end
    end
end

m      = 3;
sigmao = -log(exp(-16))*(m+1)/(2*120*pi*PL*dx);
d      = PL*dx;
SigCon = sigmao/(d^m);

for row = 1 : YCELLS
    for col = 1 : XCELLS
        if col <= PL + 1
            % A6|i,j
            % A5|i+1,j
            if col == PL + 1
                A6 = 2*c/s/dx;
                A5 = 2*c/s/dx;
            else
                A6 = (2*c*epso)/(s*epso*dx + 2*dx*SigCon*(((PL - col + 0.5)*dx)^m));
                A5 = (2*c*epso)/(s*epso*dx + 2*dx*SigCon*((PL - col)*dx)^m);
            end

            A((col-1)*YCELLS + row,(col)*YCELLS + row) = A6*A5;

            % A5|i,j
            A5_1 = (2*c*epso)/(s*epso*dx + 2*dx*SigCon*(((PL - col + 1)*dx)^m));
            A7   = (s*sin(phi)*dx - 4*c)*dx*A6/4/c/dx;
            A8   = (s*sin(phi)*dx + 4*c)*dx*A6/4/c/dx;
            if col == PL + 1
                A1 = -2*c/s/dx + 0.5*sin(phi);
                A2 = 2*c/s/dx + 0.5*sin(phi);
            else
                A1 = -2*c/s/dx - 4*c*SigCon*(((PL - col + 0.5)*dx)^m)/s/s/epso/dx +
                    0.5*sin(phi) + SigCon*(((PL - col + 0.5)*dx)^m)*sin(phi)/s/epso;
                A2 = 2*c/s/dx + 4*c*SigCon*(((PL - col + 0.5)*dx)^m)/s/s/epso/dx +
                    0.5*sin(phi) + SigCon*(((PL - col + 0.5)*dx)^m)*sin(phi)/s/epso;
            end
            A((col-1)*YCELLS + row,(col-1)*YCELLS + row) = -A6*A5 - A6*A5_1 + A7*A2 + A8*A1 - 1;

            if col ~= 1
                A((col-1)*YCELLS + row,(col-2)*YCELLS + row) = A6*A5_1;
            end

            if row ~= YCELLS
                A((col-1)*YCELLS + row,(col-1)*YCELLS + row + 1) = A7*A1;
            else
                A((col-1)*YCELLS + row,(col-1)*YCELLS + 1) = A7*A1;
            end

            if row ~= 1
                A((col-1)*YCELLS + row,(col-1)*YCELLS + row - 1) = A8*A2;
            else
                A((col-1)*YCELLS + row,(col-1)*YCELLS + YCELLS) = A8*A2;
            end
        elseif col >= XCELLS_PS + PL
            % A6|i,j
            % A5|i+1,j
            if col == XCELLS_PS + PL
                A6 = 2*c/s/dx;
            end
        end
    end
end

```

```

    A5 = 2*c/s/dx;
else
    A6 = (2*c*epso)/(s*epso*dx + 2*dx*SigCon(((col - XCELLS_PS - PL - 0.5)*dx)^m));
    A5 = (2*c*epso)/(s*epso*dx + 2*dx*SigCon(((col - XCELLS_PS - PL)*dx)^m));
end

if col ~= XCELLS
    A((col-1)*YCELLS + row,(col)*YCELLS + row) = A6*A5;
end

% A5|i,j
if col == XCELLS_PS + PL
    A5_1 = 2*c/s/dx;
else
    A5_1 = (2*c*epso)/(s*epso*dx + 2*dx*SigCon(((col - XCELLS_PS - PL - 1)*dx)^m));
end
A7 = (s*sin(phi)*dx - 4*c)*dx*A6/4/c/dx;
A8 = (s*sin(phi)*dx + 4*c)*dx*A6/4/c/dx;
if col == XCELLS_PS + PL
    A1 = -2*c/s/dx + 0.5*sin(phi);
    A2 = 2*c/s/dx + 0.5*sin(phi);
else
    A1 = -2*c/s/dx - 4*c*SigCon(((col - XCELLS_PS - PL - 0.5)*dx)^m)/s/s/epso/dx +
        0.5*sin(phi) + SigCon(((col - XCELLS_PS - PL - 0.5)*dx)^m)*sin(phi)/s/epso;
    A2 = 2*c/s/dx + 4*c*SigCon(((col - XCELLS_PS - PL - 0.5)*dx)^m)/s/s/epso/dx +
        0.5*sin(phi) + SigCon(((col - XCELLS_PS - PL - 0.5)*dx)^m)*sin(phi)/s/epso;
end
A((col-1)*YCELLS + row,(col-1)*YCELLS + row) = -A6*A5 - A6*A5_1 + A7*A2 + A8*A1 - 1;
A((col-1)*YCELLS + row,(col-2)*YCELLS + row) = A6*A5_1;

if row ~= YCELLS
    A((col-1)*YCELLS + row,(col-1)*YCELLS + row + 1) = A7*A1;
else
    A((col-1)*YCELLS + row,(col-1)*YCELLS + 1) = A7*A1;
end

if row ~= 1
    A((col-1)*YCELLS + row,(col-1)*YCELLS + row - 1) = A8*A2;
else
    A((col-1)*YCELLS + row,(col-1)*YCELLS + YCELLS) = A8*A2;
end
else
if Media(row,col) == VACUUM
    K = 2*c/(DebyeMediaLaguerre(VacuumEpsDebye,s,0) + 2*c*etao*Sigma(row,col));
elseif Media(row,col) == MED1
    K = 2*c/(DebyeMediaLaguerre(Med1EpsDebye,s,0) + 2*c*etao*Sigma(row,col));
else
    K = 2*c/(s + 2*c*etao*Sigma(row,col));
end

A((col-1)*YCELLS + row,(col-1)*YCELLS + row) = -8*c*K/s/dx/dx - 1
+ s*sin(phi)*sin(phi)*K/2/c;

A((col-1)*YCELLS + row,(col-2)*YCELLS + row) = 2*c*K/s/dx/dx;
A((col-1)*YCELLS + row,(col)*YCELLS + row) = 2*c*K/s/dx/dx;

if row ~= YCELLS
    A((col-1)*YCELLS + row,(col-1)*YCELLS + row + 1) = 2*c*K/s/dx/dx - sin(phi)*K/dx;
else
    A((col-1)*YCELLS + row,(col-1)*YCELLS + 1) = 2*c*K/s/dx/dx - sin(phi)*K/dx;
end

if row ~= 1
    A((col-1)*YCELLS + row,(col-1)*YCELLS + row - 1) = 2*c*K/s/dx/dx + sin(phi)*K/dx;
else

```



```

A6 = (2*c*epso)/(s*epso*dx + 2*dx*SigCon*(((col - XCELLS_PS - PL - 0.5)*dx)^m));
A5 = (2*c*epso)/(s*epso*dx + 2*dx*SigCon*(((col - XCELLS_PS - PL)*dx)^m));
end

% A5|i,j
if col == XCELLS_PS + PL
    A5_1 = 2*c/s/dx;
    B1 = 0;
else
    A5_1 = (2*c*epso)/(s*epso*dx + 2*dx*SigCon*(((col - XCELLS_PS - PL - 1)*dx)^m));
    B1 = (2*sin(phi)*SigCon*(((col - XCELLS_PS - PL - 0.5)*dx)^m))/s/epso;
end
A7 = (s*sin(phi)*dx - 4*c)*dx*A6/4/c/dx;
A8 = (s*sin(phi)*dx + 4*c)*dx*A6/4/c/dx;

for p = 0 : 1 : q - 1
    A3 = B1 + 2*sin(phi)*(q-p) - 4*c/s/dx;
    A4 = B1 + 2*sin(phi)*(q-p) + 4*c/s/dx;
    if row == YCELLS
        bsum = bsum + (s*dx/c)*A6*A5*Qy(row,col+1,p+1) - (s*dx/c)*A6*A5_1*
            Qy(row,col,p+1) - A7*A3*Pz(1,col,p+1) - (A7*A4 + A8*A3 - s*dx*A6/c)
            *Pz(row,col,p+1) - (A8*A4)*Pz(row-1,col,p+1) + (4*A7*(q - p) -
            s*sin(phi)*dx*A6/2/c)*Qx(1,col,p+1) + (4*A8*(q - p) - s*sin(phi)*
            dx*A6/2/c)*Qx(row,col,p+1);
    elseif row == 1
        bsum = bsum + (s*dx/c)*A6*A5*Qy(row,col+1,p+1) - (s*dx/c)*A6*A5_1*
            Qy(row,col,p+1) - A7*A3*Pz(row+1,col,p+1) - (A7*A4 + A8*A3 -
            s*dx*A6/c)*Pz(row,col,p+1) - (A8*A4)*Pz(YCELLS,col,p+1) + (4*A7*
            (q - p) - s*sin(phi)*dx*A6/2/c)*Qx(row+1,col,p+1) + (4*A8*(q - p)
            - s*sin(phi)*dx*A6/2/c)*Qx(row,col,p+1);
    else
        bsum = bsum + (s*dx/c)*A6*A5*Qy(row,col+1,p+1) - (s*dx/c)*A6*A5_1*
            Qy(row,col,p+1) - A7*A3*Pz(row+1,col,p+1) - (A7*A4 + A8*A3 - s*dx
            *A6/c)*Pz(row,col,p+1) - (A8*A4)*Pz(row-1,col,p+1) + (4*A7*(q - p)
            - s*sin(phi)*dx*A6/2/c)*Qx(row+1,col,p+1) + (4*A8*(q - p) - s*
            sin(phi)*dx*A6/2/c)*Qx(row,col,p+1);
    end
end
b(brow,1) = bsum;

else
    if Media(row,col) == VACUUM
        K = 2*c/(s + 2*c*etao*Sigma(row,col));
        epsr_1 = s;
        epsr_2 = s;
    elseif Media(row,col) == MED1
        K = 2*c/(DebyeMediaLaguerre(Med1EpsDebye,s,0) + 2*c*etao*Sigma(row,col));
        epsr_1 = DebyeMediaLaguerre(Med1EpsDebye,s,q-p);
        epsr_2 = DebyeMediaLaguerre(Med1EpsDebye,s,q-p-1);
    else
        K = 2*c/(s + 2*c*etao*Sigma(row,col));
        epsr_1 = s;
        epsr_2 = s;
    end

    for p = 0 : 1 : q - 1
        if row == 1
            bsum = bsum + (2*K/dx)*(Qy(row,col+1,p+1)-Qy(row,col,p+1)) +
                (sin(phi)*K/dx)*(Pz(row+1,col,p+1)-Pz(YCELLS,col,p+1)) + (-2*K/dx)
                *(Qx(row+1,col,p+1)-Qx(row,col,p+1)) + (K/c)*(0.5*epsr_1+0.5*epsr_2-
                s*sin(phi)*sin(phi))*Pz(row,col,p+1);
        elseif row == YCELLS
            bsum = bsum + (2*K/dx)*(Qy(row,col+1,p+1)-Qy(row,col,p+1)) +
                (sin(phi)*K/dx)*(Pz(1,col,p+1)-Pz(row-1,col,p+1)) + (-2*K/dx)
                *(Qx(1,col,p+1)-Qx(row,col,p+1)) + (K/c)*(0.5*epsr_1+0.5*
                epsr_2-s*sin(phi)*sin(phi))*Pz(row,col,p+1);
        else

```

```

        bsum = bsum + (2*K/dx)*(Qy(row,col+1,p+1)-Qy(row,col,p+1)) +
        (sin(phi)*K/dx)*(Pz(row+1,col,p+1)-Pz(row-1,col,p+1)) + (-2*K/dx)
        *(Qx(row+1,col,p+1)-Qx(row,col,p+1)) + (K/c)*(0.5*epsr_1+0.5*epsr_2
        -s*sin(phi)*sin(phi))*Pz(row,col,p+1);
    end
end

%TF/SF
if col == IL
    bsum = bsum + (-2*c*K/s/dx/dx)*Pzinc(q+1,1);
    for p = 0 : 1 : q - 1
        bsum = bsum + (2*K/dx)*(-Qyinc(p+1,1));
    end
end
b(brow,1) = bsum;
end
end

x = Ainv*b;

for row = 1 : YCELLS
    for col = 1 : XCELLS
        Pz(row,col,q+1) = x((col-1)*YCELLS + row,1);
        if col == IL
            Pz(row,col,q+1) = Pz(row,col,q+1) + Pzinc(q+1,1);
        end
    end
end

A1 = (s*dx*sin(phi) - 4*c)/2/s/dx;
B = (s*dx*sin(phi) + 4*c)/2/s/dx;
C = 2*c/s/dx;
for row = 1 : YCELLS
    for col = 1 : XCELLS
        bsum = 0;
        if col <= PL + 1
            if col == PL + 1
                A1u = -2*c/s/dx + 0.5*sin(phi);
                A2 = 2*c/s/dx + 0.5*sin(phi);
                B1 = 0;
            else
                A1u = -2*c/s/dx - 4*c*SigCon*(((PL - col + 0.5)*dx)^m)/s/s/epso/dx
                + 0.5*sin(phi) + SigCon*(((PL - col + 0.5)*dx)^m)*sin(phi)/s/epso;
                A2 = 2*c/s/dx + 4*c*SigCon*(((PL - col + 0.5)*dx)^m)/s/s/epso/dx
                + 0.5*sin(phi) + SigCon*(((PL - col + 0.5)*dx)^m)*sin(phi)/s/epso;
                B1 = (2*sin(phi)*SigCon*(((PL - col + 0.5)*dx)^m))/s/epso;
            end
            if row == 1
                bsum = A1u*Pz(row,col,q+1) + A2*Pz(YCELLS,col,q+1);
            else
                bsum = A1u*Pz(row,col,q+1) + A2*Pz(row-1,col,q+1);
            end
            for p = 0 : 1 : q - 1
                A3 = B1 + 2*sin(phi)*(q-p) - 4*c/s/dx;
                A4 = B1 + 2*sin(phi)*(q-p) + 4*c/s/dx;
                if row == 1
                    bsum = bsum + A3*Pz(row,col,p+1) + A4*Pz(YCELLS,col,p+1)
                    - 4*(q-p)*Qx(row,col,p+1);
                else
                    bsum = bsum + A3*Pz(row,col,p+1) + A4*Pz(row-1,col,p+1)
                    - 4*(q-p)*Qx(row,col,p+1);
                end
            end
            Qx(row,col,q+1) = bsum;
        elseif col >= XCELLS_PS + PL

```

```

if col == XCELLS_PS + PL
    A1u = -2*c/s/dx + 0.5*sin(phi);
    A2 = 2*c/s/dx + 0.5*sin(phi);
    B1 = 0;
else
    A1u = -2*c/s/dx - 4*c*SigCon*(((col - XCELLS_PS - PL - 0.5)*dx)^m)/
    s/s/epso/dx + 0.5*sin(phi)+ SigCon*(((col - XCELLS_PS - PL - 0.5)*dx)^m)
    *sin(phi)/s/epso;
    A2 = 2*c/s/dx + 4*c*SigCon*(((col - XCELLS_PS - PL - 0.5)*dx)^m)/
    s/s/epso/dx + 0.5*sin(phi) + SigCon*(((col - XCELLS_PS - PL - 0.5)*dx)^m)
    *sin(phi)/s/epso;
    B1 = (2*sin(phi)*SigCon*(((col - XCELLS_PS - PL - 0.5)*dx)^m))/s/epso;
end
if row == 1
    bsum = A1u*Pz(row,col,q+1) + A2*Pz(YCELLS,col,q+1);
else
    bsum = A1u*Pz(row,col,q+1) + A2*Pz(row-1,col,q+1);
end
for p = 0 : 1 : q - 1
    A3 = B1 + 2*sin(phi)*(q-p) - 4*c/s/dx;
    A4 = B1 + 2*sin(phi)*(q-p) + 4*c/s/dx;
    if row == 1
        bsum = bsum + A3*Pz(row,col,p+1) + A4*Pz(YCELLS,col,p+1)
        - 4*(q-p)*Qx(row,col,p+1);
    else
        bsum = bsum + A3*Pz(row,col,p+1) + A4*Pz(row-1,col,p+1)
        - 4*(q-p)*Qx(row,col,p+1);
    end
end
Qx(row,col,q+1) = bsum;
else
    bsum = (-2*c/s/dx + 0.5*sin(phi))*Pz(row,col,q+1);
    if row ~= 1
        bsum = bsum + (2*c/s/dx + 0.5*sin(phi))*Pz(row-1,col,q+1);
    else
        bsum = bsum + (2*c/s/dx + 0.5*sin(phi))*Pz(YCELLS,col,q+1);
    end

    for p = 0 : 1 : q - 1
        if row ~= 1
            bsum = bsum + sin(phi)*Pz(row,col,p+1) + ...
            sin(phi)*Pz(row-1,col,p+1) - 2*Qx(row,col,p+1);
        else
            bsum = bsum + sin(phi)*Pz(row,col,p+1) + ...
            sin(phi)*Pz(YCELLS,col,p+1) - 2*Qx(row,col,p+1);
        end
    end
    Qx(row,col,q+1) = bsum;
end
end
end

for row = 1 : YCELLS
    for col = 1 : XCELLS + 1
        bsum = 0;

        if col <= PL + 1
            A5 = (2*c*epso)/(s*epso*dx + 2*dx*SigCon*(((PL - col + 1)*dx)^m));
            if col == 1
                bsum = A5*Pz(row,col,q+1);
            else
                bsum = A5*Pz(row,col,q+1) - A5*Pz(row,col-1,q+1);
            end
            for p = 0 : 1 : q - 1
                bsum = bsum - (s*dx/c)*A5*Qy(row,col,p+1);
            end
        end
    end
end

```

```

        end
        Qy(row,col,q+1) = bsum;
    elseif col >= XCELLS_PS + PL + 1
        % A5|i,j
        A5 = (2*c*epso)/(s*epso*dx + 2*dx*SigCon*(((col - XCELLS_PS - PL - 1)
        *dx)^m));
        if col == XCELLS + 1
            bsum = -A5*Pz(row,col-1,q+1);
        else
            bsum = A5*Pz(row,col,q+1) - A5*Pz(row,col-1,q+1);
        end
        for p = 0 : 1 : q - 1
            bsum = bsum - (s*dx/c)*A5*Qy(row,col,p+1);
        end
        Qy(row,col,q+1) = bsum;
    else
        bsum = (2*c/s/dx)*Pz(row,col,q+1) - (2*c/s/dx)*Pz(row,col-1,q+1);
        if col == IL
            bsum = bsum + (-2*c/s/dx)*Pzinc1(q+1,1);
        end

        for p = 0 : 1 : q - 1
            bsum = bsum - 2*Qy(row,col,p+1);
        end

        Qy(row,col,q+1) = bsum;
    end
end
end
end
fid = fopen('Pzmatlabout.dat','w');
for idx = 0 : 1 : M - 1
    fprintf(fid,'%15.12f\n',Pz(10,200,idx+1));
end
fclose(fid);
end

```

Appendix F

ADE (Auxiliary Differential Equation) formulation for TM_z case (Debye media)

$$E_z|_{i,j}^{n+1} = \left[\frac{2\varepsilon_o\varepsilon_\infty + \sum_{p=1}^N \beta_p - \sigma\Delta t}{2\varepsilon_o\varepsilon_\infty + \sum_{p=1}^N \beta_p + \sigma\Delta t} \right] E_z|_{i,j}^n + \frac{2\Delta t}{2\varepsilon_o\varepsilon_\infty + \sum_{p=1}^N \beta_p + \sigma\Delta t} \left[\frac{H_y|_{i+1,j}^{n+0.5} - H_y|_{i,j}^{n+0.5}}{\Delta x} - \frac{H_x|_{i,j+1}^{n+0.5} - H_x|_{i,j}^{n+0.5}}{\Delta y} - \frac{1}{2} \sum_{p=1}^N (1 + k_p) J_z^p|_{i,j}^n \right] \quad (\text{F.1})$$

$$J_z^p|_{i,j}^{n+1} = k_p J_z^p|_{i,j}^n + \beta_p \left[\frac{E_z|_{i,j}^{n+1} - E_z|_{i,j}^n}{\Delta t} \right] \quad (\text{F.2})$$

$$k_p = \frac{1 - \frac{\Delta t}{2\tau_p}}{1 + \frac{\Delta t}{2\tau_p}}; \quad \beta_p = \frac{\varepsilon_o \Delta \varepsilon_p \Delta t}{\tau_p (1 + \frac{\Delta t}{2\tau_p})}$$

$$H_x|_{i,j+1}^{n+0.5} = H_x|_{i,j+1}^{n-0.5} - \frac{\Delta t}{\mu_o \Delta y} [E_z|_{i,j+1}^n - E_z|_{i,j}^n] \quad (\text{F.3})$$

$$H_y|_{i+1,j}^{n+0.5} = H_y|_{i+1,j}^{n-0.5} + \frac{\Delta t}{\mu_o \Delta x} [E_z|_{i+1,j}^n - E_z|_{i,j}^n] \quad (\text{F.4})$$